



University of Calabria

Department of Physics and Chemistry

*Reflection Spectroscopic Ellipsometry
investigations of reciprocal interactions between
organic-inorganic layered structures*

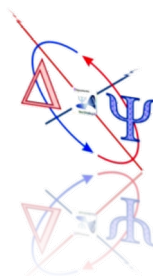
By

Stefano D'Elia

*Dissertation for the Degree of Doctor of Philosophy in
"Science and Technology of Mesophases and Molecular Materials"*

XXI° Cycle

FIS/01



*Candidate
Stefano D'Elia*

*Supervisor
Prof. Carlo Versace*

*Coordinator
Prof. Carlo Versace*

Academic year 2007/2008

Ringraziamenti

Ringrazio il Dipartimento di Fisica e il CNR-LICRYL Laboratory dell'Università della Calabria per aver sostenuto lo sviluppo dei lavori di ricerca mostrati in questo manoscritto ad altri ancora. Voglio in particolare esprimere la mia gratitudine alle persone con le quali ho collaborato ed interagito in tutti questi anni.

Speciali ringraziamenti al Prof. Alexander G. Petrov, Prof. Mathias Schubert, Dr. Tino Hofmann ed al gruppo di ellissometria della Lincoln-Nebraska University (USA).

Acknowledgments

I thank to the Department of Physics and CNR-LICRYL Laboratory of the University of Calabria for supporting me during the PhD program. Particularly, I would like to express my gratitude to all the people which I have collaborated with in developing the interesting scientific materials presented in this Ph.D. dissertation.

Special thanks to Prof. Alexander G. Petrov, Prof. Mathias Schubert, Dr. Tino Hofmann, and the ellipsometry group of the Lincoln-Nebraska University (USA).

Dedica



*Al mio nipotino
Riccardo
giunto tra noi nella notte del
26 Giugno 2008 alle ore 23:28.*

*to my parents
And
to Myself
Stefano D'Elia*

*3 - 25 - 15 - 21 - 23 - 1
"Chouwa" or "Cyouwa"*

CONTENTS

Acknowledgment	01
Contents	05
Abstract	13
Chapter 1 - Introduction	17
<i>Chapter 1 - Reference</i>	20
Chapter 2 - Polarized Light and Ellipsometry	25
<i>Introduction</i>	25
2.1. <i>Polarization of Light</i>	25
2.2. <i>Standard Ellipsometry</i>	28
2.3. <i>Single film placed on the substrate</i>	30
2.4. <i>Experimental Setup</i>	33
2.5. <i>Optical Model and Spectroscopic Ellipsometry Data Analysis</i>	34
<i>Chapter 2 - Reference</i>	36
Chapter 3 – Ferroelectric thin films obtained by sol-gel synthesis: Optical and Structural Characterization	39
Introduction	39
3.1. Characterization of the substrates and of the Indium Tin Oxide (ITO)	41
<i>“Ellipsometry investigation of the effects of annealing temperature on the optical properties of indium tin oxide thin films studied by Drude-Lorentz model”</i>	41
<u>Stefano D’Elia</u> , Federica Ciuchi, Nicola Scaramuzza, Giuseppe Strangi, Carlo Versace, Carlo Vena, and Roberto Bartolino	
INFN-CNR-LICRYL Laboratory and CEMIF.CAL, Department of Physics, University of Calabria, via P.Bucci 31C, Rende (CS), I- 87036 (ITALY)	
Submitted to SURFACE SCIENCE (2008)	
3.1.1. Appendix A	64
<i>Effects of annealing temperature on the structural and morphological properties of high quality indium tin oxide thin films: Effects on the morphological properties</i>	

3.1.2. Appendix B	65
<i>Effects of annealing temperature on the structural and morphological properties of high quality indium tin oxide thin films: Validity of the Burstein-Moss model</i>	
	67
3.1.3. Appendix C	
<i>Check of the validity of the ITO optical model. (near UV – Far-IR)</i>	
3.2. Ellipsometry characterization of Lead Zirconate Titanate thin films – PZT	71
<i>“Thermally induced modifications of the optic properties of Lead Zirconate Titanate thin films obtained on different substrates by sol-gel synthesis”</i>	
	71

Stefano D’Elia¹, Marco Castriota¹, Alfonso Policicchio², Carlo Versace¹, Nicola Scaramuzza¹, Enzo Cazzanelli¹, Raffaele Agostino², Carlo Vena¹, Giuseppe Strangi¹ and Roberto Bartolino¹

¹INFM-CNR-LICRYL Laboratory and CEMIF.CAL, Department of Physics, University of Calabria, via P.Bucci 31C, Rende (CS), I-87036 (ITALY)

²Department of Physics, University of Calabria, via P.Bucci 31C, Rende (CS), I-87036 (ITALY)

Accepted

JOURNAL OF APPLIED PHYSICS (2008)

3.2.1. Appendix A	101
<i>Optical model used for the Intrinsic Silicon wafer</i>	
3.3. ITO/PZT interface effect	103
<i>(Application in the asymmetric nematic liquid crystal cells)</i>	
<i>“Effects of thermal treatments on structural and optical properties of Lead Zirconium Titanate thin films obtained by sol gel technique”</i>	
	103

Marco Castriota, **Stefano D’Elia**, Salvatore Marino, Enzo Cazzanelli, Nicola Scaramuzza, Carlo Versace and Roberto Bartolino

CNR-LICRYL Laboratory and CEMIF.CAL, Department of Physics, University of Calabria, via P.Bucci 31C, Rende (CS), I-87036 (ITALY)

**Submitted to
THIN SOLID FILMS (2008)**

3.4.	Far-IR ellipsometry characterization of the PZT thin films obtained by sol-gel synthesis onto ITO substrates and annealed at different temperatures	123
	<i>(Lincoln Nebraska University - 2008)</i>	
	<i>Supervisors: Prof. Mathias Schubert and Dr. Tino Hofmann</i>	
	Introduction	123
	3.4.1. Far-IR model dielectric function	123
	3.4.2. Materials and methods	124
	3.4.3. Experimental results and discussion	125
	<i>Float glass characterization</i>	125
	<i>Indium tin oxide (ITO) characterization</i>	129
	<i>Lead zirconium titanate (PZT) characterization</i>	133
	<i>Acknowledgements</i>	147
	Chapter 3 - Reference	148
	Chapter 4 - Self-Assembly of surfactant molecules	149
	Introduction	149
	4.1. Angle contact and energy: Young condition	149
	4.2. Ultra thin films problem in spectroscopic reflection ellipsometry. Outline	151
	4.3. Self-Assembly and molecular order	155
	<i>“Influence of drying temperature on closed-packed structures of silanized mono-layers deposited on indium tin oxide (ITO) substrates”</i>	155
	<u>Stefano D’Elia</u>¹, Valentin Barna², Nicola Scaramuzza, Giuseppe Strangi, and Roberto Bartolino	
	¹ Department of Physics, University of Calabria, via P.Bucci 31C, Rende (CS), I-87036 (ITALY)	
	² Faculty of Physics, University of Bucharest, PO Box Mg-11, 077125, Bucharest, Romania	
	Submitted to	
	SURFACE SCIENCE (2008)	
	4.3.1. Appendix A	177
	<i>Check of the validity of the ellipsometric experimental data acquired on the glass/ITO substrates and DMOAP thin films</i>	
	Chapter 4 - Reference	182

Chapter 5 – Summary and Outlook	185
Chapter 5 - Reference	189
APPENDIX – Other publications	
APPENDIX - A	191
APPENDIX - B	195
List of own publications	201
Scientific Curriculum Vitae	205

*Reflection Spectroscopic Ellipsometry
investigations of reciprocal interactions between
organic-inorganic layered structures*

By

Stefano D'ELia

A DISSERTATION

*Presented to the Department of Physics
At the University of Calabria
In Partial Fulfillment of Requirements
For the Degree of Doctor of Philosophy in
"Science and Technology of Mesophases and Molecular
Materials"*

XXI° Cycle

FIS/01

*Under Supervision of Professor Carlo Versace
Arcavacata di Rende (CS), Italy.*

November 2008

Abstract

Layered media play a very important role in many applications of modern technology and nanotechnology science, and thin films are significant in many industrial applications. Thin films have been successfully used in many new technological applications, i.e. organic optoelectronic devices (Organic Light-Emitting Diodes (OLED), Light Emitting Polymers (LEP) and Organic Electro-Luminescence (OEL)); metamaterials technological designs for optical applications. Other important applications for thin films is represented by the self-assembly of organic materials, by which monomolecular substrates can be created for developing new nanophotolithographical systems.

For researching novel technological applications for thin film materials, that are presently used only in a limited number of cases, any experimental investigations in this direction are extremely valuable.

In this dissertation, ellipsometrical technique, together with other several experimental methods have been used for studying organic and inorganic thin films. The properties of inorganic (or organic) systems play an important role to the properties of organic (or inorganic) ones. The reciprocal interactions between organic-inorganic structures were investigated considering different physical systems.

Lead Zirconium Titanate $\text{PbZr}_{0.53}\text{Ti}_{0.47}\text{O}_3$ (PZT) thin films have been obtained by sol-gel synthesis, deposited on different substrates (float glass, Indium Tin Oxide (ITO) - coated float glass and intrinsic silicon wafer) and later subjected to different thermal treatments. Morphological and structural properties of both PZT thin films and substrates have been investigated by Scanning Electron Microscope (SEM) and their structure was determined by Energy Dispersive X-ray analysis (EDX). Moreover, Variable Angle Spectroscopic Ellipsometry (VASE) provided relevant information on the electronic and optical properties of the samples.

The growth of two different crystalline phases, pyrochlore and ferroelectric perovskite, as a function of annealing temperature, has been associated to the changing optical absorption spectra. In particular, the optical constants dispersion for PZT deposited on ITO-coated float glasses shown a small absorption resonance in the near IR region, not observed in the PZT films deposited on other substrates; this absorption resonance was explained by considering interfacial effects between ITO and PZT layers. This hypothesis is also supported by EDX measurements, showing an interdiffusion of lead and indium ions across the PZT-ITO interface, that can generate a peculiar charge distribution in this region. Moreover, a specific resonance, attributed to a particular charge distribution at the interface, has been detected when thin PZT films are deposited on ITO substrates. Finally, the behaviors of these films

in rectifying the electro-optical response of asymmetric nematic liquid crystal cells have been tested. The electro-optical response can be attributed possibly to the charge distribution present at the PZT-ITO interface, found by means of ellipsometrical investigations.

Molecular organization of self-assembled n-dimethyl-n-octadecyl-3-aminopropyltrimethoxysilylchloride (DMOAP) layers on ITO coated glass substrates was thoroughly investigated. The layer thickness for each deposition was determined by VASE, while from static contact angle measurements we deduced valuable information regarding the ordering of the molecular structures at solid-air interface. In particular, the DMOAP thin film formation was studied for two different drying temperatures (85°C and 120°C). While at $T_{\text{drying}}=85^{\circ}\text{C}$ we observed the formation of a molecular monolayer characterized by a closed-packed structure, at the higher temperature the DMOAP molecules 'bend' at the substrate as they stack in relatively disordered clusters. A qualitative interpretation of this phenomenon is given, in good agreement both with the obtained experimental data and experimental investigation reported in scientific literature. The observations regarding the DMOAP molecular level organization in function of substrate temperature could bring essential information to the self assembly research community and also explain some important physical phenomena occurring at interfaces.

The most commonly used substrates in the previously described experiments were represented by indium tin oxide (ITO) thin films. For obtaining information concerning the organic-inorganic interactions, the transparent conductive oxide (TCO) was well investigated. Float glass substrates covered by high quality ITO thin films were subjected for an hour to single thermal treatments at different temperatures between 100°C and 600°C. In order to study the electric and optical properties of both annealed and not annealed ITO-covered float glasses, ellipsometry, spectrophotometry, impedance analysis, and X-Ray measurements were performed. Moreover, variable angle spectroscopic ellipsometry provides relevant information on the electronic and optical properties of the samples. We estimated the optical density for ITO layers and determined that ITO surface roughness increases with the annealing temperature. In the near-IR range, the extinction coefficient decreases while the maximum of the absorption in the near UV range shift towards low photon energy as the annealing temperature increases. Spectrophotometrical technique was used to estimate the optical band-gap energy for the samples. The thermal annealing strongly changes the structural and optical properties of ITO thin films, as the ITO thin film absorbs oxygen from air during the thermal curing. Absorption decreases the oxygen vacancies and increases the crystalline order of the ITO thin films as confirmed both by ellipsometry and X-ray measurements.

The ellipsometrical investigation of the ITO thin films (as well as the new TCO materials by themselves) is very important for properly starting the investigation of new electro-optical devices.

The electronic structure of the ITO material greatly influences the correct operation of the devices based on organic materials, for example electrochromic devices; new solar cells devices based on the new conductive polymers; electro- and photo-luminescent devices (OLED, LEP, OEL), and other systems. Many scientific publications can be found in literature showing the solid state physics to be equally connected to molecular physics. For this reason, new projects and applications could be created by suitably blending these scientific fields of research.

Chapter 1

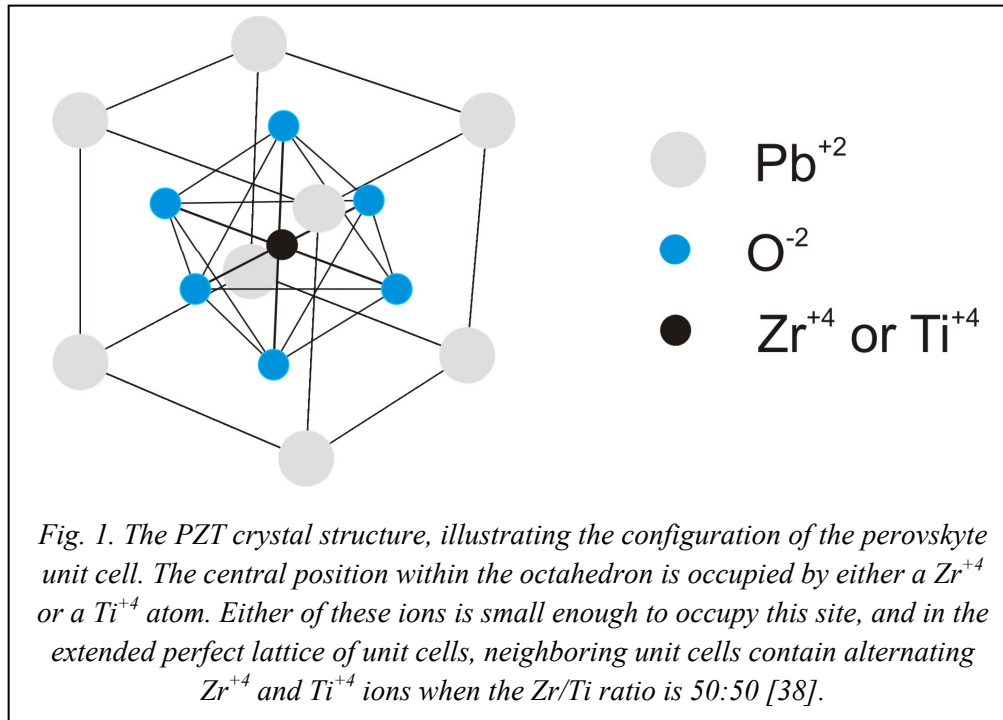
Introduction

Thin films are thin material layers ranging from fractions of a nanometer to several micrometers in thickness. Layered media play a very important role in many applications of modern technology and nanotechnology science, therefore the thin films technology are important in many industrial applications. In order to realize this assertion, we introduce some examples in which the thin films technology is very important and still under investigation: organic optoelectronic devices (Liquid Crystal Displays [1, 2, 3, 4, 5] (LCD), Organic Light-Emitting Diode [6, 7] (OLED), Light Emitting Polymer [8] (LEP) and Organic Electro-Luminescence [9] (OEL), et al.); meta-material design for optical devices [10, 11, 12], linear and nonlinear optical applications [13, 14] (multilayered photonic crystals, nano-structured layer, surface optical coatings, et al.); electronic semiconductor devices (solar cells [15], integrated nanotechnology, solid states memory [16], et al.). Other important applications of thin films technology are the Self-assembly of organic materials, by which monomolecular thin films can be created [17, 18].

In order to find new technological applications for thin film materials, actually used only in a limited number of cases, any experimental investigations around these films are important. In this dissertation, the ellipsometry investigation, supported by other experimental techniques have been used to study some organic and inorganic thin films. The properties of inorganic (organic) systems play an important role to the properties of organic (inorganic) systems. The reciprocal interaction between organic-inorganic systems are investigated in two different physical systems. The first one is a ferroelectric thin films, obtained by sol-gel synthesis by combining organic molecules [19, 20]. These organic precursors transform themselves in the inorganic ferroelectric material by thermal annealing process. The second physical system studied is the order formation of self-assembly monolayer of surfactant molecules on a Transparent Conductive Oxide (TCO).

Piezoelectric ceramic films are characterized by interesting dielectric, pyroelectric, piezoelectric and electro-optical properties. These materials are ferroelectric in perovskite crystalline phase [21]. An example of piezoelectric ceramic is Lead Zirconate Titanate $\text{Pb}(\text{Zr}_x, \text{Ti}_{1-x})\text{O}_3$ (PZT). Its perovskite structure is face-centered cubic, more exactly, the corner-sharing oxygen octahedral are linked together in a regular cubic array with smaller cations (Zr^{+4} or Ti^{+4}) occupying the central octahedral site, and the larger lead cations (Pb^{+2}) filling the interstices

between octahedra in the large site. In the Fig. 1 is shown the configuration of the perovskite unit cell.



The position of the central ions can be distorted by applying an external electric field. The dislocation of the central atom induce a polarization, that remain unchanged in time duration [16]. This induced polarization is associate with changing of birefringence of the ceramic (Kerr effect) [22]. These related effects play an important role to the technological application of ferroelectric films: electro-optic modulators [23], light-beam switching shutters [24]. The PZT material is characterized by high refractive index and low extinction coefficient in visible spectra. These properties are compatible with the optical waveguide applications, where thin film of PZT material, surrounded by other material with lower refractive index, may confine the light by total internal reflection [12]. The PZT material is also used in Far-IR detector in the design of bolometer detector, the pyroelectric property of PZT are important in this type of instruments [25]. A multilayer structure composed by three layer, where the PZT is surrounded by two metallic ultra thin films, shows interesting dielectric properties in the THz frequency: this layer stack has shown to be a magnetic resonator. Its characteristic frequency has been measured by means ellipsometry characterization, and it has been observed negative effective dielectric constant in the THz frequency [10]. In order to optimize this complex structure and push towards high frequency this dielectric property, both the dielectric properties of the PZT material in Far-IR spectra and the multilayer structure design are actually under investigation of the authors of this works [10]. Ferroelectric Random Access Memory (FeRAM) application are another important application of the ferroelectric thin films [16].

Other interesting application of the PZT material has been suggested by some experimental investigation carried out in the INFN-CNR-LICRYL Laboratory of the Department of Physics of the University of Calabria. Interesting perspectives now arise for the applications of these films as rectifying layers, which modify the electro-optical response of liquid crystals. In the past years, metal oxides with mixed ionic and electronic conduction properties have been tested as rectifying layers in asymmetric nematic liquid crystal cells (ANLCC) [26-30], and their rectifying effect has been explained by an internal electric field due to the formation of double charged layers at the interfaces, allowed by the charge carriers mobility. The same rectifying effect can be obtained by using PZT ferroelectric layer in ANLC cells [31], on the basis of different physical effects: in this latter case a permanent internal field, opposite (in polarity) to the external field, is generated by a polar orientation of the ferroelectric film.

The PZT thin films have been obtained by sol-gel synthesis, deposited on different substrates (float glass, indium tin oxide (ITO) coated float glass and intrinsic silicon wafer) and later subjected to different thermal treatments. The morphologic and the structural properties of both PZT thin films and substrates have been investigated by Scanning Electron Microscope (SEM) and their composition was determined by Energy Dispersive X-ray analysis (EDX). Moreover, variable angle spectroscopic ellipsometry provides relevant information on the optical properties of the samples. In particular, the optical constants dispersion of PZT deposited on ITO-coated float glasses shows a small absorption resonance in the near IR region, not observed in PZT films deposited on the other substrates, so that such absorption resonance can be explained by interfacial effects between ITO and PZT layers. This hypothesis is also supported by EDX measurements, showing an inter-diffusion of lead and indium ions, across the PZT-ITO interface, that can generate a peculiar charge distribution in this region [19, 20]. This interface effect may be connected to the electro-optical response, observed in the ANLCC, and previously introduced [31].

The spontaneous process by which some particles, nanoparticles and molecules organize themselves in ordered structures is indicated with Self-Assembly (SA) process. The SA process of amphiphilic molecules allows obtaining molecular thin films with superb chemical and mechanical properties [17, 18], characterized by high order degree. This molecular thin films have been used to develop new nanolithography technique [32], new experimental technique applied to the nanotechnology [33] and new results in the branch of the biologic and pharmaceutical science [34]. Many of these results are directly rely to the order degree of the molecular thin films. The SA molecular order can be controlled by different experimental procedures used during the deposition phase - depending on the utilized molecular species [35, 36]. By combining the ellipsometry technique and

static contact angle measurements, it is possible to deduce valuable information regarding the ordering at molecular level of a self assembly monolayer [36].

This dissertation consists of five chapters and is organized as follows. In Chapter 1 introduction and motivation to this work is described. Chapter 2 gives, briefly, information about both the standard ellipsometry technique (theory) and modellization processes of multilayer structures.

Chapter 3 is separated in different sections. In these sections, we will show the structural properties of the PZT thin films. In order to study the complex physical systems, obtained combining a TCO and an organic thin film that last one transforms itself in piezoelectric film by annealing process, all materials of this multilayer system have been studied, separately, by ellipsometry investigation at different annealing temperatures. The effect of the annealing process on the optical properties of the glass substrates and ITO thin film have been investigated [37], afterwards, we will discuss about piezoelectric thin film [19, 20].

In brief section of the Chapter 3, we will show the preliminary results regarding the thermal modification of PZT thin films, that have been observed by using far - IR ellipsometry technique. These experimental investigations, performed at the University of Nebraska-Lincoln (USA) and under the supervision of the Prof. Mathias Schubert [39], is still in progress.

Chapter 4 discusses the organic thin films obtained by SA process. The influence of drying temperature on the self-assembly molecular order of silanized monolayers, deposited on indium tin oxide (ITO) substrates, is presented [36]. The conclusions and comments of the works presented in this dissertation are made in Chapter 5.

Finally, the appendix sections show additional and independent works, developed in different other collaborations.

Chapter 1 - Reference

[1] M. Vilfan, I. Drevensek Olenik, A. Mertelj, M. Copic, "Aging of surface anchoring and surface viscosità of a nematic liquid crystals on photoaligning PVCi", *Physical Review E*, **63**,061709, (2001).

[2] M. Schadt, K. Schmitt, V. Kozenkov and Chigrinov, *Japan J. Appl. Phys.* **31**, 2155 (1992).

[3] E. B. Priestley, Peter J. Wojtowicz, Ping Sheng, "Introduction to liquid crystals", New York, (1975).

[4] T. Katoh, Y. Zhang, "Deposition of Teflon-polymer thin films by synchrotron radiation photodecomposition", *App. Surf. Scien.* **138-139**, 165-168, (1999).

[5] R. Schwodiauer, G. S. Neugschwandtner, S. Bauer-Gogonea, S. Bauer, "Dielectric and electret properties of nanoemulsion spin-on polytetrafluoroethylene films", *Appl. Phys. Lett.*, **76**(18) (2000).

- [6] Jonathan R. Tischler, M. Scott Bradley, and Vladimir Bulovi, "Strong Coupling in a Microcavity LED", *Phys. Rev. Lett.* **95**, 036401 (2005)
- [7] Neal R Armstrong, R Mark Wightman, and Erin M Gross "Light-Emitting Electrochemical Processes", *Annual Review of Physical Chemistry*, **52**: 391-422 (2001)
- [8] J.H. Burroughes, N. Patel, C. Foden, M. Leadbeater, M. Roberts, "High performance light emitting polymer diodes", *Lasers and Electro-Optics*, 2003. CLEO '03. Conference on, 1-6 June 2003, p. 892- 892
- [9] T Mori, K Miyachi and T Mizutani, "A study of the electroluminescence process of an organic electroluminescence diode with an Alq3 emission layer using a dye-doping method", *J. Phys. D: Appl. Phys.* **28** 1461-1467 (1995).
- [10] Zhiming Huang, Jianqiang Xue, Yun Hou, Junhao Chu, and D. H. Zhang, "Optical magnetic response from parallel plate metamaterials", *Physical Review B*, **74**, 193105 (2006).
- [11] Shuang Zhang, Wenjun Fan, B. K. Minhas, Andrew Frauenglass, K. J. Malloy, and S. R. J. Brueck, "Midinfrared Resonant Magnetic Nanostructures Exhibiting a Negative Permeability" *Phys. Rev. Lett.*, **94**, 037402 (2005).
- [12] Dong Zheng-Gao, Zhu Shi-Ning, and Liu Hui, "Numerical simulations of negative-index refraction in a lamellar composite with alternating single negative layers", *Chinese Physics*, **15** (8), August 2006.
- [13] Pochi Yeh "Optical Waves in Layered Media", WILEY, John Wiley & Sons, New York (1988)
- [14] Pochi Yeh "Introduction to Photorefractive Nonlinear Optics", WILEY, John Wiley & Sons, New York (1993)
- [15] King, R. R., Law, D. C., Edmondson, K. M., Fetzer, C. M., Kinsey, G. S., Yoon, H., Sherif, R. A., and Karam, N. H. "40% efficient metamorphic GaInP/GaInAs/Ge multijunction solar cells." *Applied Physics Letters* **90**, 183516 (2007).
- [16] Hiroshi Ishiwara, Masanori Okuyama, Yoshihiro Arimoto, "Ferroelectric Random Access Memories. Fundamentals and Applications", Springer-Verlag Berlin Heidelberg (2004).
- [17] Abraham Ulman, "An Introduction to Ultrathin Organic Films from Langmuir-Blodgett to Self-Assembly", Academic Press, 1991
- [18] M.C. Petty, "Langmuir-Blodgett films. An introduction", University of Durham, UK, Cambridge Univ. Press, 1996.
- [19] Marco Castriota, **Stefano D'Elia**, Salvatore Marino, Enzo Cazzanelli, Nicola Scaramuzza, Carlo Versace and Roberto Bartolino, "Effects of thermal treatments on structural and optical properties of Lead Zirconium Titanate thin films obtained by sol gel technique", submitted to THIN SOLID FILMS (2008).
- [20] **Stefano D'Elia**, Marco Castriota, Alfonso Policicchio, Carlo Versace, Nicola Scaramuzza, Enzo Cazzanelli, Raffaele Agostino, Carlo Vena, Giuseppe Strangi and

Roberto Bartolino, "Thermally induced modifications of the optic properties of Lead Zirconate Titanate thin films obtained on different substrates by sol-gel synthesis", accepted, *JOURNAL OF APPLIED PHYSICS* (2008).

[21] D. Damjanovic "Ferroelectric, dielectric and piezoelectric properties of ferroelectric thin films and ceramics. Laboratory of ceramics", (Swiss Fed. Inst. of Techn.-EPFL, 1015 Lausanne, Switzerland, 1998).

[22] Jyrki Lappalainen, Jussi Hiltunen and Vilho Lantto, "Characterization of optical properties of nanocrystalline doped PZT thin films", *J. Eur. Cer. Soc.* **25**(12), (2005), 2273-2276; Ludovic Eusobas, Miroslav Jelinek, Francois Flory, Emmanuel Drouard, Jan Lancok, Jean-Jacques Simon, Thomas Mazingue, "Optical and electro-optical properties of pulse laser deposited PLZT thin films", *Opt. Eng.* **42**(12) 3579-3584 (2003).

[23] Masafumi NAKADA, Hiroki TSUDA, Keishi OHASHI and Jun AKEDO, "Aerosol Deposition on Transparent Electro-Optic Films for Optical Modulators", *IEICE Transactions on Electronics* (2007) E90-C(1):36-40.

[24] Electro-optic light shutter, United States Patent 4621903.

[25] Michael A. Todd, Paul A. Manning, Paul P. Donohue, Alan G. Brown, Rex Watton, "Thin film ferroelectric materials for microbolometer arrays", *Proc. SPIE Vol. 4130*, p. 128-139, *Infrared Technology and Applications XXVI*; Weiguo Liu, Bin Jiang, and Weiguang Zhu, "Self-biased dielectric bolometer from epitaxially grown Pb(Zr,Ti)O₃ and lanthanum-doped Pb(Zr,Ti)O₃ multilayered thin films", *Appl. Phys. Lett.* **77**, 1047 (2000).

[26] S. Marino, M. Castriota, V. Bruno, E. Cazzanelli, G. Strangi, C. Versace, N. Scaramuzza, *J. Appl. Phys.* **97**, (2005) 013523-1.

[27] M. Castriota, S. Marino, C. Versace, G. Strangi, N. Scaramuzza, E. Cazzanelli, *Molecular Crystals and Liquid Crystals*, **429**, (2005) 237.

[28] G. Strangi, E. Cazzanelli, N. Scaramuzza, C. Versace, R. Bartolino, *Phys. Rev. E* **62**, (2000) 2263.

[29] E. Cazzanelli, S. Marino, V. Bruno, M. Castriota, N. Scaramuzza, G. Strangi, C. Versace, R. Ceccato, G. Carturan, *Solid State Ionics* **165**, (2003) 201.

[30] V. Bruno, M. Castriota, S. Marino, C. Versace, G. Strangi, E. Cazzanelli, N. Scaramuzza, *Molecular Crystals and Liquid Crystals* **441**, (2005) 27.

[31] S. Marino, M. Castriota, G. Strangi, E. Cazzanelli, N. Scaramuzza, *J. Appl. Phys.* **102**, (2007) 013112-1.

[32] R.K. Smith, P.A. Lewis, P.S. Weiss, "Review – Patterning self-assembled monolayers", *Progress in Surface Science* **75** (2004) 1-68

[33] Mary E. Anderson, Charan Srinivasan, J. Nathan Hohman, Erin M. Carter, Mark W. Horn, and Paul S. Weiss, "Combining Conventional Lithography with Molecular Self-Assembly for Chemical Patterning", *Adv. Mater.* **18** (2006), 3258-3260.

[34] George M. Whitesides and Mila Boncheva, "Beyond molecules: Self-assembly of mesoscopic and macroscopic components", *Proc Natl Acad Sci U S A.* 2002 April 16; **99**(8): 4769–4774; Lorena Nasalean, Stéphanie Baudrey, Neocles B. Leontis,

and Luc Jaeger, "Controlling RNA self-assembly to form filaments", *Nucleic Acids Res.* 2006; **34**(5): 1381–1392.

[35] J.B. Brzoska, N. Shahidzadeh, F. Rondelez, "Evidence of a transition temperature for the optimum deposition of grafted monolayer coatings", *Nature* **360**(1992), 719-721

[36] **Stefano D'Elia**, Valentin Barna, Nicola Scaramuzza, Giuseppe Strangi, and Roberto Bartolino "The influence of drying temperature on closed-packed structures of silanized mono-layers deposited on indium tin oxide (ITO) substrates", (in this PhD thesis: chapter 4). Submitted to SURFACE SCIENCE.

[37] **Stefano D'Elia**, Federica Ciuchi, Carlo Versace, Nicola Scaramuzza, Giuseppe Strangi, Carlo Vena and Roberto Bartolino, "Ellipsometry investigation of the effects of annealing temperature on the optical properties of indium tin oxide thin films studied by Drude-Lorentz model" (in this PhD thesis: chapter 3, sect: 3.1). Submitted to SURFACE SCIENCE.

[38] M. J. Bazack, J. R. Williams, J. M. Ferraro, Z. C. Feng, and R. E. Jones, Jr., "Physical characterization of $Pb_1Zr_{0.2}Ti_{0.8}O_3$ prepared by sol-gel process" *J. Electrochem. Soc.* **142**(2) (1995).

[39] **Prof. Mathias Schubert** "Complex Materials Optics Network - University of Nebraska-Lincoln, Department of Electrical Engineering, and Nebraska Center for Materials and Nanoscience". Link Web: <http://ellipsometry.unl.edu/index.php>

Chapter 2

Polarized Light and Ellipsometry

Introduction

Ellipsometry is a powerful optic technique, that has confirmed to be particularly useful for the study of organic and inorganic monolayer and multi-layers thin films. When the polarized electromagnetic (e.m.) wave interact with a medium, it changes both its polarization states and amplitude. The measure of the polarized modification of the e.m. wave allow us to study the physical systems.

Ellipsometry characterization of the thin films allows the simultaneous determination both of the morphological and structural properties both of the thin films and complex optical systems. These properties can be estimated by using an optical model that describe the interaction of the e.m. wave with the physical systems. In order to describe an optical system, both morphological properties (layer thickness, surface roughness, optical axis, et al.) and structural properties (dielectric function, we) have to introduce in the optical model.

In this section, we will introduce briefly, the fundamental notions both of the theory of ellipsometry and the modeling of the optical physical systems.

2.1. Polarization of Light

The spatial and temporal dependence of the electric field $\vec{E}(\vec{r}, t)$ in a uniform, isotropic medium of the complex permittivity $\tilde{\epsilon}$, is described by the wave equation [1, 2]

$$\left[\nabla^2 - \frac{\epsilon(\omega)}{c^2} \frac{\partial^2}{\partial t^2} \right] \vec{E}(\vec{r}, t) = 0 \quad (2.1)$$

where ω is the angular frequency of the light wave, and c is the light velocity in vacuum.

This wave equation accepts, as useful and general solution, the monochromatic plane wave propagating along the z-axis of an orthogonal coordinate system:

$$\vec{E}(z, t) = \text{Re} \left\{ \begin{bmatrix} E_x \\ E_y \end{bmatrix} e^{i(k_z z - \omega t)} \right\} \quad (2.2)$$

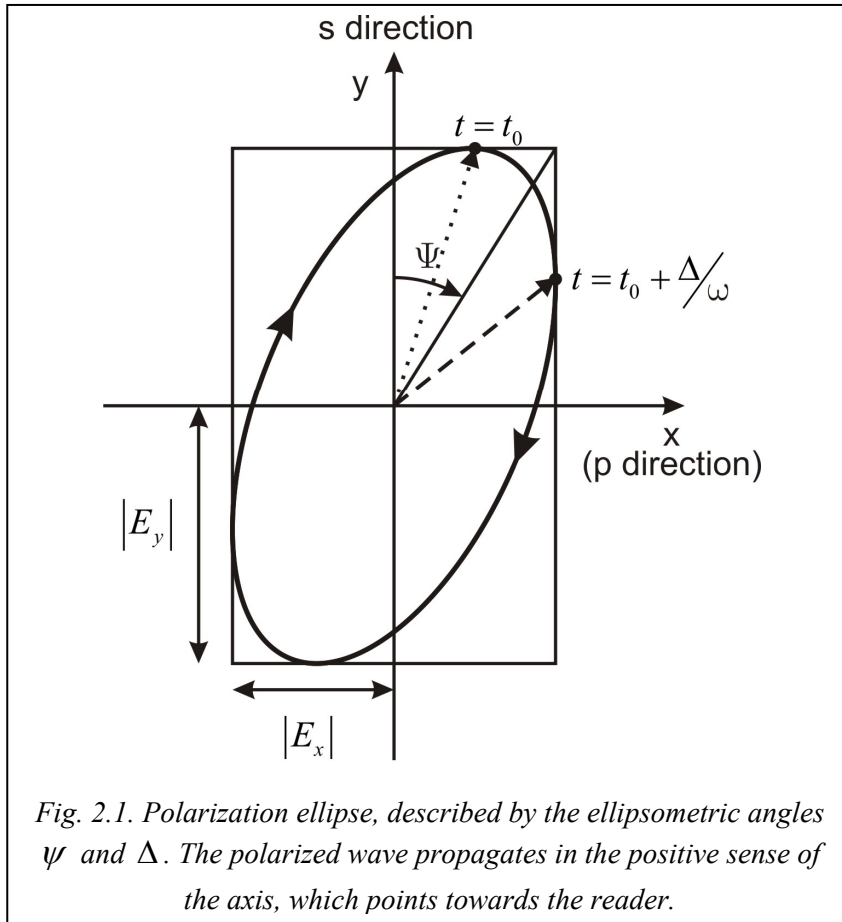
Here E_x and E_y are the complex amplitudes of \vec{E} along the x- and y-axis [1, 2].

In order to satisfy the wave equation, Eq. (2.1), the non vanishing component of the propagation vector of the plane wave of the Eq. (2.2) assumes the values given by the dispersion equation:

$$k_z = \frac{\omega}{c} \sqrt{\tilde{\epsilon}} = \frac{\omega}{c} \tilde{n} \quad (2.3)$$

where $\tilde{n} = n + ik = \sqrt{\tilde{\epsilon}}$ is the complex refractive index of the medium. By choosing the plane-wave solution, Eq. (2.2), with time dependence of $\exp(-i\omega t)$, we are adopting the standard physics convention, where the imaginary parts of $\tilde{\epsilon}$ and \tilde{n} are positive. Another convention, in which the two imaginary parts are negative (usually preferred in optics) is easily recognizable, since all expressions containing $\tilde{\epsilon}$ and \tilde{n} become complex conjugate.

The most general polarization state of a monochromatic wave, Eq. (2.2), is elliptic. The endpoint of the electric-field intensity vector describes an elliptic trajectory in any plane perpendicular to the direction of propagation (z-axis). An example of the elliptic polarization is shown in Fig. 2.1.



The wave is assumed to propagate along z-axis of the right-handed Cartesian coordinate system x - y - z. One revolution of the electric-field vector is completed in the time interval of $2\pi/\omega$. The time evolution can be described as a superposition of harmonic vibrations along two perpendicular axes (x - y). If these two components are shifted in phase, the endpoint of the electric-field vector is elliptic.

In the Fig. 2.1, the amplitude of the electric field in the x and y directions are denoted by $|E_x|$ and $|E_y|$, respectively. The time dependence of the vector $\vec{E}(t)$ of the Eq. (2.2) in the plane $z = 0$ can be written by using the following complex form [1, 2]:

$$\vec{E}(t) = \begin{bmatrix} E_x(t) \\ E_y(t) \end{bmatrix} = \text{Re} \left\{ \begin{bmatrix} |E_x| e^{i\Delta} \\ |E_y| \end{bmatrix} e^{i\omega(t-t_0)} \right\} \quad (2.4)$$

At the time $t = t_0$, the y component is at its maximum value ($|E_y|$). In the Fig. 2.1, it is indicated by the dotted arrow. The maximum value of the x component is obtained after the time interval of Δ/ω (dashed arrow). The angle between the dotted and dashed vectors is related to the relative phase Δ of the two components of the electric-field along x- and y-directions. For positive values of Δ , the polarization state is elliptic right-handed polarization. For negative values of Δ the polarization state is elliptic left-handed polarization. The values of Δ are limited to the interval from zero to 2π [1, 2].

In order to define completely the state of the elliptic polarization, the amplitudes $|E_x|$ and $|E_y|$ are indispensable. Only the relative amplitude $\frac{|E_x|}{|E_y|}$ is important in ellipsometric measurements. This ratio is independent from the light intensity, in fact multiplying both $|E_x|$ and $|E_y|$ by a constant the light intensity changes [1, 2].

The relative amplitude can be expressed by the angle Ψ shown in Fig. (2.1) by using the trigonometric formula:

$$\tan \Psi = \frac{|E_x|}{|E_y|} \quad (2.5)$$

where the values of Ψ are limited to the interval from zero to $\pi/2$.

By using both the relative phase Δ and amplitude Ψ , the elliptic polarization of Eq. (2.4) can be expressed by the Jones vector

$$\begin{bmatrix} \sin \Psi e^{i\Delta} \\ \cos \Psi \end{bmatrix} \quad (2.6)$$

where Ψ and Δ are two real angles. Special cases of a general elliptic polarization are:

- **Linear polarization**, for which $\Delta = 0$ or π . This case corresponds, respectively, to the vibrations of the components along x and y in phase, or with the opposite phase. The ellipse collapse into the linear segment as shown in the Fig. 2.2.
- **Circular polarization**, for which $\Psi = \pi/4$ and $\Delta = \pi/2$ (right-handed circularly polarized), or $\Delta = -\pi/2$ (left-handed circularly polarized).

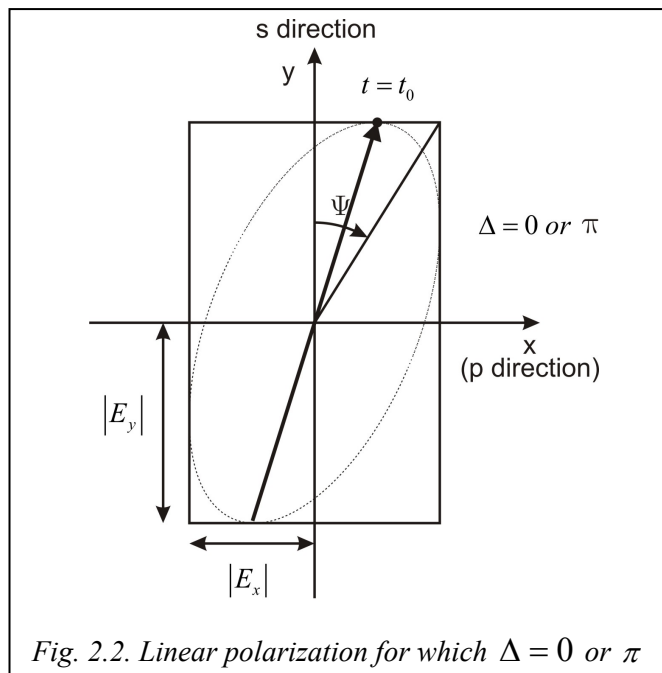
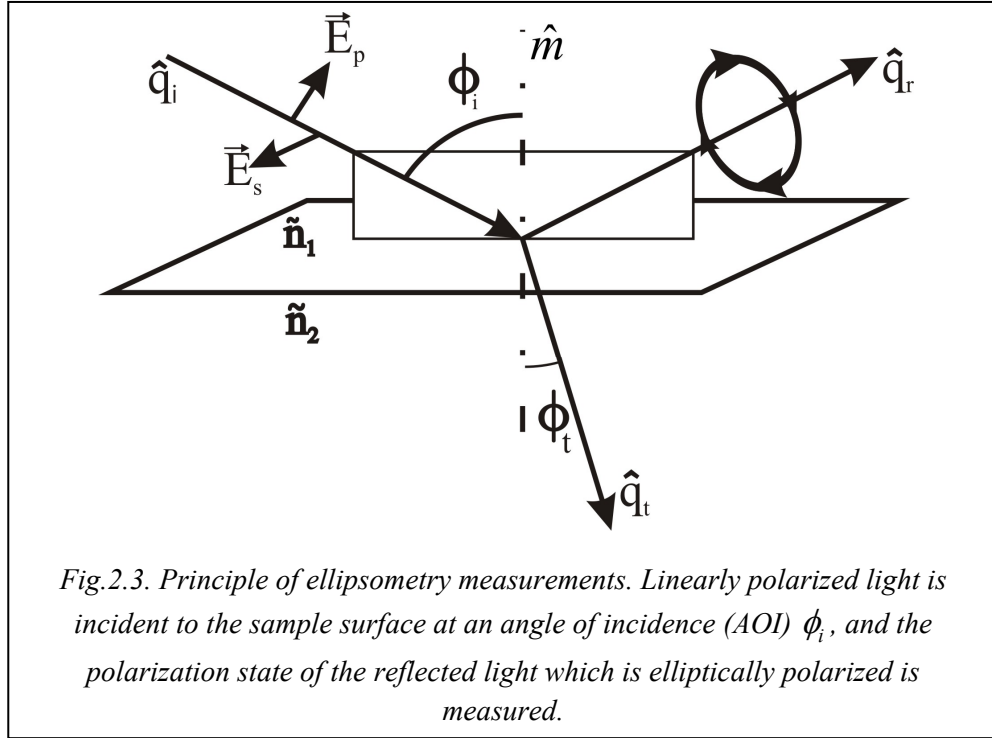


Fig. 2.2. Linear polarization for which $\Delta = 0$ or π

2.2. Standard Ellipsometry

Ellipsometry is an optical technique that measure the changes in the polarization states of light reflected (transmitted) from a surface of material being studied. The electric field of the incident light is decomposed into two components, E_{ip} and E_{is} parallel (p) and perpendicular (s) to the plane of incidence, respectively as illustrated in Fig. 2.3.



The reflection coefficient of the light at a given angle of incidence (AOI) ϕ_i can be expressed by Fresnel's equation [1, 3]

$$\frac{E_{rp}}{E_{ip}} = \tilde{r}_p = \frac{\tilde{n}_2 \cos \phi_i - \tilde{n}_1 \cos \phi_t}{\tilde{n}_2 \cos \phi_i + \tilde{n}_1 \cos \phi_t} \quad (2.7)$$

$$\frac{E_{rs}}{E_{is}} = \tilde{r}_s = \frac{\tilde{n}_1 \cos \phi_i - \tilde{n}_2 \cos \phi_t}{\tilde{n}_1 \cos \phi_i + \tilde{n}_2 \cos \phi_t}$$

where \tilde{r}_p (\tilde{r}_s) is the complex Fresnel reflection coefficient for the polarization component of reflected electric field E_{rp} (E_{rs}), parallel (orthogonal) to the plane of incidence, \tilde{n}_1 (\tilde{n}_2) is the complex index of refraction for medium 1 (medium 2), and ϕ_i (ϕ_t) is the angle of incidence (transmission).

The complex Fresnel reflection coefficients can be expressed in Euler's complex form as

$$\tilde{r}_p = |\tilde{r}_p| e^{i\delta_{rp}} \quad (2.8)$$

$$\tilde{r}_s = |\tilde{r}_s| e^{i\delta_{rs}} \quad (2.9)$$

where δ_{rp} (δ_{rs}) is the phase shift upon reflection for p (s) component.

In the general case of a multilayer structure with multiple interfaces, overall reflection coefficients are referred to as R_p and R_s , we will discuss this case further below.

Ellipsometry measures the complex ratio ρ of the parallel to perpendicular reflection coefficients:

$$\rho = \frac{R_p}{R_s} = \tan \psi e^{i\Delta} \quad (2.10)$$

where $\tan \psi = |R_p|/|R_s|$ and $\Delta = \delta_{rp} - \delta_{rs}$. The Eq. 2.10 is called Standard Ellipsometry equation and it is useful to study the isotropic and homogeneous materials. The measured ratio of reflection coefficient ρ is usually expressed in terms of ellipsometric parameters (angles) ψ and Δ , where $\tan \psi$ represents the relative amplitude attenuation and Δ corresponds to the phase shift between the p and s components of the reflection coefficients.

The measured ρ can be converted directly into a pseudo dielectric function [1, 2]:

$$\langle \varepsilon \rangle = \langle \varepsilon_1 \rangle + i \langle \varepsilon_2 \rangle = \sin^2 \phi_i \left[1 + \tan^2 \phi_i \left(\frac{1 - \rho}{1 + \rho} \right)^2 \right] \quad (2.11)$$

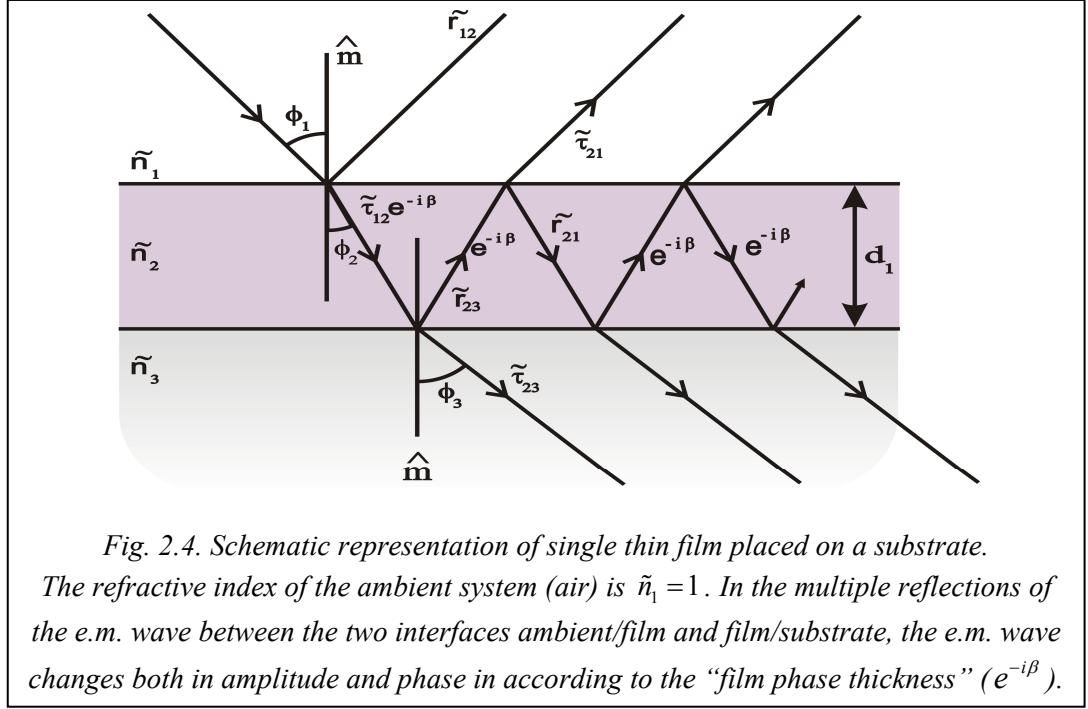
This pseudo dielectric function would be identical to the intrinsic dielectric function of the substrate material if there were no over layers [1, 2].

In order to study anisotropic materials, the Generalized Ellipsometry (GE) theory is required for a full interpretation of the ellipsometry measurements [1, 2, 4, 5, 6].

2.3. Single film placed on the substrate

A typical optical system, very important in the theory of ellipsometry, is the single film (thickness d_1 and complex refractive index \tilde{n}_2) placed on the substrate (complex refractive index \tilde{n}_3). This case is important in order to study the more complex optical system of multilayer structure [1, 7].

The Fig. 2.4 shows the schematic representation of the substrate/film/ambient system. We suppose the ideal case i.e. the interface between the different homogeneous and isotropic medium materials are perfectly flat and parallel. The Fig. 2.4, the symbol \tilde{r}_{ij} (\tilde{t}_{ij}) denotes the complex Fresnel reflection (transmission) coefficient, at the interface ij (for example, $ij = 12$ denotes the e.m. wave passing through the interface from medium \tilde{n}_1 to medium \tilde{n}_2). The complex Fresnel transmission equations can be found in literature [1, 3].



In the Fig. 2.4, the incident light beam, that impinges on the interface 1-2, is subject both to reflection (\tilde{r}_{12}) and refraction (\tilde{t}_{12}) processes. The refracted light beam, that pass through the medium \tilde{n}_2 , is subject, at the second interface 2-3, both to reflection (\tilde{r}_{23}) and refraction (\tilde{t}_{23}) processes.

Inside thin film, the reflected light beam at the interface 2-3 will impinge on the interface 1-2 (in this case from medium 2 to medium 1). At this interface, the light beam is subject both to reflection (\tilde{r}_{21}) and refraction (\tilde{t}_{21}). These multiple reflection and refraction could be reiterate for infinite number of times. Therefore, the two equations (2.12) have to be satisfied

$$\begin{aligned} \tilde{r}_{21} &= -\tilde{r}_{12} \\ \tilde{t}_{12}\tilde{t}_{21} &= 1 - \tilde{r}_{12}^2 \end{aligned} \tag{2.12}$$

By using Jones matrix formalism [3, 7, 8] and both the complex Fresnel reflection coefficients (Eq. 2.7) and Fresnel transmission coefficients [1, 3], it is possible calculate, the complex Fresnel reflection and transmission coefficients for this optical system. They are given by

$$R_t = \frac{\tilde{r}_{12} + \tilde{r}_{23}e^{-i2\beta}}{1 - \tilde{r}_{12}\tilde{r}_{23}e^{-i2\beta}} \tag{2.13}$$

$$T_t = \frac{\tilde{r}_{12}\tilde{r}_{23}e^{-i\beta}}{1 + \tilde{r}_{12}\tilde{r}_{23}e^{-i2\beta}}$$

The phase angle is given by

$$\beta = 2\pi \left(\frac{d_1}{\lambda} \right) \sqrt{\tilde{n}_2^2 - \tilde{n}_1^2 \sin^2 \phi_1} \quad (2.14)$$

it describe the phase variation of the e.m. wave during its multiple reflection inside the film. The phase angle (Eq. 2.14) is called also *film phase thickness*.

The Eq. (2.13) can be expressed in the coordinate system, defined by the two polarization components direction s and p. In these polarization components the complex Fresnel reflection coefficients are given by

$$R_p = \frac{\tilde{r}_{12p} + \tilde{r}_{23p}e^{-i2\beta}}{1 - \tilde{r}_{12p}\tilde{r}_{23p}e^{-i2\beta}} = |R_p| e^{i\Delta_{rp}} \quad (2.15)$$

$$R_s = \frac{\tilde{r}_{12s} + \tilde{r}_{23s}e^{-i2\beta}}{1 - \tilde{r}_{12s}\tilde{r}_{23s}e^{-i2\beta}} = |R_s| e^{i\Delta_{rs}}$$

To conclude, the complex ratio ρ (*standard equation of reflection ellipsometry*), defined for the single thin film placed on the substrate systems, is given by

$$\rho = \frac{R_p}{R_s} = \tan \psi e^{i\Delta} = \frac{\tilde{r}_{12p} + \tilde{r}_{23p}e^{-i2\beta}}{1 - \tilde{r}_{12p}\tilde{r}_{23p}e^{-i2\beta}} \cdot \frac{1 - \tilde{r}_{12s}\tilde{r}_{23s}e^{-i2\beta}}{\tilde{r}_{12s} + \tilde{r}_{23s}e^{-i2\beta}} \quad (2.16)$$

where $\tan \psi = \frac{|R_p|}{|R_s|}$ and $\Delta = \Delta_{rp} - \Delta_{rs}$ are the ellipsometric angles.

If we explain the mathematical dependency of the Fresnel coefficients (Eq. 2.15), from the parameters \tilde{n}_1 , \tilde{n}_2 , \tilde{n}_3 , ϕ_1 , ϕ_2 , and ϕ_3 and considering the Snell's law given by

$$\tilde{n}_1 \sin \phi_1 = \tilde{n}_2 \sin \phi_2 = \tilde{n}_3 \sin \phi_3, \quad (2.17)$$

it is possible observe that the complex ratio ρ (Eq. 2.16) is a mathematical function of nine parameters [1]. Four of these parameters are known ($\tilde{n}_1 = 1$, AOI: ϕ_1 , wave length: λ), the last five parameters are unknown (\tilde{n}_2 , \tilde{n}_3 , and d_1):

$$\rho = \tan \psi e^{i\Delta} = \rho(\tilde{n}_1, \tilde{n}_2, \tilde{n}_3, d_1, \phi_1, \lambda). \quad (2.18)$$

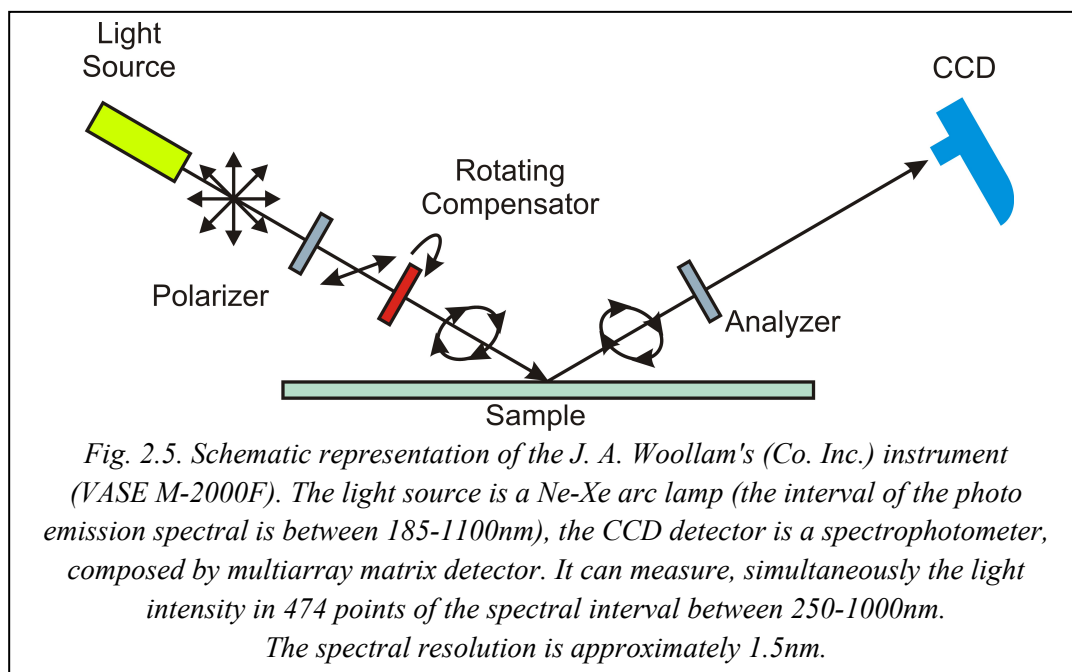
The total number of equations, considering both the real and imaginary part of the Eq. 2.17 and 2.18, is adequate to calculate the five unknown parameters. The solution of the system of equations (inversion of the exact equation of reflection ellipsometry) can be completely calculated by using a computer [1].

2.4. Experimental Setup

In order to measure the state of the polarized light, different ellipsometry techniques exist, and are used. They are based on different position of the optical devices (polarizer, compensator, and analyzer) compared both to the position of the light source and of the surface of the sample [1, 2].

The Polarization Modulation Ellipsometry (PME) technique uses a photoelastic modulator in order to modulate, with harmonic oscillation, the polarization of the incident light. The frequency of this modulation is fixed and its value depends by experimental setup [1, 2].

J.A. Woollam's instrument (VASE M-2000F), used in the our experiments, is a typical ellipsometry that use the PME technique for measuring the ellipsometry angles. The M-2000F instrument is a Rotating Compensator Ellipsometry (RCE). The angular velocity of the compensator is $\Omega = 50\text{Hz}$. The Fig. 2.5 shows the schematic configuration of the optical devices.



The optical configuration of the M-2000F ellipsometer is denoted as P(RC)SA.

Light Source \Rightarrow *Polarizer* \Rightarrow *Rotating Compensator (RC)* \Rightarrow
Sample \Rightarrow
Analyzer \Rightarrow *Detector*

The light intensity, versus wavelength, is measured by CCD detector. The mathematical expression of the light intensity, can be calculate by theoretical studying of the optical system showed in Fig. 2.5, for example, by using the Jones's matrix formalism. This mathematics problem was discussed fully in literature [1, 9, 10, 11].

The calculated light intensity can be expressed in a Fourier's formula given by this equation

$$I(C_t) = A_0 + A_2 \cos 2C_t + B_2 \sin 2C_t + A_4 \cos 4C_t + B_4 \sin 4C_t \quad (2.19)$$

where $C_t = C(t)$ is the phase modulation introduced by the rotating compensator.

The Fourier's coefficients can be calculated by using the integral formulas given by:

$$\begin{aligned} A_0 &= \frac{1}{\pi} \int_0^\pi I(C_t) dC_t, \\ A_2 &= \frac{2}{\pi} \int_0^\pi I(C_t) \cos 2C_t dC_t, \\ B_2 &= \frac{2}{\pi} \int_0^\pi I(C_t) \sin 2C_t dC_t, \\ A_4 &= \frac{2}{\pi} \int_0^\pi I(C_t) \cos 4C_t dC_t, \\ B_4 &= \frac{2}{\pi} \int_0^\pi I(C_t) \sin 4C_t dC_t, \end{aligned}$$

where $I(C_t)$ is the general equation calculated by using Jones's matrix formalism.

The Fourier's coefficients are function of many parameters: optical properties of the optical devices; calibration parameters of the optical devices and CCD detector; and obviously, the complex Fresnel coefficients that describe of the sample.

The electronic devices of the Woollam's ellipsometry measure the Fourier's coefficients by using the Fourier transformation, calculated by means the integration time $C_t = C(t)$, on the light intensity acquired as electronic signal by the CCD. The internal program control of the instruments calculates the ellipsometry angles spectra.

2.5. Optical Model and Spectroscopic Ellipsometry Data Analysis

Ellipsometry is a model dependent technique, the measured ellipsometry angles don't give direct information about the properties of the sample. Typical, a sample consist in a substrate covered by a multilayer structure with multiple interfaces. Each layer is characterized by a thickness and a dielectric function. In a ideal layer stack, the thickness of each layer remain homogeneously constant, therefore, all interfaces

are parallel respect to the surface substrate. In the previous section, we have introduced an easy example: the theoretical ellipsometry angles have been calculated for an easy example: single thin film placed on a substrate.

The modelling process consist in the building of an optical model. An optical model, defined for a sample, is a mathematical law, obtained by using the Jones or Muller matrix formalism, able to simulate the optical path of the light in the sample. Therefore, the optical model has consider both the morphological properties (surface roughness, porosity and more) and the structural properties (dielectric function, anisotropy and more).

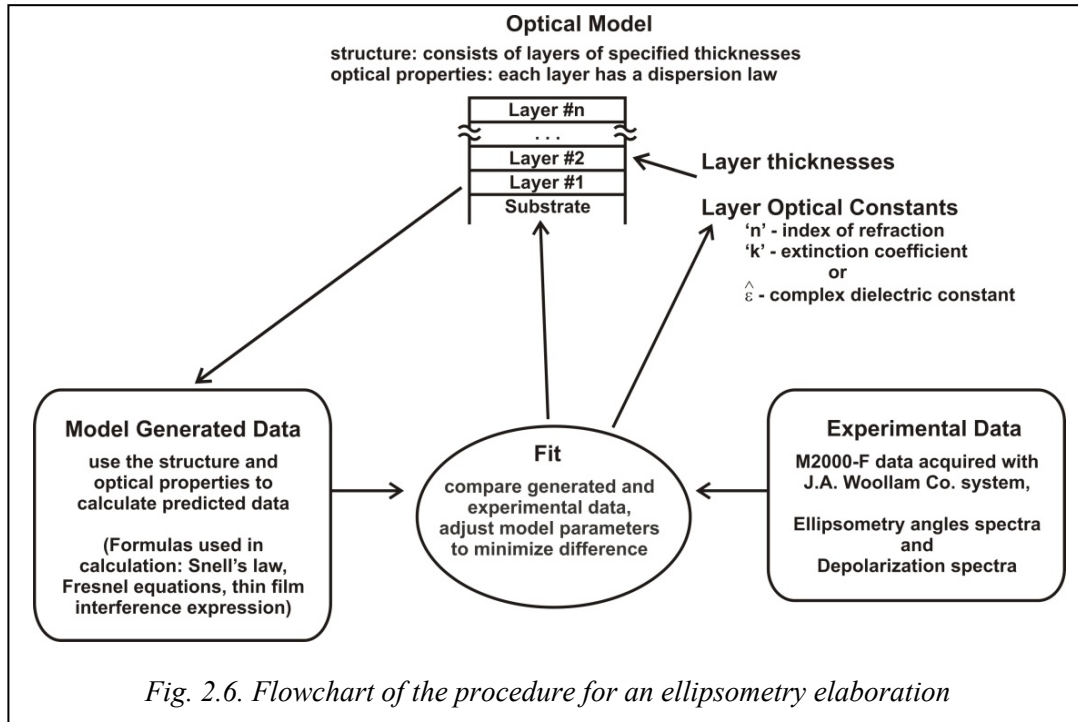
In the case where microscopic roughening, intermixing, or porosity occurs, the Bruggeman Effective Medium Approximation (BEMA) is used to model the optical constants of the rough or porous overlayer or interface [2, 12]. It is assumed that the spatial wavelength of the microstructure is much smaller than the wavelength of light. The BEMA gives the effective dielectric function ε of a microscopic mixture of two materials with known dielectric function ε_a and ε_b by solving the equation for ε given by

$$f_a \frac{\varepsilon_a - \varepsilon}{\varepsilon_a + 2\varepsilon} + f_b \frac{\varepsilon_b - \varepsilon}{\varepsilon_b + 2\varepsilon} = 0 \quad (2.20)$$

where f_a and f_b are the volume fractions of materials a and b, respectively, and $f_a + f_b = 1$. The surface roughness and the porosity, for example, can described by using BEMA model by mixing the void ($\varepsilon_a = 1$) and the medium ε_b .

Assuming that we have measured ellipsometric data of a sample under investigation, as a function of wavelength and angle of incidence. We also have an optical model for our sample. This optical model is a function of many parameters that describe the sample. In order to obtain these physical parameters, we can vary some parameters in the optical model such that ellipsometric data calculated from the model matches our experimental data as closely as possible. In other words, we have compared the generated and experimental data by means the fitting procedures.

The Fig. 2.5 shows by a diagram representation the general procedure to follow to study a sample by ellipsometric experiment.



First of all, we must define a function which represents the quality of the match between the data calculated from the model and the experimental data. This function, called *maximum likelihood estimator*, is expressed by Mean-Squared Error (MSE), it is defined by

$$MSE = \frac{1}{2N - M} \sum_{i=1}^N \left[\left(\frac{\Psi_i^{\text{mod}} - \Psi_i^{\text{exp}}}{\sigma_{\Psi,i}^{\text{exp}}} \right)^2 + \left(\frac{\Delta_i^{\text{mod}} - \Delta_i^{\text{exp}}}{\sigma_{\Delta,i}^{\text{exp}}} \right)^2 \right] \quad (2.21)$$

where N is the number of data points, M is the number of the fitting parameters, $(\Psi^{\text{exp}}, \Delta^{\text{exp}})$ and $(\Psi^{\text{mod}}, \Delta^{\text{mod}})$ are the measured and modeled ellipsometric angles respectively, while $\sigma_{\Psi}^{\text{exp}}$ and $\sigma_{\Delta}^{\text{exp}}$ are the standard deviations of the measured ellipsometric angles. The modeled ellipsometric angles $(\Psi^{\text{mod}}, \Delta^{\text{mod}})$ are functions of the all fit parameters that define the multilayer optical models.

The best fit parameter values have been calculated by means of the software of the ©J.A. Woollam Co., Inc. WVASE32™ (ver. 3.668) [13]. This application uses the nonlinear Levenberg-Marquardt algorithm to determine the minimum value of the Mean Square Error (MSE).

Chapter 2 - Reference

- [1] R. M. A. Azzam, N. M. Bashara, "Ellipsometry and Polarized Light" (third printing), North-Holland, Elsevier Science Publishers B. V., Amsterdam, (1992).
- [2] H. G. Tompkins, E. A. Irene, "Handbook of Ellipsometry", William Andrew Publishing, Springer (2005).
- [3] Pochi Yeh, Claire Gu, "Optics of Liquid Crystal Displays", John Wiley & Sons, Inc (1999).

- [4] M. Schubert, “Generalized ellipsometry and complex optical system”, *Thin Solid Films* 313-314 (1998) 323-332.
- [5] M. Schubert, “Polarization-dependent optical parameters of arbitrarily anisotropic homogeneous layered systems”, *Physical Review B*, Vol. 53, N. 8 (1996).
- [6] M. Shubert, B. Rheinlander, C. Cramer, H. Schmiedel, J.A. Woollam, et al., “Generalized transmission ellipsometry for twisted biaxial dielectric media: application to chiral liquid crystals”, *J. Opt. Soc. Am. A*, Vol. 13, N. 9, (1996).
- [7] Pochi Yeh “*Optical Waves in Layered Media*”, WILEY, John Wiley & Sons, New York (1988).
- [8] C. Gu, Pochi Yeh, “Extended Jones matrix method. II”, *J. Opt. Soc. Am. A*, Vol. 10, N. 5, (1993).
- [9] P. S. Hauge, F. H. Dill, “A Rotating-Compensator Fourier Ellipsometer”, *Optics communications*, Vol. 14, Num. 4, p. 431-437, (1975).
- [10] J. H. W. G. den Boer, G. M. W. Kroesen, F. J. de Hoog, “Spectroscopic rotating compensator ellipsometry in infrared: retarder design and measurement”, *Meas. Sci. Technol.* 8, 484-492, (1997).
- [11] **Stefano D’Elia** “Deposizione e caratterizzazione ellissometrica di film sottili molecolari”, Cap. 3, Master's Degree Thesis in Physical Science (11 November 2003), (Laurea in Fisica), Department of Physics, University of Calabria, Super advisor: Prof. Carlo Versace.
- [12] D. E. Aspnes, *Thin Solid Films* **89**, (1982) 249.
- [13] <http://www.jawoollam.com/index.html>

Chapter 3

Ferroelectric transparent thin films obtained by sol-gel synthesis: Optical and Structural Characterization

Introduction

The PZT thin films have been obtained by sol-gel synthesis, deposited on different substrates (float glass, indium tin oxide (ITO) coated float glass and intrinsic silicon wafer) and later subjected to different thermal treatments. The morphologic and the structural properties of both PZT thin films and substrates have been investigated by Scanning Electron Microscope (SEM) and their composition was determined by Energy Dispersive X-ray analysis (EDX). Moreover, variable angle spectroscopic ellipsometry provides relevant information on the optical properties of the samples. In particular, the optical constants dispersion of PZT deposited on ITO-coated float glasses shows a small absorption resonance in the near IR region, not observed in PZT films deposited on the other substrates, so that such absorption resonance can be explained by interfacial effects between ITO and PZT layers. This hypothesis is also supported by EDX measurements, showing an inter-diffusion of lead and indium ions, across the PZT-ITO interface, that can generate a peculiar charge distribution in this region [1, 2]. This interface effect may be connected to the electro-optical response, observed in the ANLCC [3].

In order to optimize the electro-optical properties of the ferroelectric films, many aspects have to be studied such as: the influence of the production methods (for example effect of the thermal annealing); the influence of the conductive substrates. These one have impacted on the optical, structural and morphological properties of such ferroelectric thin films.

The optical characterization of substrates and thin film samples was performed by using the Spectroscopic Ellipsometry (SE) technique. The VASE M2000F (J.A. Woollam) rotating compensator ellipsometer (RCE) was used in the 250-1000 nm

wavelength range. Spectra were collected at different incident angles to increase the accuracy of layer modeling.

The structural and morphological properties are estimated by using multilayer optical models compatible with both the ellipsometry results and the layer structures of our samples. Each layer was depicted by optical model whose fit parameters were the layer thickness and the frequency dispersion of its complex optical constants. The optical models, chosen to characterize the substrates and the PZT samples, have been proposed taking into account the main characteristics of the studied physical systems.

In a preliminary study, we have estimated the optical models of the substrates, without PZT depositions, annealed at different temperatures in the range 100-700 °C with steps of 100°C and treatment duration of one hour. These optical models will be used to study the optical property variations of the PZT depositions annealed at the same temperatures.

3.1. Characterization of the substrates and the Indium Tin Oxide (ITO)

*ELLIPSOMETRY INVESTIGATION OF THE EFFECTS OF
ANNEALING TEMPERATURE ON THE OPTICAL PROPERTIES
OF INDIUM TIN OXIDE THIN FILMS STUDIED BY DRUDE-
LORENTZ MODEL*

Stefano D'Elia, Federica Ciuchi, Nicola Scaramuzza*, Carlo Versace, Giuseppe Strangi, Carlo Vena, and Roberto Bartolino.

INFN-CNR-LICRYL Laboratory and CEMIF.CAL, Department of Physics,
University of Calabria, via P.Bucci 31C, Rende (CS), I-87036 (ITALY).

* Author for correspondence

E-mail corresponding author: scaramuzza@fis.unical.it

Submitted to SURFACE SCIENCE (2008)

Abstract

Float glass substrates covered by high quality ITO thin films (Balzers) were subjected for an hour to single thermal treatments at different temperature between 100°C and 600°C. In order to study the electric and optical properties of both annealed and not annealed ITO-covered float glasses, ellipsometry, spectrophotometry, impedance analysis, and X-Ray measurements were performed. Moreover, variable angle spectroscopic ellipsometry provides relevant information on the electronic and optical properties of the samples. The estimated optical density for ITO layer and ITO surface roughness increases with the annealing temperature. In the near-IR range, the extinction coefficient decreases while the maximum of the absorption in the near UV range shift towards low photon energy as the annealing temperature increases. Spectrophotometry was used to estimate the optical band-gap energy of the samples. The thermal annealing changes strongly the structural and optical properties of ITO thin films, because during the thermal processes, the ITO thin film absorbs oxygen from air. This oxygen absorption decrease the oxygen

vacancies and increase the crystalline order of the ITO thin films as confirmed both by ellipsometry and X-ray measurements.

1. Introduction

Indium tin oxide (ITO) is a transparent conductive oxide, intensively used in optoelectronic devices like thin films coating. This conducting oxide exhibits interesting optical and electronic properties [1,2,3,4,6]: high optical transmittance, over 90% from visible to near infrared (near-IR) spectra, with high reflectance in infrared spectra (IR); low resistivity between 10^{-5} and 10^{-4} Ωcm and n-type semiconductor properties with a band gap between 3.7 and 4.5 eV.

All these property have led to a wide range of technical applications. The ITO is used in liquid crystal displays, organic light-led devices, solar cells, thin films transistor, sensors, energy-efficient window applications and other.

The ITO physical properties result from its nature being an n-type semiconductor. The free electrons are obtained both from creation of oxygen vacancies or from external doping with tin (Sn) metal [1,2,3,4]. However, in ITO, the Sn-doping and the oxygen vacancies together contribute to the high conductivity, the oxygen vacancies act as ionized donors and donate two electrons for conduction.

The ITO is essentially formed by the substitution doping of In_2O_3 with Sn, which replaces the In^{3+} ions from the cubic bixbyte structure of indium oxide [1,7]. The Sn atom forms an interstitial bond with oxygen and exist like SnO or SnO_2 according with the chemical valence of +2 or +4, respectively. This valence state has directly related to the ITO conductivity. The lower valence state reduces the carrier density because a hole is created which acts as a trap for the electrons and reduces the conductivity. When the SnO_2 or Sn^{4+} state is predominant, the tin ion acts as a cationic donor in the In_2O_3 lattice, providing an electron to the conduction band [7].

The importance of the oxygen vacancies have been studied by effect of the O_2 pressure during ITO depositions by DC or RF sputtering. It has been observed that, for a constant concentration of Sn-dopand, exists an oxygen pressure therefore the ITO resistivity is minimum [1,2,5,8].

The carrier mobility is influenced by the crystalline state of ITO structure. It has been observed that high crystalline state, obtained by increasing the substrate temperature at 200-300 $^\circ\text{C}$, improve the conductivity [1,3,4,9].

In this work we study the effect of the annealing processes on the optical and electrical properties of the high quality indium tin oxide films industrially produced by Balzers Thin Films FAB [10].

Many optical devices nowadays are build up with transparent substrates with conductive properties obtained by covering the glass substrate by an indium tin oxide (ITO) thin film. Generally the construction of most electro-optical devices requires that different organic and inorganic materials like liquid crystals, polymers, surfactants or oxides are deposited on the ITO films, so the characteristics of the device are very sensitive to changes of the ITO properties. In order to optimize the optical behavior of these layered structures with respect to their electrical properties,

often the glass-ITO substrates undergo a after deposition thermal treatment, but the annealing processes can change both the ITO properties and the samples properties itself.

In fact the annealing processes can modify the ITO properties such as: sheet resistivity, optical band-gap energy, carrier concentrations, crystalline structure and consequently optical dispersion law. Hence for specific technological applications, the annealed films must be characterized from appropriate morphological, structural and electrical properties. For example, an interface effect has been observed in the multilayer structure, where the ITO film was covered by lead zirconate titanate material obtained by sol-gel synthesis [10]. Such effect depends by the thermal annealing of the sample required to obtain a ferroelectric film on transparent conductive oxide, like ITO film.

2. Experimental

Large sheets (425x320mm) of 1.1mm thick float glass covered by ITO thin film (nominal sheet resistance, $R_{sh}=25\Omega/\square$), manufactured by Balzers Thin Films [11], have been prepared in small slides (20x30mm). In order to optically characterize the float glass substrates, from some slides the ITO coating thin films has been removed by heated piranha solution ultrasonic cleaning. The piranha solution is a mixture of sulfuric acid and hydroxide peroxide with ratio concentration 7:3. When the hydroxide peroxide is added to sulfuric acid the exothermic and aggressive reaction can dissolve organic and inorganic materials [12]. The ITO films were completely removed by means of three treatments in the piranha solution.

Finally, the ITO-covered float glasses and ITO-uncovered float glasses have been ultrasonically cleaned in chloroform and then in acetone. After these processes, all samples have been ultrasonically cleaned in distilled water, to eliminate the residual solvent traces. In the final step, the substrates have been dried in furnace at 100°C for 30 minutes duration.

Micro-chemical analysis by Energy Dispersive X-ray (EDX) investigations by using scanning electron microscope (FEI Quanta 400) have been performed on the ITO-covered glass slides. The chemical composition analysis (data not shown) allow us to estimate the concentration of the atomic Sn-dopant in In_2O_3 , the measured value is about 7-8 %.

The clean glass/ITO slides have been annealed in air at different temperatures in the range [100°C - 600°C] for one hour; afterwards they have been studied to estimate their optical and electrical properties.

The optical characterization of both float glass substrates and ITO/glasses samples have been performed by Spectroscopic Ellipsometry (SE). The VASE M2000F (J.A.

Woollam) rotating compensator ellipsometer (RCE) was used to measure the ellipsometric angles Ψ and Δ spectra, in the wavelength range between 250nm - 1000nm. The Ψ and Δ spectra were measured at different angles of incidence (AIO) to increase the accuracy of layer modeling. The structural and morphological properties have been estimated from the ellipsometric characterization by using a multilayer optical model compatible with the layer structures of our samples. Each layer was defined by its optical model which fit parameters are the thickness and the complex dispersion law [38]. The optical model and the best fit parameter values have been calculated by means of the WVASE32 application (J.A. Woollam). Such software determines the minimum value of the likelihood estimator function, Mean Square Error (MSE), using the nonlinear Levenberg-Marquardt algorithm. The figure of merit, MSE, is a measure of the goodness of the fit [12], and it is defined by

$$MSE = \frac{1}{2N - M} \sum_{i=1}^N \left[\left(\frac{\Psi_i^{\text{mod}} - \Psi_i^{\text{exp}}}{\sigma_{\Psi,i}^{\text{exp}}} \right)^2 + \left(\frac{\Delta_i^{\text{mod}} - \Delta_i^{\text{exp}}}{\sigma_{\Delta,i}^{\text{exp}}} \right)^2 \right]$$

where N is the number of data points, M is the number of the fitting parameters, $(\Psi^{\text{exp}}, \Delta^{\text{exp}})$ and $(\Psi^{\text{mod}}, \Delta^{\text{mod}})$ are the measured and modeled ellipsometric angles, respectively while σ_{Ψ} and σ_{Δ} are the standard deviations of the measured ellipsometric angles. The modeled ellipsometric angles $(\Psi^{\text{mod}}, \Delta^{\text{mod}})$ are functions of the all fit parameters which define the multilayer optical models.

The Varian Cary-5E spectrophotometer has been used to measure the transmittance spectra both of the float glass slides and of the ITO-covered float glass slides in the wavelength range 250-1100 nm and at normal angle of incidence.

The electric impedance spectra of the ITO films have been studied by an Agilent 4294A Precision Impedance Analyzer. The measurements have been performed by using two close (about 1 mm) gold tipped electrodes. The measurements were performed at room temperature. In figure 1, we show the equivalent circuit model used to estimate the resistivity R_{ITO} (Ω/\square) of the annealed ITO thin films (R_i and C_i represent the resistance and capacitance of the electrode and of the instrument).

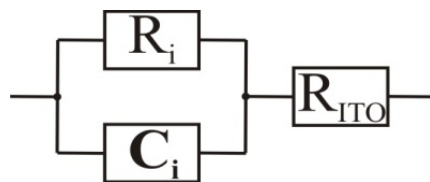


Figure 1: Equivalent circuit used to estimate the resistivity R_{ITO} (Ω/\square) of the annealed ITO thin films.

The resistivity is related to the measured resistance R_{ITO} (Ω/\square) by:

$$\rho_{\text{ITO}}^{(\text{electric measur.})} (\Omega\text{cm}) = R_{\text{ITO}} \cdot d_{\text{ITO}} \quad (1)$$

where d_{ITO} is the thickness of the ITO thin films estimated by ellipsometric characterization.

X ray diffraction has been performed in a standard Bragg Brentano geometry (θ - 2θ) with $k_{\alpha 1}$ and $k_{\alpha 2}$ Cu radiation and in asymmetric geometry (incident angle 1° ,

Soller slits in the detector path) with pure $k_{\alpha 1}$ Cu radiation, for comparison in a D8 Bruker axs reflectometer.

3. Results and discussion

3.1 Structural optical models for the samples

The analysis of the ellipsometric data requires a multilayer optical model of the samples. In order to describe the variations of the structural and morphological properties of both the float glass and the ITO thin film as function of the annealing temperature, we have chosen to estimate an optical model for each annealed sample. All these models have been compared among them.

The float glass substrates have been modeled by means of the Cauchy dispersion law with the Urbach law to characterize the absorbing properties of the glass substrates [13]. On the contrary, the ITO thin films have been modeled by two superimposed layers (see figure 2): the deeper layer describes the conductive and dielectric properties; the upper layer describes the surface roughness of the ITO thin films.

Surface roughness (EMA model)
ITO layer
Float glass 1.1mm

Figure 2: ITO layer is modeled by using the sum of Drude (conductive property) and Lorentz (dielectric property) oscillators. Surface roughness is modeled by using EMA model (mixing the Lorentz oscillator and Void).

The dielectric and conductive properties of the ITO layer (figure 2) have been simulated by means a linear combination of a Lorentz oscillator and a Drude oscillator. The mathematic expression of the complex dielectric function [13] is given by

$$\tilde{\varepsilon}_{ITOlayer}(h\nu) \equiv \varepsilon_1 + i\varepsilon_2 = \varepsilon_{1\infty} + \frac{A_L}{E_L^2 - (h\nu)^2 - iB_L h\nu} + \frac{-A_D}{(h\nu)^2 - iB_D h\nu} \quad (2)$$

where $\varepsilon_{1\infty}$ is a background high-frequency dielectric constant; ε_1 and ε_2 are the real and imaginary parts of the complex dielectric function, respectively; $A_L(\text{eV}^2)$, $B_L(\text{eV})$, $E_L(\text{eV})$ introduce the amplitude, the damping factor and the central energy of Lorentz oscillator; while $A_D(\text{eV}^2)$, $B_D(\text{eV})$ are the Drude oscillator parameters.

The dielectric properties of ITO thin films are characterized by the Lorentz oscillator i.e. the second term of the complex dielectric function $\tilde{\varepsilon}_{ITOlayer}(h\nu)$. The

behavior of the dispersion law in the near UV spectral region is described by this Lorentz oscillator, which determines the variation of the optical band-gap energy. The Drude oscillator i.e. the third term of the complex dielectric function $\tilde{\epsilon}_{ITOlayer}(h\nu)$ describe the free-carriers in the near-IR spectra and, as a consequence, the conductive properties of the ITO films. The amplitude A_D (eV²) of the Drude oscillator is proportional to the carrier concentration density and it is related to the plasma frequency by:

$$\omega_p^2 = \frac{N_c e^2}{m_e^* \epsilon_0} = \frac{A_D}{\hbar^2} \quad (3)$$

The parameter B_D (eV) is proportional to the collision frequency ω_τ defined by

$$\omega_\tau = \frac{\rho_{ITO} N_c e^2}{m_e^*} = \frac{B_D}{\hbar} \quad (4)$$

where e is the electron charge; m_e^* is the effective electron mass; ϵ_0 is the permittivity of free space; \hbar is Plank constant; and ρ_{ITO} (Ωcm) is the ITO resistivity.

The collision frequency can be related to the collision processes between the free charge carriers and the ionized impurities in the polycrystalline structure of the ITO. These ionized impurities are originated from both the oxygen vacancies and the Sn-doping. Hamberg and Granqvist have shown that these impurities are important for the carrier mobility properties in the ITO material [1,14]. The collision frequency ω_τ is inversely proportional to the carrier mobility μ by:

$$\mu = \frac{e}{\omega_\tau m_e^*} = \frac{1}{\rho_{ITO} N_c e} \quad (5)$$

The collision frequency and carrier mobility give us information about the behavior of the defect density in the ITO lattice structure, i.e., it give us information about the crystalline order [1,14].

The ITO thin films resistivity can be calculate by using the Eqs. (3) and (4)

$$\rho_{ITO} = \frac{B_D}{A_D} \hbar / \epsilon_0 \quad (6)$$

The surface roughness layer is modeled by using an effective-medium approximation with a mixture of voids ($\epsilon_{void} = 1$) and a Lorentz oscillator ($\tilde{\epsilon}_{ITO\ srough}$) given by:

$$\tilde{\epsilon}_{ITO\ srough}(h\nu) \equiv \epsilon_1 + i\epsilon_2 = \epsilon_\infty^{ito} + \frac{A_{ito}}{E_{ito}^2 - (h\nu)^2 - iB_{ito}h\nu}$$

where ϵ_∞^{ito} is a background high-frequency dielectric constant and A_{ito} (eV²), B_{ito} (eV), E_{ito} (eV) are the amplitude, the damping factor and the central energy, respectively, of Lorentz oscillator that describes such layer.

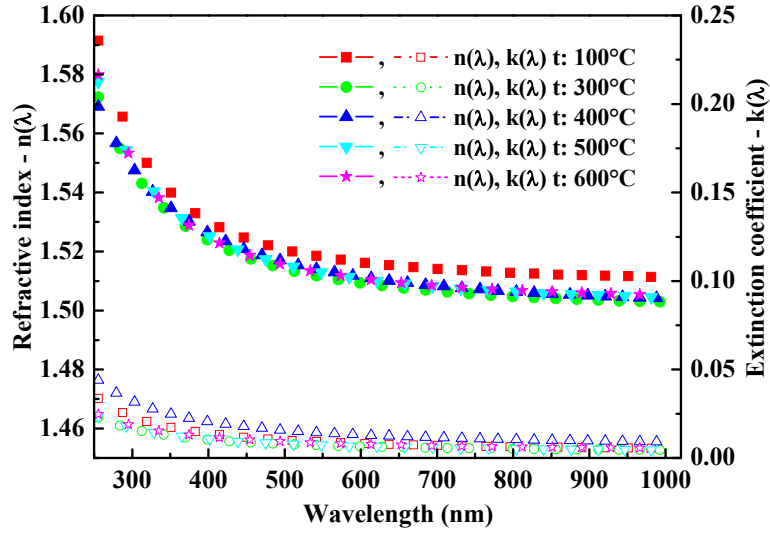
The complex effective dielectric function of the roughness layer, $\tilde{\epsilon}_{srough}$, was calculated by the Bruggeman effective medium approximation (EMA) [13,15]:

$$f_{ITO} \frac{\tilde{\epsilon}_{ITO srough} - \tilde{\epsilon}_{srough}}{\tilde{\epsilon}_{ITO srough} + 2\tilde{\epsilon}_{srough}} + f_{void} \frac{\epsilon_{void} - \tilde{\epsilon}_{srough}}{\epsilon_{void} + \tilde{\epsilon}_{srough}} = 0$$

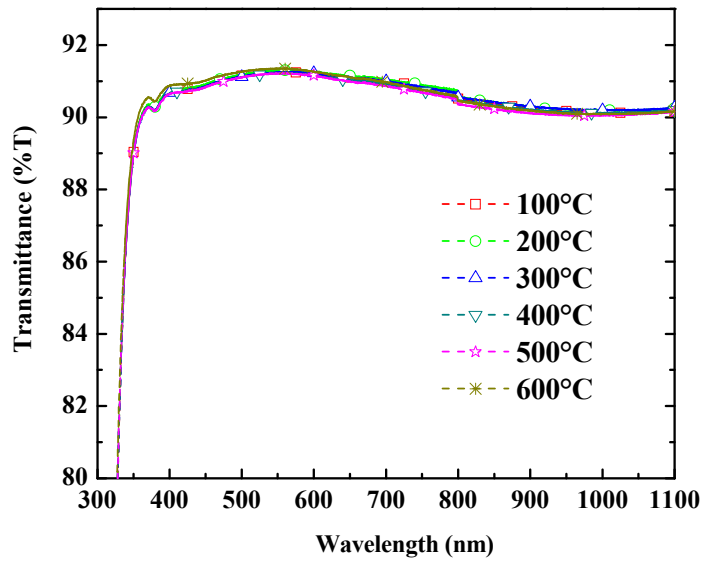
where f_{ITO} and f_{void} are the volume fractions of the two medium mixed together, and they must satisfy the condition $f_{ITO} + f_{void} = 1$.

3.2 Structural and morphological properties of the samples

The ellipsometric and spectrophotometric characterizations of the float glass substrate prove that the dispersion law didn't change much when the annealing temperature increase in the range between 100 and 600°C. The figure 3 show the dispersion laws estimated by using the optical model for the glass substrate previously described and the normal transmittance spectra performed on the same glass samples.



(a)



(b)

Figure 3: Dispersion laws estimated of the annealed float glasses by ellipsometry characterization (a) and normal transmittance spectra acquire on same samples (b).

The optical properties of float glass samples remain constant when annealing temperature increase.

We have chosen to neglect these small variations in the dispersion law of the float glass substrate, when we analyzed the optical model of ITO layer. The dispersion law estimated for the float glass annealed at 100°C has been used to define the optical models for ITO/glass samples. In fact, the small variations highlighted in the glass dispersion law vs. thermal annealing are negligible with respect to the optical property variations of the annealed ITO thin films.

The optical models used to study the annealed ITO thin films (figure 2) allowed us to simulate the measured ellipsometry angles with low MSE values.

The figure 4 and figure 5, respectively, show two examples of the fit results estimated for the ITO layer annealed at 100°C and 600°C.

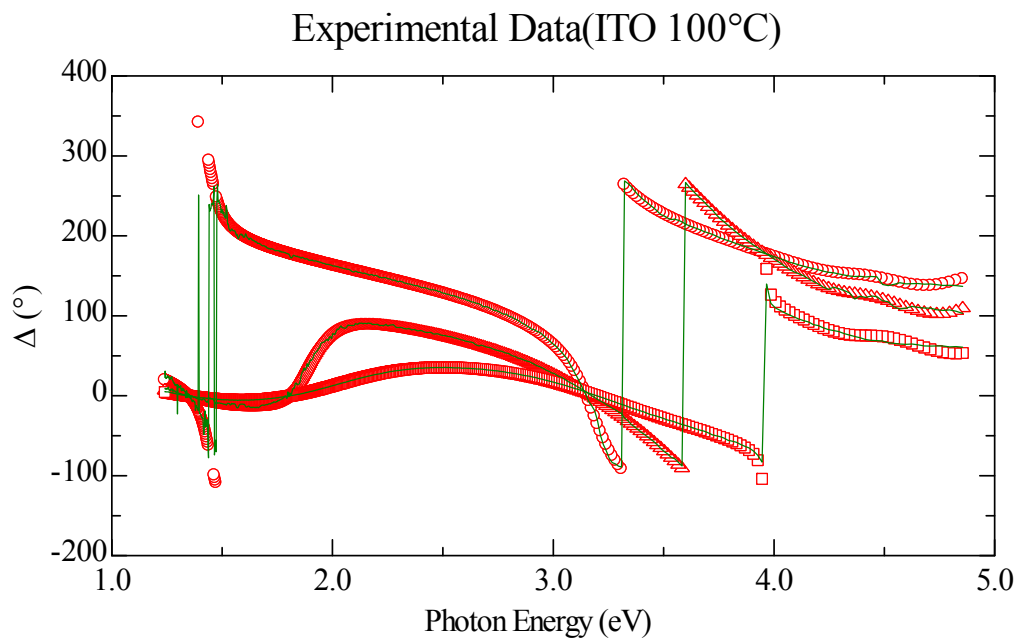
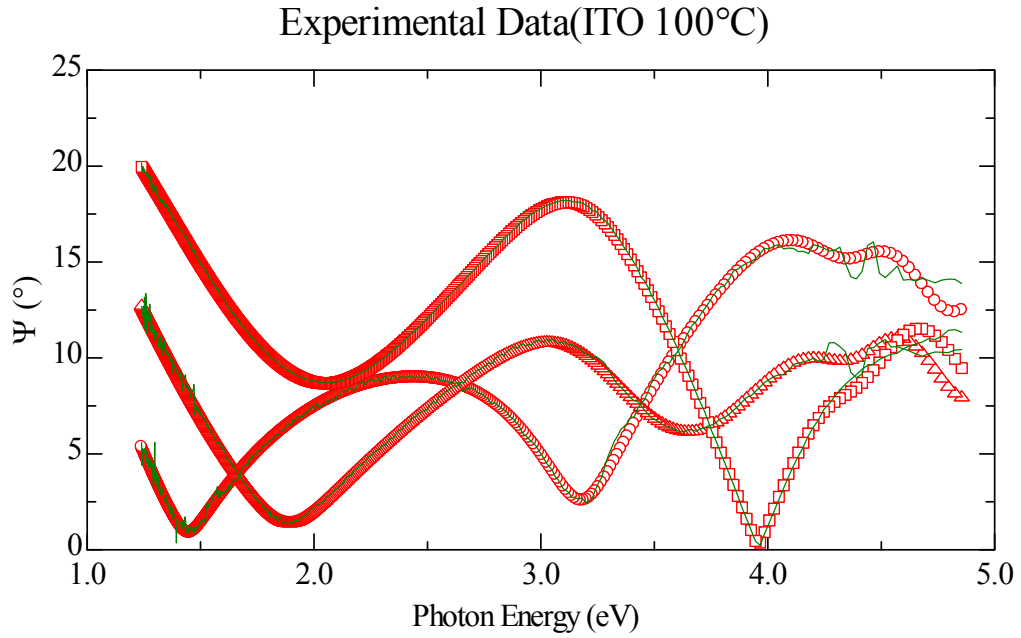


Figure 4: Experimental (solid curves) and fitted data (geometric symbols) for different AIO: 60° (circles); 65° (triangles); 70° (squares). The ITO layer was annealed at 100°C.

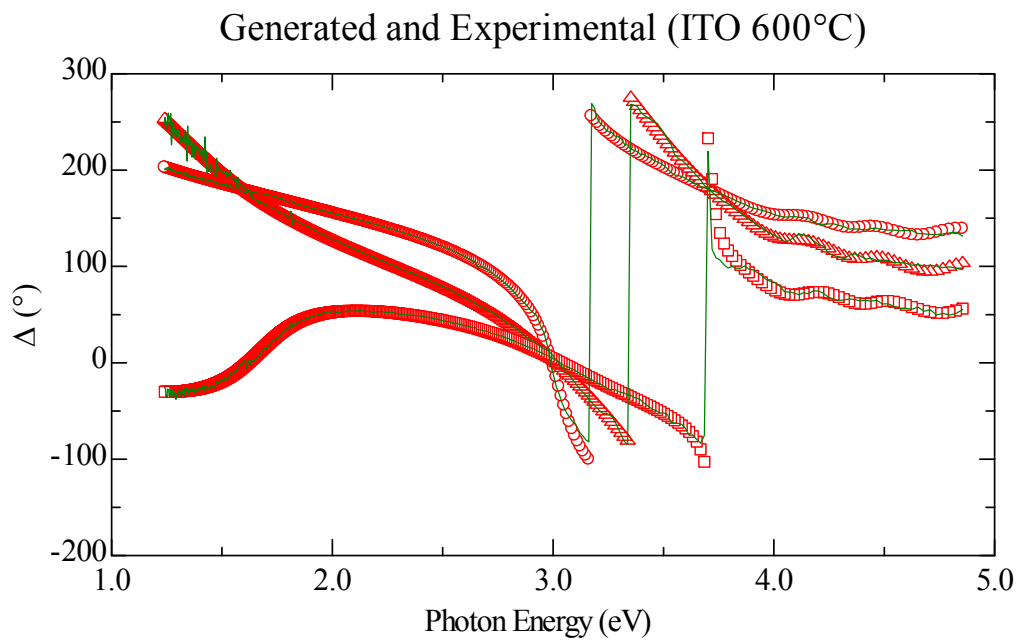
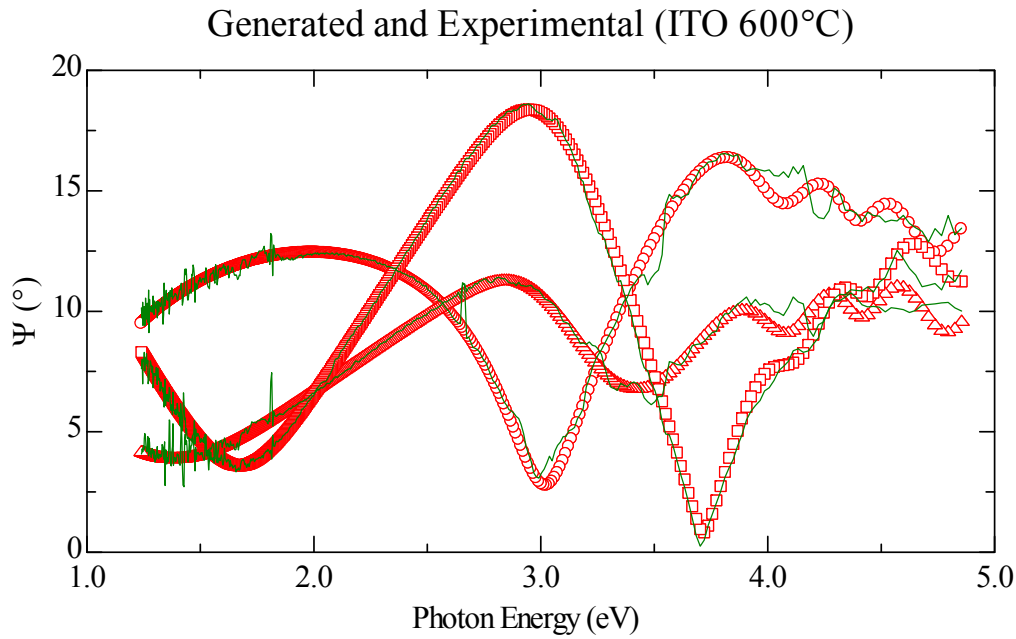
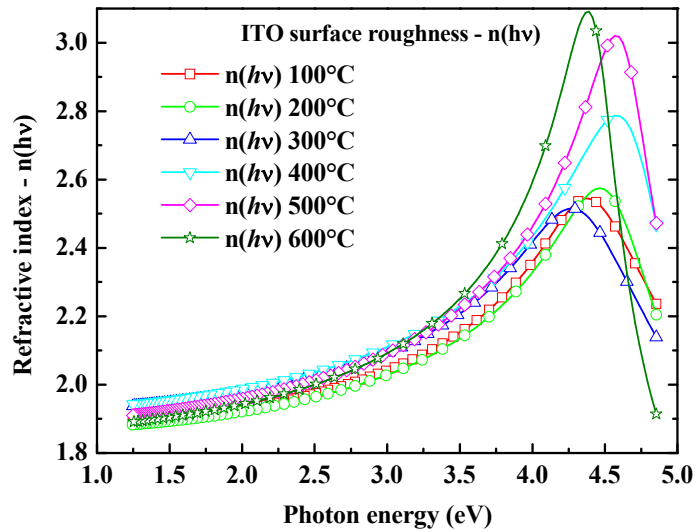


Figure 5: Experimental (solid curves) and fitted data (geometric symbols) for different AIO: 60° (circles); 65° (triangles); 70° (squares). The ITO layer were annealed at 600°C

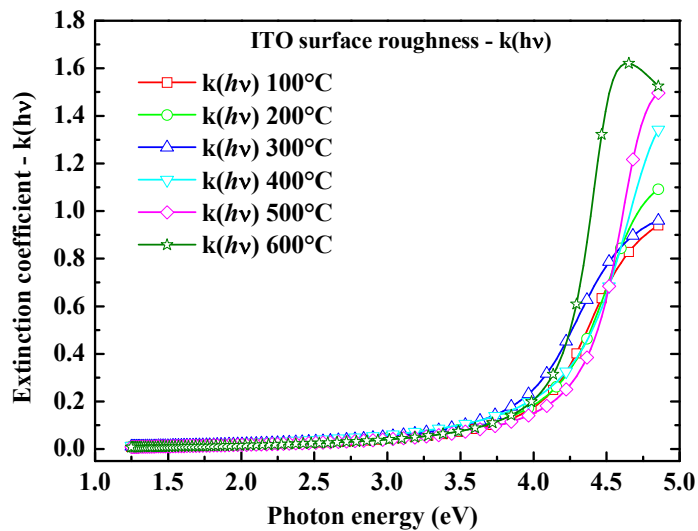
The ITO thickness was found to be about 105 ± 4 nm and remain constant with the annealing processes.

The dispersion laws of the annealed ITO layer and ITO surface roughness, estimated by fit elaboration, are showed in the figure 6. The estimated optical density for ITO layer and for ITO surface roughness increases with the annealing temperature. In the near-IR range, the extinction coefficient decreases while the maximum of the absorption in the near UV range shift toward low photon energy

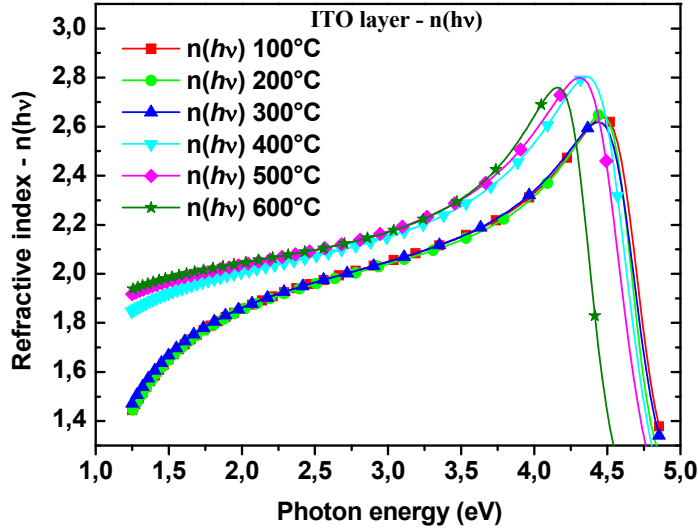
with the annealing temperature. The dispersion laws in the near-IR and in the near UV spectra describe, respectively, the variation of the conductive properties and of the optical band-gap energy when the annealing temperature of the ITO film change (figure 6c-d).



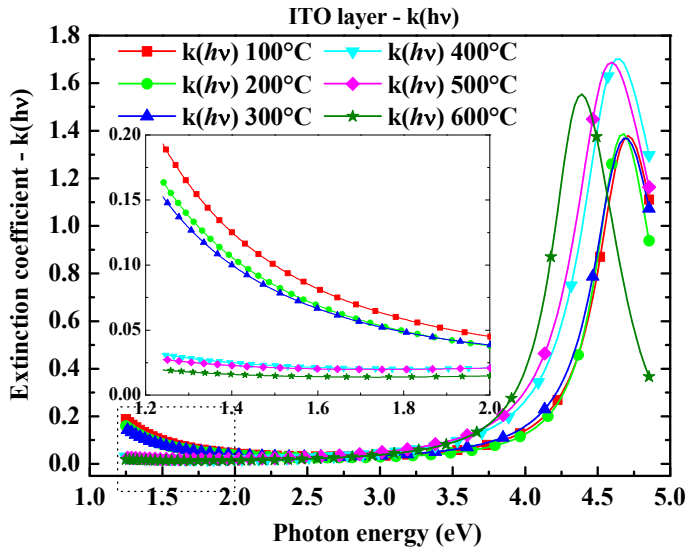
(a)



(b)



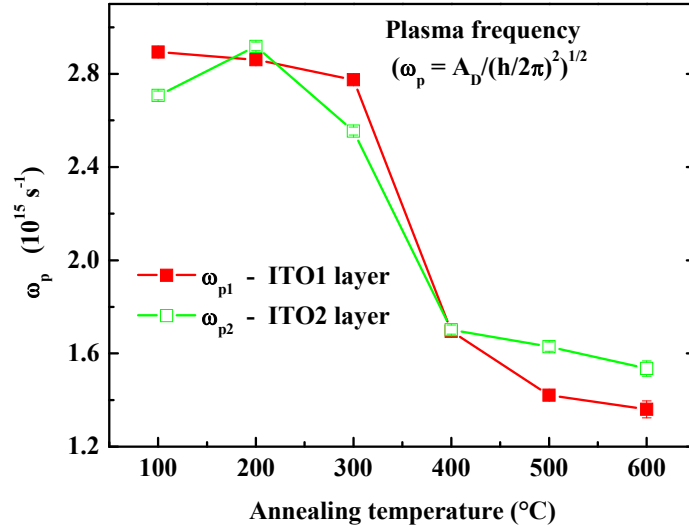
(c)



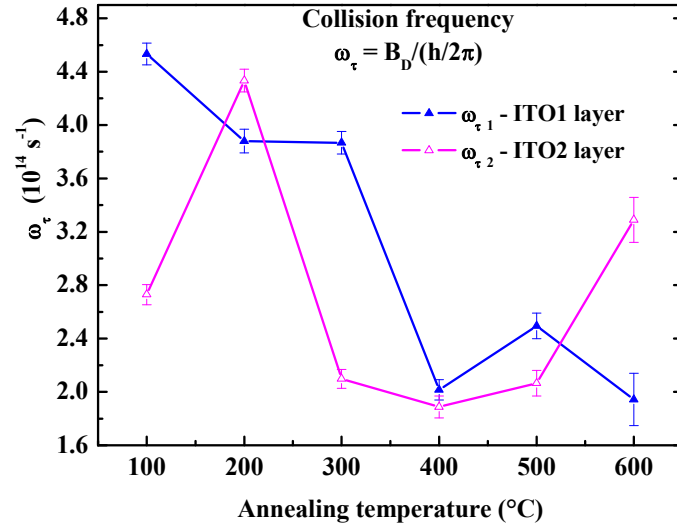
(d)

Figure 6: Optical properties of the surface roughness describe the dielectric behavior (a), these layers were modeled by using the mixing of ITO material and voids. Optical property of ITO layer (b) shows the maximum absorption in the near UV region that it shifts towards low energy and the carrier density decrease when the annealing temperature increases.

The Drude oscillator in the optical model for “ITO layer” describes the dispersion law in the near-IR range (figure 2). The fit parameters $A_D(\text{eV}^2)$ and $B_D(\text{eV})$ of this oscillator were used to calculate the plasma frequency $\omega_p(\text{s}^{-1})$ (figure 7a) and the collision frequency $\omega_\tau(\text{s}^{-1})$ (figure 7b), by the eqs. (2) and (3).



(a)



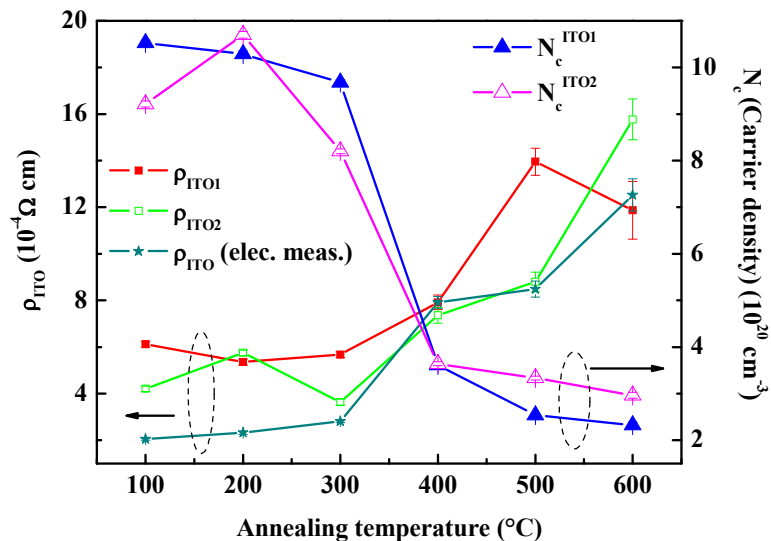
(b)

Figure 7: The Drude's fit parameters have been used to estimate the plasma (a) and collision frequencies (b). ITO1 (or 2) indicate the experimental results estimated for two set of the same ITO film samples studied.

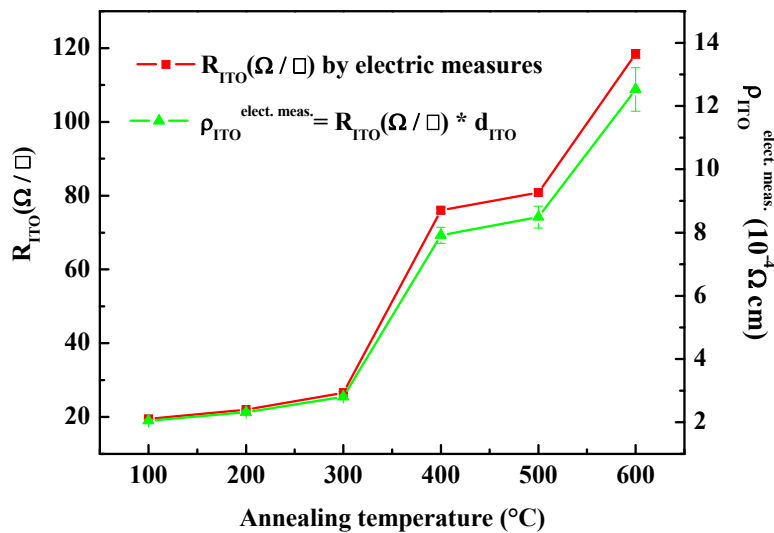
From figure 7 is possible to observe that the plasma frequency and the collision frequency decrease when the annealing temperature increase. By using the Eqs. (2) and (5), respectively, we have estimated (figure 8) the carrier density N_c (cm^{-3})

and resistivity $\rho_{ITO} (\Omega cm)$ for the two set of samples of the same kind of ITO film (ITO1 or 2).

In order to estimate the carrier density (Eq. 1), we have assumed a constant effective electron mass $m^* = 0.4m_e$, proposed by Hamberg and Granqvist [1] for an ITO thin film with sheet resistivity of $27(\Omega/\square)$.



(a)



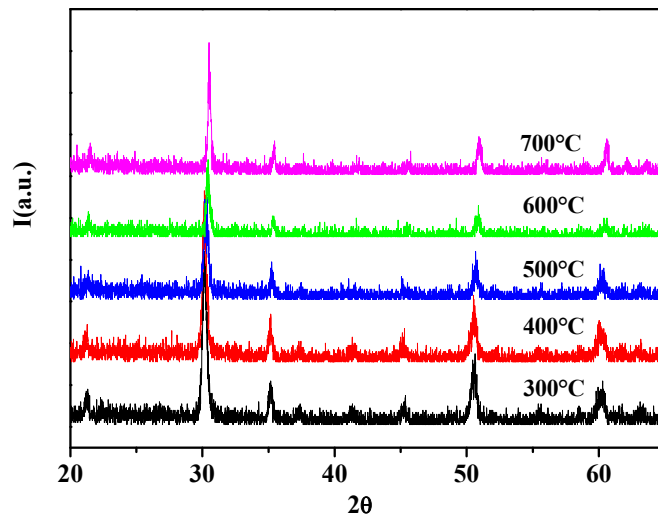
(b)

Figure 8: The carrier density (triangles) and ITO resistivity (squares) (a) were estimated for the two set of samples, the effective electron mass was $m^* = 0.4m_e$ [1]. The resistivity estimated by electric measurements (stars) was calculated from the electric measurements (b) by using Eq. (1). d_{ITO} is the thickness estimated for the ITO film by ellipsometry measurements. ITO1 (or 2) indicate the experimental results estimated for two set of the same ITO film samples studied.

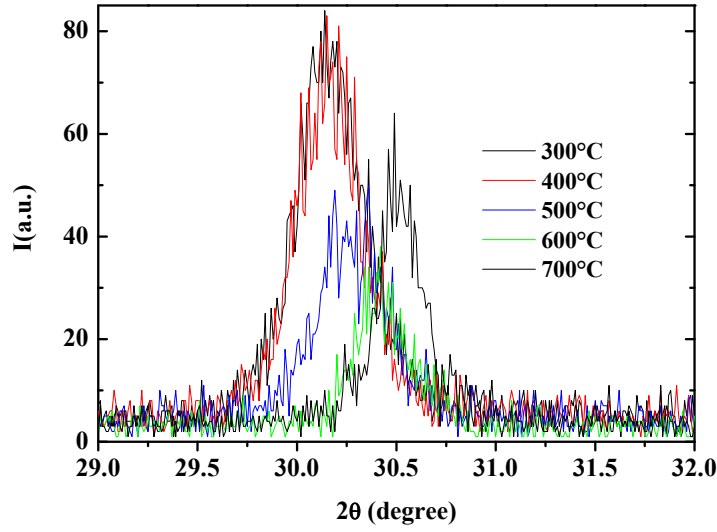
The figure 8 shows that, when the annealing temperature increases, the carrier density decrease and the resistivity increase. The resistivity variation at different annealing temperature, estimated by ellipsometry characterization for the two set of samples (open and full squares in figure 8a), is close to the resistivity values (stars symbols in figure 8a), estimated by the electric measurements (figure 8b). This is in agreement with the experimental observations reported in literature [1,2,3,4,5], in fact the annealing processes favor the thermal oxygen diffusion in the ITO thin films.

Therefore we suggest that this oxygen absorption process from the ITO film, decrease the density of the oxygen vacancies in the ITO crystalline structure. Consequently, the structural defects generated by these oxygen vacancies [1,3] decrease therefore the crystalline order will increase.

The recorded spectra at different annealing temperature are reported in figure 9. In figure 9b a zoom around [2,2,2] peak is reported.



(a)



(b)

Figure 9: X-ray diffraction measurements of ITO films at different temperatures: (a) all 2θ range, (b) enlargement of [222] peak.

It is clear that the annealing temperature induces a small shift of all the ITO peaks starting from 600 degrees. We fitted the more intense peak to determine precisely its width, then considering that the instrumental resolution (measured on Si111 perfect crystal) is small (0.007°) compared to the crystallites peaks we calculated the crystallites dimension using the Debye-Sherrer equation:

$$\Delta(2\theta) = \frac{0.9\lambda}{L \cos(\theta)}. \text{ The results are reported in table 1. From this analysis we can infer}$$

that the sample becomes more crystalline overcoming 600 °C annealing temperature.

T (°C)	$\sigma(\text{deg})$	L(Å)
300	0.173 ± 0.003	476 ± 10
400	0.166 ± 0.003	496 ± 10
500	0.179 ± 0.005	460 ± 15
600	0.143 ± 0.005	575 ± 20
700	0.114 ± 0.003	722 ± 10

Table 1: FWHM (full width at half maximum) of more intense crystalline peak and related crystalline sizes.

In literature is reported that the carrier mobility is directly proportional to the crystalline order [1,3], and it may be indirectly measured by studying the variation of the collision frequency (figure 7b) estimated by ellipsometry characterization. In that figure, we have observed that the collision frequency decrease with annealing temperature therefore the crystalline order increase and this is agreement with the X-ray measurements.

The optical band-gap energy of the annealed ITO thin films have been studied by using both the extinction coefficients estimated the ellipsometry characterization and the normal transmittance measured by spectrophotometry technique.

In the figure 10 are showed the measured normal transmittance spectra at different annealed temperatures. It is worthwhile observe that when the annealing temperature increase the slope of the transmittance curve, in the range 300-400 nm (near-UV), shift towards to higher wavelengths.

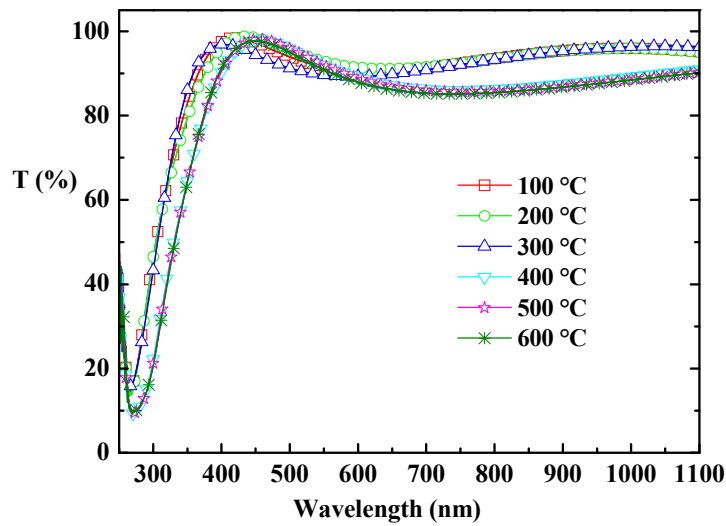


Figure 10: Normal transmittance spectra acquired on the annealed ITO thin films. The maximum transmittance in visible spectra was found about 90%.

The normal transmittance spectra have been used to calculate the absorption coefficient (data not shown) by the formula:

$$\alpha(h\nu) = \frac{1}{d_{ITO}} \ln \left[\frac{100}{T_{\%}(h\nu)} \right]$$

where $T_{\%}(h\nu)$ is the measured transmittance and $d_{ITO} = ITO_{layer} + ITO_{s.rough}$ is the ITO thickness estimated by ellipsometry technique.

The extinction coefficients $k(h\nu)$, estimated by ellipsometry characterization, are used to calculate the absorption coefficient $\alpha(h\nu)$ versus photon energy $h\nu$ (data not shown) by the formula:

$$\alpha(h\nu) = 4\pi \frac{k(h\nu)}{\lambda}$$

where h is the Plank constant and λ is the wavelength of the light.

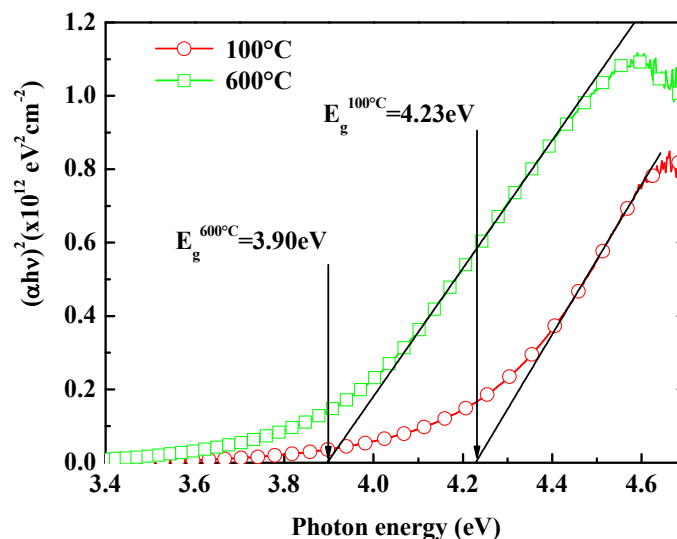
The optical band-gap energies for ITO thin films can be estimated by using the allowed direct transition model [1, 16]. If exciton formation is neglected, the form of the absorption coefficient α as function of photon energy $h\nu$ depend on the joint density of the states, $N(e)$, involving the band across the Fermi level.

For simple parabolic bands and allowed direct transitions, the typical expression of the absorption coefficient $\alpha(h\nu)$, is:

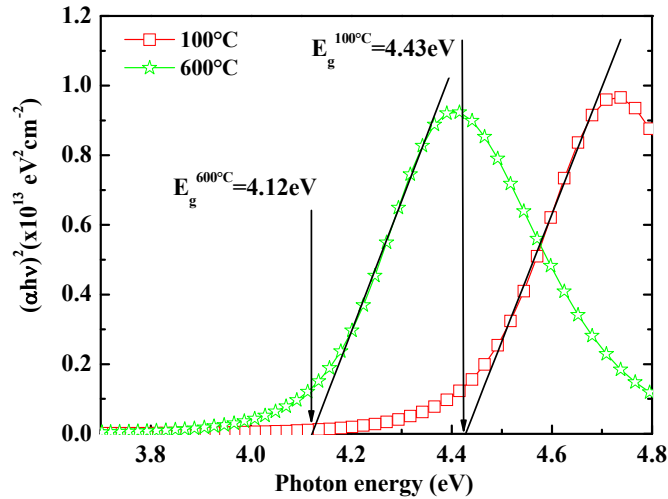
$$(\alpha h\nu)^2 = A(h\nu - E_g^{opt}), \quad \text{with } h\nu > E_g^{opt}$$

where E_g^{opt} is gap energy and A is a constant, proportional to the probability of electron transition between occupied and empty states [16].

The figure 11 show the $(\alpha h\nu)^2$ functions, measured at 100°C and 600°C, versus photon energy $h\nu$, estimated by the transmittance (figure 11a) and by ellipsometry characterizations (figure 11b). We can extract the band gap by linear fit of the function $(\alpha h\nu)^2$ immediately above the edge. The band gap is taken to be the intercept of the line estimated by linear fit with photon energy axis (see figure 11a-b).



(a)



(b)

Figure 11: The $(\alpha h\nu)^2$ functions versus photon energy $h\nu$, estimated by normal transmittance (a) and ellipsometry characterizations (b), were comparing together. The pictures show examples of band-gap energy estimations at 100°C and 600°C.

The figure 12 show the optical band-gap energies calculated, by the ellipsometry characterization, for the two set of ITO samples (1 and 2). The band-gap energies, estimated by spectrophotometry measurements, are compared with that.

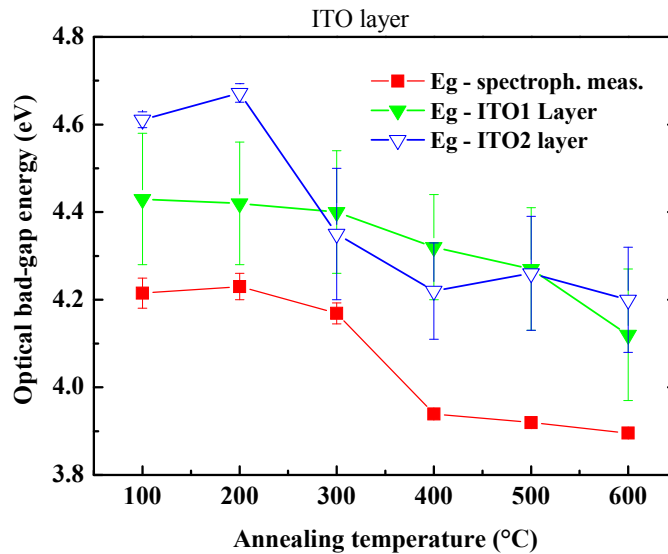


Figure 12: The gap energy of ITO layer obtained by ellipsometry characterization (triangles) decrease when the annealing temperature increases, as well as the gap energies estimated by transmittance measurements (squares).

From the figure 12 is possible to observe that the optical band-gap energies estimated by ellipsometry characterization are greater than the gap energy values estimated by transmittance measurements. The difference is about 0.2-0.4eV. Similar different values have been observed by other authors [17]. A possible explanation could be that the ellipsometry characterization depends from an optical model that describe the physical system, therefore we can suppose that the ellipsometry characterization is more precise than spectrophotometry one.

In first approximation, the variation of the optical band-gap energy versus annealing temperature can be described by using the Burstein-Moss theory [1,18]. When the carrier density decrease, the conductive band is emptied of the electrons, therefore the photon energy needs, to the electron transition between the high energy level of the valence band and the low free level energy of the conductive bands, decrease [3]. This gap energy is the optical band gap energy E_g (eV).

In according to the Burstein-Moss (B-M) model, the gap energy shift is proportional to $N_c^{2/3}$ (N_c is the carrier density) by the formula:

$$E_g = E_{g0} + \Delta E_g^{BM}, \quad \text{where} \quad \Delta E_g^{BM} = \frac{\hbar^2}{2m^*} (3\pi^2)^{2/3} \cdot N_c^{2/3} \quad (7)$$

The B-M model describe the optical band-gap energy of ITO like a variation ΔE_g^{BM} , respect to the In_2O_3 optical band-gap energy $E_{g0} = 3.75\text{eV}$, generated from the increasing of the carrier density by using Sn-dopant or caused by oxygen vacancy [1].

In this work the main cause of the decreasing of the band-gap energy, when the annealing temperature increase, is the thermal oxygen absorption by ITO thin film. This process decreases the oxygen vacancies in the ITO structure and therefore the carrier concentration. The figure 13 shows the linear variation of the estimated optical band-gap energies versus the carrier density $N_c^{2/3}$, in according with the B-M model.

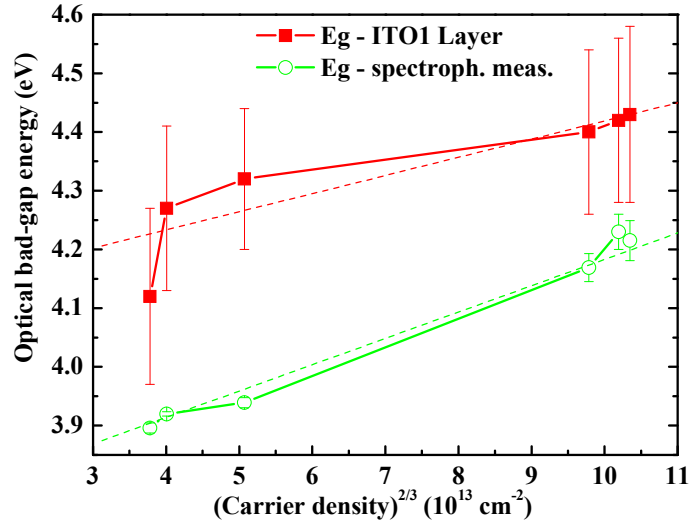


Figure 13: The optical band-gap energy estimated by the ellipsometry (squares) and transmittance (circles) measurements for each annealing temperature are plotted versus the carrier density shown in figure 8a. The dash lines are drawn only to guide the eye.

The carrier density has been estimated by the Eq. (2) with $m^* = 0.4m_e$ [1]. In the figure 13, the difference between the experimental data is about 0.2-0.4eV as previously showed [17].

4. Conclusion

Float glass substrates covered by high quality ITO thin films (Balzers) were subjected for an hour to single thermal treatments at different temperature between 100°C and 600°C. In order to study the electric and optical properties of both annealed and not annealed ITO-covered float glasses, ellipsometry, spectrophotometry, impedance analysis, and X-Ray measurements were performed. The dispersion law of the float glass slides do not depends on annealing temperature as emphasized by the transmittance measurements. By this preliminary study, we have chosen a common dispersion law for the float glass substrates, which were used to define the optical models for the ITO thin films.

The ellipsometric optical models, used to characterize the ITO thin film and to study the thermal modification of its structural properties, were defined by two layers: the first one describes the dielectric surface roughness properties; the second one describes the ITO thin film properties.

The second layer is defined by a sum of the Lorentz oscillator to describe bound carriers (dielectric properties) and Drude oscillator to describe the free-carriers (conductive properties). This optical model allowed estimating the dispersion laws and structural properties (plasma frequency, collision frequency, carrier density, resistivity and optical band-gap energy) of the annealed ITO samples.

Advanced spectrophotometry has been used to estimate the optical band-gap energy of the same samples. The optical band-gap energy estimated by transmittance measurements were smaller than band-gap energy obtained by ellipsometric characterization. The difference between the two results was found in the range between 0.2 and 0.4eV.

Transmittance and impedance characterizations have been compared to ellipsometry investigations to complete our scientific picture.

The thermal annealing changes strongly the structural and optical properties of ITO thin films, because during the thermal processes, the ITO thin film absorbs oxygen from air. This oxygen absorption decreases the oxygen vacancies and increase the crystalline order of the ITO thin films as confirmed both by ellipsometry and X-ray measurements.

The plasma frequency decrease in the range of $2.9 \times 10^{15} \text{ (s}^{-1}\text{)}$ to $1.2 \times 10^{15} \text{ (s}^{-1}\text{)}$, and the collision frequency decrease in the range of $4.6 \times 10^{14} \text{ (s}^{-1}\text{)}$ to $1.6 \times 10^{14} \text{ (s}^{-1}\text{)}$.

By using these two functions we have obtained that, when the annealing temperature increases the carrier density and optical band-gap energy decrease according with the Burstein-Moss theory, while the resistivity increases accordingly with electrical measurements performed on the same samples. The optical band-gap energy was found to decrease in the range of 4.5eV to 4.2eV when the annealing temperature increases.

References

- [1] I. Hamberg and C.G. Granqvist, "Evaporated Sn-doped In₂O₃ films: Basic optical properties and applications to energy-efficient windows", *J. Appl. Phys.* **60** (11) 1986 - R123.
- [2] M. Berder, W. Seelig, C. Daube, H. Frankenberger, B. Ocker, J. Stollenwerk "Dependence of oxygen flow on optical and electrical properties of DC-magnetron sputtered ITO films", *Thin Solid Films* **326**(1998) 72-77.
- [3] J.R. Bellingham, W.A. Phillips and C.J. Adkins, "Electrical and optical properties of amorphous indium oxide" *J. Phys.: Condens. Matter* **2**(1990) 6207-6221.
- [4] F. O. Adurodija, H. Izumi, T. Ishihara, H. Yoshioka, M. Motoyama, and K. Murai, "Influence of substrate temperature on the properties of indium oxide thin films", *J. Vac. Sci. Technol. A*, **18**(3)(2000)814-818.
- [5] M. Buchanan, J.B. Webb and D.F. Williams, "Preparation of conducting and transparent thin films of tin-doped indium oxide by magnetron sputtering", *Appl. Phys. Lett.* **37** (2) 1980.
- [6] V. Teixeira, H.N. Cui, L.J. Meng, E. Fortunato, R. Martins, "Amorphous ITO thin films prepared by DC sputtering for electrochromic applications", *Thin Solid Films* **420-421** (2002) 70-75.

- [7] John C.C. Fan, John B. Goodenough, "X-ray photoemission spectroscopy studies of Sn-doped indium-oxide films", *J. Of Appl. Phys.* **48**(8) 1977.
- [8] John C.C. Fan, Frank J. Bachner and George H. Foley, "Effect of O₂ pressure during deposition on properties of rf-sputtered Sn-doped In₂O₃ films", *Applide Phys. Lett.* **31**(11) 1977.
- [9] F.O. Adurodija, L. Semple, R. Bruning, "Crystallization process and electro-optical properties of In₂O₃ and ITO thin films", *J. Mater. Sci.* **41** (2006)7096-7102.
- [10] S. Marino, M. Castriota, G. Strangi, E. Cazzanelli, and N. Scaramuzza "Asymmetric nematic liquid crystal cells containing lead zirconium titanate (PZT) films", *J. Appl. Phys.* **102**, 013112 (2007); S. D'Elia, M. Castriota et al., "Thermally induced modifications of the optic properties of Lead Zirconate Titanate thin films obtained on different substrates by sol-gel synthesis" accepted, *J. Appl Phys.* (2008).
- [11] Genell Med auf Floarglas - Balzers Thin Films Prod. ID. BD051149, BATCH 1400-655-(1999)
- [12] Yi Liu, Lauren K. Wolf, and Marie C. Messmer "A Study of Alkyl Chain Conformational Changes in Self-Assembled n-Octadecyltrichlorosilane Monolayers on Fused Silica Surfaces", *Langmuir* **17**(2001) 4329-4335.
- [13] Harland G. Tompkins, E. A. Irene, "Handbook of Ellipsometry", William Andrew Publishing, Springer (2005).
- [14] J. Ederth, A. Hultaker, G.A. Niklasson, P. Heszler, A.R. Van Doorn, M.J. Jongorius, D. Burgard, and C.G. Granqvist, "Thin porous indium tin oxide nanoparticle films: effects of annealing in vacuum and air", *Appl. Phys. A* **81** (2005).1363-1368
- [15] D. E. Aspnes, *Thin Solid Films* **89**,(1982) 249.
- [16] N.F. Mott, E.A Davis, "Electronic processes in non-crystalline materials", second edition Clarendon press, Oxford (1979).
- [17] H. Lee, Y.S. Kang, S-J Cho, Bo Xiao, H. Morkoc, T.D. Kang, G. S. Lee, J Li, S-H Lee, P.G. Snyder, J.T. Evans, "Dielectric function and electronic band structure of lead zirconate titanate thin films", *Jour. of App. Physic* **98** (2005). 094108
- [18] E. Burstein, "Anomalous Optical Absorption Limit in InSb", *Phys. Rev.* **93** (1954) 632

INFN-CNR-LICRYL Laboratory and CEMIF.CAL, Department of Physics, University of Calabria, via P.Bucci 31C, Rende (CS), I-87036 (ITALY).

3.1.1. Appendix A. Effects of annealing temperature on the structural and morphological properties of high quality indium tin oxide thin films: Effects on the morphological properties.

The variations of the morphological properties of the ITO films versus the annealing temperature are showed in Fig. 3.1.

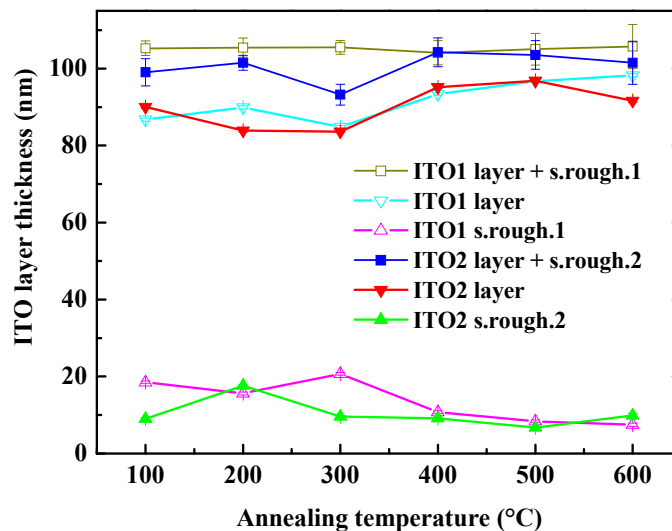
In the picture, the thickness (Fig. 3.1a) and the void volume fraction (Fig. 3.1b), for two set of samples, are showed. The morphological fit parameters are estimated by using the ITO optical model showed in the last section.

The ITO film thickness is given by the sum of the thickness estimated for the layer called “ITO layer” and its surface roughness (ITO s. rough.).

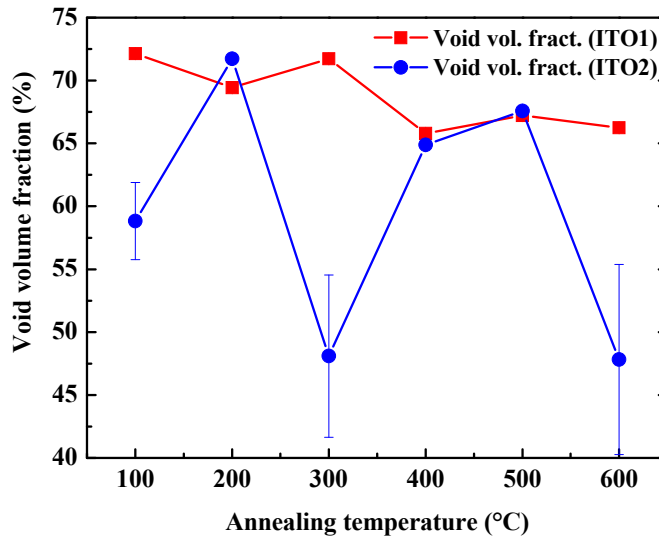
$$ITO1 \text{ (or 2) film thickness} = ITO \text{ 1(or 2)} + s. \text{ rough.1 (or 2)}$$

The ITO film thickness is drawn by using square symbols. (Void (full) symbols are used for the first (second) set of sample ITO1 (ITO2)). We can observe that after the thermal annealing, the ITO film thickness remain unchanged.

The estimated void volume fraction values (Fig. 3.1b), calculated for the two set of samples (full squares: ITO1 and full circles: ITO2, respectively), decrease when the annealing temperature increase. We suggest that the thermal annealing favors the reduction of the structural defect in the surface roughness layer.



(a)



(b)

Fig.3.1. (a) the ITO layer and surface roughness thickness are plotted for the two set of the samples ITO1 and ITO2. The sum of the two layers (ITO film thickness) is plotted in same picture (squares). The solid curve is drawn only to guide the eye.

3.1.2. Appendix B. Effects of annealing temperature on the structural and morphological properties of high quality indium tin oxide thin films: Validity of the Burstein-Moss model.

In the last section, we have showed that the optical band gap energy value (sect. 3.1, Fig. 12) decreases when the annealing temperature increases. We have observed, also, that this variation is linearly proportional to the variation of the carrier density, in according to the Burstein-Moss model. The Fig 3.2 shows this effect of thermal annealing on the optical properties of the ITO film.

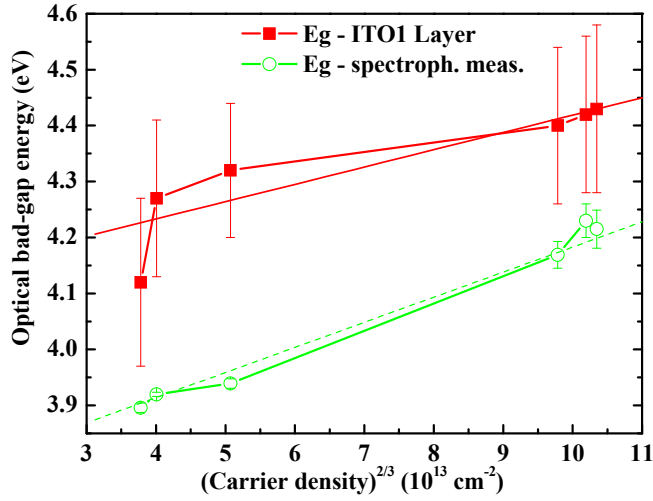


Fig. 3.2. The optical band-gap energy estimated by the ellipsometry (squares) and transmittance (circles) measurements for each annealing temperature are plotted versus the carrier density shown in fig 7a. The solid and dash lines are the linear fit.

By using Eq. (6) shown in the section 3.1 i.e.

$$E_g = E_{g0} + \Delta E_g^{BM}, \quad \text{where} \quad \Delta E_g^{BM} = \frac{\hbar^2}{2m^*} (3\pi^2)^{2/3} \cdot N_c^{2/3},$$

we have estimated E_{g0} and $\frac{\hbar^2}{2m^*} (3\pi^2)^{2/3}$ by means a linear fit on the data shown in the Fig. 3.1. The linear equation is given by:

$$E_g = E_{g0} + \left(\frac{\hbar^2}{2m^*} (3\pi^2)^{2/3} \right) \cdot N_c^{2/3} \quad \rightarrow \quad y = E_{g0} + Bx$$

The calculus has been performed by using both the points estimated by ellipsometry and spectrophotometry technique.

We have estimated by using transmittance measurements these two fit parameters:

$$E_{g0} = 3.734 \pm 0.012 eV \quad \text{and} \quad B = (4.49 \pm 0.27) \cdot 10^{-15} \text{ eVcm}^2.$$

While, by using the estimated ellipsometric data, we have found:

$$E_{g0} = 4.11 \pm 0.15 eV \quad \text{and} \quad B = (3.1 \pm 1.9) \cdot 10^{-15} \text{ eVcm}^2;$$

These results are close to the literature value of the optical band-gap energy of indium oxide ($E_{g0} = 3.75eV$) and to the theoretical parameter

$$B = \frac{\hbar^2}{2m^*} \left(3\pi^2 \right)^{2/3} \approx 9 \cdot 10^{-15} eVcm^2, \text{ calculated by using } m^* = 0.4m_e.$$

In our calculus we have neglected the variation of the constant effective electron mass caused by the thermal annealing, therefore, the difference observed in our estimated values may be attributed to the approximation used.

The Burstein-Moss theory is valid only for low dopant concentration in fact, if the carrier density changes strongly, it changes also the constant effective electron mass, and the density of the states are distorted by charge effects. This effect of the carrier density variation on the Burstein-Moss model has been studied by Hamberg and Granqvist [4], in their full paper concerning the ITO transparent conductive oxide.

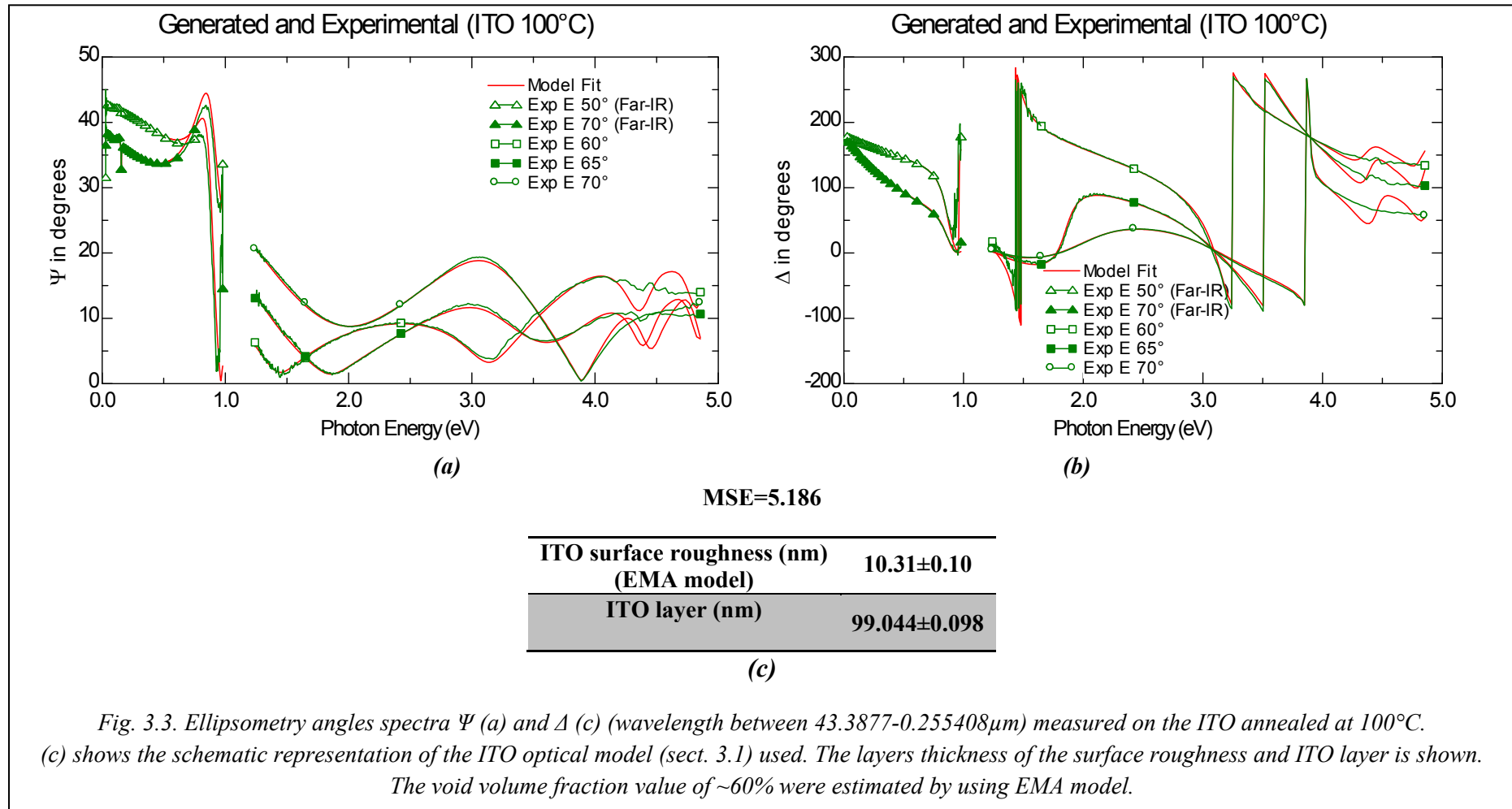
3.1.3. Appendix C. Check of the validity of the ITO optical model. (near UV – Far-IR)

The ITO optical model, described in the last section (3.1), has been tested with the far-IR ellipsometry angles spectra measures, collected by using the far-IR ellipsometry instrument at the Nebraska-Lincoln University.

In the last section of this chapter, we will show the preliminary results, concerning the far-IR Spectroscopic Ellipsometry characterization both of the annealed glass/ITO and glass/ITO/PZT samples.

These far-IR ellipsometry angles spectra has been appended to the middle IR-Visible-near UV ellipsometry angles measures, acquired at the University of Calabria by using the J.A. Woollam's Spectroscopic Ellipsometry (VASE M2000F).

The Fig. 3.3 shows the experimental and generated ellipsometry angles spectra (photon energy from 0.0285795eV (43.3877 μ m) to 4.85497eV (0.255408 μ m)) and at different AIO for the ITO/glass substrates annealed at 100°C. In the same picture, the best MSE and fit parameters estimated are showed.



3.2. Ellipsometry characterization of Lead Zirconate Titanate thin films – PZT

THERMALLY INDUCED MODIFICATIONS OF THE OPTIC PROPERTIES OF LEAD ZIRCONATE TITANATE THIN FILMS OBTAINED ON DIFFERENT SUBSTRATES BY SOL-GEL SYNTHESIS

Accepted JOURNAL OF APPLIED PHYSICS (2008)

Stefano D'Elia¹, Marco Castriota¹, Alfonso Policicchio², Nicola Scaramuzza^{1,*}, Carlo Versace¹, Enzo Cazzanelli¹, Raffaele Giuseppe Agostino², Carlo Vena¹, Giuseppe Strangi¹ and Roberto Bartolino¹.

1) INFN-CNR-LICRYL Laboratory and CEMIF.CAL, Department of Physics, University of Calabria, via P.Bucci 33B, Rende (CS), I-87036 (ITALY).

2) Department of Physics, University of Calabria, via P.Bucci 33B, Rende (CS), I-87036 (ITALY).

* Author for correspondence

Abstract

Lead Zirconium Titanate $\text{PbZr}_{0.53}\text{Ti}_{0.47}\text{O}_3$ (PZT) thin films have been obtained by sol-gel synthesis, deposited on different substrates (float glass, ITO-coated float glass and intrinsic silicon wafer) and later subjected to different thermal treatments. The morphologic and the structural properties of both PZT thin films and substrates have been investigated by Scanning Electron Microscope (SEM) and their composition was determined by Energy Dispersive X-ray analysis (EDX). Moreover, variable angle spectroscopic ellipsometry provides relevant information on the electronic and optical properties of the samples. In particular, the optical constants dispersion of PZT deposited on ITO-coated float glasses shows a small absorption resonance in the near IR region, not observed in PZT films deposited on the other substrates, so that such absorption resonance can be explained by interfacial effects between ITO and PZT layers. This hypothesis is also supported by EDX measurements, showing an interdiffusion of lead and indium ions, across the PZT-ITO interface, that can generate a peculiar charge distribution in this region.

1. Introduction

Electro-optic ceramics have attracted great interest for their applications, like infrared detectors, electro-optic modulators, light-beam switching shutters, waveguides, ferroelectric random access memory (FRAM), microelectromechanical actuators and other applications [1-3]. Recently, hybridized semiconductors with insertions of perovskite oxide materials have been investigated [4].

Among various electro-optic ceramics, lead zirconate titanate (PZT) thin films are widely used, due to their good ferroelectric and piezoelectric properties, high optical transmittance, low reflectance, and strong electro-optic Kerr effect.

Interesting perspectives now arise for the applications of these films as rectifying layers, which modify the electro-optical response of liquid crystals. In the past years, metal oxides with mixed ionic and electronic conduction properties have been tested as rectifying layers in asymmetric nematic liquid crystal cells (ANLCC) [5-9], and their rectifying effect has been explained by an internal electric field due to the formation of double charged layers at the interfaces, allowed by the charge carriers mobility. The same rectifying effect can be obtained by using PZT ferroelectric layer in ANLC cells [10], on the basis of different physical effects: in this latter case a permanent internal field, opposite (in polarity) to the external field, is generated by a polar orientation of the ferroelectric film.

To optimize this electro-optical application of ferroelectric films, many phenomena need to be studied, for instance the role played by the production methods, the influence of the substrate and the effect of the thermal treatments on the optical, structural and morphological properties of the films. In particular, important investigations have to be performed about the interface effect between PZT ferroelectric layer and transparent conductive oxide (TCO) thin films, both for well known indium-tin-oxide (ITO) and for the new semiconductor-like TCO materials as zinc-doped Al_2O_3 (AZO) and Ga_2O_3 (GZO), recently proposed as transparent electrodes [11].

In this work PZT ($\text{PbZr}_{0.53}\text{Ti}_{0.47}\text{O}_3$) thin films have been obtained by sol-gel synthesis on different substrates (float glass, ITO-coated float glass and intrinsic silicon wafer). Different thermal annealing processes have been tested, to investigate eventual temperature-driven changes in structural and morphological properties of amorphous PZT. These modifications were extensively investigated by spectroscopic ellipsometry (SE), which allows also to study the interface effects between the PZT thin films and the substrates.

2. Experimental

2.1. Sol-gel synthesis of the $PbZr_{0.53}Ti_{0.47}O_3$

Lead Zirconate-Titanate ($PbZr_{0.53}Ti_{0.47}O_3$ - PZT) thin films, were obtained by hybrid (carboxylate and alkoxides) [12] sol gel route and spin coating deposition of the obtained mother solution on different substrates.

The synthesis procedure of our PZT [10] has been developed by modifying some particular aspect of the synthesis process already used in previously works [13-15]. The used reagents (all supplied by Sigma-Aldrich) are Lead(II) acetate trihydrate ($Pb(CH_3COO)_2 \cdot 3H_2O$, 99.999 %), Zirconium(IV) propoxide solution ($Zr(C_3H_7O)_4$, 70 wt. % in 1-propanol), Titanium(IV) isopropoxide ($Ti[(CH_3)_2CHO]_4$, 99.999 %), glacial acetic acid (CH_3COOH , 99.99+ %), n-Propanol anhydrous ($CH_3CH_2CH_2OH$, 99.7%), anhydrous Ethylene glycol ($HOCH_2CH_2OH$, 99.8%). The solution was synthesized in a “humidity free” Glove Box insuring a dry Argon atmosphere.

To obtain stable mother solution, 10.43 g of $Pb(CH_3COO)_2 \cdot 3H_2O$ have been dissolved in CH_3COOH by stirring and heating the solution up to 80°C for fifteen minutes. The amount of $Pb(CH_3COO)_2 \cdot 3H_2O$ has been calculated to obtain a 10% excess in mole of lead, which compensate the lead loss (as PbO) occurring during the process. The amount of acetic acid has been chosen in order to have its molar number twice the sum of the molar number of lead, zirconium and titanium.

After two minutes at 80 °C, the heater was set at 70°C and when the solution reached this temperature, the stoichiometric amount of $Zr(C_3H_7O)_4$ solution, have been added. As it was already reported [16], by adding zirconium butoxide, we observed a temperature increase of $\approx 10^\circ C$.

After fifteen minutes, when the temperature is again 70°C and all the particles eventually formed are dissolved, $Ti[(CH_3)_2CHO]_4$, in its stoichiometric ratio, was added. The resulting solution has been stirred for one hour at 70°C, for an additional hour on a cold stirrer (room temperature) and, finally we left the solution for another hour on a room temperature stage without stirring it. Successively, with the solution held at room temperature, CH_3COOH have been added and the resulting solution has been left to stir for fifteen minutes. The amount of acetic acid used is such that the total molar number present in solution is twenty-five times the titanium molar number [17].

The addition of the acetic acid, at this step, slows down the reaction that otherwise occurs when the n-propanol is added, with the consequent formation of a white precipitate [13,15]. At this point 23.10 g of $CH_3CH_2CH_2OH$ have been added and the obtained solution was stirred for fifteen minutes.

Subsequently, 1.16 g of $HOCH_2CH_2OH$ have been added to obtain homogeneous film (1ml of $HOCH_2CH_2OH$ for each 10 g $Pb(CH_3COO)_2 \cdot 3H_2O$) [13] and then the

solution has been sealed with parafilm and left to stir for one night at room temperature.

Finally, the solution has been removed from the glove box and 9 g of bidistilled water have been added before its use in the spin coating procedure, to obtain a concentration of 0.38(4) mol/l for the final $\text{PbZr}_{0.53}\text{Ti}_{0.47}\text{O}_3$ solution.

2.2. Substrates and samples preparation

Substrates with different structural and morphological properties were used: intrinsic silicon wafers, float glasses and ITO covered float glasses (nominal sheet resistivity, $R_{\text{sh}}=25\Omega/\square$, Balzers FAB Thin Films [18]).

These substrates were submitted to an accurate cleaning procedure to remove all surface impurities, without damaging the surface. All samples have been ultrasonically cleaned in a chloroform solution, then in an acetone solution and finally cleaned in bidistilled water for tree times to eliminate eventual residual solvent traces. Finally, the substrates have been dried in furnace at 100°C for 30 minutes in air.

The $\text{PbZr}_{0.53}\text{Ti}_{0.47}\text{O}_3$ solution is spread on the substrates using a SC10 spin coater (produced by CaLCTec s.r.l.) at 1200 rpm for 25 s. The deposited film is placed on a hot plate for 5 minutes at 300°C to evaporate the organic solvent used in the sol solution. Finally, different samples are obtained by thermal treatments of the deposited film to temperatures in the 100°C - 700°C range, with the same procedure described above.

2.3. Measurement techniques

The optical characterization of substrates and thin film samples was performed by using the Spectroscopic Ellipsometry (SE) technique. The VASE M2000F (J.A. Woollam) rotating compensator ellipsometer (RCE) was used in the 250-1000 nm wavelength range. Spectra were collected at different incident angles to increases the accuracy of layer modeling.

The structural and morphological properties are estimated by using multilayer optical models compatible with both the ellipsometric results and the layer structures of our samples. Each layer was depicted by optical model whose fit parameters were the layer thickness and the frequency dispersion of its complex optical constants [19].

The optical model and the best fit parameter values have been calculated by means of the WVASE32 application using the nonlinear Levenberg-Marquardt algorithm, which determines the minimum value of the Mean Square Error (MSE). The figure of merit, MSE, is a measure of the likelihood of the fit [19], and it is defined by

$$MSE = \frac{1}{2N - M} \sum_{i=1}^N \left[\left(\frac{\Psi_i^{\text{mod}} - \Psi_i^{\text{exp}}}{\sigma_{\Psi,i}^{\text{exp}}} \right)^2 + \left(\frac{\Delta_i^{\text{mod}} - \Delta_i^{\text{exp}}}{\sigma_{\Delta,i}^{\text{exp}}} \right)^2 \right]$$

where N is the number of data points, M is the number of the fitting parameters, $(\Psi^{\text{exp}}, \Delta^{\text{exp}})$ and $(\Psi^{\text{mod}}, \Delta^{\text{mod}})$ are the measured and modeled ellipsometric angles respectively, while σ_{Ψ} and σ_{Δ} are the standard deviations of the measured ellipsometric angles. The modeled ellipsometric angles $(\Psi^{\text{mod}}, \Delta^{\text{mod}})$ are functions of the all fit parameters that define the multilayer optical models.

A Varian 5E spectrophotometer has been used to perform the transmittance spectra measurements. Energy Dispersive X-ray (EDX) analysis were performed by using a Scanning Electron Microscopy (SEM) Quanta FEG 400 F7 produced by FEI. The EDX measurements were collected at three different beam energies (10, 15, 30 kV) in order to determine the elemental depth profile composition and morphological properties of the PZT samples.

3. Results

3.1. Multilayer optical models

In a preliminary study, we have estimated the optical models of the substrates, without PZT depositions, annealed at different temperatures in the range 100-700 °C with steps of 100°C and treatment duration of one hour. These optical models will be used to study the optical property variations of the PZT depositions annealed at the same temperatures.

The float glass substrates were described by an optical Cauchy model [19] for the dispersion law, and by the Urbach model [19] for the extinction law. The intrinsic silicon wafer was described by the optical model created by Herzinger [20], while the Lorentz optical model [19] was used for both the annealed ITO thin films and PZT samples.

The ITO thin film has been modeled by using two layers with different conductive or dielectric properties: the first one describes the bulk; the second one describes the rough surface of the ITO thin films. The bulk layer has been simulated by using a linear sum of Drude oscillators [19] (conductive properties) and Lorentz oscillators (dielectric properties). The roughness of the surface layer was defined by using the effective-medium approximation with a mixture of a Lorentz oscillator layer (ϵ_{ITO}) and voids ($\epsilon_{\text{void}} = 1$). The complex effective dielectric function (ϵ_{srough}) was calculated by the Bruggeman effective medium approximation (EMA) [19, 21]:

$$f_{ITO} \frac{\epsilon_{ITO} - \epsilon_{\text{srough}}}{\epsilon_{ITO} + 2\epsilon_{\text{srough}}} + f_{\text{void}} \frac{\epsilon_{\text{void}} - \epsilon_{\text{srough}}}{\epsilon_{\text{void}} + \epsilon_{\text{srough}}} = 0$$

where f_{ITO} and f_{void} are the volume fractions of the ITO phase and voids respectively, and they must satisfy $f_{ITO} + f_{\text{void}} = 1$.

In Table I is reported a schematic representation of the optical models used to characterize the substrates annealed at the different temperatures.

Float glass 1.1mm

(a) Refractive index of the float glass is modeled by using Cauchy dispersion law; Extinction index modeled by using Urbach absorption law.

S₂O₃ layer (5÷25nm)
Intrinsic silicon wafer (0.8mm)

(b) Intrinsic silicon wafer is modeled by using the optical model estimated by Herzinger [20].

Surface roughness (EMA model) 10÷20nm
ITO layer 85÷90nm
Float glass 1.1mm

(c) ITO layer is modeled by using the sum of the Drude (conductive property) and Lorentz (dielectric property) oscillators. Surface roughness is modeled by using EMA model (mixing the Lorentz oscillator and Void).

Table I: Multilayer optical models used to characterize the substrates annealed at different temperatures. We estimate an optical model parameters for each temperature and for each substrate. (a) Optical properties of the float glass do not change with annealing temperature; (b) The thickness of silicon oxide increase when the annealing temperature increase; (c) Optical properties of ITO layer change strongly with the annealing temperature.

Three Lorentz oscillators have been introduced to simulate the pseudo-dielectric functions of the PZT layer. Two of the oscillators describe the pyrochlore and perovskite phases [22,23]; while the last oscillator describes the gap energy in the Deep UV (DUV) spectral region [23].

When the PZT was placed on ITO-coated float glass, a correct description of its pseudo-dielectric function requires the introduction of a further Lorentz oscillator. This oscillator has its characteristic resonance energy in the NIR region.

The surface roughness of the PZT films is taken into account by an effective-medium approximation model (EMA) with mixture of PZT layer and void. Also in

this case, the Bruggeman EMA was used to estimate the effective dielectric function of the PZT roughness (see Table II).

Surface roughness (EMA model)
PZT layer
Substrate (a), (b) or (c)

Table II: The multilayer optical model used to characterize the PZT layers annealed at the temperatures $T_i(^{\circ}\text{C})$. The multilayer optical model of the substrate at same temperature $T_i(^{\circ}\text{C})$ has fixed during the fit analysis. The substrates can be: (a) float glass, (b) float glass covered by ITO, (c) intrinsic silicon wafer (Tab.I).

3.2. Optical and morphological properties of the substrates

Each sample is described by an appropriate optical model changing with substrate composition, annealing temperature and multilayer structure. Their comparison allows us to investigate the structural and morphological modifications of the used substrates.

The dispersion laws of the optical constants estimated for the float glasses annealed at different temperatures are shown in figure 1.

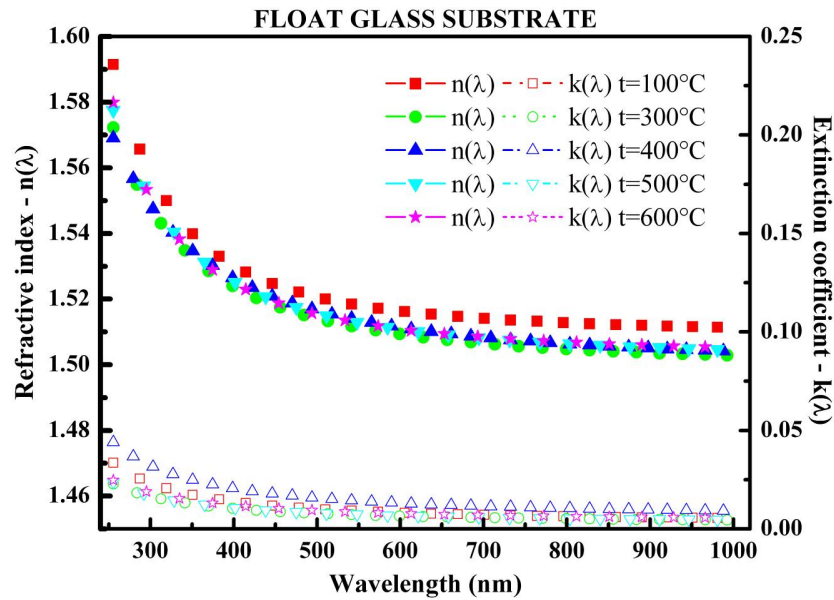


Figure 1: Dispersion of the optical constants estimated for the float glasses annealed at different temperatures.

It is evident that the dispersion laws, defined for each optical model, have no remarkable dependence on the annealing process. These results are supported also by the transmittance optical characterization of the float glasses, as shown in figure 2.

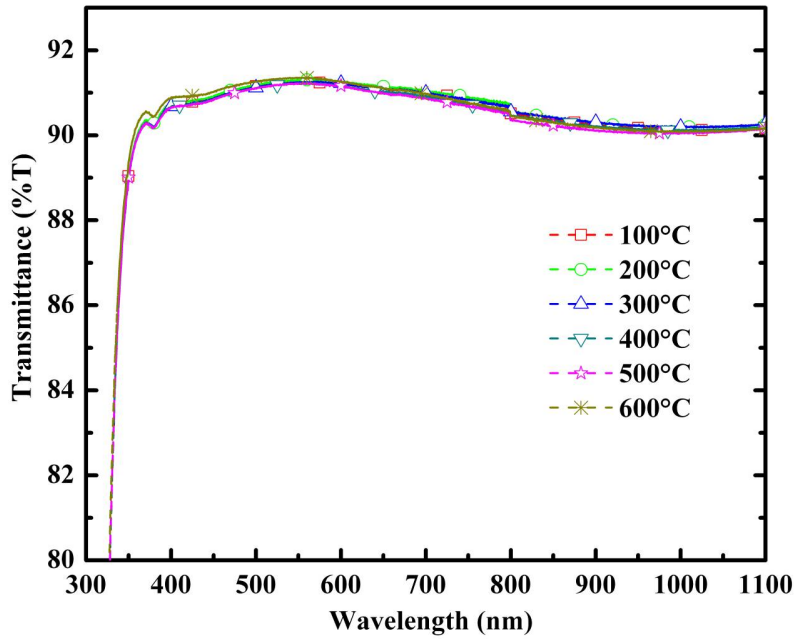


Figure 2: Transmittance measured on the annealed glass substrates. The annealing temperatures are indicated in figure.

The evaluation of the parameters used in the optical model [20], reproducing the measured ellipsometric angles collected on the silicon substrates annealed at different temperatures, shows that only the silicon oxide layer thickness increases with the annealing temperature (see Figure 3), while the other parameters remain practically unchanged.

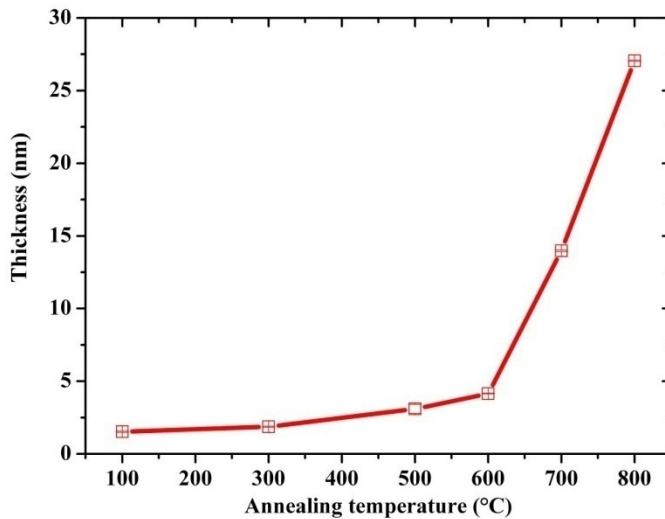
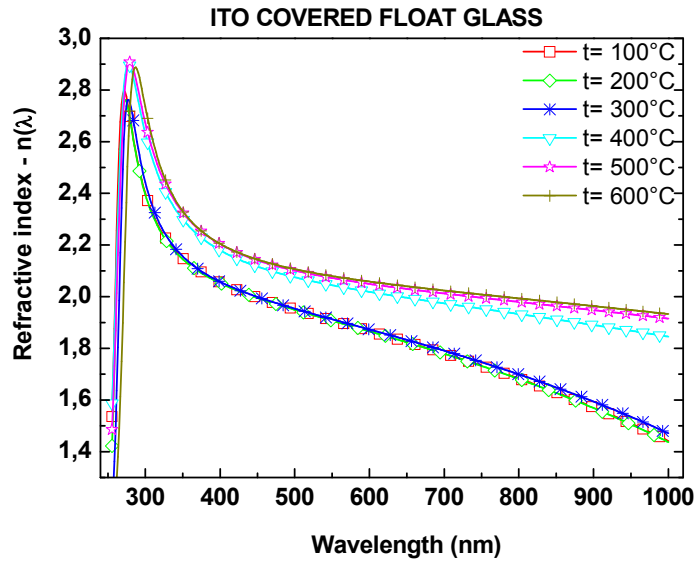
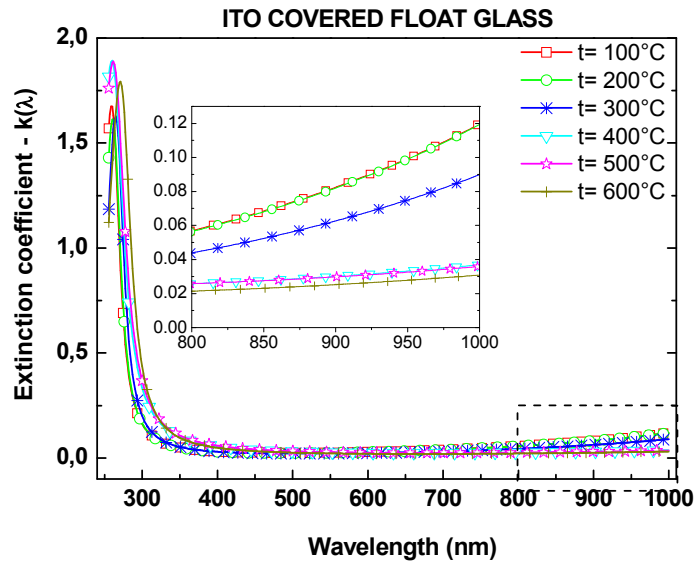


Figure 3: Evaluated silicon oxide layer thickness versus the annealing temperature of the Silicon substrate.

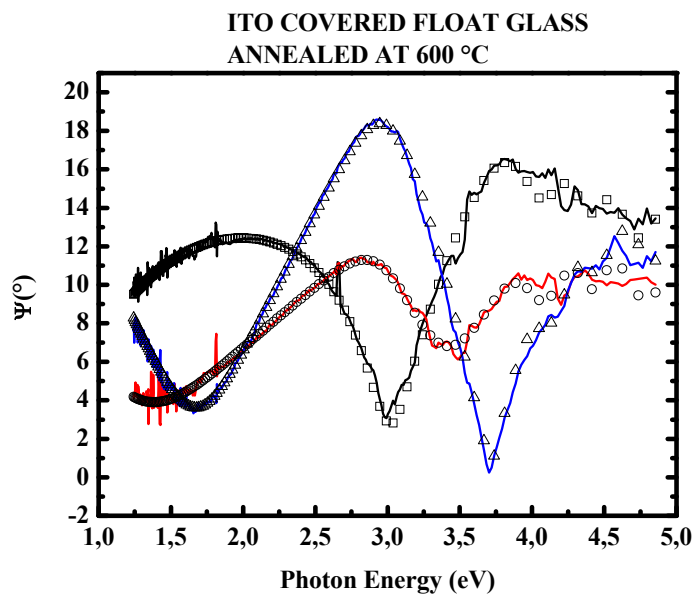
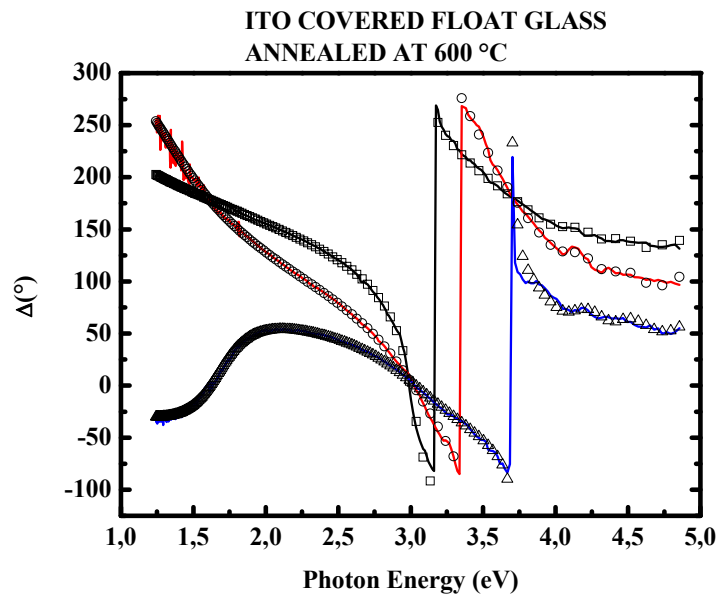
On the contrary, the measurements on samples of ITO-coated float glass show significant changes of the optical properties of the ITO thin films, depending on the annealing temperature (see Figure 4).



(a)



(b)



(c)

Figure 4: Optical properties estimated by using the multilayer optical models for ITO-covered glasses (Tab. 1(c)). The enlargement of the NIR spectra (b) shows the reduction of carrier concentration when annealing temperature increases (Drude theory for free carriers). In the pictures (c) are shown the experimental values (solid curves) and fitted data (geometric symbols) of the characteristic ellipsometric angles ψ and Δ , for different angles of incidences: 60° (squares); 65° (circles); 70° (triangles). The ITO layer is annealed at 600°C

The optical properties estimated from ITO-coated float glasses, annealed at different temperature, have been used to estimate the optical band gap energies, as discussed in the (3.3) paragraph. The evaluated ITO thickness exhibits only small changes versus annealing temperature, while the electrical (measured sheet resistivity) and optical band gap energies remain constants for treatments between 100 and 300°C (see Figure 5).

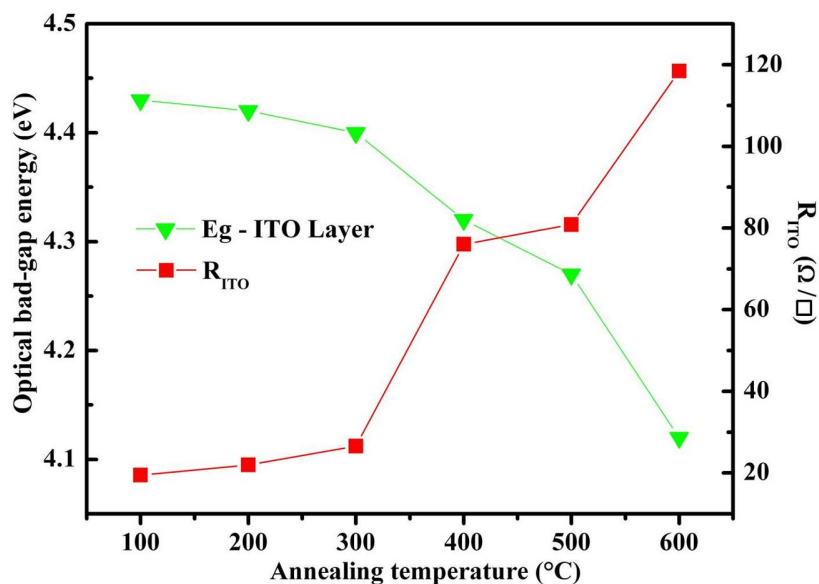


Figure 5: The sheet resistivity (red squares) versus annealing temperature increase from 20 Ω/\square , measured when the annealing temperature were between 100-300°C, to the 120 Ω/\square when the annealing temperature were 600°C. When the resistivity increase, the optical band gap energy (green triangles) decrease in according to the Burstein-Moss model.

The typical model used to describe the high conductivity of the ITO takes into account the carrier density determined both by the oxygen vacancies and by the tin atoms substituted for indium, that acts as donor when their oxidation state is Sn^{4+} [24-26]. The carrier mobility depends on the ITO crystalline state [26-29]. It was observed that oxygen plays an important role for the ITO conductivity as well as the amount of Sn doping [26, 30]. In this framework, when the oxygen vacancies density decrease the carrier concentration also decrease.

The adsorption of the atmospheric oxygen into ITO thin film, associated to the annealing process, induces the decrease of the oxygen vacancies in the ITO lattice structure. Therefore, the density of the carrier concentration decrease, the resistivity of ITO thin film increase and the optical band-gap energy decrease.

The dependence of ITO optical properties from the annealing temperature can be described by the Burstein-Moss model [31], which is typically used to study the

dependence of semiconductors properties on both temperature and dopant concentration [26, 32].

3.3. Structural and morphological properties of the samples (substrates/PZT)

Different experimental observations on the ferroelectric PZT thin films, obtained by sol-gel synthesis and deposited on various substrates, indicate that these films are not a significant barrier for the atmospheric oxygen. In fact, during the heat-treatment the oxygen atoms diffuse through PZT layer towards the substrate [33-35]. The oxygen thermal diffusion is an important problem regarding the electro-optical and electronic application of these ferroelectric thin films. Moreover, both the electro-optical and optical responses of the ferroelectric layers depend from the interface substrate/ferroelectric films [35].

On the basis of such evidences, we can assume that, the changes of the substrates during the thermal process, induced by the structural reorganization as well as by the thermal adsorption of atmospheric oxygen, are slightly affected by the presence of the PZT layer. In particular, the structural and morphological properties of silicon wafer and ITO are strongly dependent on the oxygen adsorption while the float glass substrates are only slightly influenced (Figure 1 and 2).

As already stated, the parameters optical models estimated of each substrate for different temperature have been used to study the temperature dependence of PZT films properties. The results for the uncoated substrate at T_i , has been used to evaluate the optical model parameters of the PZT layer annealed at the same temperature.

The fit procedure has been performed using the optical models obtained for the substrates, maintaining the same fit parameters of substrates and estimating only the fit parameters of the PZT layers. Figure 6 reports the results obtained in this way, showing a fairly good agreement between experimental data and model results.

These experimental observations justify the assumed optical models for the samples Glass/ITO/PZT. The atmospheric oxygen can diffuse through the PZT thin films and change the structural and morphological properties of ITO layers.

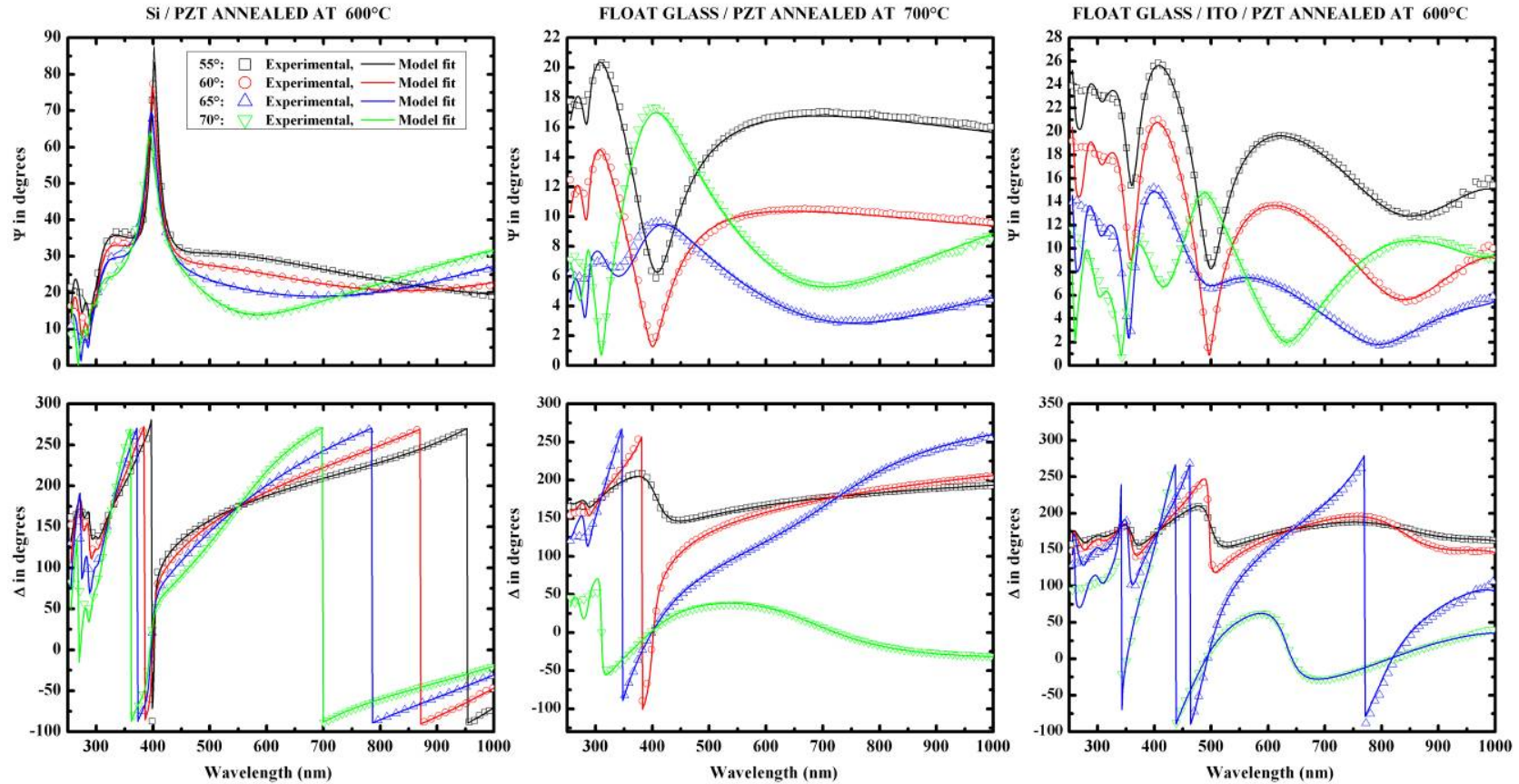


Figure 6: Generated and Experimental data examples for different PZT samples: silicon/PZT substrates (annealed at 600°C) (a); float glass/PZT (annealed at 700°C) (b); float glass/ITO/PZT (annealed at 600°C) (c).

The estimated dispersion laws of optical constants for PZT layers annealed at different temperature and on the different substrates are shown in figure 7.

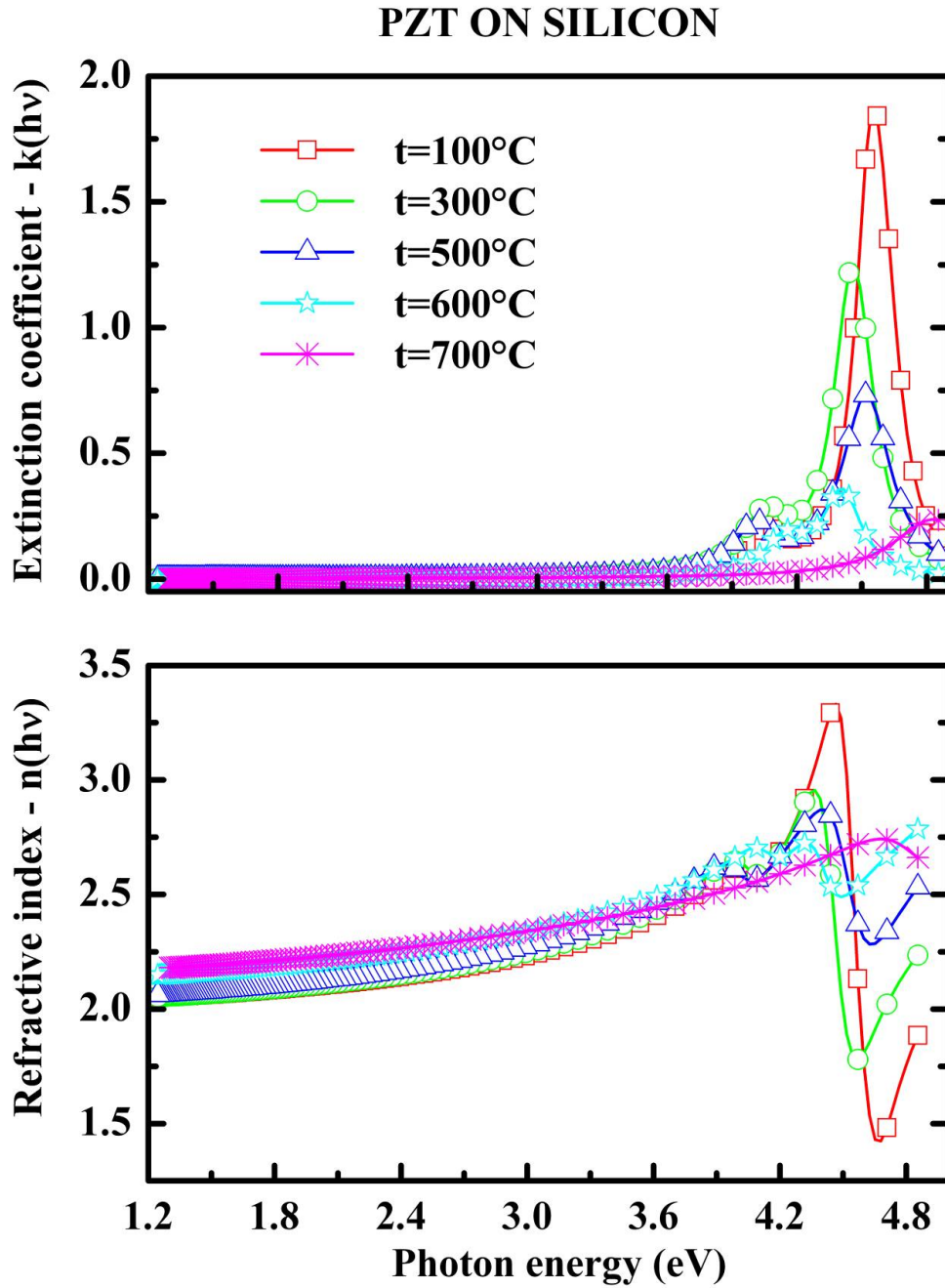


FIGURE 7a

PZT ON FLOAT GLASS

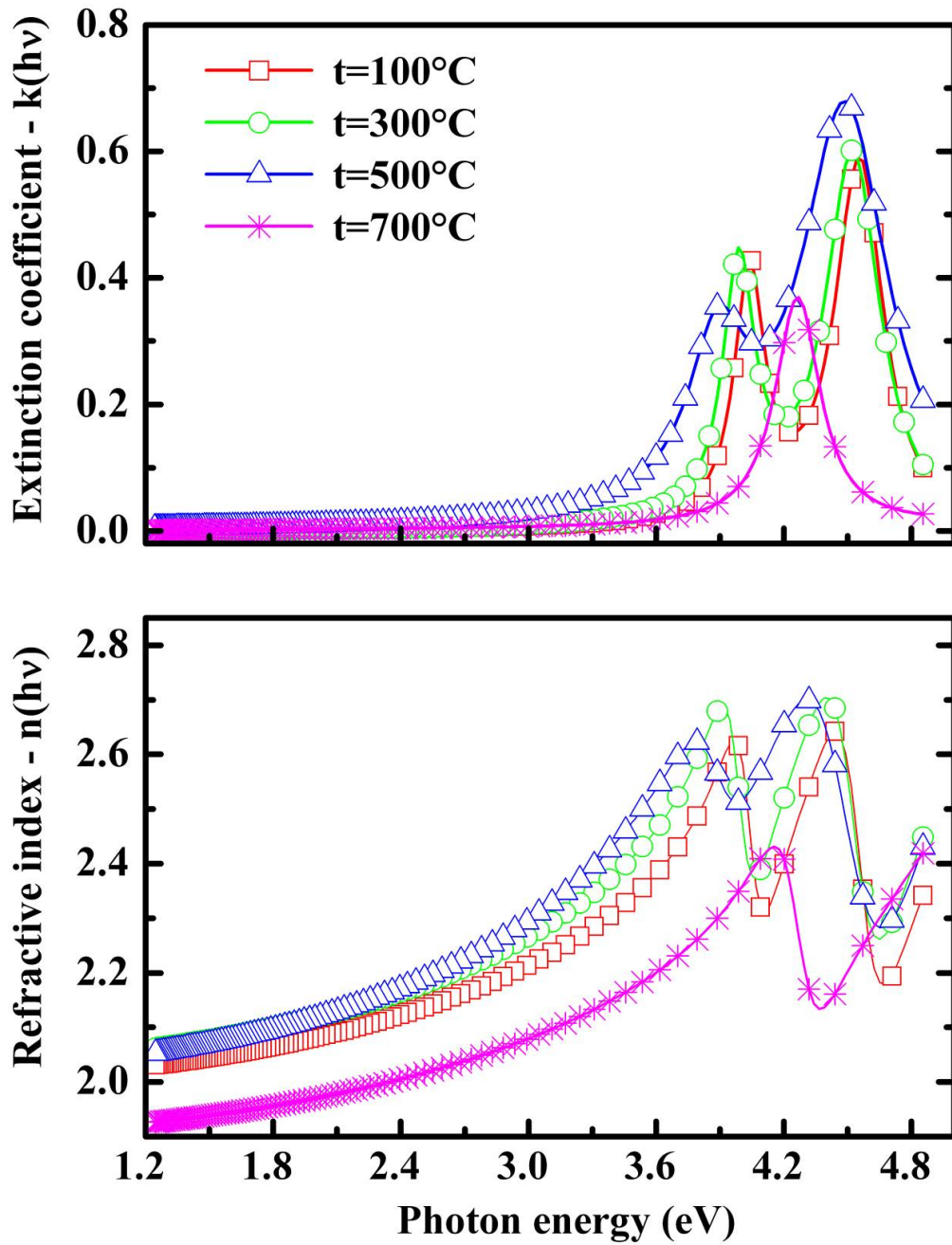


FIGURE 7b

PZT ON ITO COVERED FLOAT GLASS

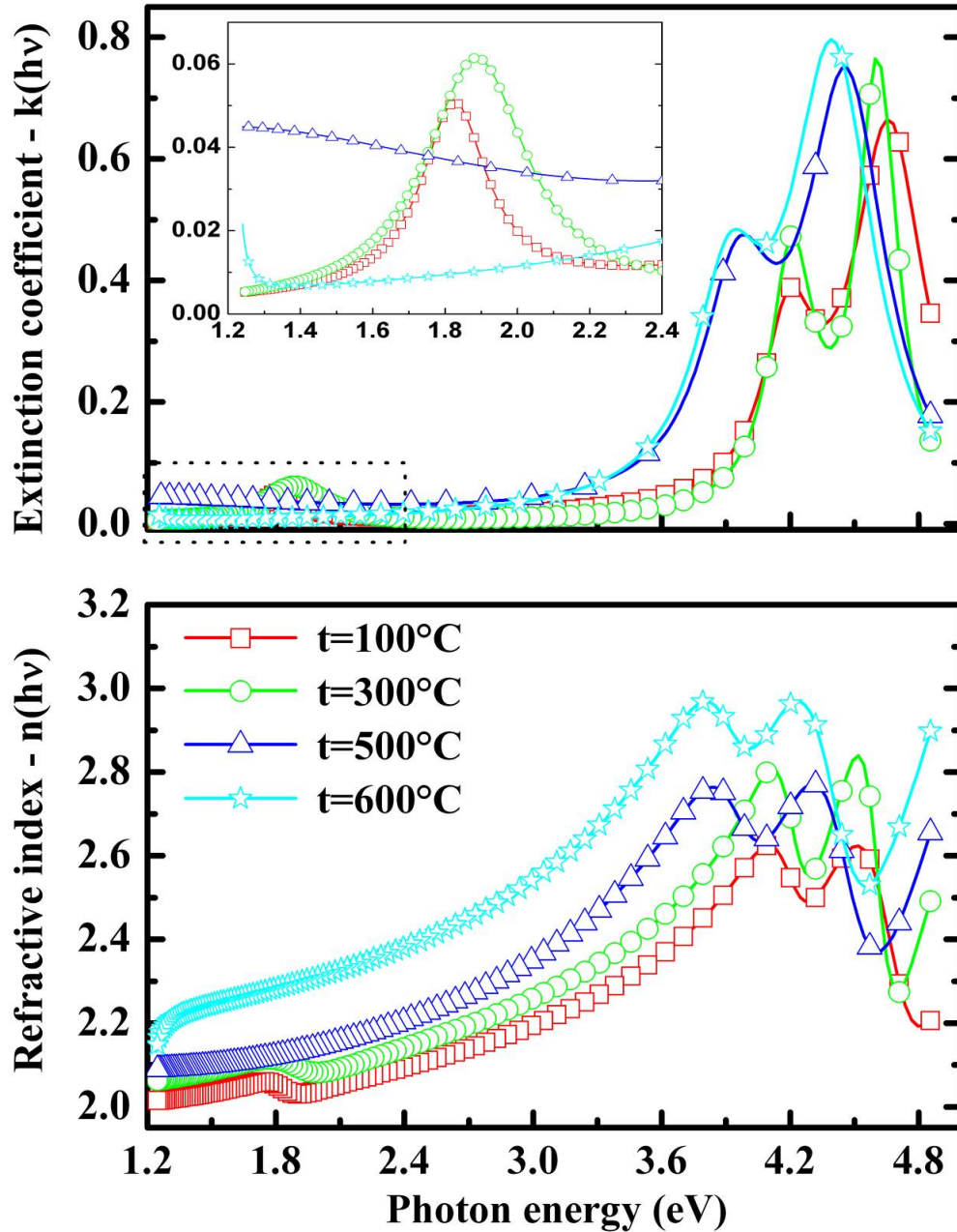


FIGURE 7c

Figure 7: Dispersion laws estimated for PZT layers deposited on intrinsic silicon wafer (a); float glass (b); float glass coated by ITO thin film (c), respectively. In all cases the refractive index increase versus annealing temperature as the PZT thin films change from amorphous to crystalline phase.

From the figure is possible to distinguish two absorption resonances in the Near-UV region, due to the presence of the two structural phases of PZT layers: the pyrochlore and ferroelectric perovskite phases [22, 23], respectively. It is possible also to observe a small peak in the NIR region that appears for high annealing temperature of PZT material deposited on ITO-coated float glass (see Figure 7(c) inset). This resonance is not observed in the dispersion curves relative to the other samples (float glass/PZT and silicon wafer/PZT). Such band seems to move towards lower energies for increasing annealing temperature, as shown in figure 8.

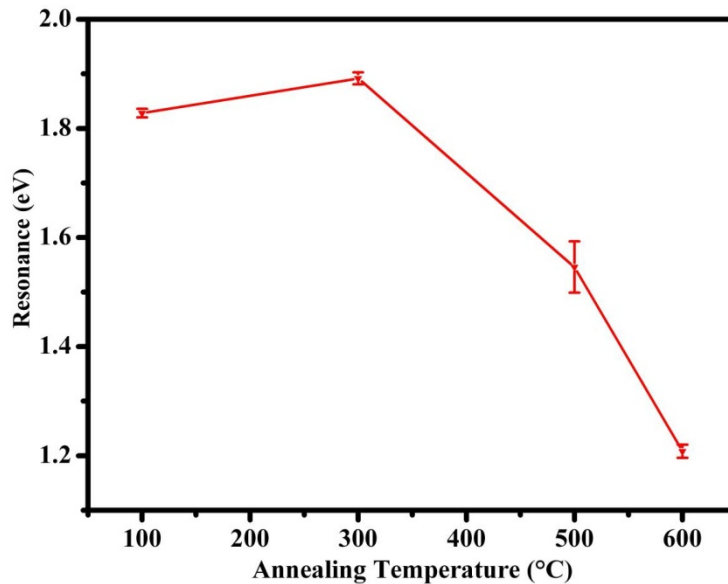


Figure 8: The peak position of the small resonance in the NIR region, characteristic of glass/ITO/PZT samples, as determined by a Lorentzian fit.

Some more information about the phenomena occurring in glass/ITO/PZT samples under high temperature treatments can be provided by the investigation of the elements redistribution as a consequence of the annealing.

Energy Dispersive X-ray (EDX) analysis has been performed using three different beam energy (10, 15, 30 kV). Figure 9 shows the compositional depth profile of some elements extracted from the EDX data for the Glass/ITO/PZT samples annealed at 600°C and 700°C. Depth profile data are obtained taking into account the primary electron penetration depth for the beam energy. Further details are reported in [36-38].

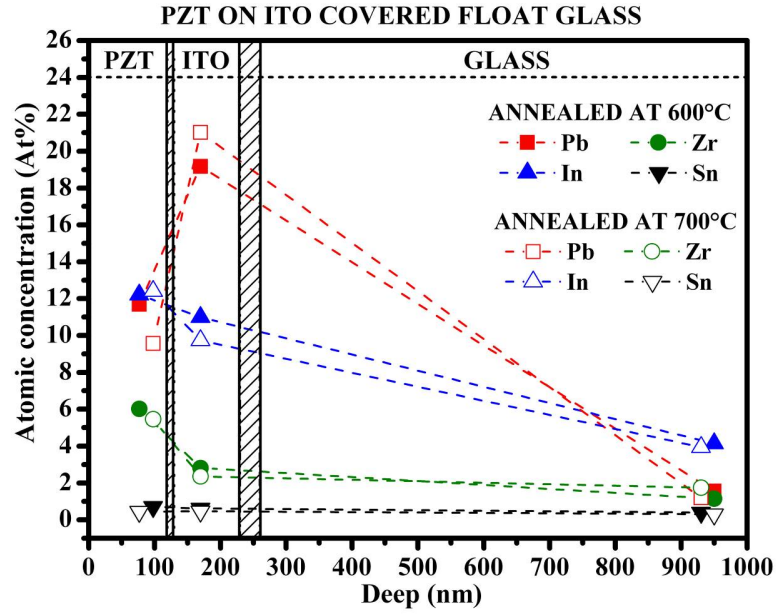


Figure 9: The compositional depth profile of some elements in the Glass/ITO/PZT samples annealed at 600°C and 700°C

From the figure 9 is evident that for high annealing temperatures lead and indium ions interdiffusion across the PZT–ITO interface increase and this probably gives an intermediate layer formation between the PZT and ITO layers. No-inter diffusion of PZT film elements is observed for the other samples (data not shown). Lead ions interdiffusion has been observed also in other experiments [39]. We can tentatively associate the NIR resonance feature to the formation of an “intermediate layer” having a peculiar charge distribution, which generates a potential barrier at the ITO/PZT interface. Similar to that observed is analogues systems [51]. Further necessary characterizations of this layer are under way.

The extinction coefficients of PZT thin films annealed at different temperatures have been used to estimate the optical band gap energies of the pyrochlore and perovskite phases. Moreover, the electron transitions gaps energies have been estimated by using the typical model used to describe an allowed direct transition [40].

If exciton formation is neglected, the form of the absorption coefficient α as function of photon energy $h\nu$ depend on the joint density of the states, $N(E)$, involving the band across the Fermi level. For simple parabolic bands and allowed direct transitions, the typical expression of the absorption coefficient $\alpha(h\nu)$, is:

$$(\alpha h\nu)^2 = A(h\nu - E_g^{opt}), \quad \text{with} \quad h\nu > E_g^{opt}$$

where E_g^{opt} is gap energy and A is a constant, proportional to the probability of electron transition between occupied and empty states [40]. The extinction

coefficients $k(\lambda)$, estimated by ellipsometry characterization, are used to calculate the absorption coefficient $\alpha(h\nu)$ versus photon energy $h\nu$ by using the wellknown formula:

$$\alpha(h\nu) = 4\pi \frac{k(h\nu)}{\lambda}$$

where h is the Plank constant and λ is the light wavelength.

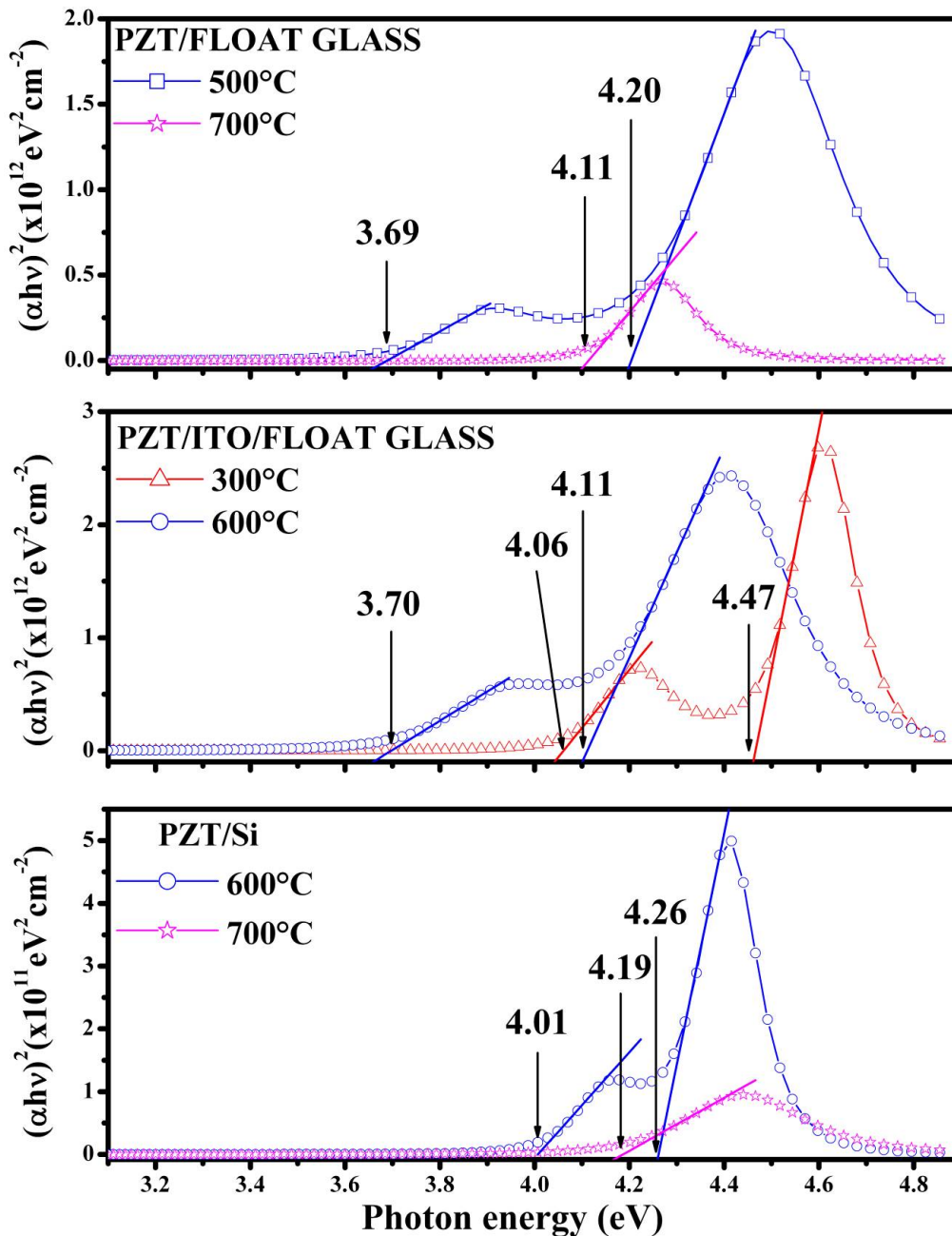


Figure 10: Optical band-gap energy has been extracted by linear fit of the function $(\alpha h\nu)^2$ immediately above the edge. The band gap is taken to be the intercept of the line estimate by linear fit with photon energy axis.

Figure 10 show the $(\alpha hv)^2$ functions versus photon energy hv , estimated by using the model previously described. We can extract the band gap by linear fit of the function $(\alpha hv)^2$ immediately above the edge for each absorption peak. The estimated band gap is the intercept of this line with photon energy axis. The optical band gaps energies estimated by using this linear extrapolation, are shown in figure 11 as function of the annealing temperature, and compared with the values of band-gap energies of the pyrochlore and perovskite phases reported from Okada, for PZT films produced by r.f. diode sputtering of a target with stoichiometric ratio Zr/Ti=52/48 [22].

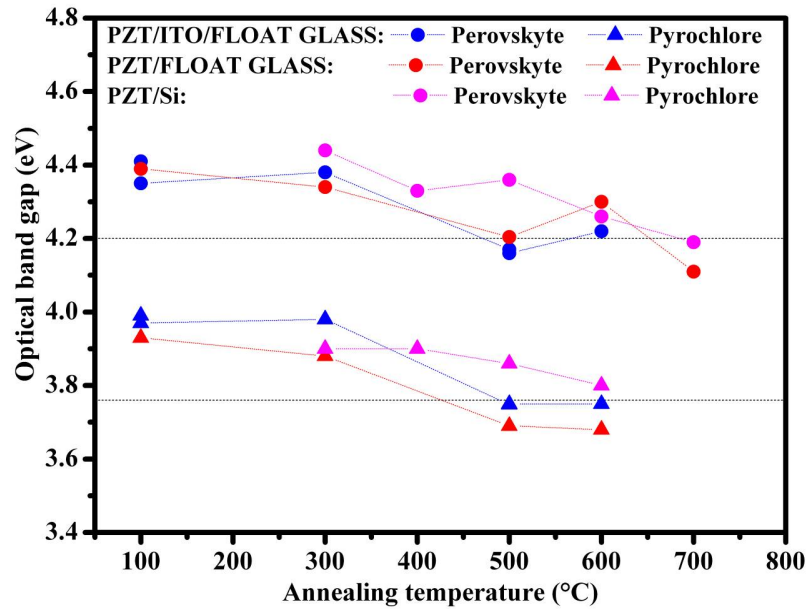


Figure 11: Optical band gap values as extracted from Fig. 10 data.

In that study, Okada estimated, by optical absorption measurements, that the optical band-gap for the pyrochlore phase was $E_g^{py} = 3.76 eV$, and for the perovskite phase was $E_g^{pv} = 4.21 eV$. Recent works show similar estimated values of the optical band gap energy for the pyrochlore and perovskite phases obtained by sol gel synthesis and r.f. sputtering [23,41,42].

Our estimated band-gap energy values are consistent with those reported in literature so that we can assign the lower values to pyrochlore phase and the higher ones to perovskite phase.

PZT layers obtained by different techniques have been studied, using spectrophotometry and spectroscopic ellipsometry techniques [22,23,41,43], in order to measure the optical band-gap energy and other optical properties, and it has been found that the gap-energy values are influenced by different experimental parameters: *i.e.* they depend on the deposition technique and on its peculiar parameters as well as on the zirconium and titanium stoichiometry [42-44]. In fact

the band-gap energy of the PZT films with perovskite structure decreases as Ti content increases, having its typical value 4.2 eV when the Ti fraction is between 0.45 and 0.55. These values are consistent with our investigations where the Ti content was 0.47.

Figure 12 shows the changes in the estimated PZT thickness during the thermal annealing processes. The thickness slowly decrease as the temperature increases from 100°C to 500°C and collapse to about the 50%, of its initial value when the temperature reaches 600/700 °C.

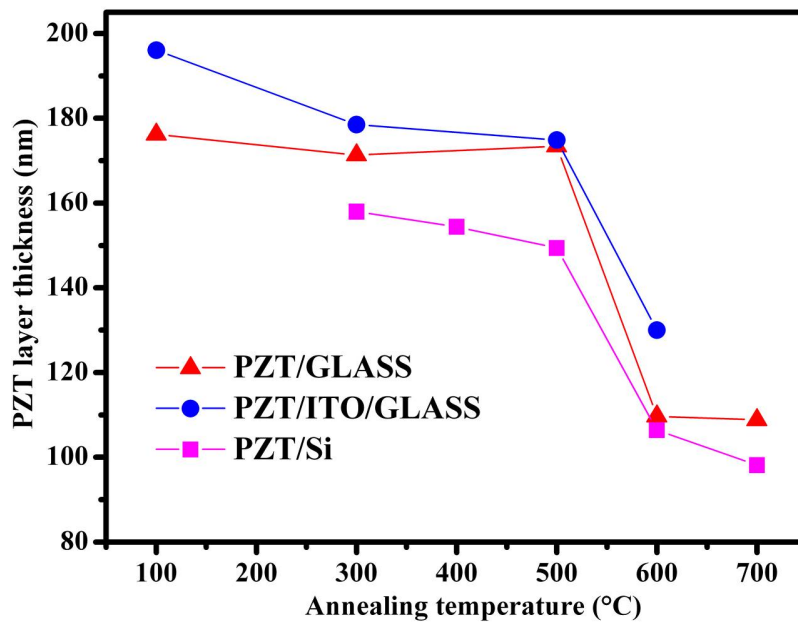


Figure 12: Evaluated PZT layer thickness for films deposited on various substrates.

The study of the PZT optical band-gap energies and thicknesses allows us to fully characterize the changes in morphological and structural properties with the annealing temperature.

Accordingly to our date the annealing temperature is lower than 600°C, the perovskite ($E_g^{opt} \approx 4.2eV$) and pyrochlore ($E_g^{opt} \approx 3.7eV$) phases are simultaneously presents. The optical band gaps energies slowly decrease towards the gap energy values reported in the literature when the annealing temperature increase from 100 to 600°C.

When the annealing temperature is higher than 600°C, the pyrochlore phase is completely converted in perovskite phase. In fact, the optical absorption relative to pyrochlore phase disappears (figure 10) when the annealing temperature is 700°C.

Note that the band gap evaluation as well as all the parameters evaluated from the ellipsometric measurements are missing for the glass/ITO/PZT samples heated at 700°C. The reason of this concerns the deformation of the samples surfaces induced by the different thermal expansion coefficients of the different layers [45].

During the heat treatments, the defects in the PZT layer decrease because the residual impurities (e.g. water, residual organic, etc.) coming from the sol-gel synthesis are throw out from the PZT lattice structures.

This description is consistent with some models that are able to describe the microstructure evolution of the PZT layers obtained by sol-gel synthesis [46-48].

The structure of the as-deposited PZT layer is amorphous but it is converted by the annealing processes into a polycrystalline structure [22, 47]. The sequence of pictures in the figure 13, obtained by the SEM instrument, show the morphological evolutions of PZT film deposited on ITO-coated float glass after annealing at different temperatures.

When the annealing temperature increases, flower-like shaped dendritic structures, called “rosetta” appear on the sample surface. Similar surface patterns has been observed on the float glass and silicon wafer substrates (images not shown). These structures show crystalline structure and ferroelectric properties [49]. The crystallization process occurring during high temperatures treatments modifies the electronic properties of the films: in fact, it has been observed that the optical band gap of amorphous PZT films is greater than polycrystalline ones [50].

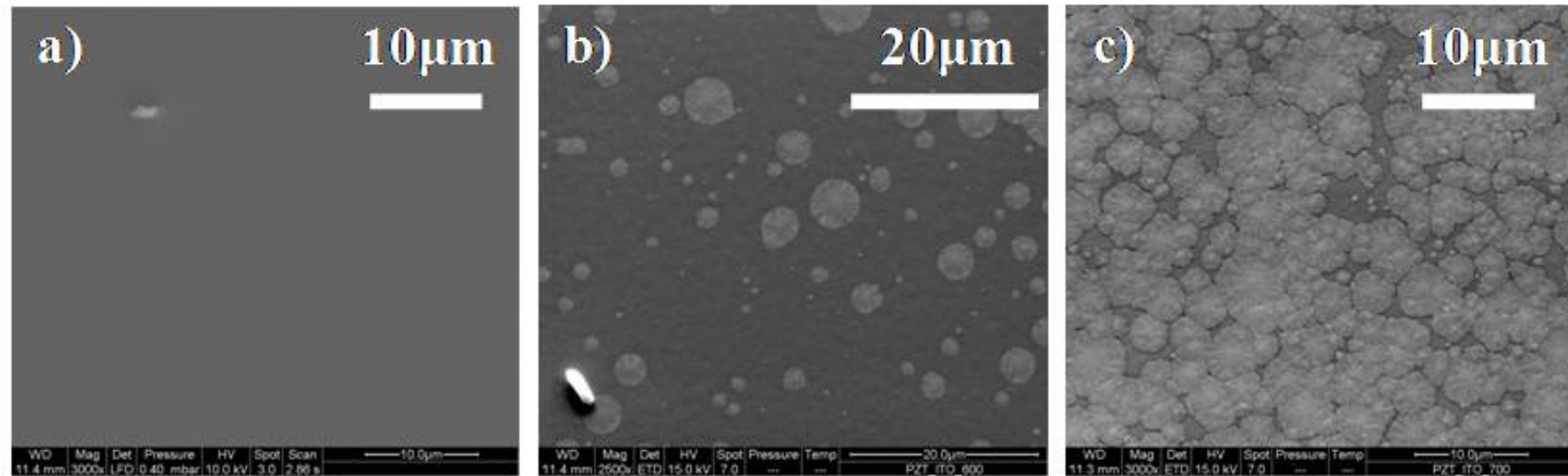


FIGURE 13

Figure 13: SEM images of the PZT deposited on ITO covered glasses annealed at (a) 400 °C (b) 600 °C (c) and 700 °C. The morphological evolution as function of the annealing temperature can be seen. It possible to observe the typical microscopic “rosetta” structure (c).

4. Discussion

We used the optical model estimated for the uncoated substrate, at every temperature, to describe the PZT behavior annealed at the same temperature. This hypothesis of an independent thermal evolution allows us to simulate, with good approximation, all the measured ellipsometric angles acquired on different samples. We obtained good results also with the optical models of the system glass/ITO/PZT.

The optical models of the PZT layers deposited on float glasses, silicon wafers and ITO-coated float glasses, estimated for each annealing temperature, show that structural properties modifications of these thin films, obtained by sol-gel synthesis on different substrates, are similar.

The heating process allows the elimination of water molecules and residual organic impurities from the PZT layers, even for lower annealing temperatures. The as-deposited PZT layer on different substrates is amorphous, but with increasing annealing temperatures a transformation toward a crystalline phase occurs and consequently an increase in the optical density is observed.

This is good agreement between the changes in the optical band gap energy estimated for the samples deposited on the three substrates. We have observed that the optical band-gap energies of the perovskite and pyrochlore phases are simultaneously presents below 600 °C while for higher temperature the pyrochlore phase was completely transformed in perovskite phase.

The optical band gap energy decrease towards the typical values of the band gap energy of the pyrochlore phase (3.7eV) and perovskite phases (4.2eV) when the annealing temperature is between 100 - 500 °C.

The slowly decrease of the measured optical band-gap energies, towards the gap energies reported in literature, can be justified taking into account two different effects: the decrease of defects density and the corresponding increase of polycrystalline phase.

During these structural modifications, caused by the annealing process, the thickness of the PZT layers decrease slowly for temperature between 100-500 °C, and collapses of the 50% when the temperature is near to 600°C. This structural reorganization indicates the transition from amorphous to polycrystalline phase as it confirmed by the SEM images.

The ellipsometry characterization allows us to observe an interesting effect between PZT layers and substrates. The dispersion laws of PZT deposited on ITO covered float glasses show a small absorption resonance in the near IR region. This one is not observed in the samples of PZT deposited on float glass and intrinsic silicon wafer substrates. We suggest that this absorption resonance depends on the interfacial effects between ITO thin films and PZT material.

5. Conclusion

Lead Zirconate-Titanate (PZT) thin films, with stoichiometric ratios indicated by the formula $\text{PbZr}_{0.53}\text{Ti}_{0.47}\text{O}_3$, were obtained by hybrid (carboxylate and alkoxides) sol-gel route and spin coating deposition of the obtained mother solution on different substrates (float glasses, ITO coated float glasses, and intrinsic silicon wafers) and the effects of different thermal treatments on the structural and morphological properties of PZT films and substrates have been investigated. Preliminary investigations on the bare substrates indicate that the float glasses and silicon wafers properties did not change with the annealing. On the contrary, changes of structural and morphological properties were found for ITO thin films because the annealing favors the thermal adsorption of the atmospheric oxygen. Consequently we measured an increase of the sheet resistance and decrease of the optical band gap, in good agreement with the Burstein-Moss model. The substrates properties and their changes under annealing are not appreciably influenced by the presence of deposited PZT layers, because these layers are not a significant barrier for the oxygen diffusion into the substrate materials.

The EDX measurement show an interdiffusion of lead and indium ions, across the PZT-ITO interface, generating probably a peculiar intermediate layer between the PZT and ITO layers. The new band detected on the NIR region can be attributed to the charge distribution in this region. Structural and chemical characterizations of such layer are in progress.

Acknowledgements

The authors wish to thank Giuseppe De Santo and Tiziana Barone for their essential contribution during the PZT thin layers preparation, Emanuela Bruno, Giovanni Desiderio and Salvatore Abate for the SEM imaging, Salvatore Marino and Maria P. De Santo for the scientific discussion.

References

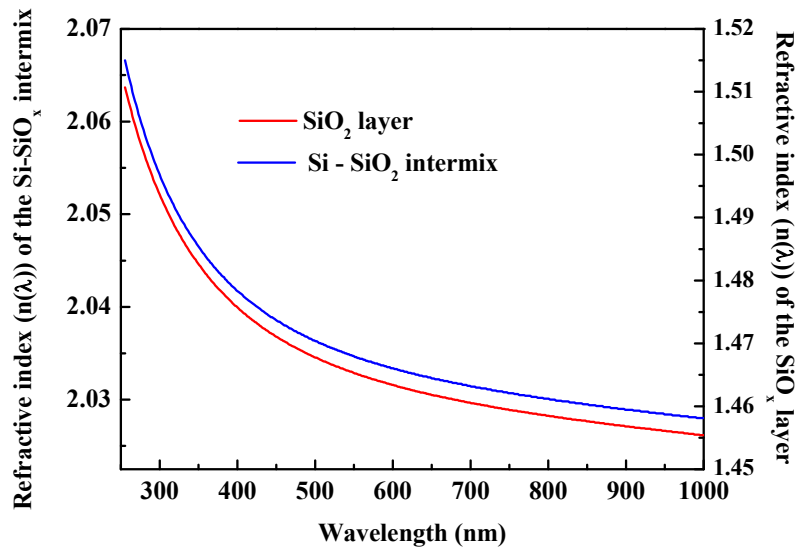
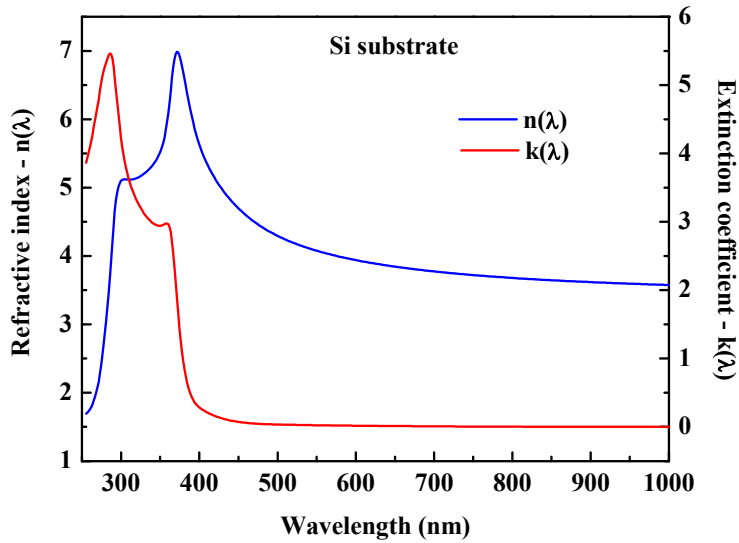
- [1] D. Damjanovic "Ferroelectric, dielectric and piezoelectric properties of ferroelectric thin films and ceramics. Laboratory of ceramics", (Swiss Fed. Inst. of Techn.-EPFL, 1015 Lausanne, Switzerland, 1998).
- [2] K. Uchino, *Ferroelectric Devices* (Marcel Dekker, New York, 2000).
- [3] Y. Xu, *Ferroelectric and their Applications* (North-Holland, Tokyo, 1991).
- [4] B. Li, P. T. Lai, G. Q. Li, S. H. Zeng, M. Q. Huang, *Smart Mater. Struct.* **9** (4), (2000) 498-501.
- [5] S. Marino, M. Castriota, V. Bruno, E. Cazzanelli, G. Strangi, C. Versace, N. Scaramuzza, *J. Appl. Phys.* **97**, (2005) 013523-1.
- [6] M. Castriota, S. Marino, C. Versace, G. Strangi, N. Scaramuzza, E. Cazzanelli, *Molecular Crystals and Liquid Crystals*, **429**, (2005) 237.
- [7] G. Strangi, E. Cazzanelli, N. Scaramuzza, C. Versace, R. Bartolino, *Phys. Rev. E* **62**, (2000) 2263.
- [8] E. Cazzanelli, S. Marino, V. Bruno, M. Castriota, N. Scaramuzza, G. Strangi, C. Versace, R. Ceccato, G. Carturan, *Solid State Ionics* **165**, (2003) 201.

- [9] V. Bruno, M. Castriota, S. Marino, C. Versace, G. Strangi, E. Cazzanelli, N. Scaramuzza, *Molecular Crystals and Liquid Crystals* **441**, (2005) 27.
- [10] S. Marino, M. Castriota, G. Strangi, E. Cazzanelli, N. Scaramuzza, *J. Appl. Phys.* **102**, (2007) 013112-1.
- [11] T. Minami, *Semicond. Sci. Technol.* **20**, (2005) S35–S44.
- [12] R. W. Schwartz, T. Schneller and R. Waser, *C. R. Chim.* **7**, (2004) 433-461.
- [13] G. Yi, Z. Wu, M. Sayer, *J. Appl. Phys.* **64**, (1988) 2717-2723.
- [14] C. R. Martin, I. A. Akasay, *J. Phys. Chem. B* **107**, (2003) 4261-4268.
- [15] Y. J. Song, Ph.D Thesis, Virginia Polytechnic Institute and State University, (Blacksburg, Virginia, USA, 1998).
- [16] R. A. Assink, R. W. Schwartz, *Chem. Mater.* **5**, (1993) 511-517.
- [17] A. S. Mischenko, Q. Zhang, J. F. Scott, R. W. Whatmore, N. D. Mathur, *Science* **311**, (2006) 1270-1271.
- [18] Genell Med auf Floarglas - Balzers Thin Films Prod. ID. BD051149, BATCH 1400-655-(1999)
- [19] H. G. Tompkins, E. A. Irene, “Handbook of Ellipsometry”, William Andrew Publishing, Springer (2005).
- [20] C. M. Herzinger, B. Johs, W. A. McGahan, J. A. Woollam, W. Paulson, *J. Appl. Phys* **83** (6), (1998) 3323.
- [21] D. E. Aspnes, *Thin Solid Films* **89**, (1982) 249.
- [22] A. Okada, *J. Appl. Phys.* **48** (7) (1977) 2905-2909.
- [23] H. Lee, Y.S. Kang, S-J. Cho, B. Xiao, H. Morkoc, T. D. Kang, S. Lee J. Li, S-H. Wei, P.G. Snyder, J. T. Evans, *J. Appl. Phys.* **98**, (2005) 094108.
- [24] J. C.C. Fan, F. J. Bachner, and G. H. Foley, *Appl. Phys. Lett.* **31** (11), (1977) 773-775.
- [25] J. C.C. Fan, J. B. Goodenough, *J. Appl. Phys.* **48** (8), (1977) 3524-3531.
- [26] I. Hamberg, C.G. Granqvist, *J. Appl. Phys.* **60** (11) (1986) R123-R159.
- [27] F.O. Adurodija, L. Semple, R. Bruning, *J. Mater. Sci.* **41**, (2006) 7096-7102.
- [28] F.O. Adurodija, H. Izumi, T. Ishihara, H. Yoshioka, M. Montoyama, and K. Murai, *J. Vac. Sci. Technol. A* **18** (3), (2000) 814-818.
- [29] M. Buchanan, J.B. Webb, and D.F. Williams, *Appl. Phys. Lett.* **37** (2), (1980) 213-215.
- [30] M. Berder, W. Seelig, C. Daube, H. Frankenberger, B. Ocker, J. Stollenwerk, *Thin Solid Films* **326**, (1998) 72-77.
- [31] E. Burstein, *Phys. Rev.* **93**, (1954) 632-633.
- [32] J.R. Bellingham, W.A. Phillips and C.J. Adkins, *J. Phys.: Condens. Matter* **2**, (1990) 6207-6221.
- [33] Y. Matsui, M. Suga, M. Hiratani, H. Miki and Y. Fujisaki, *Jpn. J. Appl. Phys.* **36** (2), (1997) 1239-1241.
- [34] S.G. Lee, K-T. Kim, Y.H. Lee, *Thin Solid Films* **372**, (2000) 45-49.

- [35] Y. J. Song, H.H. Kim, S.Y. Lee, D.J. Jung, B. J. Koo, N. W. Chang, C. J. Kim, K. Kim, *Integrated Ferroelectrics* **31**, (2000) 351-358.
- [36] K. Kanaya and S. Okayama, *J. Phys. D: Appl. Phys.*, **5**, (1972) 43-58.
- [37] T. Suzuki, N. Endo, M. Shibata, S. Kamasaki, T. Ichinokawa, *J. Vac. Sci. Technol. A* **22** (1), (2004) 49-52.
- [38] J. I. Goldstein, H. Yakowitz, "Practical scanning electron microscopy, Electron and Ion Microprobe Analysis" (Plenum Press, New York and London 1975).
- [39] D.P. Vijay, S.B. Desu, *J. Electrochem. Soc.* **140** (9), (1993) 2640-2645.
- [40] N.F. Mott, E.A. Davis, "Electronic processes in non-crystalline materials", second edition (Clarendon press, Oxford - 1979).
- [41] Z. Hu, Z. Huang, Z. Lai, G. Wang, J. Chu, *Thin solid films* **437**, (2003) 223-229.
- [42] S. Yang, D. Mo and X. Tang, *Ferroelectrics*, **287**, (2003) 35-46.
- [43] M.P. Moret, M.A.C. Devillers, K. Worhoff, P.K. Larsen, *J. App. Phys.* **92** (1), (2002) 468-474.
- [44] S. Yang, D. Mo and X. Tang, *J. of Mater. Sci.* **37**, (2002) 3841-3845
- [45] V. Craciun, D. Craciun, X. Wang, T. J. Anderson, R. K. Singh, *J. Optoelectronics and Adv. Mat.* **5** (2), (2003), 401-408.
- [46] A. Wu, P. M. Vilarinho, I. M. M. Salvado, and J. L. Baptista, *J. Am. Ceram. Soc.* **83** (6), (2000) 1379-1385.
- [47] S. Trolrier-McKinstry, J. Chen, K. Vedam, and R. E. Newnham, *J. Am. Ceram. Soc.* **78** (7), (1995) 1907-1913.
- [48] C. H. Peng, S. B. Desu, *J. Am. Ceram. Soc.* **77** (6), (1994) 1486-1492.
- [49] E. Bruno, M. P. De Santo, M. Castriota, S. Marino, G. Strangi, E. Cazzanelli, N. Scaramuzza, *J. App. Phys.* **103**, (2008) 064103.
- [50] S. Yang, Y. Zhanget, D. Mo, *Materials Science and Engineering B* **127**, (2006) 117-122.
- [51] V. M. Voora, T. Hofmann, M. Brandt, M. Lorenz, M. Grundmann, N. Ashkenov, and M. Schubert, in press on *J. Electron. Mater* (2008).

3.2.1. Appendix A. Optical model used for the intrinsic Silicon wafer

In the last section, we had showed some experimental results concerning the effect of annealing properties on the intrinsic silicon wafer substrates. The optical model built by C. M. Herzinger [5], is shown in this appendix section. The multilayer structure and the dispersion laws of the layers are showed in Fig. 3.2, while some fit elaborations are showed in the Fig. 3.3.

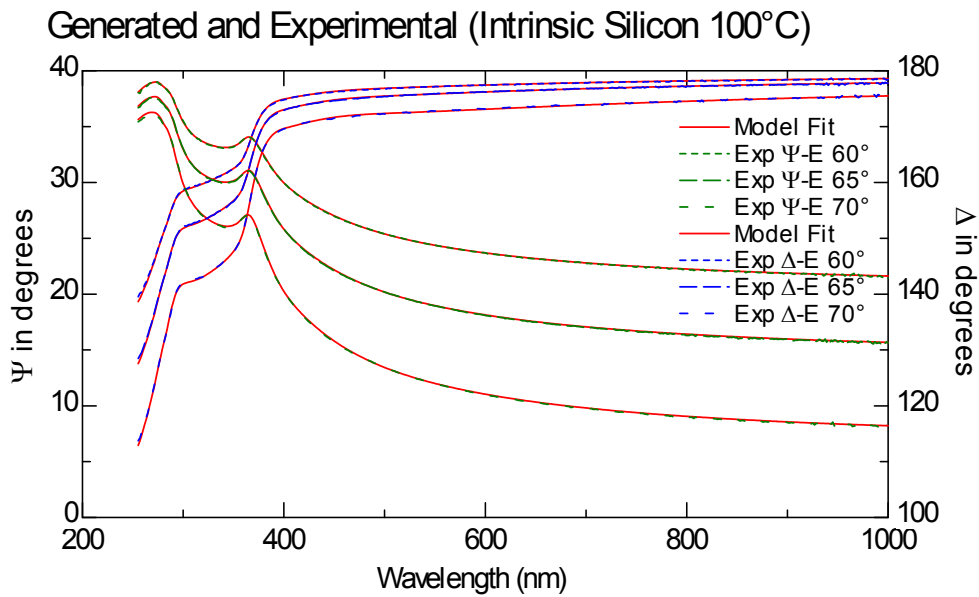


2	sio2 layer	27.059 nm
1	si - sio2 intermix	0.519 nm
0	si substrate	1 mm

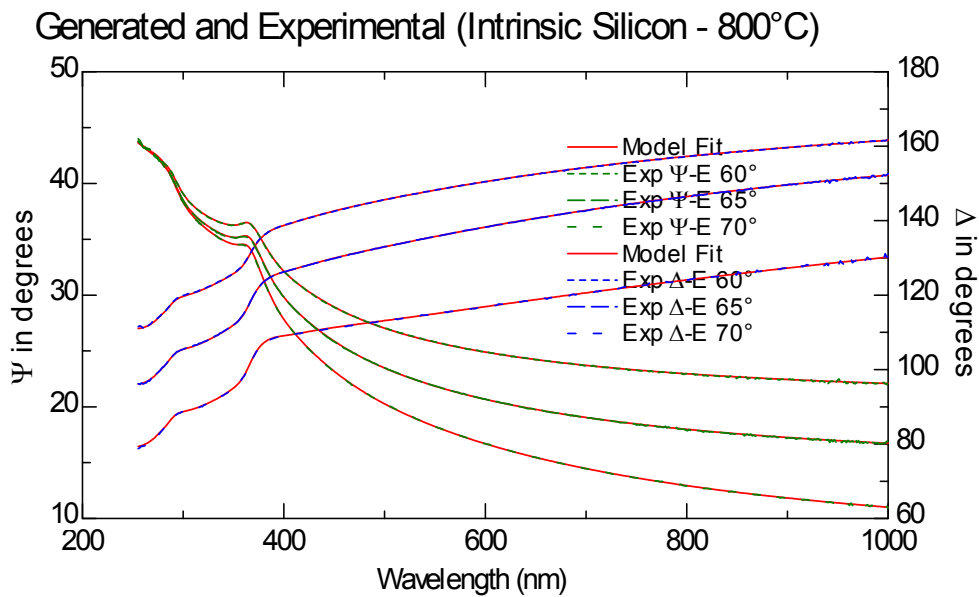
(c)

Fig.3.2. Intrinsic silicon wafer optical model. C. M. Herzinger [4]. (a) dispersion law of silicon substrates; (b) the refractive index SiO₂ layer (red line), and the Si-SiO₂ intermix layer (blue line). (c) multilayer structure. The intermix layer thickness remains constant during thermal annealing (data not shown).

Figure 3.3



(a)



(b)

Fig. 3.3. Generated and experimental ellipsometry angles estimated for intrinsic silicon wafer annealed at 100°C (a), and at 800°C (b).

3.3. ITO/PZT interface effect.

(Application in the asymmetric nematic liquid crystal cells)

EFFECTS OF THERMAL TREATMENTS ON STRUCTURAL AND OPTICAL PROPERTIES OF LEAD ZIRCONIUM TITANATE THIN FILMS OBTAINED BY SOL GEL TECHNIQUE

Submitted to THIN SOLID FILMS (2008)

Marco Castriota, Stefano D'Elia, Salvatore Marino, Enzo Cazzanelli, Nicola*

Scaramuzza, Carlo Versace and Roberto Bartolino.

CNR-LICRYL Laboratory and CEMIF.CAL, Department of Physics, University of
Calabria, via P.Bucci 31C, Rende (CS), I-87036 (ITALY).

CORRESPONDING AUTHOR: castriota@fis.unical.it

Thin films of Lead Zirconate Titanate (PZT) have been obtained by a modified sol-gel route on float glass and Indium Tin Oxide (ITO) covered float glass substrates. Different thermal treatments have been performed on the deposited films, in the range between 100 to 700 °C. The optical properties of these deposited films have been investigated by using spectroscopic ellipsometry. The growth of two different crystal phases, pyrochlore and ferroelectric perovskite, as a function of annealing temperature, has been associated to the changing optical absorption spectra. Moreover, a specific resonance, attributed to a particular charge distribution at the interface, has been detected when thin PZT films are deposited on ITO substrates. Finally, the performances of these films in rectifying the electro-optical response of asymmetric nematic liquid crystal cells have been tested.

Introduction

Electro-optic ceramics are considered very interesting materials for their technological applications such as: infrared detectors, electro-optic modulators, light-beam switching shutters, waveguides, ferroelectric random access memories (FRAM), microelectromechanical actuators.¹⁻³ Among these materials, lead zirconate titanate (PZT) received great attention because of its ferroelectric and piezoelectric properties, associated to high optical transmittance, low reflectance and strong electro-optic Kerr effect.⁴

Due to their good optical properties, PZT thin films have been used recently as electrodes in asymmetric nematic liquid crystal cells (ANLCC), where they induce a polarity-sensitive electro-optical response of liquid crystal layers.⁵ Such effect has been previously obtained by inserting in ANLC cells thin films of metal oxides like WO_3 , and V_2O_5 , well-known for their applications to electrochromism; in fact the combination of electronic and ionic conductivity allowing for the electrochromic effect explains also the occurrence of peculiar charge distributions at the interfaces of these films inside ANLC cells, inducing internal electric fields which can modify the electro-optical effect of external applied fields.⁶⁻⁹

In the case of inserted PZT films a different mechanism should be invoked: the internal field producing the electro-optical rectified response should be related to the polarization of ferroelectric PZT.⁵

Thin films of lead zirconate titanate can be obtained by different techniques. In this work, they have been obtained by sol gel synthesis, since it results to be one of the more versatile techniques to obtain large area electrodes, necessary for some technological development.

The synthesis method reported in this work represent an improvement of the procedures used in previously works¹⁰⁻¹², obtained by modifying some aspects such as temperature and processing time. Moreover, a great attention has been given to the study of thermally induced transformation of the as-deposited films. The PZT films deposited on different substrates have been subject to annealing processes at several different temperatures, to evaluate the effect of such treatments on the PZT structural morphology. The same kind of thermal treatment have been also performed on the substrates without PZT films, to discriminate between thermally induced transformations of PZT films and the ones of the substrates.

To gain information about the electronic and optical properties of the different systems film-substrate obtained by the thermal treatments, the ellipsometric spectroscopy technique has been used. The optical models necessary to fit the ellipsometric data of both the substrates and the PZT layers have been chosen taking into account the main physical and chemical properties of the investigated layers. The float glass substrates were described by an optical Cauchy model for the dispersion law of the refractive index and by the Urbach model for the extinction coefficient, while a Lorentz optical model was used for both the annealed ITO thin films and PZT samples.¹³

The ITO characterization has been performed by using different models for both ITO bulk and ITO rough surface. The bulk layer has been simulated by using a linear sum of Drude oscillators (conductive properties) and Lorentz oscillators (dielectric properties).¹³ The optical properties due to roughness of the surface layer were simulated by using the Bruggeman Effective-Medium Approximation (EMA), which combines a ITO layer containing a Lorentz oscillator (ϵ_{ITO}) and a layer made by voids (ϵ_{void}).¹⁴

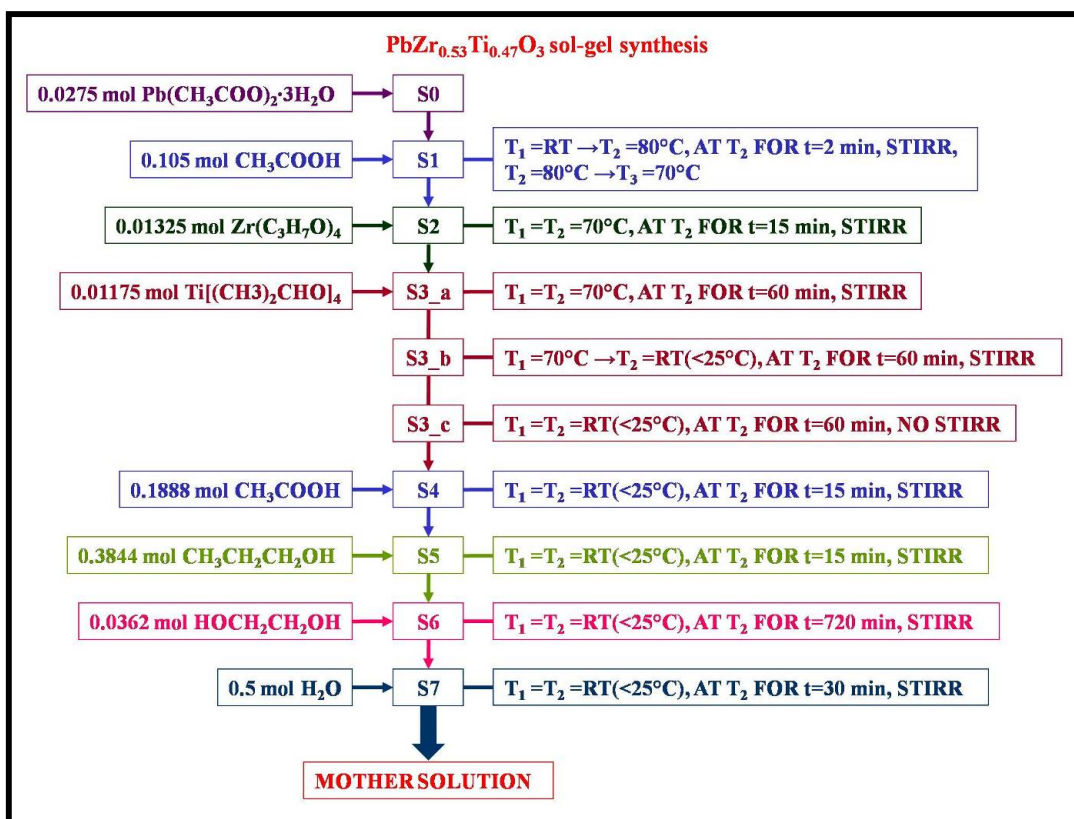
Experimental

PZT sol- gel synthesis and thin films deposition:

Lead Zirconate Titanate $\text{PbZr}_{0.53}\text{Ti}_{0.47}\text{O}_3$ (PZT) thin films, were obtained by hybrid (carboxylate and alkoxides) sol gel route and spin coating deposition of the obtained mother solution on float glasses and ITO (indium tin oxide)-glasses (sheet resistivity $\square_s = 20 \Omega/\square$, Unaxis GmbH and $R_{\text{sh}}=25\Omega/\square$, Balzers FAB) substrates.

The reagents (all supplied by Sigma-Aldrich) used are Lead(II) acetate trihydrate ($\text{Pb}(\text{CH}_3\text{COO})_2 \cdot 3\text{H}_2\text{O}$, 99.999 %), Zirconium(IV) propoxide solution ($\text{Zr}(\text{C}_3\text{H}_7\text{O})_4$, 70 wt. % in 1-propanol), Titanium(IV) isopropoxide ($\text{Ti}[(\text{CH}_3)_2\text{CHO}]_4$, 99.999 %), Acetic acid glacial (CH_3COOH , 99.99+ %), n-Propanol anhydrous ($\text{CH}_3\text{CH}_2\text{CH}_2\text{OH}$, 99.7%), Ethylene glycol anhydrous ($\text{HOCH}_2\text{CH}_2\text{OH}$, 99.8%). Bi-distilled water has been used when necessary.

The PZT mother solution sol-gel synthesis is schematized in Scheme 1 where the amount of the reagents and the operational conditions are indicated.



Scheme 1. PbZr_{0.53}Ti_{0.47}O₃ (PZT) mother solution sol gel synthesis with the number of mole of each reagent and the procedure at each stage indicated. (RT indicates room temperature).

Except for the solution S7 (Scheme 1), the synthesis has been carried out under Argon atmosphere, inside an “humidity free” Glove Box, with water and oxygen concentrations lower than 0.01 ppm. The glove box has been equipped by two magnetic stirrers (thermal controlled) and by a technical balance. The chosen amount of Pb(CH₃COO)₂·3H₂O has been calculated in such a way to obtain a 10% excess in mole of lead, which compensate the lead loss (as PbO) which occurs during the process. The amount of acetic acid used, in this work, is such that the total mol number of the acetic acid present in solution is twenty-five times the titanium mol number.¹⁰⁻¹² As it can be seen in Scheme 1, in order to obtain stable mother solution, the Pb(CH₃COO)₂·3H₂O have been dissolved in CH₃COOH, (Scheme 1), making the solution indicated as S1) by stirring and heating the solution up to 80°C for fifteen minutes. After two minutes at 80 °C, the heater was set at 70°C and when the solution was cooled down to the latter temperature the Zr(C₃H₇O)₄ solution, has been added (Scheme 1, solution S2). Later on, after fifteen minutes, when the temperature is again 70°C and all the particles eventually formed are dissolved, the

Ti[(CH₃)₂CHO]₄ was added (Scheme 1, solution S3_a). The resulting solution has been stirred for one hour at 70°C, for another hour on a cold stirrer (room temperature) (Scheme 1, solution S3_b) and left for another hour on a room temperature stage without stirrer (Scheme 1, solution S3_c).

When the solution is cooled down to room temperature, the rest part of CH₃COOH has been added (Scheme 1, solution S4) and the solution has been left to stir for 15 minutes. At this point the CH₃CH₂CH₂OH (Scheme 1, solution S5) has been added and again stirred for others 15 minutes.

At this time, the HOCH₂CH₂OH (Scheme 1, solution S6) has been added in order to obtain homogenous film (1 ml of HOCH₂CH₂OH for each 10 g Pb(CH₃COO)₂·3H₂O)¹⁰⁻¹² and then the solution has been sealed with parafilm and left to stir for one night.

Finally, the solution has been removed from the glovebox and 9 ml of bidistilled water have been added (Scheme 1, solution S7) before the spin coating.

The float glass and the ITO glasses substrates have been previously ultrasonically cleaned^{5,6} and an SC10 CaLCTec s.r.l. spin coater has been used for the deposition. PZT thin films have been obtained at 1200 rpm for 25 s. Such films have been placed on a hot plate for 5 minutes at 300°C.

Later on, the films were subjected, for an hour, to different single thermal treatment in an oven in temperature range between 100 °C and 700 °C, each one separated by 100°C step.

Spectroscopic ellipsometry:

The optical characterization of substrates and thin film samples was performed by using the Spectroscopic Ellipsometry (SE) technique. The VASE M2000F (J.A. Woollam) rotating compensator ellipsometer (RCE) was used in the 250-1000 nm wavelength range. The ellipsometric spectra have been collected at different incident angles to improve the accuracy of layer modelling.

The structural and morphological properties have been estimated by using multilayer optical models compatible with the ellipsometric experimental results. Each layer has been depicted by an optical model whose fitting parameters were both thickness and its complex dispersion law¹³.

The optical models together with the best fitting values have been calculated by WVASE32 application using the nonlinear Levenberg-Marquardt algorithm, which determines the minimum value of the Mean Square Error (MSE) which is a measure of the likelihood of the fit ¹³.

Electro-optical responses collected by ANLC cells:

The ANLC cells have been obtained by following the same procedure described before.⁵⁻⁹ The ITO-coated glasses were used in ANLC cells as counter electrodes with respect to the PZT samples which were the working electrodes.

The electro-optical responses have been obtained by using a polarizing microscope Axioskop Pol (Zeiss). The transmitted light intensities have been collected by using a large area silicon photodiode (Hamamatsu) mounted on the polarizing microscope. The electrical signals proportional to the light intensities were collected by a digital oscilloscope (Tektronics, Mod. TDS 784). White light (the bulb of the microscope) have been used as light source. Without any applied voltage the maximum of the transmitted light it is obtained, since the liquid crystal is in planar alignment. When the external voltage is applied the liquid crystal switches toward the homeotropic alignment and simultaneously the light collected by the photodiode decreases.

Results and Discussion

The PZT layer has been simulated by three Lorentz oscillators to generate its pseudo-dielectric functions. When the PZT was placed on ITO covered float glass (Table 1), the introduction of a further Lorentz oscillator was necessary to generate a pseudo-dielectric function well fitting the ellipsometric experimental data. The surfaces roughness of PZT films has been simulated by using the Bruggeman EMA models with mixture of PZT layer and void, in similar way to the procedure applied to ITO substrates, obtaining as final result an effective dielectric function of the PZT roughness.

	Optical Models			
	(a)	(b)	(c)	(d)
Layer 1	Float Glass 1.1 mm	Float Glass 1.1 mm	Float Glass 1.1 mm	Float Glass 1.1 mm
Layer 2	/	ITO 85 ÷ 90 nm	PZT	ITO 85 ÷ 90 nm
Layer 3	/	Surface Roughness (EMA Model) 10 ÷ 20 nm	Surface Roughness (EMA Model)	Surface Roughness (EMA Model) 10 ÷ 20 nm
Layer 4	/	/	/	PZT
Layer 5	/	/	/	Surface Roughness (EMA Model)

Table 1. Description of the optical models used to characterize the samples and substrates annealed at the different temperatures.

The dispersion laws of the optical constants, estimated for the float glasses annealed at different temperatures, are shown in Figure 1. It can be seen that the dispersion law for the float glasses substrates is not affected by the thermal annealing, while on the contrary the optical investigation performed on the ITO covered float glasses shows that the optical properties of such substrate depend on the annealing temperature (Figure 1). The evaluated ITO thickness has small changes with temperature.

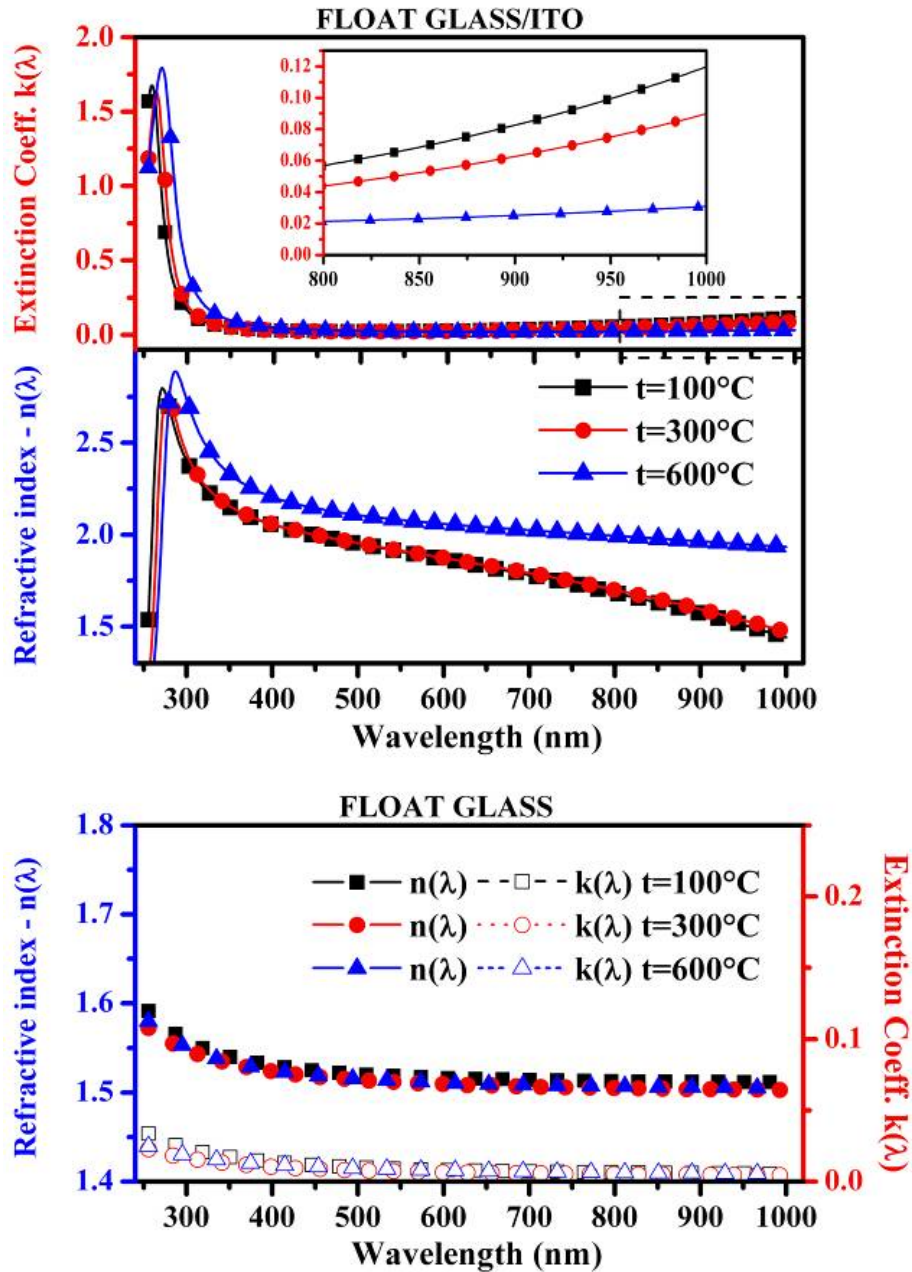


Figure 1. Dispersion laws estimated by using the multilayer optical models described in Table 1 for the float glasses and the ITO covered float glasses substrates annealed at different temperatures. The enlargement of the NIR spectra (on the top) shows the reduction of carrier concentration as well as the annealing temperature increases (Drude theory for free carriers).

The typical model used to describe the conductivity of the ITO takes into account the carrier density determined both by the oxygen vacancies and by the doping tin atoms, acting as electron donors when the tin oxidation state is (IV), as in SnO_2 .¹⁵⁻¹⁷ Of course, the annealing treatment, performed in oxidizing atmosphere, promotes the

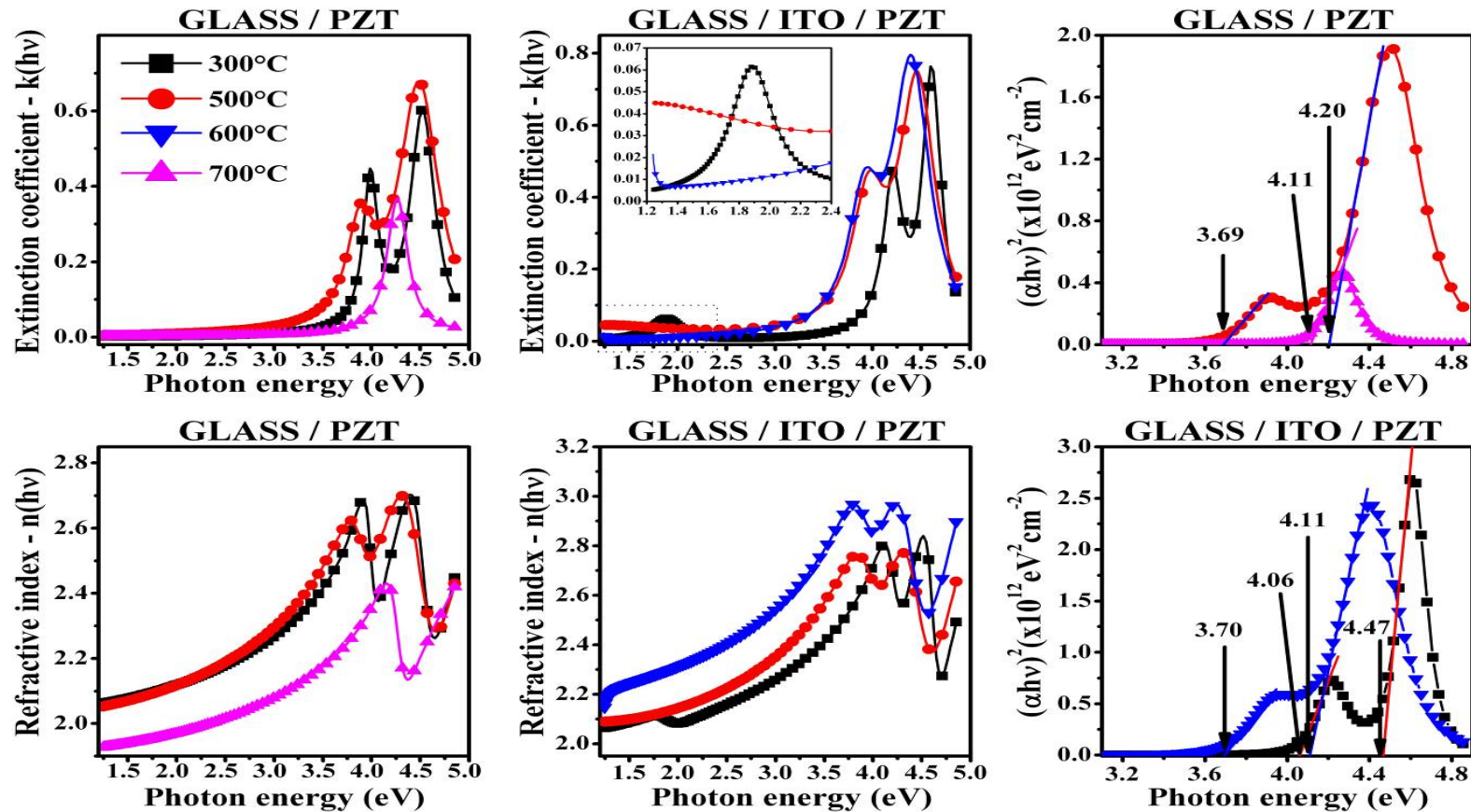
oxidation of the layer (reducing the oxygen vacancies and consequently reducing the amount of the charge carriers) increasing the resistivity of the ITO layers.

The presence of the PZT layer does not change appreciably the oxidation phenomena for the ITO layer. In fact, different experimental observations on the ferroelectric PZT thin films, obtained by sol-gel synthesis and deposited on various substrates, show that these films are not acting as barrier for the atmospheric oxygen which can perform the oxidation of the ITO layer^{18,19}. Thus, it is possible to assume that, during the thermal processes, the changes in structural and morphological properties of the substrates are only slightly affected by the presence of PZT thin layers.

The fitting procedure were performed by using the optical models obtained for the substrates at each temperature, maintaining the same fit parameters relative to the substrates, estimating only the fitting parameters of the PZT layers.

The estimated dispersion laws of PZT layers annealed at different temperature and on the different substrates are shown in Figure 2, where it is possible distinguish two absorption resonances in the Near-UV region. These bands are assigned to the presence of the two structural phases of PZT layers: the pyrochlore and ferroelectric perovskite phase.^{20,21}

Figure 2. On the left and on the middle: dispersion laws estimated for PZT layers deposited on float glasses and ITO float glasses substrates; on the right: optical energies band-gaps extracted by linear fit of the function $(\alpha h\nu)^2$ immediately above the edge (see text).



Moreover, a new small peak in the NIR region occurs for the PZT layer deposited on ITO coated glass, subjected to the higher temperature annealing treatments (see Figure 2). Such band, not detected for the others samples, seems to move towards lower energies as well as the annealing temperature increases. It has been tentatively assigned to the peculiar charge distribution at the interface, which constitutes some kind of “intermediate layer” between ITO and PZT interface. Further investigations are on the way in order to better characterize such NIR-resonance.

The extinction coefficients of PZT thin films annealed at different temperatures have been used to estimate the optical band gaps energies of the pyrochlore and perovskite phases. Moreover, the electron transitions gaps energies have been estimated by the typical model used to describe an allowed direct transition.²²

Neglecting the exciton formation, the form of the absorption coefficient α as function of photon energy $h\nu$ depends on the joint density of the states, $N(E)$, involving the band across the Fermi level. For simple parabolic bands and direct transitions (allowed), the typical expression of the absorption coefficient $\alpha(h\nu)$, is:

$$(\alpha h\nu)^2 = A(h\nu - E_g^{opt}) \quad \text{with } \nu > E_g^{opt} \quad (1)$$

where E_g^{opt} is the energy gap and A is a constant, proportional to the probability of electron transition between occupied and empty states.²² The extinction coefficients $k(\lambda)$, estimated by ellipsometry, are used to calculate the absorption coefficient $\alpha(h\nu)$ versus photon energy $h\nu$ by using the well-known formula:

$$\alpha(h\nu) = 4\pi \frac{k(h\nu)}{\lambda} \quad (2)$$

where, h is the Plank constant and λ is the light wavelength.

In Figure 2 (on the right) are shown the $(\alpha h\nu)^2$ functions versus photon energy $h\nu$, estimated as described above. The band gaps can be extracted by linear fit of the function $(\alpha h\nu)^2$ immediately above the edge of each absorption peak. The band gaps, obtained calculating the intercept of these lines with the photon energy axis, are indicated in Figure 2. First of all, it can be noticed that for the Glass/PZT sample annealed at 700°C only one band appears and the associated band gap falls at 4.11 eV, while when the sample are treated at 500°C two bands occur at 3,69 eV and 4.20

eV. In summary, the optical band gaps obtained for the Glass/ITO/PZT samples are 3,70 eV and 4.11 eV, for the sample annealed at 600°C and 4,06 eV and 4.47 eV, for the samples annealed at 300°C. The NIR shift of the bands (and of the relative optical band gaps energies values) as well as the annealing temperature increases, observed in the Figure 2, is due to the PZT structural evolution from amorphous to polycrystalline phase.²³⁻²⁵

Such values are consistent with the literature data that assign the lowest value, obtained from each sample, to the presence of the pyrochlore phase and the highest to the presence of ferroelectric perovskite phase, of the PZT with the same stoichiometric ratio (Zr=0.53, Ti=0.47).^{20,21,26-29} It means, that when the annealing temperature is lower than 600°C, the pyrochlore ($E_g^{opt} \approx 3.7 eV$) and the perovskite ($E_g^{opt} \approx 4.2 eV$) phases are coexisting. On the contrary, when the annealing temperature is higher than 600°C, the pyrochlore phase is completely converted in ferroelectric perovskite phase; for instance, in the GLASS/PZT sample annealed at 700°C (see Figure 2), the only band detected is assigned to the ferroelectric perovskite phase (the sample GLASS/ITO/PZT annealed at 700°C, has been not characterized by ellipsometry because of its deformation after such annealing treatment). However, the thermal induced structural evolution, similar to that observed on GLASS/PZT sample annealed at 700°C, has been detected by AFM and EFM (Electrostatic Force Microscopy) investigations, where the presence of ferroelectric dendritic structures has been shown. These evidences indicate the same evolution of the PZT layer on GLASS/ITO substrates when such samples are subjected to the highest thermal annealing process.³⁰

Such structural evolutions are at the basis of the effect observed when GLASS/ITO/PZT samples are used as electrode in ANLC cells. In Figure 3 are shown the electro-optical responses measured in ANLC cells, containing as electrodes GLASS/ITO/PZT samples annealed at 500°C (on the bottom) and 600°C (on the top).

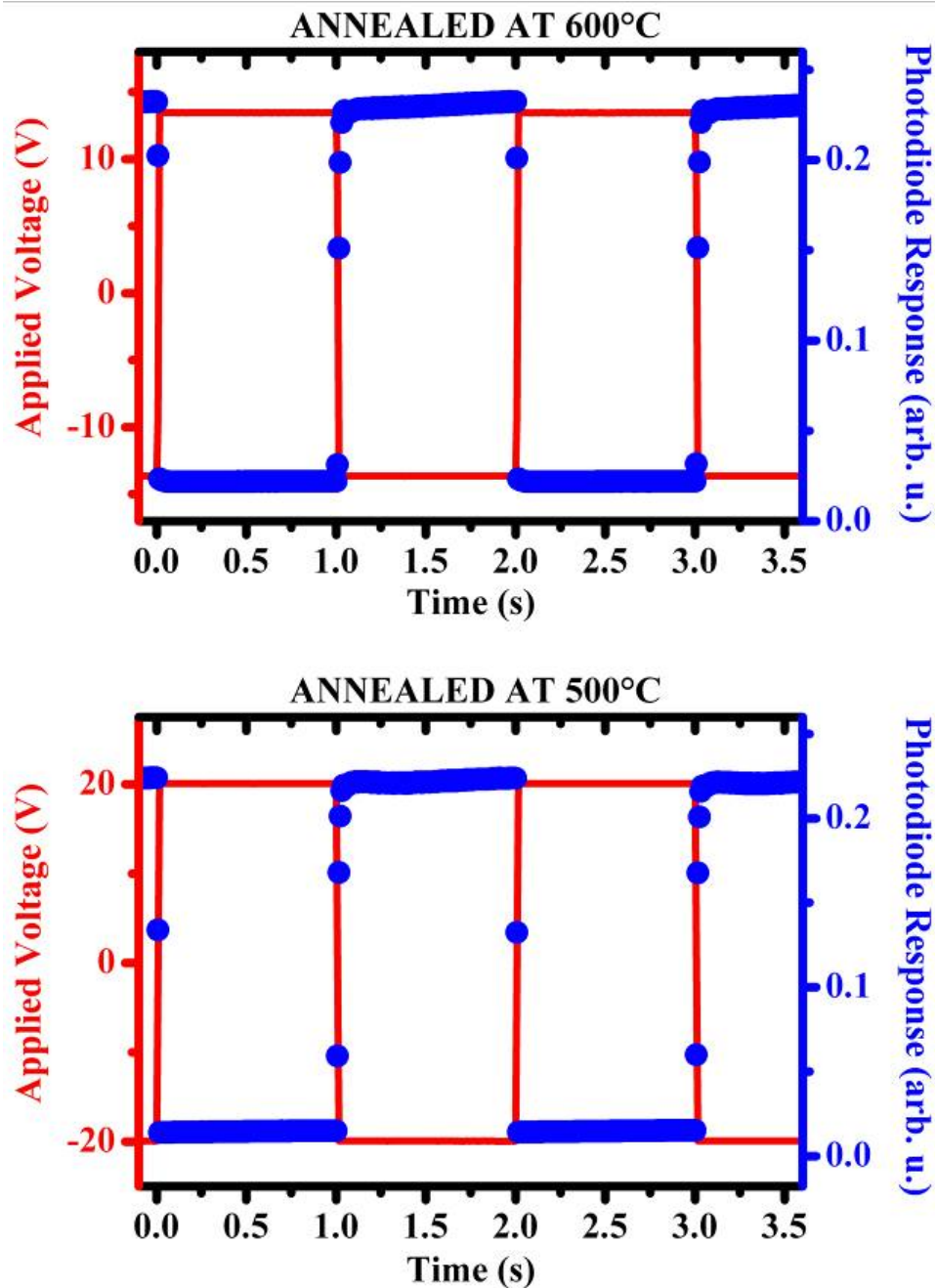


Figure 3. Electro-optical responses (blue circle) of ANLC cells containing PZT layers annealed at 500°C (on the bottom) and 600°C (on the top) when the external applied voltage is applied (red solid line).

The same optical responses are obtained from the two cells (Figure 3), polarity sensitive in both the cases: the liquid crystals molecules are affected by the electric field only for positive voltages while for negatives ones they do not switch. (It should be remembered that at the beginning the maximum of the light is collected by

the photodiode; when the liquid crystals molecules change the initial alignment the light intensity decreases).⁵ Such kind of response generates a plot (see Figure 3) where transmitted light intensity and applied voltage appear “in opposition of phase”. The same behavior has been obtained also in ANLC cells where the electrode was made by WO₃ film annealed at 600°C, while in the case of WO₃ films annealed at 100°C the electro-optical response appears “in phase” to the applied voltage⁶⁻⁹. On the contrary, by using PZT films the observed electro-optical responses appear always “in opposition of phase”, independently from the annealing temperature.⁵

However, the electrooptic efficiency of the devices results remarkably dependent on the annealing temperature of the electrode films. In fact, in order to obtain the same polarity sensitive electro-optical responses, a voltage twice higher should be used for the ANLC cell containing PZT films annealed at 500°C with respect to that used for the ANLC cell containing PZT films annealed at 600°C. As reported above, the increasing of the annealing temperatures favors the formation of the ferroelectric perovskite structures, which remains the only existing structure for the highest annealing temperatures. It is possible to assign to the increasing presence of such structure the better efficiency obtained from the ANLC cell made with the PZT sample annealed at 600°C.

Conclusion

In conclusion, an easy way to grow Lead Zirconium Titanate, PbZr_{0.53}Ti_{0.47}O₃, (PZT) films, with stoichiometric amount indicated in the formula, has been obtained by hybrid (carboxylate and alkoxides) sol gel route and spin coating deposition of the mother solution on different substrates (float glasses, ITO covered float glasses) is shown.

The thermal induced structural evolutions of such films have been studied by spectroscopic ellipsometry. It has been seen that for lower temperatures annealing the PZT layer is quite amorphous and it become polycrystalline when the annealing temperature increases. Two phases have been identified, by comparison of the optical band gaps obtained during this work to the literature data: the pyrochlore phase and the ferroelectric perovskite phase. It has been shown that the ferroelectric perovskite phase is the only phase which remains when the annealing temperature is 700°C. The greatest amount of ferroelectric perovskite structures obtained by the higher annealing temperatures has been associated to the best efficiency, in the

electro-optical response, obtained in asymmetric nematic liquid crystals (ANLC) cell having PZT electrodes annealed at 600°C.

The formation, thermally induced, of a peculiar interlayer between the ITO and PZT interface has been hypothesized. It should be responsible of the new band detected on the NIR region. Structural and chemical characterizations of such new layer are on the way. The preliminary Raman spectroscopic investigations seem to be very promising in order to individuate the nature of such novel layer.

ACKNOWLEDGMENT. The authors wish to thank Dr. Giuseppe De Santo and Dr. Tiziana Barone for their essential contribution during the PZT thin layers preparation.

REFERENCES

- (1) Damjanovic, D. *Ferroelectric, dielectric and piezoelectric properties of ferroelectric thin films and ceramics. Laboratory of ceramics*; Departement of Material Scienze-Swiss Federal Institute of Tecnology-EPFL: 1015 Lausanne, Switzerland, 1998.
- (2) Uchino, K. *Ferroelectric Devices*; Marcel Dekker: New York, 2000.
- (3) Xu, Y. *Ferroelectric and their Applications*; North-Holland: Tokyo, 1991.
- (4) Lappalainen, J.; Hiltunen, J.; Lantto, V. *Journal of the European Ceramic Society* **2005**, *25*, 2273.
- (5) Marino, S.; Castriota, M.; Strangi, G.; Cazzanelli, E.; Scaramuzza, N. *Journal of Applied Physics* **2007**, *102*, 013112-1. Paper selected for the April 9, **2007** issue of "Virtual Journal of Nanoscale Science & Technology".
- (6) Castriota, M.; Marino, S.; Versace, C.; Strangi, G.; Scaramuzza, N.; Cazzanelli, E. *Molecular Crystals and Liquid Crystals* **2005**, *429*, 237.
- (7) Strangi, G.; Cazzanelli, E.; Scaramuzza, N.; Versace, C.; Bartolino, R. *Phys. Rev E* **2000**, *62*, 2263.
- (8) Cazzanelli, E.; Marino, S.; Bruno, V.; Castriota, M.; Scaramuzza, N.; Strangi, G.; Versace, C.; Ceccato, R.; Carturan, G. *Solid State Ionics* **2003**, *165*, 201.
- (9) Bruno, V.; Castriota, M.; Marino, S.; Versace, C.; Strangi, G.; Cazzanelli, E.; Scaramuzza, N. *Molecular Crystal Liquid Crystal* **2005**, *441*, 27.
- (10) Yi, G.; Wu, Z.; Sayer, M. *J. Appl. Phys.* **1988**, *64*, 2717.
- (11) Martin, C. R.; Akasay, I. A. *J. Phys. Chem. B* **2003**, *107*, 4261.
- (12) Song, Y. *J. Ph.D Thesis*; Virginia Polytechnic Institute and State University, Blacksburg: Virginia, USA, 1998.

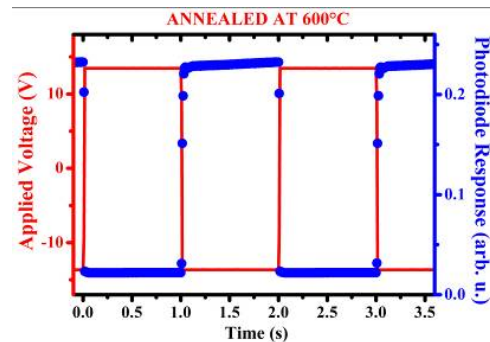
- (13) Tompkins, G. H.; Irene E. A. *Handbook of Ellipsometry*; William Andrew Inc: Norwich, New York, 2005.
- (14) Aspnes, D. E. *Thin Solid Films* **1982**, *89*, 249.
- (15) Adurodija, F. O.; Semple, L.; Bruning, R. *J. Mater. Sci.* **2006**, *41*, 7096.
- (16) Berder, M.; Seelig, W.; Daube, C.; Frankenberger, H.; Ocker, B.; Stollenwerk, J. *Thin Solid Films* **1998**, *326*, 72.
- (17) Hamberg, I.; Granqvist, C. G. *J. Appl. Phys.* **1986**, *60*, R123.
- (18) Matsui, Y.; Suga, M.; Hiratani, M.; Miki, H.; Fujisaki, Y. *J. Appl. Phys.* **1977**, *36*, 1239.
- (19) Lee, S. G.; Kim, K. T.; Lee, Y. H. *Thin Solid Films* **2000**, *372*, 45.
- (20) Okada, A. *J. Appl. Phys.* **1977**, *48*, 2905.
- (21) Lee, H.; Kang, Y. S.; Cho, S. J.; Xiao, B.; Morkoc, H.; Kang, T. D.; Lee, G. S.; Li, J.; Wei, S. H.; Snyder, P. G.; Evans, J. T. *J. Appl. Phys.* **2005**, *98*, 094108.
- (22) Mott, N. H.; Davis E. A. *Electronic Processes in Non-Crystalline Materials*; Clarendon Press: Oxford, UK, 1979.
- (23) Wu, A.; Miranda Salvado, I. M.; Vilarinho, P. M.; Baptista, J. L. *Journal of the American Ceramic Society* **2000**, *83*, 1379.
- (24) Trolrier-McKinstry, S.; Chen, J.; Vedam, K.; Newnham, R. E. *Journal of the American Ceramic Society* **1995**, *78*, 1907.
- (25) Peng, C. H.; Desu, S. B. *Journal of the American Ceramic Society* **1994**, *77*, 1486.
- (26) Hu, Z.; Huang, Z.; Lai, Z.; Wang, G.; Chu, J. *Thin Solid Films* **2003**, *437*, 223.
- (27) Moret, M. P.; Devillers, M. A. C.; Worhoff, K.; Larsen, P. K. *J. Appl. Phys.* **2002**, *92*, 468.
- (28) Yang, S.; Mo, D.; Tang, X. *Ferroelectrics* **2003**, *287*, 35.
- (29) Yang, S.; Mo, D.; Tang, X. *J. Mater. Sci.* **2002**, *37*, 3841.
- (30) Bruno, E.; De Santo, M. P.; Castriota, M.; Marino, S.; Strangi, G.; Cazzanelli, E.; Scaramuzza, N. *J. Appl. Phys.* **2008**, *103*, 064103.

The table of contents

**Marco Castriota, Stefano D'Elia,
Salvatore Marino, Enzo Cazzanelli,
Nicola Scaramuzza, Carlo Versace and
Roberto Bartolino**

Structural and Optical evolutions thermal induced of Lead Zirconium Titanate thin films obtained by sol gel

Polarity sensitive electro-optical response obtained by Asymmetric Nematic Liquid Crystals (ANLC) cell made by using a $\text{PbZr}_{0.53}\text{Ti}_{0.47}\text{O}_3$ (PZT) films as working electrode. The PZT layer, made by sol gel, annealed at 600°C for one hour allows to obtain the ANLC device with the best efficiency, since at this temperature the formation of PZT in ferroelectric perovskite phase which promotes such effect increases.



3.4. Far-IR ellipsometry characterization of the PZT thin films obtained by sol-gel synthesis onto ITO substrates and annealed at different temperatures.

Supervisors: Prof. Mathias Schubert and Dr. Tino Hofmann.

Lincoln Nebraska University, April-June 2008.

Preliminary results.

Introduction

This section shows some preliminary experimental results, concerning the far-IR ellipsometry investigations of the structural and optical thermal induced modification of the PZT thin films obtained by sol-gel synthesis previously reported.

This experimental measurements have been performed in the University of Nebraska-Lincoln (USA), Department of Electrical Engineering, and Nebraska Center for Materials and Nanoscience. Prof. Mathias Schubert and Dr. Tino Hofmann were the supervisors.

In order to obtain new physical information, the thermal induced modifications of the dielectric function of these organic-inorganic thin film systems have been investigated by means the far-IR (1.4 - 43 μ m) ellipsometry for different annealing processes applied to the organic-inorganic samples. The PZT samples were the thin films obtained by deposition of the PZT gel solution onto ITO substrates.

The goal of this work consist to understand as the organic PZT precursors transform themselves in ferroelectric material by annealing processes. In order to obtain these information, the modifications of the typical resonances of the organic chemical groups that appear in the dielectric function were studied. By using far-IR elliposmetry, we have tried to find new information concerning the interface effect between the ITO substrates and PZT material.

This study is under investigation, therefore here we present only some preliminary information about this complex optical system characterized by the multilayer structure: float glass/ITO/PZT. Actually, there are different open questions concerning the PZT thin films annealed at different temperatures. We will show some of these open questions of this section.

3.4.1. Far-IR model dielectric function

In general, the electromagnetic waves couple with the medium, in other words, the dielectric permittivity ϵ is not equal to unity and depends on material parameters, and ϵ is a function of the wavelength of the electromagnetic wave. It also depends on the symmetry of the crystal and is influenced by chemical composition, concentration and defect properties, etc. These material properties can be studied, if we can measure and study the dielectric function.

In the far- to mid-IR wavelength range (45-1.7 μ m), the model dielectric function can be defined by the following contributions:

$$\epsilon(\omega) = \epsilon^{(FC)}(\omega) + \epsilon^{(PL)}(\omega) + \epsilon^{(AM)}(\omega) \quad (3.4.1)$$

where $\varepsilon^{(FC)}(\omega)$, $\varepsilon^{(PL)}(\omega)$, $\varepsilon^{(AM)}(\omega)$ are the contributions due to free-charge-carriers, polar lattice vibrations, and additional modes, respectively [6].

The contribution of the free-charger $\varepsilon^{(FC)}(\omega)$ to $\varepsilon(\omega)$ can be obtained from the classical equation derived by Drude to describe optical properties of free-charge-carriers in simple metals:

$$\varepsilon^{(FC)}(\omega) = -\frac{Nq^2}{\varepsilon_0 m} \cdot \frac{1}{\omega^2 + i\omega/\tau} \quad (3.4.2)$$

where m is the effective mass of the free-charge-carriers with concentration N . The vacuum dielectric permittivity and the charge of the free-charge-carrier are given by ε_0 and q , respectively.

The contribution of the polar lattice vibrations (phonons) $\varepsilon^{(PL)}(\omega)$ and of the additional modes $\varepsilon^{(AM)}(\omega)$ to $\varepsilon(\omega)$ can be described by using harmonic oscillator function with Lorentzian shape. These contributes depend by the absorption bands of molecular vibrations and the resonances of solid states.

3.4.2. Materials and methods

The samples preparation have been widely introduced in the last sections of this chapter. The $\text{PbZr}_{0.53}\text{Ti}_{0.47}\text{O}_3$ solution is spread on the substrates using a SC10 spin coater (produced by CaLCTec s.r.l.) at 1200 rpm for 25 s. The deposited film is placed on a hot plate for 5 minutes at 300°C to evaporate the organic solvent used in the sol-gel solution. This process is called also pyrolysis process, it consists in the thermo-chemical decomposition of organic materials. Finally, different samples are obtained by thermal treatments of the deposited film to temperatures in the 300°C-700°C range. In order to study the dielectric properties of the PZT sol-gel solution, one PZT sample were prepared by deposition of the gel solution onto ITO substrates and it didn't subjected to pyrolysis process.

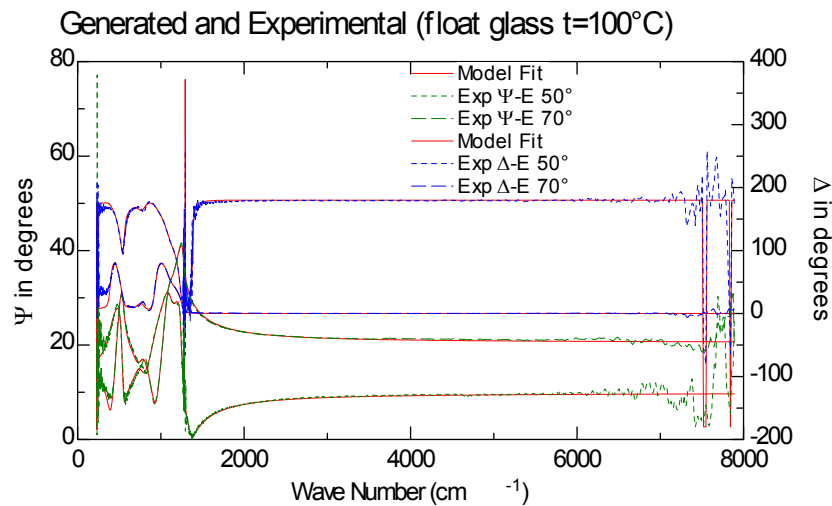
In a preliminary study, we have estimated the optical models of the substrates, without PZT depositions, annealed at different temperatures in the range 100-700 °C with steps of 100°C and treatment duration of one hour. These optical models will be used to study the optical property variations of the PZT depositions annealed at the same temperatures.

It has been observed that in the spectral range 250-1000nm, the dielectric properties of the float glass substrates subjected to annealing process change slightly (let's see section 3.1 and 3.2 of this chapter [2]). In order to prove that the dielectric function of the glass substrates does not change in far-IR spectra, the thermal induced modification of the far-IR dielectric properties of the float glass substrates were studied. Two glass substrates without both PZT and ITO thin films were annealed in air respectively at 100°C and 700°C for one hour.

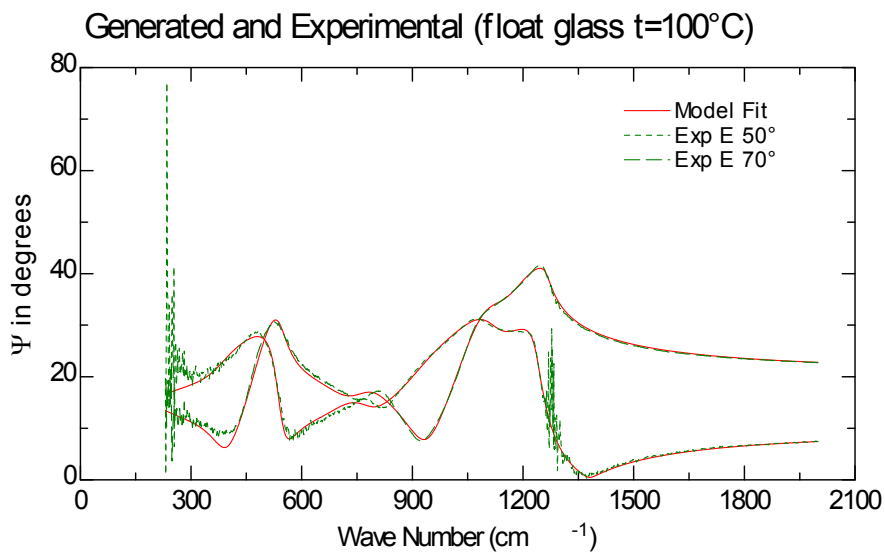
The clean glass/ITO slides have been annealed in air at different temperatures in the range [100°C - 600°C] for one hour; afterwards they have been studied to estimate their far-IR dielectric properties.

3.4.3. Experimental results and discussion.

Float glass characterization. The figure 3.4.1 shows the generated and experimental ellipsometry angles acquired onto float glass substrates annealed at 100°C for one hour. This good fit results have been obtained by using an optical model where the complex dielectric function has been modeled by using a sum of Lorentzian oscillator.



(a)



(b)

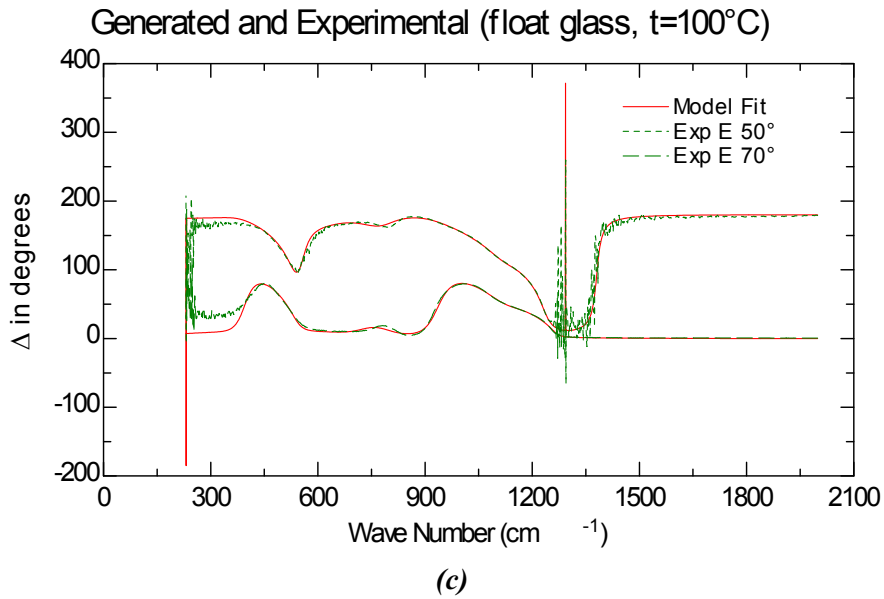
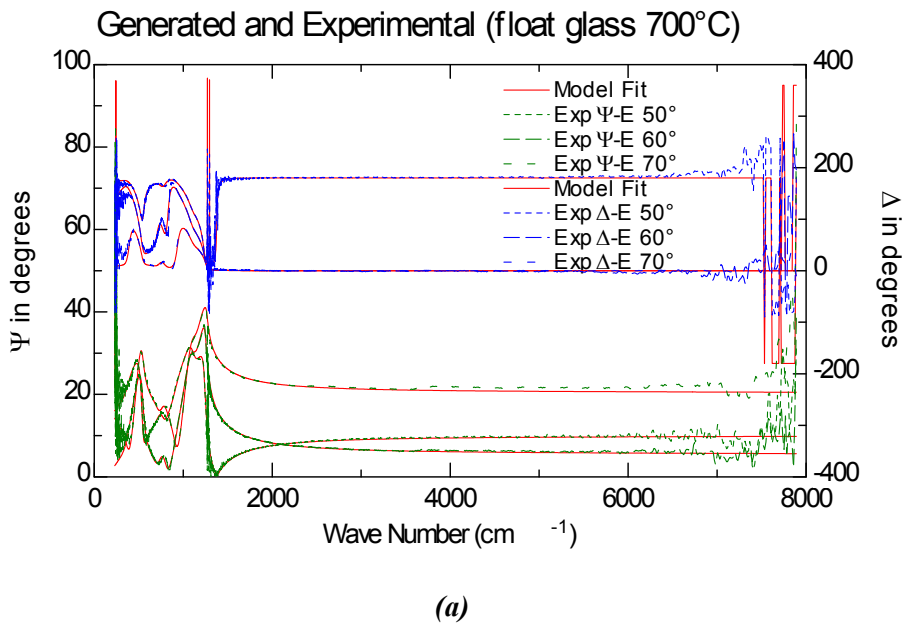


Fig. 3.4.1. Experimental and modeled data (a) for float glass substrates annealed at 100°C for one hour. (b) and (c) show an enlargement of the Ψ and Δ ellipsometry angles in the wave number range $200\text{-}2000\text{ cm}^{-1}$ (energy range $\sim 0.006\text{-}0.248\text{ eV}$). The Brewster angle for the glass is about 56.3° for a refractive index $n_{\text{glass}}=1.5$. Therefore, in order to increase the accuracy of layer modeling, two AOI were chosen, the first one smaller and the second one larger than 56.3° .



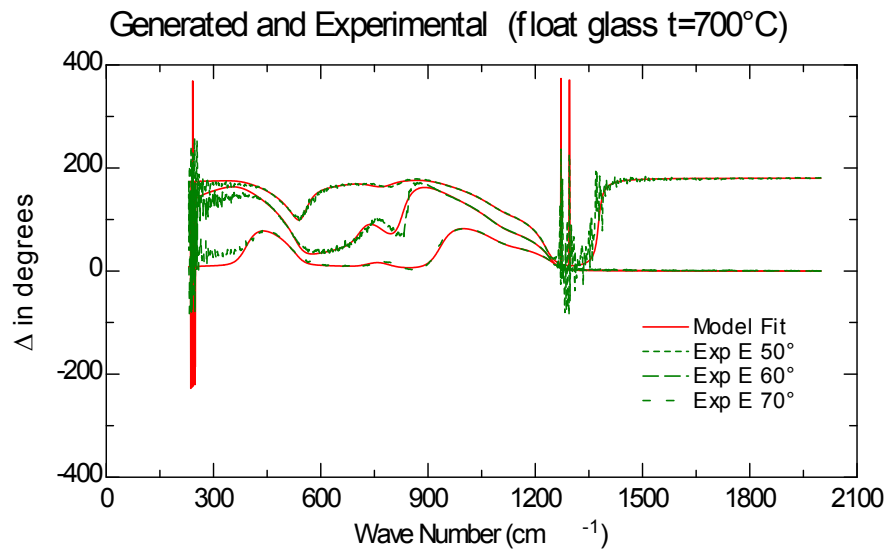
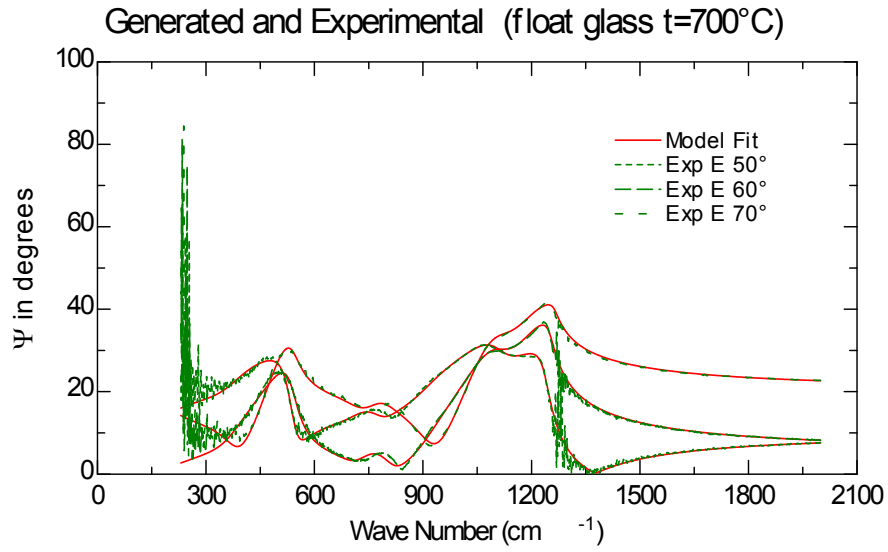


Fig. 3.4.2. Experimental and modeled data (a) for float glass substrates annealed at 700°C for one hour. (b) and (c) show an enlargement of the Ψ and Δ ellipsometry angles in the wave number range 200-2000 cm^{-1} (energy range ~ 0.006 - 0.248 eV).

The figure 3.4.3 shows the complex dielectric functions estimated for the float glass substrates annealed at 100°C and 700°C. In the wave number range 230-2000 cm^{-1} , it is possible observe two important absorption bands, first one close to 500 cm^{-1} , the second one is neighboring to 1000 cm^{-1} . The float glass material is an amorphous material (isotropic structure) in macroscopic scale. In domains with dimensions $\sim 1\text{nm}$, it is possible observed two types of inhomogeneities typical of the structure of glass: density and elastic constant fluctuations [7]. These are attributable

to the local structure of silicate glasses is rather well-known: the “building units” are similar to that of the crystalline structure of the SiO_4 tetrahedra, but at intermediate range the tetrahedra are linked together in a disordered manner, which has been shown to depend on thermal history of the glass material [7, 8]. In accordance with several experimental investigations, these resonances are related both to this local structure and to the Si-O-Si bond angles [7, 8, 9].

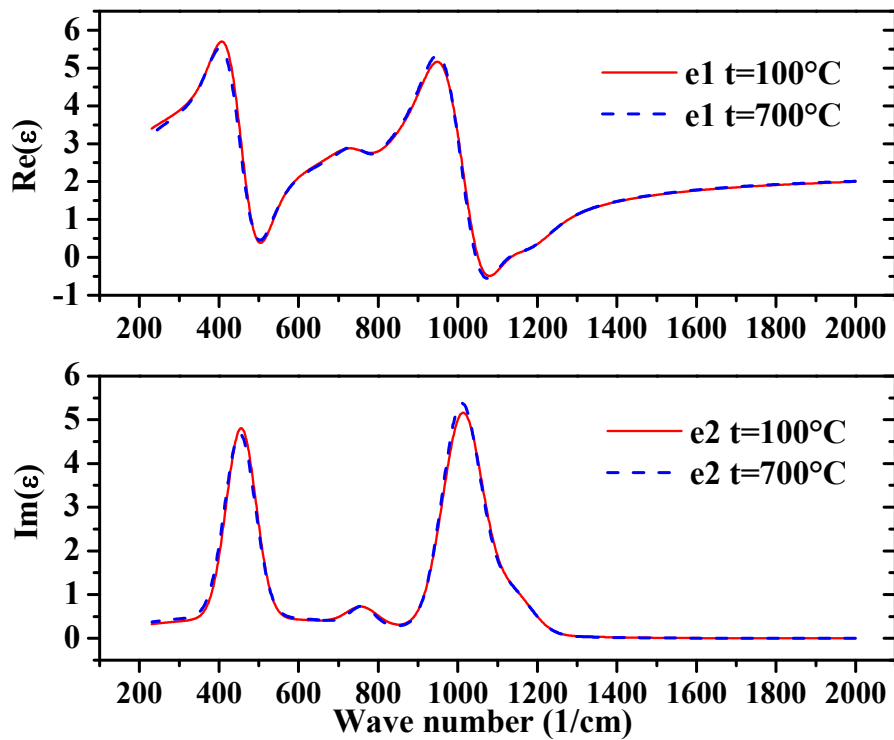


Fig. 3.4.3. Complex dielectric function for float glass annealed at 100°C and 700°C.

It has been observed that the annealing processes change this local structure. When the annealing temperature increases, these typical absorption bands are shifted to lower frequencies. The amplitude of these variations is very small [8, 9], and variations are related to the change of the Si-O-Si angles, which in turn is related to the density change. The density of silica glass increases with increasing of the annealing temperature and is inversely correlated with the Si-O-Si bond angle. Higher density glass appears to have smaller Si-O-Si bond angles and lower peak wave numbers [8, 9].

We have observed that these two resonance bands shift towards low frequencies, in accordance with the experimental investigations previously introduced. The figure 3.4.4 shows an enlargement of the second bands close to 1000cm^{-1} .

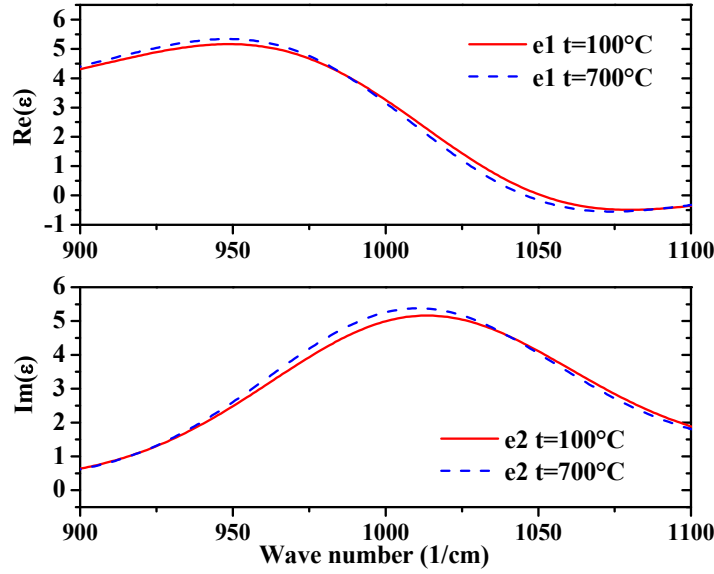


Fig. 3.4.4. Enlargement (wave number range 900-1100 cm^{-1}) of the complex dielectric function showed in figure 3.4.3. The small variation of the central frequency position of these resonance is due to the densification of the float glass because the Si-O-Si bond angle decrease when the annealing temperature increase.

Indium tin oxide (ITO) characterization. In the section 3.1 (appendix C) of this chapter, we have showed that the optical model for the ITO thin film, studied in visible spectral range 250-1000nm [section 3.1 of this thesis], can simulate very well also the ellipsometry angle acquired in far-IR spectra. Although this one, we have used a more easy optical model to study the annealed ITO thin films. The multilayer structure is showed in the figure 3.4.4.

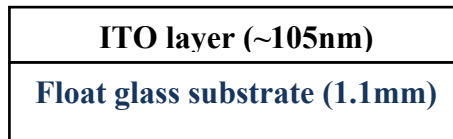


Fig. 3.4.4. The ITO thin films has been modeled by using a single layer, the complex dielectric function is described by means the Drude-Lorentz oscillator.

The complex dielectric function were modeled by using the Drude-Lorentz oscillator represent by means

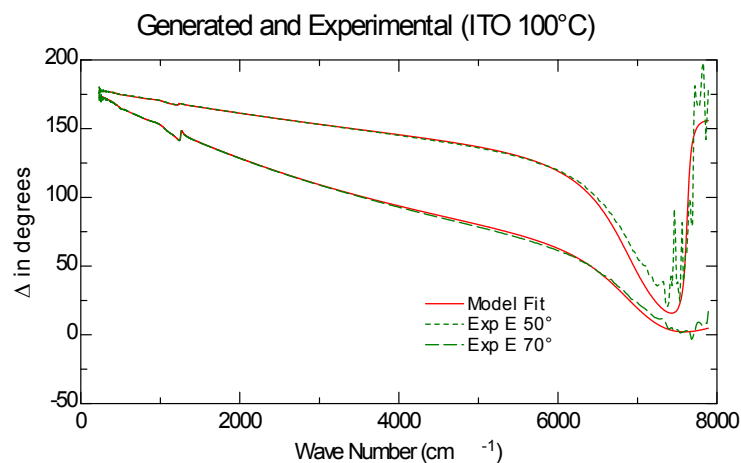
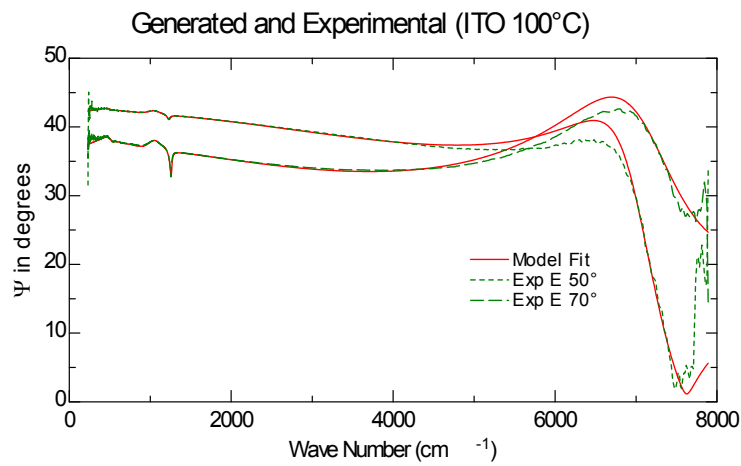
$$\tilde{\epsilon}_{Drude}(E = \hbar\omega) = \frac{-\hbar^2}{\epsilon_0 \rho (\tau \cdot E^2 + i\hbar E)} \quad \text{where } \rho = \frac{m^*}{Nq^2\tau} \quad (3.4.3)$$

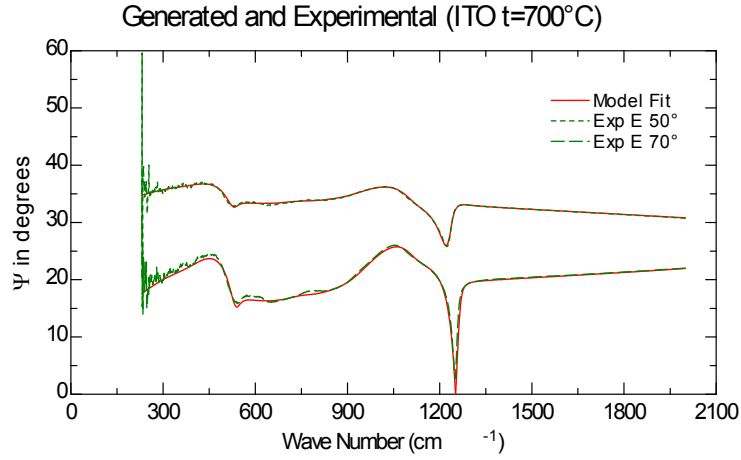
where the fit parameters are defined by resistivity $\rho(\Omega \text{ cm})$, and scattering time $\tau(\text{sec})$. The related parameters of interest are m^* (the carrier effective mass), and N (the carrier concentration in cm^{-3}). The physical constants are \hbar (Plank's constant/ π),

ϵ_0 (the vacuum dielectric constant) and the single electron charge q ($1.6 \times 10^{-19} \text{C}$). During the fit elaborations the carrier effective mass has been fixed equal to $m^*=0.4$, in according with the previously work (section 3.1 of this thesis).

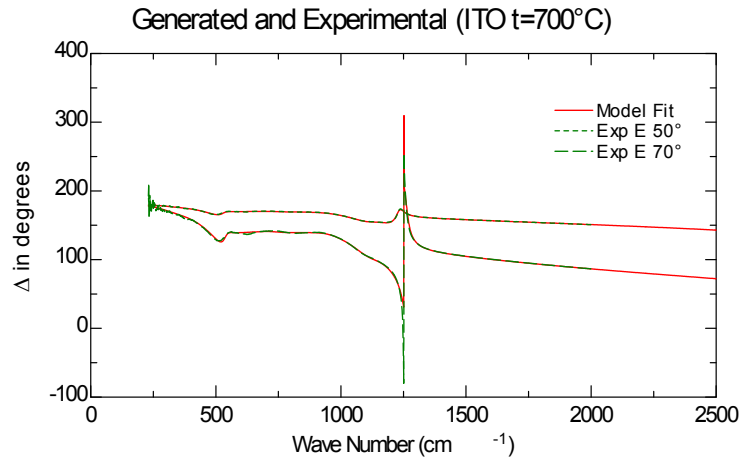
At high annealing temperature ($T_{\text{annealing}} > 300^\circ\text{C}$), it has been observed absorption bands characterized by central energy localized for wave numbers less than 400cm^{-1} ($< 0.05 \text{eV}$). In this case the complex dielectric function for the ITO layer has been modeled by a sum of the Drude-Lorentz (eq. 3.4.3) and some Lorentz oscillators. This Lorentz oscillator describe these absorption bands.

The figures 3.4.5 show some examples of the fit elaborations performed for the ITO samples annealed at different temperatures.





(c)



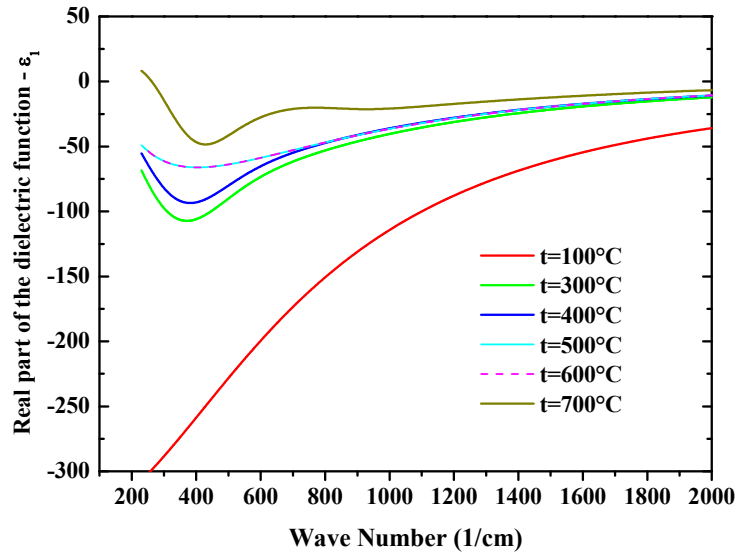
(d)

Fig. 3.4.5. Experimental and modeled ellipsometry angles for ITO samples annealed at 100°C (a, b), and 700°C (c, d) respectively.

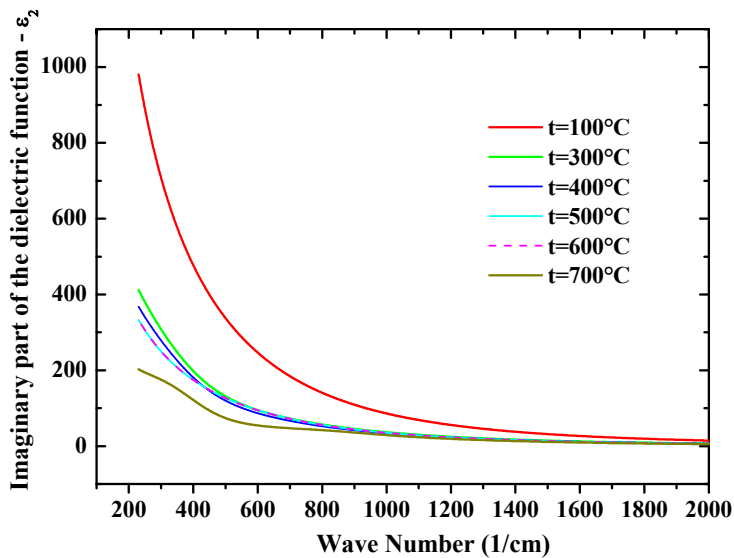
The figure 3.4.6 shows the complex dielectric function for ITO samples having different annealing treatments. When the annealing temperature is greater than 300°C, the value of the imaginary part of the $\tilde{\epsilon}$ (fig. 3.4.6 (b)) becomes small in size. Simultaneously, some absorption resonances in deep IR spectra (200-1000 cm^{-1}) seem to appear. The imaginary part of the $\tilde{\epsilon}$ decreases when the annealing temperature increases because the free-charge-carriers density decreases during the annealing process. This effect has been showed and described fully in the previous sect. (3.1) of this chapter.

The ITO thin film, used in this work and manufactured by Balzers Thin Films, is characterized by nominal sheet resistance, $R_{sh}=25\Omega/\square$. In the previous experimental investigations (section 3.1 of this thesis), we have estimate, for the ITO film annealed at 100°C, the free-charge-carriers concentration value more or less $N_c \approx 18 \times 10^{20} \text{ cm}^{-3}$.

Let's consider the equation (3.4.1), it defines the complex dielectric function in far-IR spectra. For ITO material, the contribution of the free-charger $\varepsilon^{(FC)}(\omega)$ to $\varepsilon(\omega)$ is more important than the contributions both $\varepsilon^{(PL)}(\omega)$ (the polar lattice vibrations (phonons)) and $\varepsilon^{(AM)}(\omega)$ (the additional modes).



(a)



(b)

Fig. 3.4.6. Complex dielectric functions for ITO thin films having different annealing treatment processes. When the annealing temperature increases the amplitude of the Drude-Lorentz oscillator decreases (the free-charge-carriers density decreases). Simultaneously, some phonon absorptions seem to appear.

Therefore, the characteristic absorption phonons of the ITO can be observed only when the free-charge-carriers concentration decrease. These absorption resonances

can be observed clearly when the free-charge-carriers density assumes a small value, for example in the ref. [10] are reported some absorption frequencies when the free-charge-carriers density is $N_c \approx 0.5 \times 10^{20} \text{ cm}^{-3}$. The characteristic phonons of the ITO seem to appear in this experiment when the free-charge-carriers were less than $N_c \approx 4 \times 10^{20} \text{ cm}^{-3}$ (fig. 3.4.7).

The figure 3.4.7 shows the resistivity and carrier density estimated by fit elaboration. These results are comparable to that one estimated in the previous work (section 3.1 of this chapter).

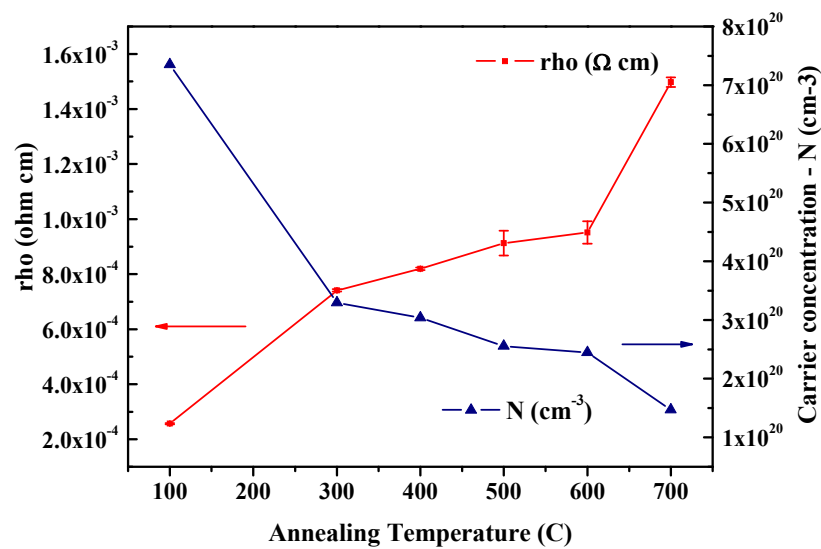


Fig. 3.4.7. Rho ($\Omega \text{ cm}$) estimated by the fit elaboration. The carrier concentration N_c (cm^{-3}) has been calculated by fixing of the carrier effective mass value $m^*=0.4$, as reported in sect. 3.1 of this thesis.

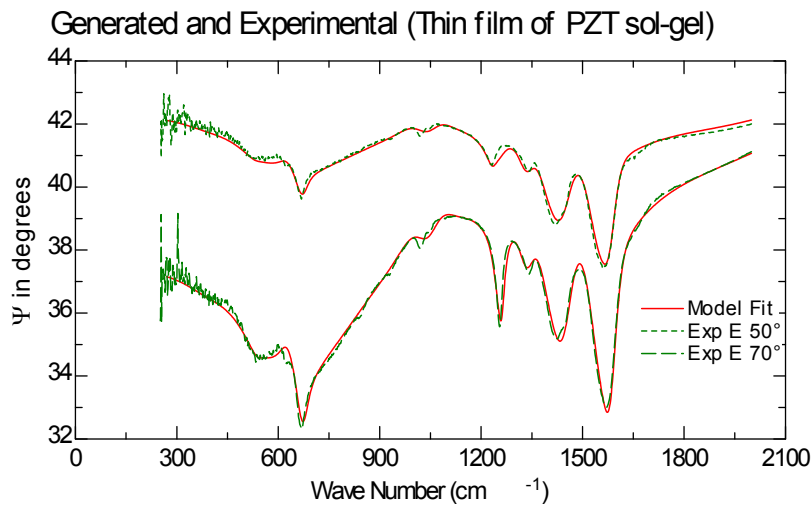
Lead zirconium titanate (PZT) characterization. As proposed in the previous work (section 3.2 of this chapter), we have assumed that the changes of the substrates during the thermal process, induced by the structural reorganization as well as by the thermal adsorption of atmospheric oxygen, are slightly affected by the presence of the PZT layer. The parameters optical models estimated of each substrate for different temperature have been used to study the temperature dependence of PZT films properties. The results for the uncoated substrate at T_i , has been used to evaluate the optical model parameters of the PZT layer annealed at the same temperature.

The fit procedure has been performed using the optical models obtained for the substrates, maintaining the same fit parameters of substrates and estimating only the fit parameters of the PZT layers.

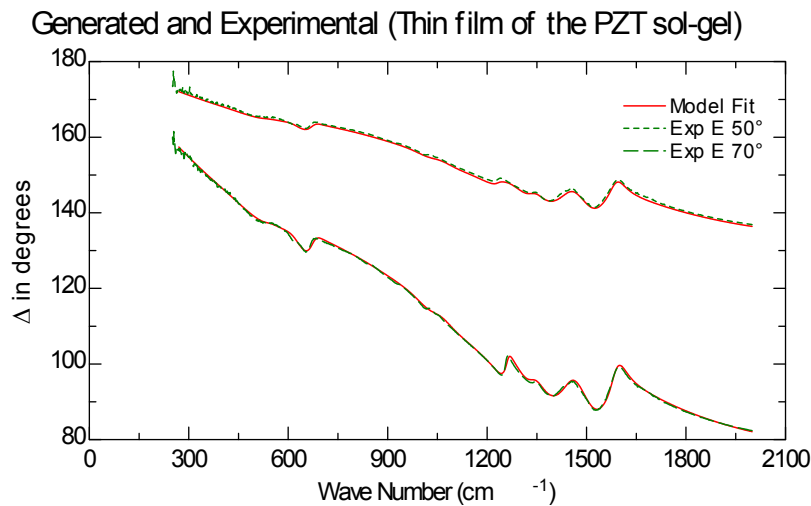
The figures 3.4.8 show some examples of the fit elaborations executed for the experimental data measured on the PZT samples having the multilayer structure glass/ITO/PZT and different annealing temperatures.

The complex dielectric function has been modeled by using a sum of Lorentz oscillators, the number of these ones depends by the number of the phonon frequencies that characterized these PZT samples.

(Figure 3.4.7)



(a)



(b)

Fig. 3.4.7 (a - b). Modeled and experimental data for Ψ (a) and Δ (b) ellipsometry angles.

The AOI were 50° and 70°

“Thin film of PZT sol-gel” represents the PZT samples made without the pyrolysis process.

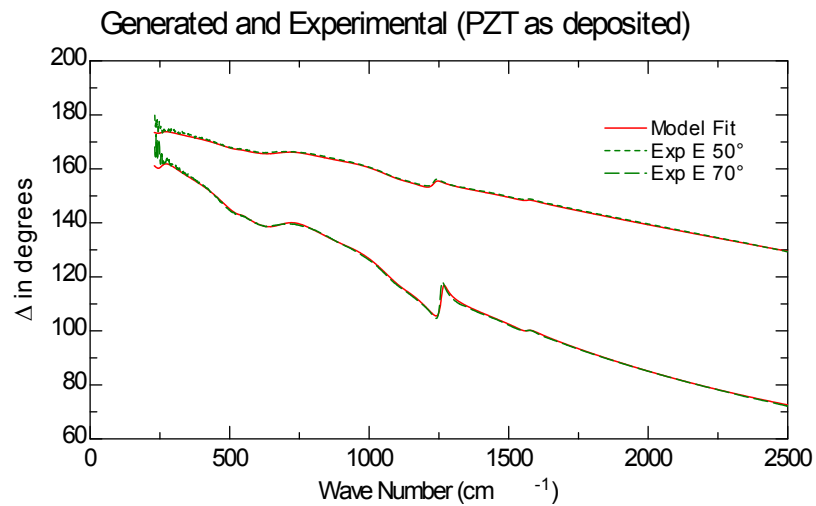
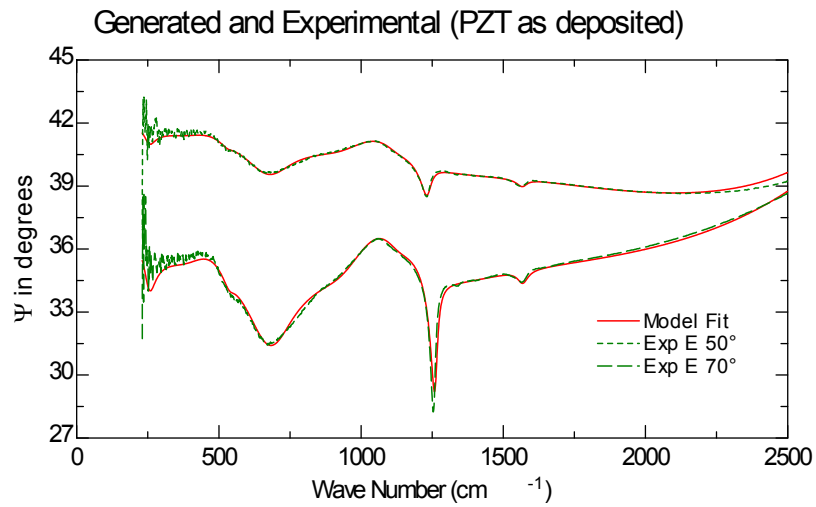


Fig. 3.4.7 (c - d). Modeled and experimental data for Ψ (c) and Δ (d) ellipsometry angles. “PZT as deposited” represents the PZT samples subjected to the pyrolysis process.

(The samples, obtained by the deposition of the gel solution onto the ITO substrate, were placed on a hot plate for 5 minutes at 300°C to evaporate the organic solvent used in the sol-gel solution).

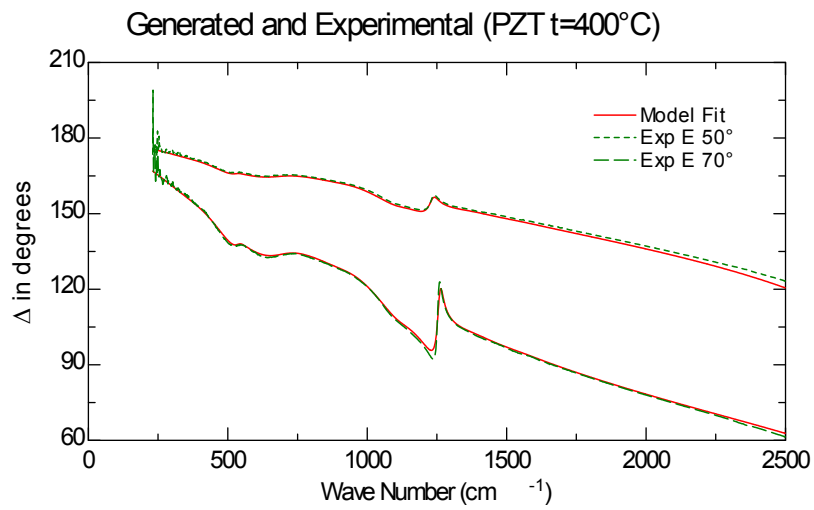
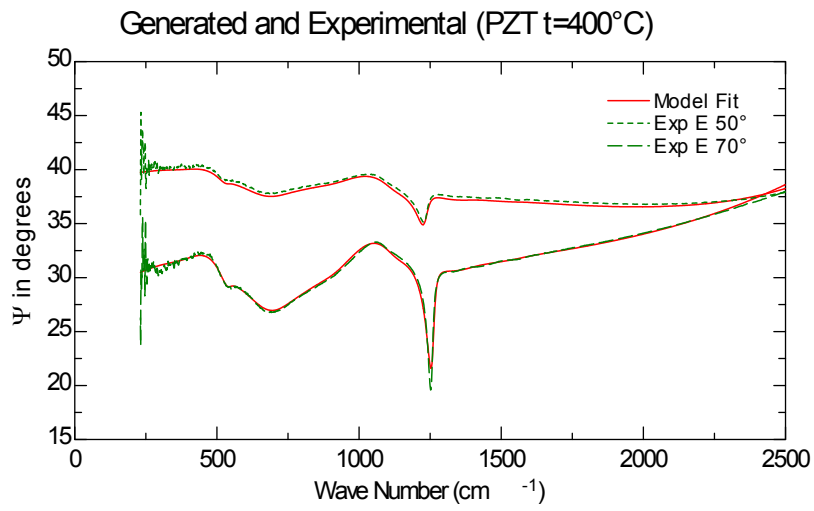
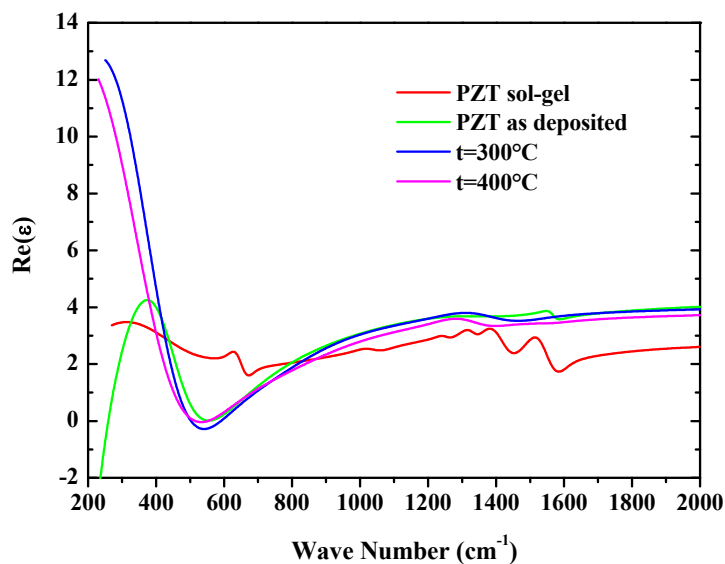
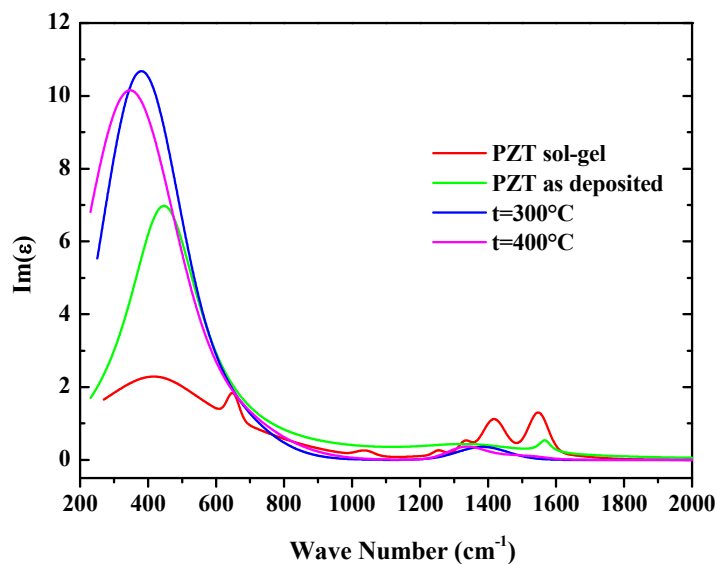


Fig. 3.4.7 (e - f). Modeled and experimental data for Ψ (e) and Δ (f) ellipsometry angles. PZT thin film annealed, for one hour, at 400°C.

The complex dielectric functions estimated for PZT samples having different thermal treatments are showed in the figure 3.4.8. The imaginary part of the complex dielectric functions (fig. 3.4.8a) show several resonances. These ones represent the characteristic vibration frequencies of the PZT thin films.



(a)

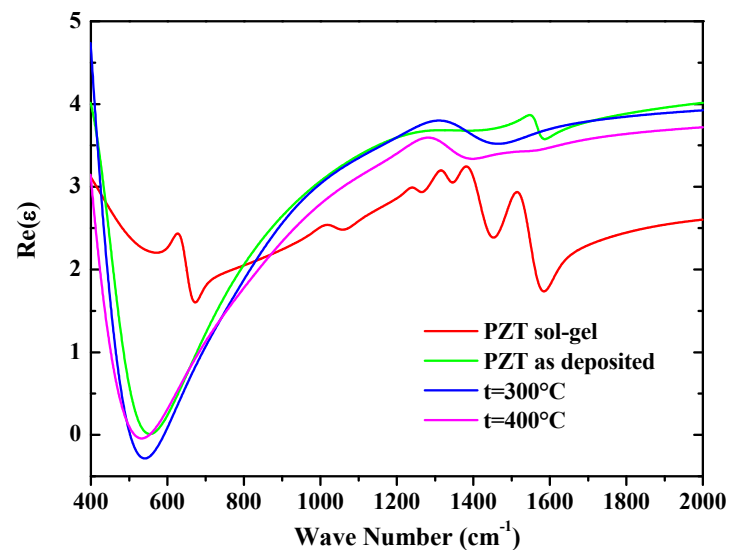


(b)

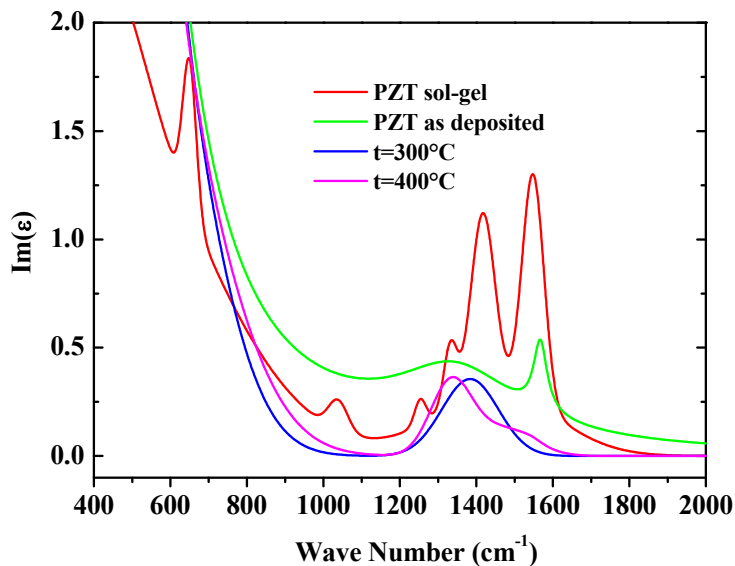
Fig. 3.4.8. Real part (a) and imaginary part (b) of the complex dielectric functions estimate for PZT samples having different annealing temperatures.

“PZT sol-gel” indicates the PZT sample prepared without the pyrolysis process, while “PZT as deposited” indicates the PZT sample prepared with pyrolysis process.

In order to show clearly the different vibration frequencies, we have plot in the figure 3.4.9, the complex dielectric functions showed in the last figure (fig. 3.4.8), but the enlargement of the ordinate axis has been performed. In the IR spectral range 1000-1800 cm^{-1} , we can observe different resonance describing the vibration frequencies of the PZT organic precursors (“PZT sol-gel”, red curve). After pyrolysis process (“PZT as deposited”, green curve), the amplitude of these resonances decrease. It is clear that some residual organic molecules remain, in fact, it is possible observe, in the same figure, the resonance close to 1600 cm^{-1} (green curve) that seem to be identical that one observed in the red curve (“PZT sol-gel”).



(a)



(b)

Fig. 3.4.8. The enlargement of the ordinate axis shows clearly the vibration frequencies characterizing the organic precursors.
(Let's observe that the Kramers-Kronig (KK) consistency is confirmed)

In the IR spectral range $1000-1800\text{cm}^{-1}$, after pyrolysis process (“PZT as deposited”), a large resonance seems to appear, actually, we think that there is the presence of organic impurity also after pyrolysis process, may be.

After pyrolysis process, when the PZT samples are subject to annealing process, new absorption resonances seem to appear. Actually, we can't give any information concerning these absorption frequencies and the chemical groups associated to these vibration frequencies showed in the figure 3.4.8.

In order to obtain a clear picture of this systems, new experimental investigations are finalized to compare these results with the RAMAN characterization. In this way, we will obtain more information about the multiple resonances, showed in the figure 3.4.8.

Other experimental data has been measured on the samples annealed at 500°C , 600°C and 700°C . During the fit elaboration of these samples, some problems were occurred: we have observed that the isotropic optical model, used for the characterization of the previous samples (PZT sol-gel, PZT as deposited, PZT annealed at 300°C and 400°C), didn't allowed us to obtain good fit results.

The SEM images showed in previous section 3.2 (page 95 of this thesis) show clearly that when the annealing temperature becomes neighbor to $500-600^{\circ}\text{C}$, appear onto the surface of the samples some structure called “rosette” [2] (fig. 3.4.9).

These rosette are characterized by crystalline structure, therefore the PZT thin films assume anisotropic property. In order to obtain information for these samples annealed at high temperature $T > 500^{\circ}\text{C}$, an anisotropic optical model is required to study the phonon structures for these samples.

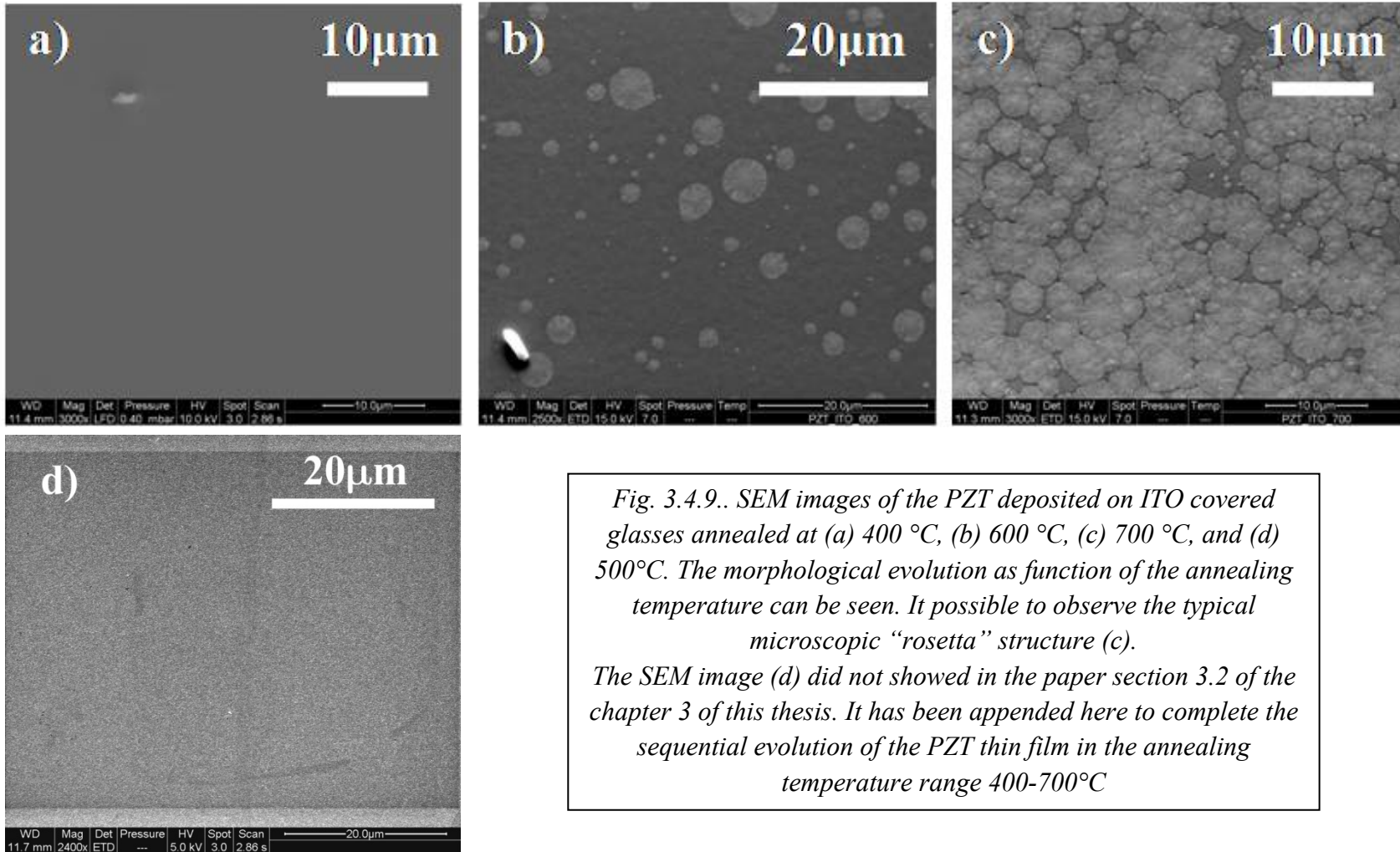


Fig. 3.4.9.. SEM images of the PZT deposited on ITO covered glasses annealed at (a) 400 °C, (b) 600 °C, (c) 700 °C, and (d) 500°C. The morphological evolution as function of the annealing temperature can be seen. It possible to observe the typical microscopic “rosetta” structure (c). The SEM image (d) did not showed in the paper section 3.2 of the chapter 3 of this thesis. It has been appended here to complete the sequential evolution of the PZT thin film in the annealing temperature range 400-700°C

However, in order to obtain some morphological information for the PZT samples annealed at 500°C, 600°C and 700°C, we have used another easy optical model: the dielectric function of the PZT layer were modeled by using the Cauchy dispersion law to describe the refractive index.

The figures 3.4.10 show the results of these fit elaboration. In deep IR spectra between 250cm⁻¹ and 900cm⁻¹, we can observe a very bad fit result. The characteristic phonon resonances for PZT material would have to be found in this spectral range [10] and the Cauchy optical model can't simulate these complex structures.

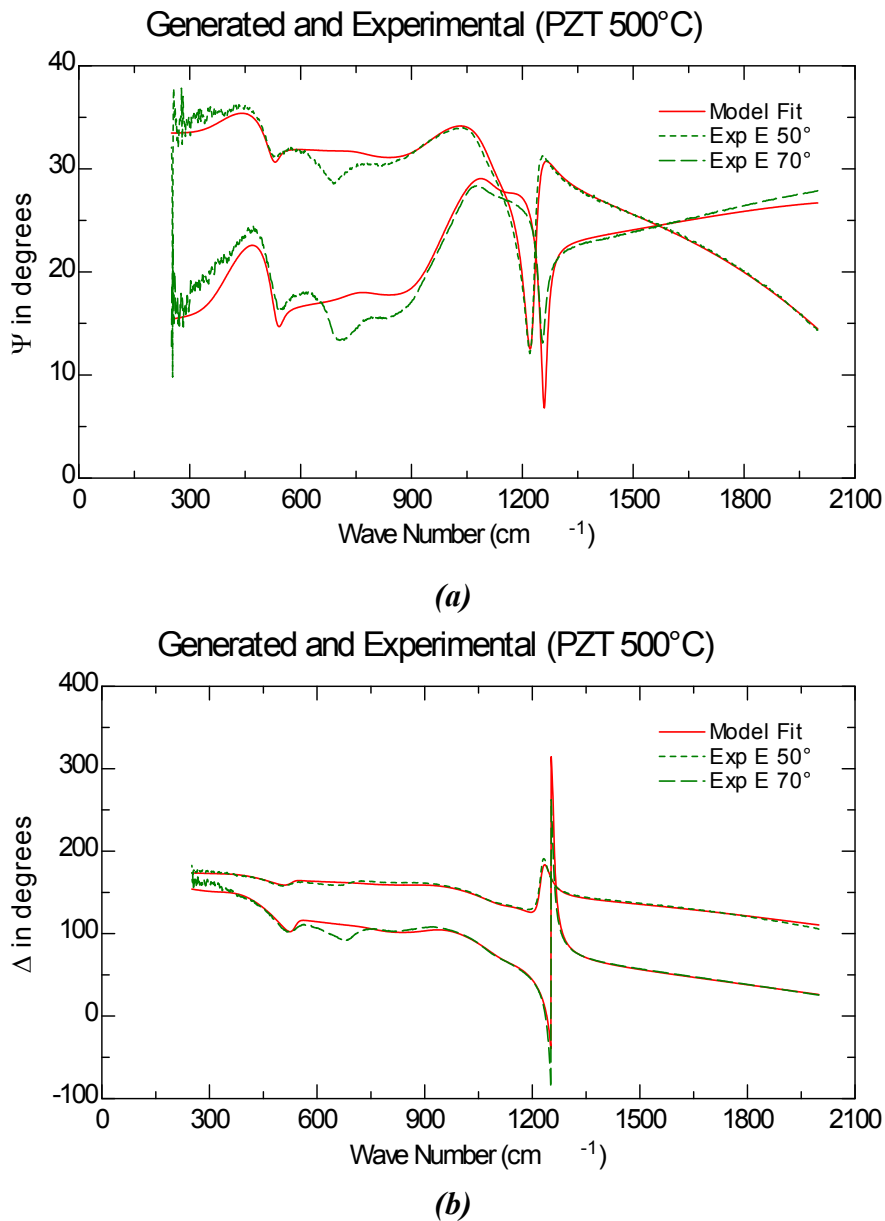
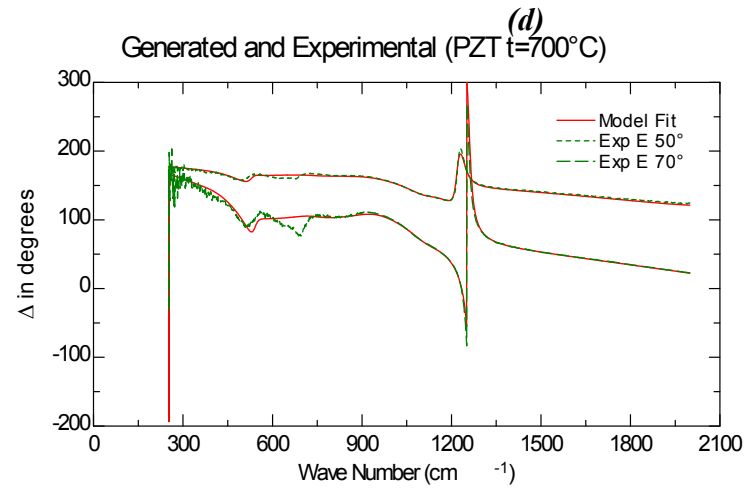
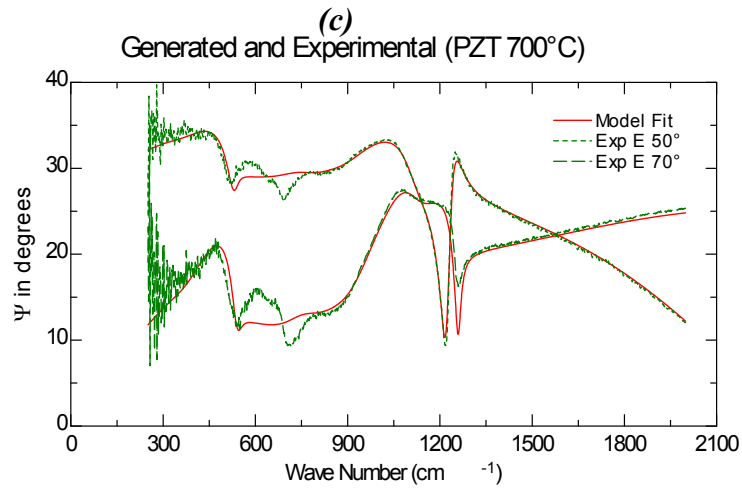
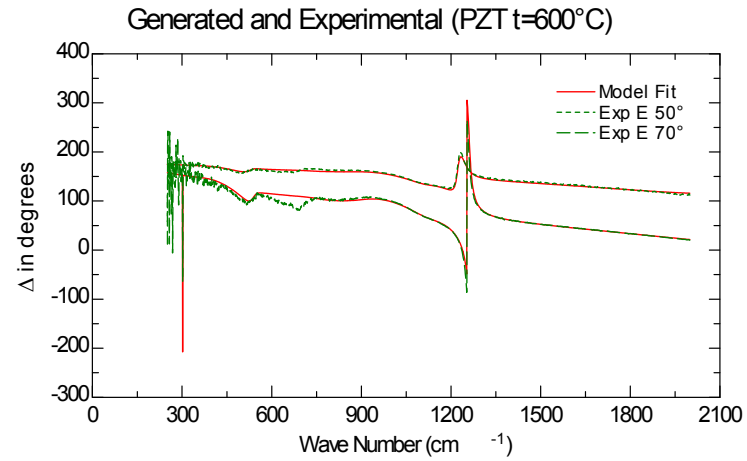
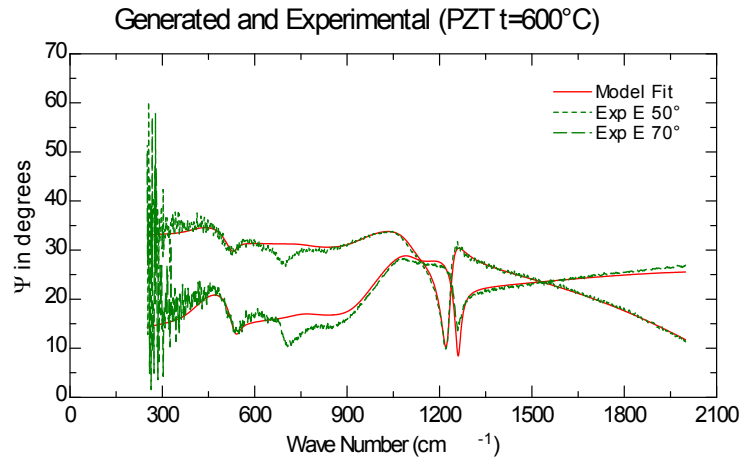


Fig. 3.4.10. Experimental and modeled data for PZT samples annealed at 500°C (a-b). In the successive page: 600°C (c-d) and 700°C (e-f).



(e)

(f)

The figure 3.4.11 shows the PZT layer thicknesses estimated for the samples having different annealing treatment processes. During the pyrolysis process, the thickness were reduced of 50%, in fact, during this process, the organic materials, used to synthesis of the PZT sol-gel are expelled. During the annealing processes, the thickness decreases of other 50%. These results are compatible with the our previous work reported in this thesis ([2] and section 3.2, Chapter 3).

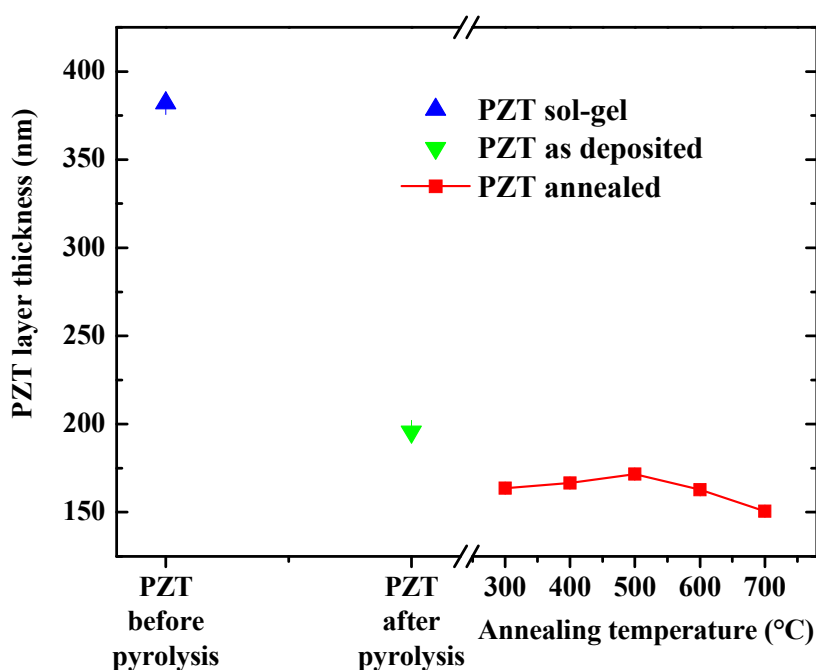


Fig. 3.4.11. The layer thicknesses estimated for the PZT samples having different thermal history. The blue and green triangle symbols represent the PZT thin film thickness before and after pyrolysis processes, respectively. The square red symbols represent the PZT layer thicknesses estimated for the annealed samples. The PZT thicknesses estimated for the samples annealed at 300°C and 400°C have been calculated by using a sum of the Lorentz oscillators, while the thickness estimated for the samples annealed at 500°C, 600°C, and 700°C have been obtained by using a Cauchy dispersion law.

Actually, this work is under investigation in collaboration with the Department of Electrical Engineering, University of Nebraska-Lincoln (USA).

Acknowledgements. I wish to thank Prof. Mathias Schubert in order to have invited myself at the University of Nebraska-Lincoln, and moreover in order to have extended the time duration of the my visit from one to two months. Thanks to Dr. Tino Hofmann to have helped me in the UNL laboratory.

Thanks to Dr. Marco Castriota for PZT materials. Thanks to Emanuela Bruno for SEM images.
(15 April 2008 - 15 June 2008)

Chapter 3 - Reference

- [1] Marco Castriota, **Stefano D'Elia**, Salvatore Marino, Enzo Cazzanelli, Nicola Scaramuzza, Carlo Versace and Roberto Bartolino, "Effects of thermal treatments on structural and optical properties of Lead Zirconium Titanate thin films obtained by sol gel technique". Submitted to *THIN SOLID FILMS* (2008).
- [2] **Stefano D'Elia**, Marco Castriota, Alfonso Policicchio, Carlo Versace, Nicola Scaramuzza, Enzo Cazzanelli, Raffaele Agostino, Carlo Vena, Giuseppe Strangi and Roberto Bartolino, "Thermally induced modifications of the optic properties of Lead Zirconate Titanate thin films obtained on different substrates by sol-gel synthesis". Accepted, *JOURNAL OF APPLIED PHYSICS*. (2008).
- [3] S. Marino, M. Castriota, G. Strangi, E. Cazzanelli, N. Scaramuzza, *J. Appl. Phys.* **102**, (2007) 013112-1.
- [4] I. Hamberg and C.G. Granqvist, "Evaporated Sn-doped In₂O₃ films: Basic optical properties and applications to energy-efficient windows", *J. Appl. Phys.* **60** (11) 1986 - R123.
- [5] C. M. Herzinger, B. Johs, W. A. McGahan, J. A. Woollam, W. Paulson, *J. Appl. Phys* **83** (6), (1998) 3323.
- [6] Mathias Schubert "Infrared Ellipsometry on Semiconductor Layer Structures. Phonons, plasmons, and polaritons", Springer, ISSN print edition: 0081-3869, electronic edition: 1615-0430.
- [7] B. Champagnon, C. Chemarin, E. Duval and R. Le Parc "Glass structure and light scattering", *Journal of Non-Crystalline Solids* **274** (2000) 81-86.
- [8] M. Tomozawa, J.-W. Hong, and S.-R. Ryu "Infrared (IR) investigation of the structural changes of silica glasses with fictive temperature", *Journal of Non-Crystalline Solids* **351** (2005) 1054–1060.
- [9] C. Lavelut, R. Le Parc, A. Faivre, and B. Champagnon, "Influence of thermal history on the structure and properties of silicate glasses", *Journal of Non-Crystalline Solids* **352** (2006) 4495–4499.
- [10] I. Hamberg and C.G. Granqvist, "Evaporated Sn-doped In₂O₃ films: Basic optical properties and applications to energy-efficient windows", *J. Appl. Phys.* **60** (11) 1986 - R123.
- [11] T. D. Kang, G. S. Lee, H. S. Lee, H. Lee, Y. S. Kang, Sang-Jun Cho, B. Xiao, H. Morkoc and Pau G. Snyder, "Infrared Ellipsometry Study on PZT Thin Films" *J. of the Korean Physical Society*, **49** (4) (2006) 1604-1610.

Chapter 4

Self-Assembly of surfactant molecules

Introduction

The spontaneous process by which some particles, nanoparticles and molecules organize them self in ordered structures is indicated with Self-Assembly (SA) process. The SA process of amphiphilic molecules allows obtaining molecular thin films with superb chemical and mechanical properties [1, 2], characterized by high order degree. This molecular thin films have been used to develop new nanolithography technique [3], new experimental technique applied to the nanotechnology [4] and new results in the branch of the biologic and pharmaceutical science [5]. Many of these results are directly rely to the order degree of the molecular thin films. The SA molecular order can be controlled by different experimental procedures used during the deposition phase - depending on the utilized molecular species [6, 7]. By combining the ellipsometry technique and static contact angle measurements, it is possible deduce valuable information regarding the ordering at molecular level of a self assembly monolayer [7].

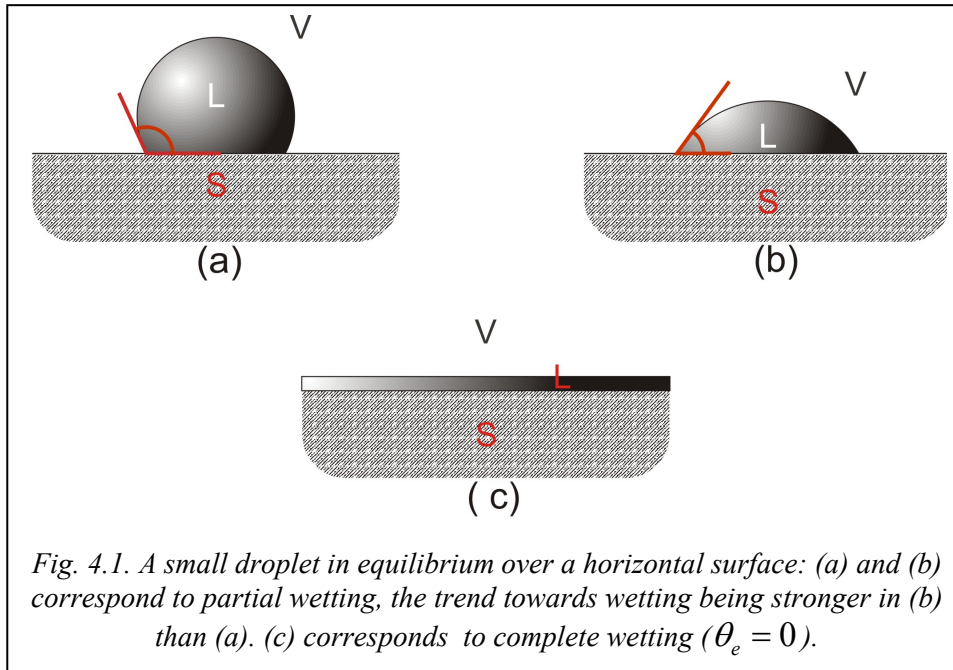
In order to introduce the physical system studied in this chapter, we give some general information about two tackled theoretical and experimental problems. First one is the angle contact measure and the wettability problems, and the second one is the ultra thin film problem in ellipsometry technique.

4.1. Angle contact and energy: Young condition

The organization of the molecules, located at the interface between two phases (for example liquid-air interface), is different from that in the bulk of the liquid (or air) phase. These molecules are completely surrounded by other molecules of the same type and are located in an isotropic environment. This symmetry is missing in the region of the interface. The molecules at the interface, fact, interact with the molecules, located in the uniform region of their own phase, in a different way than with the molecules of the nearby phase. For this asymmetry, it is need to make labour to bring a molecule from the homogeneous phase to the interface (liquid-air), and this labuor is related to the size variation of the surface of the interface. Therefore, an surface increasing of the interface dA requires an increasing of the labour, dW , proportional to $dW = \gamma dA$, where γ is called *surface tension* (free energy per unit area).

When a small liquid droplet is put in contact with a flat solid surface, an equilibrium between the three phases: solid (S), liquid (L) and air (V) occurs.

Two distinct equilibrium regimes may be found: partial wetting (Fig. 4.1a and 4.2b) with a finite *contact angle* θ_e , or complete wetting ($\theta_e = 0$) (Fig. 4.1c).



This thermodynamic equilibrium may be described by the Young equation given by:

$$\gamma_{SV} - \gamma_{SL} - \gamma_{LV} \cos \theta_e = 0 \quad (4.1)$$

where γ_{SV} , γ_{SL} , and γ_{LV} are the surface tension between the solid-air, solid-liquid, and liquid-solid interfaces, respectively. Eq. 4.1 shows that angle contact θ_e is entirely defined in terms of thermodynamic parameters: measurements on θ_e give us certain information on the interfacial energies. Usually, we know $\gamma_{LV} \equiv \gamma$ by separate measurements. Thus we are left with two unknowns (γ_{SV} , γ_{SL}) and only one datum (θ_e). But it is only the difference $\gamma_{SV} - \gamma_{SL}$ which is relevant for experiments involving the liquid.

Two cases seem to be of particular interest:

- If $\gamma_{SV} - \gamma_{SL}$ is larger than $\gamma_{LV} \equiv \gamma$, the drop tends to spread completely over the solid, resulting in a situation of complete wetting;
- If $\gamma_{SV} - \gamma_{SL}$ is a lot smaller than $\gamma_{LV} \equiv \gamma$, the drop should be sitting on the solid like a marble ($\theta_e = 180^\circ$). However, no physical systems have been reported which realizes such situation, for example, water on highly hydrophobic smooth surfaces make contact angles in the order 120° . However, different experimental investigation are reported in literature, concerning the high hydrophobic surface problems. Such physical situation is called *super hydrophobic surface* [8, 9].

Full review paper about wetting of solids by liquid can be find in literature [10].

4.2. Ultra thin films problem in spectroscopic reflection ellipsometry. Outline

Due to the continuous miniaturization in microelectronics, silicon oxide layers with a few nanometer thickness (less than 5nm) grown on silicon substrate are required. For the development of such ultrathin layers an accurate characterization technique to determine their thickness were essential. Ellipsometry is known as a sensitive and accurate non-destructive technique for characterization of multilayer structures. Ellipsometric measurements are not direct, different algorithms and methods have been developed to extract information about the optical constants and the thickness of thin layers from measured data. We have shown, that the most common technique is a regression analysis assuming a physically realistic model (optical model) for the multilayer structure (Chapter 2 of this dissertation). Therefore, when an optically isotropic film is deposited on a optically isotropic substrates, the complex refractive index and thickness d of the film are obtainable by solving the three-phase model (substrate/overlayer/ambient) to calculate the theoretical ellipsometry equation ρ .

This so-called nkd (n is refractive index; k is the extinction coefficient, and d is the thickness) problem has been investigated extensively over the last 35 years, and only in the last 10 years, it has made improvement with new digital computer. In order to solve this problem the numerical inversion of the exact equation of reflection ellipsometry is required, but the equations are typically nonlinear and transcendental equations (chapter 4 of the ref. [11]).

The inversion problem becomes particularly complex when the thickness of the film is very thin i.e. when $d/\lambda \ll 1$, where λ is the wavelength of the light, because increase the correlation between adjacent layers as the layer thickness decreases.

This problem is very complicate mathematical problem, and actually is under investigation. Different algorithms have been proposed to numerical inversion of the ellipsometry equation in the limit $d/\lambda \ll 1$. In the last international ellipsometry conference (ICES 4 – Stockholm – Sweden, June, 2007), I.K. Kim and D. E. Aspnes have proposed new mathematical approach to improve and solve the correlation between n , k , and d [12, 13, 14]. This new method allows to estimate layer thickness of transparent layer (less than 1 nm) breaking the correlation between the refractive index and thickness values.

Briefly, we introduce some useful information concerning the ellipsometry technique and the experimental method used to study thin film in the limit $d/\lambda \ll 1$. In order to understand the mathematical inversion problem in the thin-film limit, it is need answer to this question: why does the correlation problem occur between the parameters in the thin-film limit?

In the thin-film limit ($d/\lambda \ll 1$), a film can be considered transparent ($k \approx 0$). In this regime ($d \ll 10\text{nm}$), the corresponding changes in Ψ angle, in particular, become extremely smaller than Δ angle and require highly precise measurements together

with accurate calibration procedures of the instrument to determine simultaneously the thickness and refractive index [11, 15]. Therefore, in the thin-film limit, the measured Ψ angle is more susceptible to the experimental error than the measured Δ angle. This increase the interdependence between the parameters of the optical model, because after the inversion of the ellipsometry equation only the measured Δ angle is useful to estimation of the parameters by inversion of the equations, while the information given by the Ψ angle are subject to a “big error”. We recall that Δ and Ψ angles, simultaneously, are important to calculate the parameters of the optical model [11].

In order to solve the high correlation problem between the parameters of the optical model, different circumstances are required. First of all the ellipsometry angles must be measured with high precision and low error (systematic and random errors). It is worthwhile to quantify the sensitivity of ellipsometry to the presence of overlayer on a substrate whether is an intentional film or contamination. Table 1 shows calculates results for a Si surface coated with a film with $n=1.5$ and $k=0$ for 632.8nm light and angle of incidence 70° (chapter 8 of the ref. [16]).

Δ ($^\circ$)	Ψ ($^\circ$)	Thickness (nm)
179.257	10.448	0.0
178.957	10.448	0.1
178.657	10.449	0.2
178.356	10.450	0.3
178.056	10.451	0.4
177.756	10.453	0.5
176.257	10.462	1.0

Table. 1. Calculate Δ , Ψ for various film thickness with condition: $n = 1.5$ on Si, $k = 0$, 632.8nm, and $\phi = 70^\circ$. (from chapter 4, ref. [16])

Under these conditions of the calculation for an imaginary film that is similar to SiO_2 , it is seen that Δ changes by about 0.3° for 0.1nm of film, while Ψ remain unchanged. Considering that a properly aligned ellipsometry with high quality optics is capable of precision of about an order of magnitude better in Δ and Ψ from 0.01° to 0.02° , submonolayer sensitivity is readily achievable with a properly aligned and calibrated ellipsometer.

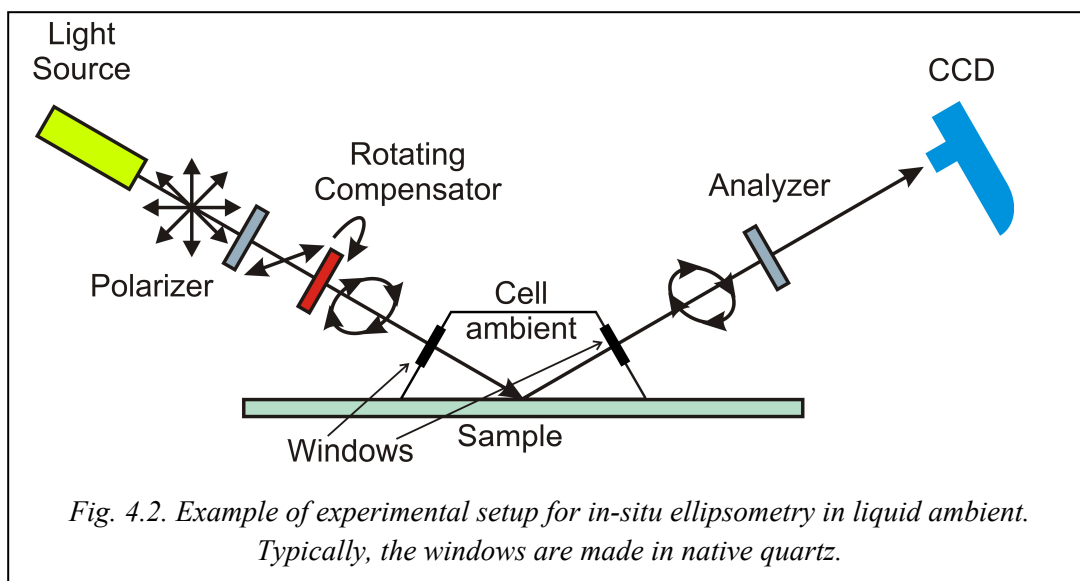
R.M.A. Azzam and N.M. Bashara have theoretically shown, the dependence of the thickness and optical properties estimated by imperfect ellipsometry angles i.e. when the ellipsometric angles are characterized by systematic and random error. These simulations have been performed for the three-phase: air/ SiO_2 /Si (chapter 4 of the ref. [11]). In the presence of experimental errors, in the ellipsometry angles, as large as -0.1 to 0.3° , it is still possible to obtain solutions for the parameters almost identical to the solution obtained when the error range is 0 to 0.01° , which is the lower limit in practice. This is true also for very thin films, for example 20\AA [11].

The sensitivity of an ellipsometry is related to the quality optics and to the technique used to measure the ellipsometry angles. At this moment, the polarization modulation ellipsometry (PME) designs allows to measure the ellipsometry angles with high precision [11, 16]. For example, the last spectroscopic ellipsometry instruments is a double rotating compensator, and it is able to measure 16 elements of the Muller matrix that describes the sample [16].

The J.A. Woolam M2000F is a single rotating compensator (RC), it can measure the Δ angles near 0° and $\pm 180^\circ$ with high precision (obviously after a good calibration!) [16], and this is very important for the study of the thickness of a transparent film in the thin-film limit [11].

Two different experimental methods are used to solve the correlations between the parameters in the thin-film limit: Multiple-Angle-of-Incidence (MAI) and Multiple-Incidence-Medium (MIM) measurements. The first measurement technique consist to measure the ellipsometry angle to different angle of incidence [11]. By mathematical and experimental simulation, R.M.A. Azzam and N.M. Bashara have shown that correlation can be solved (chapter 4 of the ref. [11]). The second measurement consist to measure the ellipsometry angles chancing the ambient medium in the three-phase system (ambient/film/substrates) [11, 15].

The first method is easy to reproduce, while on the contrary, the second method require an new experimental setup (for example a cell or an case) to perform the measurements in different ambient, because this method require different interface between the sample and the ambient. But this cell introduce other problem to calibration of the instruments [15]. It needs correct the measured ellipsometry angles, because the light beam pass through two glass windows as shown in the Fig. 4.2.



We can reassume that ellipsometry technique allows to study very thin film only by following accurate procedures before and during the ellipsometry measurements: performing an accurate calibration of the ellipsometry [11, 16]; measuring the

ellipsometry angles by MAI method, around the Brewster angle (chapter 4 of the ref. [11]), or by MIM method.

To conclude, an good optical model for substrates and for ultra-thin film are required too.

In literature can be found different experimental investigations concerning the ultra thin film problem, performed by means the ellipsometry technique, in these last 30years. Physical and chemical adsorption of molecular or atomic species on surfaces in contact with gaseous or liquid ambient has been studied in-situ by ellipsometry, for example the physical adsorption of water vapor onto etched and hydrated silicon surface or chemical adsorption of several molecules (capronic, lauric, stearic acids et al.) (chapter 6 of the ref. [11]). Oxide-film growth on surfaces of semiconductor and metals in atmospheric, controlled-gaseous, and liquid ambient are successful studied also by ellipsometry technique. The oxide-film growth rate has been studied for different material, for example, by employing oxygen pressures below 10^{-6} torr, Chou et al. (chapter 6 of the ref. [11]) succeeded in using *null ellipsometry* to resolve the initial growth of ultra-thin (0-8Å) lead oxide (PbO) on clean lead (Pb) surfaces (it has been confirmed by auger electron spectroscopy). The thickness of the growing oxide film is closely proportional to the oxygen exposure until a limiting thickness of about 6.3Å, irrespective of pressure.

In the same book [11] can be found different examples concerning also the chemical adsorption of biologic materials, studied by ellipsometry.

Spontaneous spreading of microdroplets of polymeric liquid, nematic liquid crystal and surfactant molecules have been successful archived by using the ellipsometry technique [17, 18, 19]. In these experiments the thickness of organic molecules in ultra thin film regime ($0.1 \leq d(\text{nm}) < 10$) has been measured by ellipsometry.

By using generalized ellipsometry, the weak in-plane anisotropy of Langmuir-Blodgett (LB) ultrathin films (cadmium behenate surfactant onto a hydrophilic silicon substrates) has been studied [20]. The results show that on a 19-monolayer LB film (i.e., with a thickness of $\sim 50\text{nm}$), it is possible to measure in-plane birefringence of 10^{-2} with absolute accuracy of 10^{-3} . Less accurate but still satisfactory in-plane birefringence measurements are possible on LB films as thin as 10nm (four monolayers).

In the last year (2007), I.K. Kim and D. E. Aspnes have been studied the reversible physical adsorption of water vapor on oxidized GaAs. They have proposed new method to extend the limit of the simultaneous determination of the refractive index and thickness (less than 1nm) [14].

4.3. Self-Assembly and molecular order

THE INFLUENCE OF DRYING TEMPERATURE ON THE CLOSED-PACKED STRUCTURE OF SILANIZED MONOLAYERS DEPOSITED ON INDIUM TIN OXIDE (ITO) SUBSTRATES

Submitted to SURFACE SCIENCE (2008)

Stefano D'Elia¹, Valentin Barna², Nicola Scaramuzza, Giuseppe Strangi, and
Roberto Bartolino.

¹ INFN-CNR-LICRYL Laboratory and CEMIF.CAL, Department of Physics,
University of Calabria, via P.Bucci 31C, Rende (CS), I-87036 (ITALY).

² Faculty of Physics, University of Bucharest, PO Box Mg-11, 077125, Bucharest,
Romania.

AUTHOR EMAIL ADDRESS: saramuzza@fis.unical.it

RECEIVED DATE

ABSTRACT. Molecular organization of self-assembled n-dimethyl-n-octadecyl-3-aminopropyltrimethoxysilylchloride (DMOAP) layers on ITO coated glass substrates was thoroughly investigated. The layer thickness for each deposition was determined by Variable Angle Spectroscopic Ellipsometry (VASE), while from static contact angle measurements we deduced valuable information regarding the ordering of the molecular structures at solid-air interface. In particular, the DMOAP thin film formation was studied for two different drying temperatures (85°C and 120°C). While at $T_{\text{drying}}=85^{\circ}\text{C}$ we observed the formation of a molecular monolayer characterized by a closed-packed structure, at the higher temperature the DMOAP molecules 'bend' at the substrate as they stack in relatively disordered clusters. A qualitative interpretation of this phenomenon is given, in good agreement both with the obtained experimental data and experimental investigation reported in scientific literature. The observations regarding the DMOAP molecular level organization in function of substrate temperature could bring essential information to the self

assembly research community and also explain some important physical phenomena occurring at interfaces.

KEYWORDS: Self-assembly, Ellipsometry, Thin films, Surfactant molecules, Static contact angles, Organosilicon derivatives.

Introduction.

Self-assembled monolayers (SAMs) of organic thin films demonstrate an increasing interest in many application fields over the last years. These modified surfaces find their use in pharmacologic and biological applications, but also in chemistry, material and surface science [1-6]. Recently, investigations have also been performed towards the nanotechnology area; SAMs are successfully used in the nanolithography techniques for obtaining nanometric structures [7,8]. The combination of conventional lithographical and SAM techniques will definitely find its way towards further interesting applications in the nanomaterials and nanostructures arena [9].

The Self-Assembly (SA) processes were lately analyzed in great detail and a lot of information about the physical, chemical properties and experimental parameters can be found in the research literature [1, 2, 10].

Amphiphilic molecules can organize themselves into higher order structures of molecular monolayers at various types (liquid-liquid, air-liquid, and solid-air) of boundary interfaces. Several other techniques are also used for obtaining molecular monolayers at different interfaces.

The Langmuir-Blodgett (L-B) films are amphiphilic molecular monolayers organized at one interface (typically air-liquid) that are transferred to another one (air-solid) by means of mechanical procedures [1, 8]. Such a technique allows obtaining good quality molecular monolayer thin films characterized by a high molecular order degree, but has some drawbacks as these films suffer both in chemical and mechanical stability [8]. Typically, molecular monolayers are not chemically bond at the surfaces: the interactions are electrostatic like as well as of the van der Waals (VdW) type, but also dipole-dipole, hydrophilic and hydrophobic [10].

The Self-Assembly is a spontaneous process in which the amphiphilic molecules are usually adsorbed on a solid surface. These molecules are characterized by chemical groups that possess strong affinities for the substrates. The preparation procedures for a molecular monolayer, by spontaneous adsorption of a surfactant onto a clean surface, are relatively simple. Firstly, the surface is treated by means of immersion in a surfactant solution [11] or by exposure to the surfactant vapor phase [12].

The Self-Assembly process allows obtaining molecular thin films with superb chemical and mechanical properties [8], whereas the molecular order can be controlled by different experimental procedures used during the deposition phase - depending on the utilized molecular species [1, 2, 8, 13, 14].

SAM formation of the organosilicon derivatives require hydroxylated surfaces as substrates. In fact, several experimental investigations showed that monolayers can be successfully prepared onto substrates covered by silicon oxide, aluminum oxide, glass, quartz, mica, indium tin oxide (ITO) etc [10]. A common and straightforward model used to describe the chemical adsorption of the molecules onto the oxide surfaces consists in a hydrolysis process between the hydrate surface and the hydrolysable head group of the surfactant molecules. A chemical bond between the silicon atom(s) in the polar head group of the organosilane molecules and the surface oxide is created by means of a chemical process favored by the presence of water [10, 15]. This chemical adsorption model was studied and confirmed for the SAM formation of the organosilane molecules as alkylchlorosilanes, alkylaminosilane and alkylalkoxysilane derivatives [4, 10, 15].

Brzoska [16] has observed that the SAM formation of the n-alkyltrichlorosilane thin films on hydrophilic substrates is favored by the low temperature of the solution. In fact, when the solution temperature is lower than a critical temperature, T_c , layers of high surface quality are obtained. T_c temperature is characteristic of the surfactant molecules and it is independent of the solvent being used. Brzoska observed a linear dependence of this critical temperature on the length of the chain for the molecular hydrophobic group.

The molecular order of the hydrocarbon chains in the SAM of organosilane molecules is influenced both by the surfactant and the water concentration in the solution [2, 10]. High surfactant concentration favors the formation of complex molecular structures as well as micelle, vesicle and oligomerization processes between the molecules [15]. Such processes are undesirable, as they contribute to the generation of defects in the SA thin films structure.

The surfactant concentration depends on the molecular species and on the different experimental parameters as well as on the water concentration and solution temperature [2, 10]. The molecular order of the SAM is also influenced by the solvent used in the solution [14]. These observations are very important and lead to developing a new experimental procedure for SAM formation by using mixtures of various solvents.

The growing SAMs for the organosilane molecules can be described in three stages [17, 18]. The initial part involves the chemical adsorption from solution and the island formation on the substrate surface. During this phase, a large region of the surface remains uncoated while in the covered part the hydrocarbon chains are completely disordered. The second stage is characterized by the formation of ordered molecules with closed-packet hydrocarbon chains. When the molecular chains are sufficiently close, electrostatic interactions (VdW and dipole-dipole) are involved

and they manage to support each other [8]. The long hydrophobic chains assume a closed-packed structure of the monomolecular layer characterized by an increased order with respect to the one observed in the first stage. During this second phase still only a small increase in the surface coverage occurs. The final stage is represented by a much slower adsorption process, as the surface is almost completely covered. During this step, some oligomerization processes may occur on the SAM surface, resulting in an increase of the molecular disorder [16, 19].

The spontaneous formation of the monomolecular layers occurs when the substrate is exposed to the surfactant molecules. An easy experimental procedure consists in the immersion of the substrates in the surfactant solution for a certain amount of time. When the substrate is removed from the solution some solvent molecules will however remain both onto the surfactant coated substrate and also between the hydrocarbon chains. These molecules can be removed by drying of the SAM samples in a furnace.

In this paper we study the influence of the drying temperature on the molecular organization of SAMs. Up to now this experimental parameter was very little considered in both theoretical and experimental investigations in the field, but as it will be demonstrated, it is a fundamental quantity to be taken into account. An accurate experimental setup and procedures were prepared in order to study the influence of the drying process on the molecular reorganization.

The *n,n*-dimethyl-*n*-octadecyl-3-aminopropyltrimethoxysilylchloride (DMOAP) organosilane has been used in order to study the molecular order versus the drying temperature in SAM structures.

The DMOAP molecules form an ordered SAM on oxide surfaces and the long hydrophobic chains ($17\text{CH}_2+\text{CH}_3$) assume generally an almost orthogonal orientation with respect to the substrate [4, 20] (fig.1). These molecular monolayers have been extensively investigated for liquid crystal (LC) applications [3,4]. A glass substrate covered by a SAM(s) of DMOAP surfactant can induce homeotropic alignment to a nematic liquid crystal (NLC) [21], as the nematic molecules can penetrate in between the hydrophobic chains of the surfactant [4] as shown the figure (1). The NLC molecular order obtained by using DMOAP surfactant molecules has been used recently to observe unexpected optical depolarization effects during the electrically induced Fréedericksz transition [22].

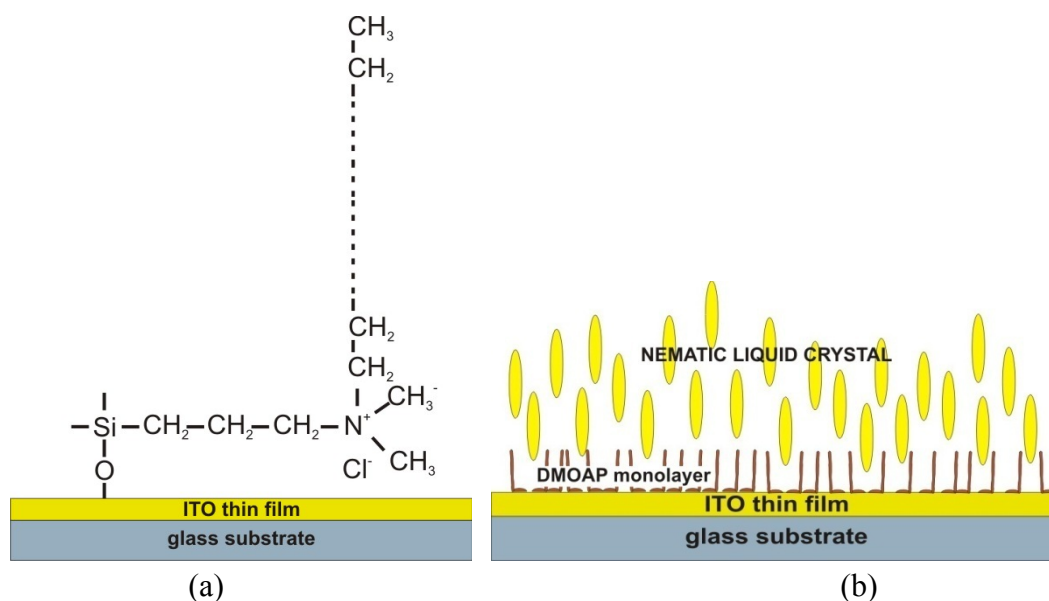


Figure 1. The chemical bond (a) between the silicon atom in the polar head group of the DMOAP molecule and the surface oxide (ITO) is created by means of a chemical hydrolysis process favored by the presence of water. The DMOAP molecules generally assume an almost orthogonal orientation with respect to the substrate and they induce a homeotropic alignment to NLCs (b).

The molecular length of a DMOAP molecule can be theoretically estimated. Different experimental observations showed that surfactant molecules increase the length of the hydrophobic tail by around 1.27\AA for one methylene group (CH_2) summed to the long hydrocarbon chain [1, 23, 15]. The methyl terminal group and polar head group also contribute to the molecular length. In order to check this, it is necessary to stress some experimental observations.

Fadeev and McCarthy studied monomolecular layers of dichloro- and trichloroalkylsilanes deposited on silicon having different length chains [19]. The layer thickness estimate for the dimethyldichlorosilanes was $\sim 3.5\text{\AA}$ (the dimethyldichlorosilanes $(\text{CH}_3)_2\text{SiCl}_2$ is a surfactant molecule with very short hydrophobic group, composed by only one methyl group). Other experimental studies concerning the alkanethiols show the contributes to the molecular length of both the terminal group of the alkyl chain and the sulfur ion polar head. For example, the carboxylic acid terminal thiols of varying chain lengths are characterized by sulfur ions in the polar head groups and by a large molecular group in the tail of the alkyl chain. For this type of molecules the contribution to the molecular length of the polar head and terminal alkyl group were estimated to be about 4.8\AA [23].

In our case, the DMOAP molecule is much more complex and definitely larger than dimethyldichlorosilanes, but in the same time similar to the alkanethiols

molecules. We estimated the reasonable size of 5Å by considering both the terminal methyl group and the large polar group of the DMOAP molecule (fig.1).

For these reasons, the DMOAP molecular length can be valued by using the previously introduced information. The 17CH₂ groups of the long DMOAP chain have the length around 21Å and if we consider both methyl and polar groups (~5Å), the DMOAP molecular length estimation is about 26Å.

The monolayer thickness of homogeneous surfaces covered by DMOAP molecules is also reported in the scientific literature. A layer thickness of 25 - 27Å inclusive has been estimated by using Atomic Force Microscope (AFM) [20], while comparable layer thicknesses were obtained by Almanza-Workman (20.7±8.5Å) by using the Spectroscopic Ellipsometry (SE) technique [24].

The molecular order of the SAM can be studied with different experimental techniques [8], such as surface second-harmonic generation (SHG) and sum-frequency generation (SFG) [4], x-ray photoelectron spectroscopy (XPS) [6], contact angle goniometry [25], spectroscopic ellipsometry and others.

The contact angle goniometry technique was often used to examine the general hydrophylicity or hydrophobicity of a surface, but it was also applied to the surface of SAMs as well [8]. The measured contact angle changes with varying film composition [26], it reflects the degree of surface order and could indicate the conformation of the functional groups at the substrate.

Let us briefly introduce the model used to describe the contact angle variation versus the composition of the monomolecular thin films. The static contact angle of a liquid on a heterogeneous surface composed by two chemical groups, characterized by the surface two covered fractions respectively f_a and f_b , can be estimated by using the phenomenological Cassie equation (eq.1) [27, 28] and the modified Cassie equation introduced by Israelachvili-Gee (eq.2) [28]:

$$\cos \theta = f_a \cos \theta_a + f_b \cos \theta_b \quad (1)$$

$$(1 + \cos \theta)^2 = f_a (1 + \cos \theta_a)^2 + f_b (1 + \cos \theta_b)^2 \quad (2)$$

where $f_a + f_b = 1$ and θ_a and θ_b are the two static contact angles of the liquid respectively on the homogeneous surface covered by the a and b type chemical groups.

In this work both the static contact angle measurements, explained by using equations (1) and (2), and SAM layer thickness, estimated by ellipsometrical investigations, were determined for the molecular organization and the SAMs formation.

Experimental

Materials. The 2-Propanol alcohol (99.8%) from Panreac and the n,n-dimethyl-n-octadecyl-3-aminopropyltrimethoxysilychloride (DMOAP) [CH₃(CH₂)₁₇(Me)₂N⁺(CH₂)₃Si(OMe)₃Cl⁻] product ~50wt.% (AT) from Sigma-Aldrich were used without a purification process. The 2-Propanol solvent is

characterized by a boiling temperature that is reported in the specification sheet to be around 81-83°C.

A solution of 0.005wt.% DMOAP mixture in 2-propanol alcohol was obtained by mixing the two components. This low surfactant concentration was chosen for reducing the probability of the micelles and vesicles formation during the SAM deposition. In order to disaggregate the DMOAP micelles and vesicles systems, the organosilane solution was first stirred for approx one hour at room temperature, and afterwards sonicated for another hour.

The SAM formation is related to the chemical reactions with the hydrate oxide surface. These processes occur mostly because of the water molecules that are present in the 2-Propanol alcohol (0.1%), so no water was added in the solution for this experiment.

Substrates and samples preparation. The substrates consisted of float glass covered by an indium tin oxide (ITO) thin film (nominal sheet resistance, $R_{sh}=25\Omega/\square$) manufactured by Balzers [29]. A rigorous cleaning procedure was applied for removing all surface impurities, but taking into account not to damage the surface. The substrates were ultrasonically cleaned in chloroform, acetone for two times and then showered bi-distilled water for three times to eliminate potential residual alcohol traces. Finally, the substrates were dried in a furnace (at 110°C) for 30 minutes.

The experimental setup used for SAMs depositions is presented in figure 2. The glass substrates were dipped in a baker containing the surfactant solution. During the SAM depositions, the surfactant solution contained in the beaker was continuously stirred while the glass surfaces were held vertical by a rack, both the beaker and the rack were made by chemically inert polytetrafluoroethylene (PTFE).

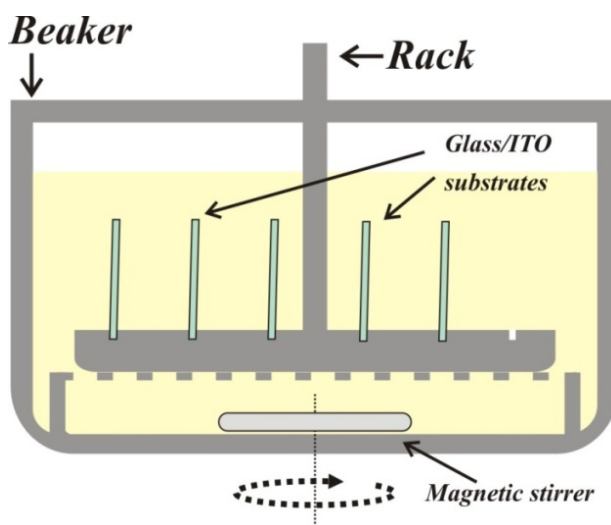


Figure 2. Schematic representation of the deposition setup: the beaker and the rack (dark grey) for vertically holding the substrates are built in Teflon® (PTFE). The surfactant solution was stirred for the entire duration of SAMs depositions.

For obtaining SAM samples with low impurities and defects, the experimental setup was kept in a laminar flow hood inside a clean room - CR (class ISO 5).

The protocol used for the surfactant depositions is the dipping treatment of the clean substrates in the DMOAP solution: N glass/ITO substrates are dipped in the DMOAP solution for approx 20 mins, and afterwards dried for more than 40 mins in the furnace (set at T_{drying} temperature). Following the annealing process one of the substrates was kept aside while the other N-1 substrates were subject to the dipping treatment process previously described. Subsequently this repetitive process, in the end, we have that the first sample was subject to one treatment (1_{dip}) while the N^{th} sample was subject to N treatments (N_{dip}).

The two different drying temperatures (T_{drying}) for evaporating the 2-propanol solvent were chosen to be 85°C and 120°C respectively. The first one was in the neighborhood of the 2-propanol boiling temperature (81-83°C) while the second one is much larger. For each T_{drying} temperatures, a set of five samples was prepared by using the deposition protocol previously described. In order to confirm the reproducibility of the experimental results, the set of five samples, dried at the lower temperature, $T_{\text{drying}} = 85^{\circ}\text{C}$ was prepared two times by using the same experimental procedures and parameters. For clarity, the two set of samples were called $T_{\text{drying}} = 85^{\circ}\text{C}$ (1st) and 85°C (2nd).

During the SAM depositions, both the DMOAP solution temperature and the atmospheric relative humidity of the microclimate in the laminar flow hood have been monitored: $T_{\text{Sol}}(\text{DMOAP}) = 20 \pm 3^{\circ}\text{C}$ and $\text{RH} = 34 \pm 2\%$. The parameters remained constant for all the depositions (which took about six hours for each set of the samples).

Experimental Measurements

Spectroscopic Ellipsometry (SE) technique was employed to determine the SAMs layer thickness. The VASE M2000F (J.A. Woollam) rotating compensator ellipsometer (RCE) was used to measure the ellipsometric angles (Ψ and Δ) spectra, in the wavelength range 250-1000nm. Measurements at different angles of incidence (AOI) were performed to increase the accuracy of layer modeling. The structural and morphological properties have been estimated from the ellipsometric characterization by using a multilayer optical model compatible with our samples. Each layer was defined by an optical model, for which the fit parameters were the thickness and complex dispersion law. The optical model and the best fit parameter values have been calculated by mean the WVASE32® application (J.A. Woollam). The software resolves the minimum values of the likelihood estimator function, Mean Square Error (MSE), using the nonlinear Levenberg-Marquardt algorithm. The figure of merit, MSE, is a measure of the fit quality [12], and it is defined by:

$$MSE = \frac{1}{2N - M} \sum_{i=1}^N \left[\left(\frac{\Psi_i^{\text{mod}} - \Psi_i^{\text{exp}}}{\sigma_{\Psi,i}^{\text{exp}}} \right)^2 + \left(\frac{\Delta_i^{\text{mod}} - \Delta_i^{\text{exp}}}{\sigma_{\Delta,i}^{\text{exp}}} \right)^2 \right],$$

where N is the number of data points, M is the number of the fitting parameters, $(\Psi^{\text{exp}}, \Delta^{\text{exp}})$ and $(\Psi^{\text{mod}}, \Delta^{\text{mod}})$ are the measured and modeled ellipsometric angles respectively, while σ_{Ψ} and σ_{Δ} are standard deviations of the measured ellipsometric angles. The modeled ellipsometric angles $(\Psi^{\text{mod}}, \Delta^{\text{mod}})$ are functions depending on all the fit parameters which define the multilayered optical model.

The CAM 200 – Optical Contact Angle Meter by KSV Instruments LTD was used to estimate the static contact angle of pure bi-distilled water on the coated DMOAP samples. The static contact angle measurements were performed at room temperature (~25°C), after 24 hours from the SAM sample deposition. The followed procedure consisted in registering the shape of a small water droplet (~4μL) placed on the coated substrate; for each measurement, ten digital photos of the shape of the water droplet were acquired after 5 minutes from the deposition of the small water droplet. These photos were used to calculate the average and indetermination value of the water static contact angle by using the software elaboration of the CAM 200 – Optical Contact Angle instrument.

Models, results and discussion

Structural and optical models. The analysis of the ellipsometric angles spectra requires a highly elaborated multilayer optical model. Moreover, for estimating the ultrathin films thickness of the DMOAP monolayer, a very accurate optical model for the substrate is essential. The optical and structural properties of the substrates purchased from Balzers were extensively studied on several previous occasions [30, 31].

The float glass substrates were studied by means of a Cauchy dispersion law, describing the refractive index that is given by the empirical formula [32]:

$$n(\lambda) = A_n + \frac{B_n}{\lambda^2} + \frac{C_n}{\lambda^4}, \text{ where } A_n > 1 \text{ and } A_n, B_n \text{ and } C_n > 0 \quad (3)$$

and also the Urbach model to characterize the extinction dispersion law [32].

The ITO thin film was modeled by using two layers (Tab. 1) with different conductive or dielectric properties: the first one describes the bulk; the second one describes the rough surface of the ITO film. The bulk layer has been simulated by using a linear sum of the Drude oscillator (conductive properties) and the Lorentz oscillator (dielectric properties) [32]. The roughness of the surface layer was defined by using the effective-medium approximation with a mixture of a Lorentz oscillator layer (ϵ_{ITO}) and voids ($\epsilon_{\text{void}} = 1$). The complex effective dielectric function (ϵ_{srough}) was calculated by the Bruggeman effective medium approximation (EMA) [32, 33]:

$$f_{ITO} \frac{\epsilon_{ITO} - \epsilon_{srough}}{\epsilon_{ITO} + 2\epsilon_{srough}} + f_{void} \frac{\epsilon_{void} - \epsilon_{srough}}{\epsilon_{void} + \epsilon_{srough}} = 0,$$

where f_{ITO} and f_{void} are the volume fractions of the ITO phase and voids respectively; and they must satisfy $f_{ITO} + f_{void} = 1$.

Surface roughness (EMA model)
ITO layer
Glass bulk 1.1mm

Table 1. ITO layer is realized by using the sum of Drude (conductive property) and Lorentz (dielectric property) oscillators. Surface roughness is modeled by using EMA model (mixing the Lorentz oscillator and Void).

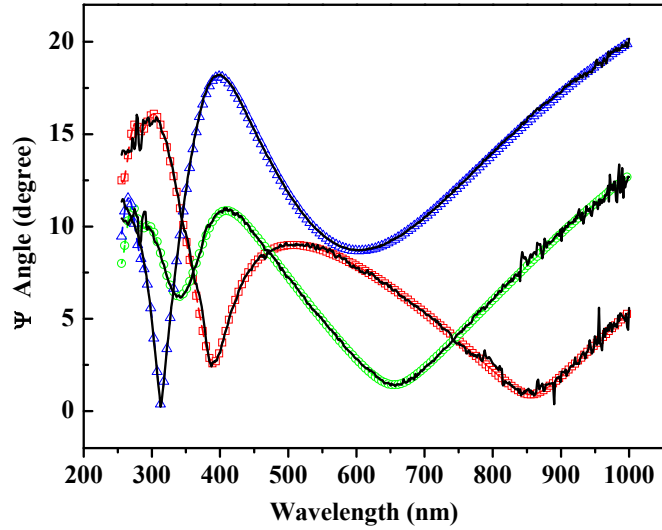
The excellent optical model that was estimated for the glass/ITO substrates [30, 31] has allowed us to study with great precision the DMOAP layer thickness. This molecular layered optical system can be considered a typical ultra thin film issue in the SE model problems, where the ratio between layer thickness (d) and light wavelength (λ) is less than one ($d / \lambda \ll 1$).

The ellipsometric angles Ψ and Δ acquired for different AOI, measured with respect to the normal to the surface and near the Brewster-angle allow us to estimate the DMOAP layer thickness with extremely high precision [34]. The refractive index difference between ITO thin film (~ 1.86 at 589nm) and DMOAP (~ 1.41 at 589nm), as reported by Sigma-Aldrich data sheet and in the literature [19, 24] favors the multiple light reflections in the thin films, therefore increasing the sensibility of the ellipsometric measurements.

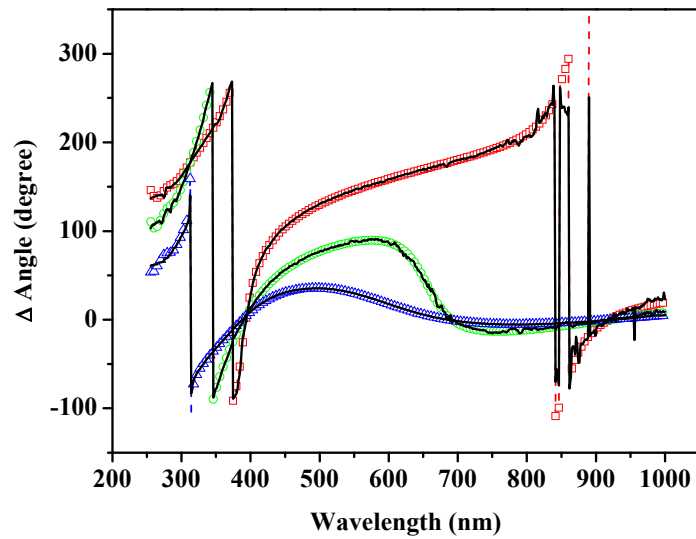
The SAM of the DMOAP molecules was then modeled by means of a single transparent layer (extinction coefficient, $k=0$). The refractive index dispersion of such molecular layer was described by using a Cauchy dispersion law, and the DMOAP layer thicknesses for the different dipping treatments (N_{dip}) were estimated in order for describing the molecular arrangements.

Experimental results and discussion.

The previously described ITO optical model allows obtaining exceptionally good fit results. An example of the fit elaboration is showed in figure (3).



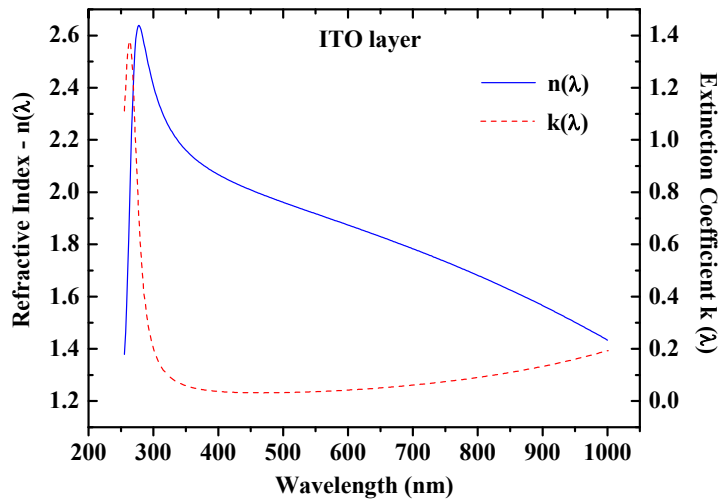
(a)



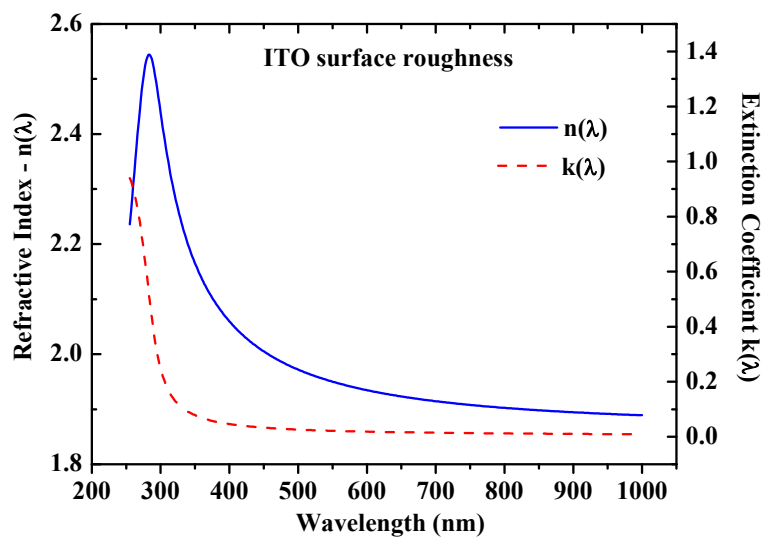
(b)

Figure 3. The ellipsometric angles Ψ (a) and Δ (b): experimental data (solid lines) and fitted results (symbols) for different AOI (angles of incidence); 60° (square), 65° (circle), 70° (triangle).

The ITO film thickness was estimated for each sample coated with DMOAP surfactant (data not shown). Figure (4) describes the morphological and optical properties of the ITO thin film.



(a)



(b)

ITO surface roughness (nm)	7.48 ± 0.40
ITO layer (nm)	98.26 ± 0.43

(c)

Figure 4. Optical properties of the “ITO layer” (a) and “surface roughness” (b) estimated for the glass/ITO substrate. The optical constants (refractive index and extinction coefficient) vs wavelength are plotted in the top panels. The ITO film thickness (c) is estimated by adding the “ITO” and “surface roughness” layers.

The structural and optical information of the ITO thin film have been fully investigated in recent papers [30, 31] and the determined optical model used extensively to examine the effects of the annealing process on both of the ITO substrate and other ferroelectric thin films. We observed that the structural and optical properties of the ITO thin film do not change too much when varying the temperature (for the temperature range 100-300 °C).

Water static contact angle measurements were performed on the clean ITO surfaces; we have obtained contact angle values between 35.5 and 38.5 degrees. These results are very close to the experimental contact angle measurements present in reference [35], obtained on glass/ITO substrates from Balzers. The high value of the contact angle is related to surface roughness of the ITO.

The DMOAP layer thicknesses estimated for the N samples subject to N_{dip} dipping treatments and dried at the temperature 85°C and 120°C, are shown in the figure (5). In order to consider the variations of the ITO layer thickness, during the fit elaborations between the different DMOAP samples, the two layer thicknesses describing the ITO thin film (surface roughness and ITO layer) was calculated together with the fit parameters of the optical model that describe the organic layer.

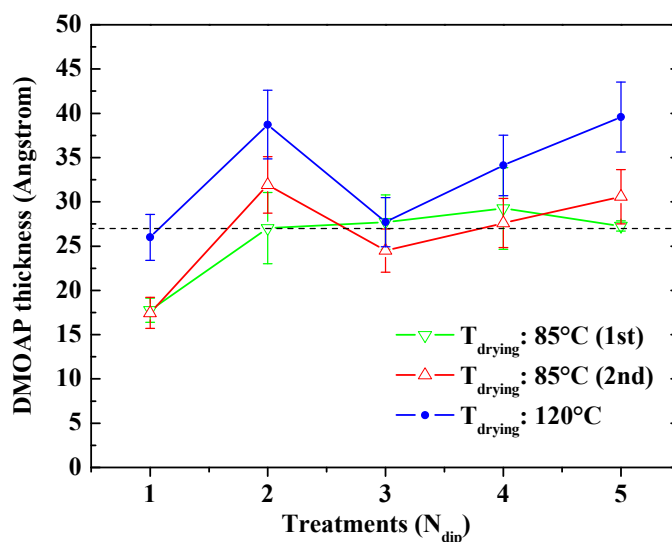


Figure 5. DMOAP layer thicknesses estimated for the samples dried at 85°C and 120°C. The dash lines limit the thickness of the DMOAP layer obtained by one and two overlaying mono molecular layers. The terms 85°C (1st) and 85°C (2nd) indicate two sets of samples prepared at different instants but at the same drying temperature (85°C) and in similar experimental conditions. The dashed line indicates the DMOAP layer thickness (~27Å) reported in literature by the reference [20, 24]

In figure (5) the dashed line indicates the average DMOAP layer thickness ($\sim 27\text{\AA}$), also reported in literature [20, 24]. Theoretical molecular length estimations (presented in the introductory paragraph of this manuscript) and the DMOAP thickness measurements (fig. 5) are fully compatible with similar information for DMOAP layer thickness extant in literature.

Figure 5 shows (void triangle symbols) the formation of a mono molecular layer after two treatments ($N_{\text{dip}} \geq 2$) when the drying temperature is 85°C , while for the 120°C (full symbols) drying temperature, we can observe the appearance of a DMOAP monolayer characterized by layer thickness little bit larger than that one obtained at low drying temperature.

In order to investigate the molecular structural reorganization, we present the water static contact angles that were measured for these particular samples. Figure 6 shows the static contact angles observed for the DMOAP samples having different drying temperatures and different number for the dipping treatment.

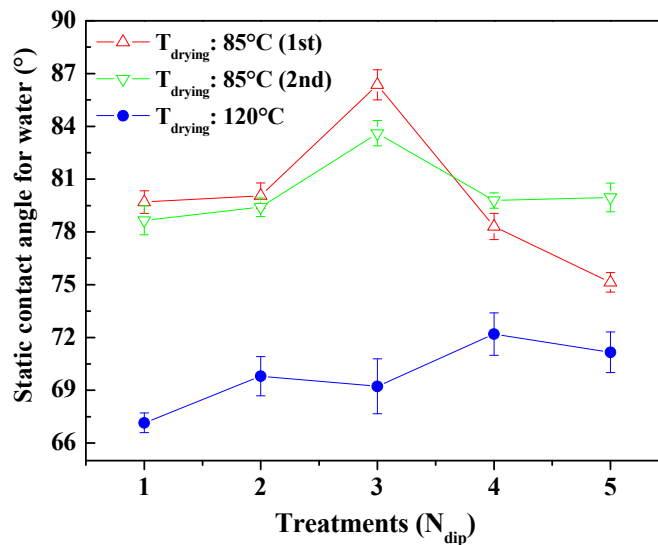


Figure 6. The contact angles acquired for DMOAP samples dried at 85°C are found to be larger than for the ones dried at 120°C . For the lower value of the drying temperature (85°C), the contact angle has the maximum value for the third dipping treatment ($N_{\text{dip}}=3$).

The experimental data demonstrate the reproducibility of the hydrophobic properties for the set of samples obtained for low drying temperature (85°C).

The contact angles acquired on DMOAP samples dried at 85°C were found to be larger than the contact angles on the DMOAP surfaces dried at 120°C . For the lower drying temperature of the DMOAP samples, the contact angle assumed maximum value for the third dipping treatment. In this point, the measured contact angle values, for the two set of studied samples, were found 86.4 ± 0.9 degrees and 83.6 ± 0.7 degrees respectively.

In order to understand correctly both DMOAP layer thickness and water static contact angle information, a schematic representation of the DMOAP molecular layer configuration was prepared (figure 7). DMOAP molecules are characterized by a head polar group with similar chemical properties of the organosilane molecules described in the introductory section. In this representation, we have supposed that the previously introduced experimental observations were also applicable for the DMOAP molecules.

In the introductory section, we described the growth of SAM surfactant molecules on a surface by means of three different stages. Figure 7 shows the molecular order configuration of the SAM for the first and second phase. The first stage can be described in the figure 7(a). The surface density of the surfactant molecules was small; therefore, the hydrocarbon chains could have collapsed on the substrate surface. In this case, the air-solid interface consists in a thin film composed by different chemical groups (methyl, methylene and head polar groups). The second stage of the SAM formation can be represented in figure 7(b). In this case, the hydrocarbon chains were packed together and, as they form a mono molecular layer on the surface. Let's considered the air-solid interface showed in figure 7(b) – we can observe that the surface fraction covered by methyl groups is larger than the surface fraction covered by methylene and head polar groups.

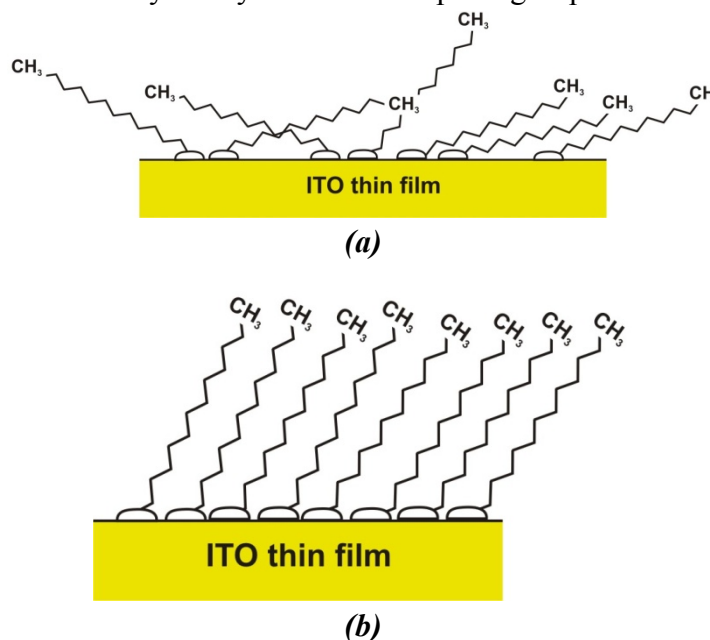


Figure 7. Schematic representation for a SAM of DMOAP. The zigzag line represents the long hydrocarbon chains, while the small “foot” represents the head polar group of the DMOAP molecule. The top picture (a) shows a representation of an disordered DMOAP monomolecular layer. Picture (b) presents ordered DMOAP layer.

Various experimental observations showed that the water contact angle on a homogeneous surface covered by methylene (CH_2) chemical groups is about 94 degrees, while the water contact angle on a homogeneous surface covered by methyl (CH_3) groups is around 110 degrees. These experimental results were obtained on homogeneous monomolecular layers deposited on very smooth silicon surfaces [19, 26]. The effects of the surface roughness on the water contact angle on the SAM of alkylsilane molecules have been previously reported in literature [36].

The water contact angle on the heterogeneous surface composed by different chemical groups can be studied by means the Cassie and Israelachvili-Gee equations (eq.1 and 2).

By considering these information, we can observe that if the hydrocarbon chains of the SAM form a closed-packet structure like showed in the figure 7(b), the air-solid interface will be more hydrophobic than the air-solid interface proposed in the figure 7(a). In the first case (fig.7a) the contact angle is given by the Cassie and Israelachvili-Gee equations, therefore resulting less than the water contact angle on a homogeneous monomolecular layer composed only by methyl (CH_3) groups, in the second case (fig.7b) the water contact angle value was close to the one for the methyl groups surface, characterized by a surface covered fraction of about one. Note that the monolayer thickness of an ordered molecular structure will be characterized by a large static contact angle.

The experimentally measured contact angle values for water were found to be lower than the ones reported in literature for the covered methyl and methylene surfaces [26], although the authors used purified surfactants in their experiments. We recall that our surfactant was not subject to any purification process. Therefore, we suggest that the observed lower contact angle values depend on two sources. Firstly, the dependence on the presence of some chemical ionic impurities (for example: chlorine and ammonium ions of the polar head) in the DMOAP surfactant mixture, but also (although is less probable) we cannot exclude the formation of a non perfect homogeneous surface.

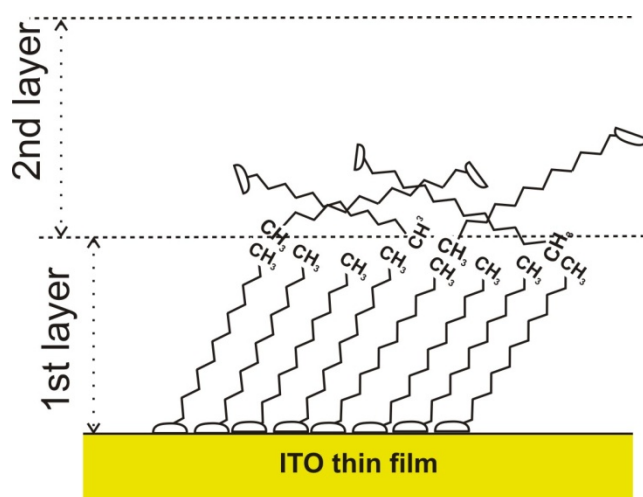
The measured contact angle values reported in this manuscript were situated between the advancing (99.1 ± 1.6 degrees) and receding (59.8 ± 1.8 degree) contact angle values measured on the covered DMOAP surfaces and reported in the ref. [24]. The theoretical and experimental interpretation of the static and dynamic wetting [25, 37] generally showed that the static contact angle value was comprised between advancing and receding contact angle. It was found that static contact angle value is equal to the average values calculated between advancing and receding contact angles.

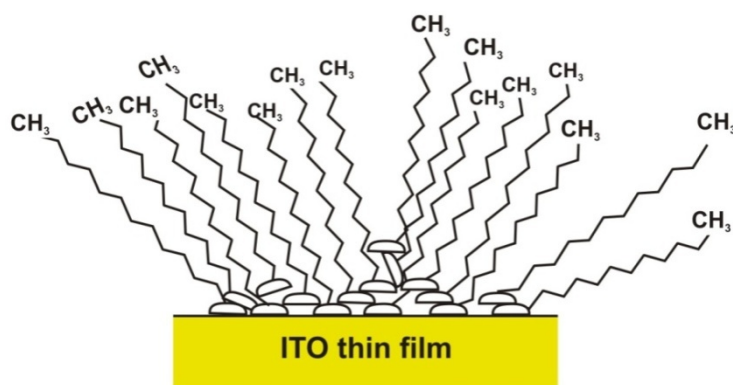
It is now possible to introduce a model that is able to explain simultaneously both the DMOAP layer thicknesses and the water contact angles.

When the drying temperature was 85°C , the maximum contact angle (fig.6) can be described by the schematic representation showed in the figure 7(b). In fact, the maximum hydrophobicity can be well justified only if there is a closed-packet molecular organization of the hydrocarbon chains. The maximum observed contact angle corresponds to the DMOAP layer thickness reported in literature [20, 24].

When the dipping treatments were different than $N_{\text{dip}} = 3$ (fig.6) , the low contact angles can be described by the schematic representation shown in figure 7(a) and 8, because only disordered hydrocarbon chains can exhibit low contact angles. Therefore, we can distinguish two cases that are compatible with the description of the previously presented SAM formation [17]. The first stage was observed for a few dipping treatments. The SA(s) were not completely formed (fig.7a), in fact, the estimated layer thickness was smaller than 27\AA (fig.5). When the dipping treatments were $N_{\text{dip}} > 3$, we can observe that the contact angle decreases and the DMOAP layer thickness was found to be a little larger than the thickness of a mono molecular layer. This situation corresponds to the third stage and it can be explained by the two schematic representations shown in figure 8.

Figure 8(a) describes the formation process of a second layer on the first close-packed DMOAP monolayer. This second molecular layer was created by the accumulation of some weakly bounded DMOAP molecules on top of the first layer. The link between the $\text{CH}_3\text{-CH}_3$ chemical groups, meaning the VdW interaction, is established between the unbounded DMOAP molecules and the terminal methyl groups of the DMOAP alkyl chains. It has been observed that the excess organosilane aggregates to some centers on the surface [20].





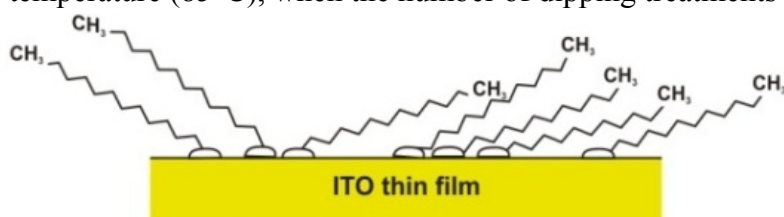
(b)

Figure 8. Schematic representation for the two possible configurations for the SAM of DMOAP molecules. (a) A second molecular layer can form on top of the first layer by means VdW electrostatic interactions between CH₃ - CH₃ chemical groups; (b) oligomerization processes can form a disordered molecular layer. The chemical bond between the polar head groups and other chemical groups is not represented. The head polar group of the DMOAP molecule is a complex chemical group and it can chemically interact with other chemical groups.

Figure 8(b) describes the second possible configuration of the molecular layer assembled on the surface. This model was introduced by Fadeev and McCarthy [19]. The molecular structure formed as a result of the rapid oligomerization of the alkylsiloxanes in the presence of water molecules. The chemical reaction involves the polar head groups, which are chemically active, favored by the presence of molecular water [19].

We suggest that the drying temperature 85°C favors the molecular configuration shown in figure 8(a). The low drying temperature has facilitated the gradual removal of the solvent molecules from the DMOAP layer. Such a slow process favors the molecular reorganization of the hydrocarbon chains of the DMOAP molecules bounded to the surface. For this reason, the DMOAP molecular configuration showed in figure 7(a) is most probable at the third treatment ($N_{\text{dip}} = 3$), whereas the DMOAP molecular configuration that is more probable for high number of dipping treatments ($N_{\text{dip}} > 3$) is shown in 8(a). In our experiment we used a low DMOAP concentration (0.005 wt.% in 2-propanol) and we did not add water in solution. These two elements have not promoted the polymerization processes described by Fadeev and McCarthy [19] (fig. 8(b)).

Figure 9 shows a model of the molecular layer evolution for the DMOAP samples dried at low temperature (85°C), when the number of dipping treatments increases.



(a)

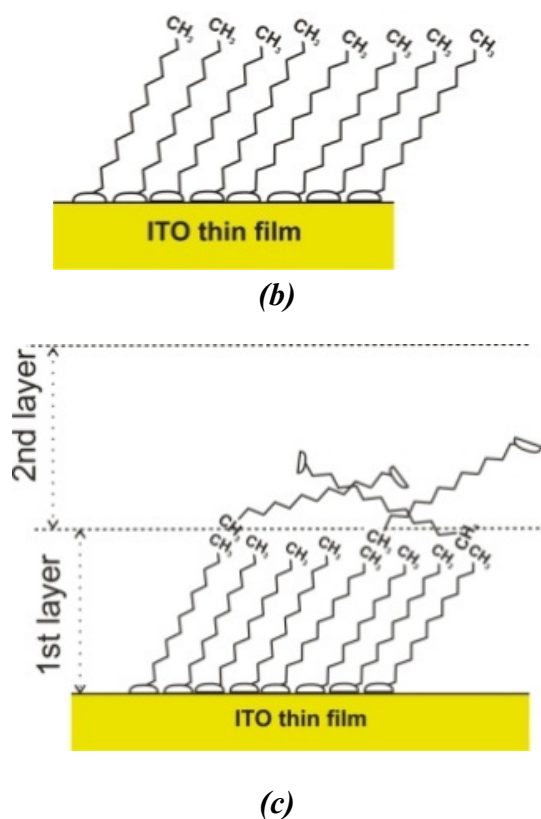


Figure 9. The sequential model ($a \rightarrow b \rightarrow c$) shows the schematic molecular configurations of the DMOAP layers obtained for drying temperature 85°C when the number of dipping treatments increases. The central picture (b) corresponds to the samples after the third treatment.

The low contact angle observed for the DMOAP samples dried at high temperature (120°C) (fig. 6) can be justified only by a disordered DMOAP molecular layer. Figure 8(b) describes the molecular configuration of the DMOAP layer obtained at this drying temperature. The larger layer thickness (fig. 5) obtained at 120°C with respect to the samples dried at 85°C suggests the fact that the high temperature induced a hydrocarbon chains rotation favoring the formation of complex and disordered molecular layers (figure 8b). The fast evaporation process of the solvent molecules from the DMOAP layer simultaneously with the high temperature can support the oligomerization process. Figure 10 shows this kind of a formation process.

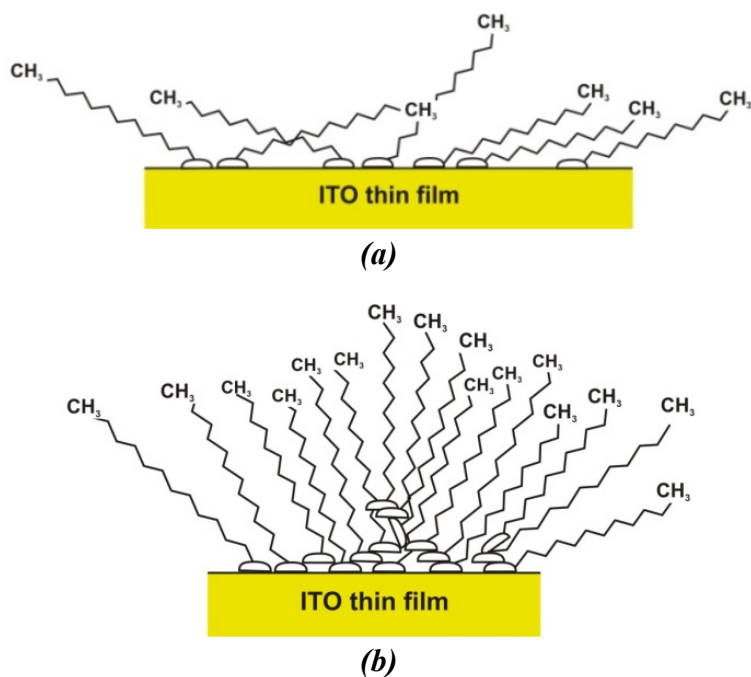


Figure 10. The picture shows a schematic molecular configuration model (a → b) of the DMOAP layers obtained at drying temperature 120°C when the dipping treatments increase in number. The high temperature favors the polymerization process within the layers (b).

This qualitative model does not consider the water molecules present at the interface between the ITO thin film and head polar chemical groups. The desorption temperature of the water molecules from ITO thin film is influenced both by the morphological structure (for example surface roughness, porosity) and the layer thickness of the ITO [38, 39, 40]. This desorption temperature value is typically larger than the desorption temperature (above 110°C) on the silicon wafer.

For this reason, water molecules can remain in different concentration on the ITO surface, even after annealing at 85°C and 120°C. These water molecules can influence the molecular reorganization of the head polar groups, therefore of the long hydrocarbon tails. New experimental investigations are actually in progress, for better understanding how the competition between the solvent, surfactant and water molecules can influence the molecular reorganization of DMOAP SAMs deposited onto ITO thin films for different drying temperatures.

Conclusions

Self-Assembled monolayers have been obtained by using DMOAP surfactant molecules on ITO thin film substrates. The protocol deposition of the DMOAP surfactant consists in a dipping treatment of the clean substrates in the DMOAP solution by means of an accurate experimental setup assembled in the clean room. We studied DMOAP thin film formation at two different drying temperatures (85°C and 120°C respectively). The layers thicknesses were determined by ellipsometry and we obtained helpful information about the molecular organization at the substrate by performing static contact angle measurements.

We propose a self-consistent model to explain the obtained experimental results. In addition, the drying temperature is demonstrated to be a relevant experimental control parameter in characterizing molecular reorganization. For $T_{\text{drying}} = 85^{\circ}\text{C}$, near the 2-propanol boiling range temperature ($81\text{-}83^{\circ}\text{C}$), we measured the maximum water contact angle value of 80° and found the layer thickness value of $26\text{-}27\text{\AA}$, which is consistent with the molecular monolayer thickness reported in literature. Therefore, at 85°C , we consent that we obtained a single monolayer of DMOAP molecules, characterized by closed-packet structure of the hydrocarbon chains. At $T_{\text{drying}} = 120^{\circ}\text{C}$, the layer thickness increases to some extent, and the acquired data reveal smaller contact angle values, suggesting that DMOAP molecules bend on the substrates and they stack in disordered formations. In this case, we expect that some solvent molecules were still present when the samples were extracted from the surfactant solution. Moderate drying temperature favored the gradual removing of the solvent molecules from the DMOAP molecular layer. Such a slow process privileged the molecular reorganization of the hydrocarbon chains inside the film, greatly increasing the molecular order. On the contrary, both a rapid removal of the solvent (at a higher drying temperature) and chemical reaction between the head polar groups inhibited the ongoing molecular reorganization reducing considerably the level of molecular ordering.

These investigations could prove very important in further analysis and understanding of self-assembly monolayer physics by showing the high impact of some initial parameters, such as the drying temperature that ought to be taken into consideration.

ACKNOWLEDGMENTS. The authors would like to thank Alfredo Pane for the essential technical support during the SAM depositions at INFM-CNR-LICRYL Laboratory and CEMIF.CAL (Department of Physics, University of Calabria) and to dr. Carlo Vena for the useful scientific discussions.

References

- [1] Petty, M.C. Langmuir-Blodgett films. An introduction, University of Durham; UK, Cambridge Univ. Press, 1996.
- [2] Ulman, A. An Introduction to Ultrathin Organic Films from Langmuir-Blodgett to Self-Assembly; Academic Press, 1991.
- [3] Blinov, L.M. Chigrinov, V.G. Electrooptic Effects in Liquid Crystal Materials, Springer-Verlag: New York, 1994.
- [4] Huang, J. H.; Superfine, R.; Shen, Y. R. Phys. Rev. A, 1990, **42**(6).
- [5] Drawhorn, R. A.; Abbott, N. L. J. Phys. Chem. 1995, **99**, 16511.
- [6] Fonseca, J. G.; Hommet, J.; Galerne, Y. Appl. Phys. Lett., 2003, **82**(1), 58.
- [7] Huie, J. C. Smart Mater. Struct. 2003, **12**, 264.
- [8] Smith, R.K.; Lewis, P.A.; Weiss, P.S. Progress in Surface Science, 2004, **75**, 1.

- [9] Anderson, M. E.; Srinivasan, C.; Hohman, J. N.; Carter, E. M.; Horn, M. W.; Weiss, P. S. *Adv. Mater.* 2006, **18**, 3258.
- [10] Ulman, A. *Chem. Rev.* 1996, **96**, 1533.
- [11] Bigelow, W. C.; Pickett, D. L.; Zisman, W.A. *J. Colloid Sci.* 1946, **1**, 513.
- [12] Nakajima, A.; Hashimoto, K.; Watanabe, T.; Takai, K.; Yamauchi, G.; Fujishima, A. *Langmuir* 2000, **16**, 7044.
- [13] Brzoska, J.B.; Shahidzadeh, N.; Rondelez, F. *Nature* 1992, **360**, 719.
- [14] McGovern, M.E.; Kallury, K.M.R.; Thompson, M. *Langmuir* 1994, **10**, 3607.
- [15] Silberzan, P.; Léger, L.; Ausserré, D.; Benattar, J. J. *Langmuir* 1991, **7**, 1647.
- [16] Brzoska, J.B.; Azouz, I. B.; Rondelez, F. *Langmuir* 1994, **10**, 4367.
- [17] Liu, Y.; Wolf, L. K.; Messmer, M.C. *Langmuir* 2001, **17**, 4329.
- [18] Davidovits, J.V.; Pho, V.; Silberzan, P.; Goldmann, M. *Surface Science* 1996, **352-354**, 369.
- [19] Fadeev, A. Y.; McCarthy, T. J. *Langmuir* 2000, **16**, 7268.
- [20] Lelidis, I.; Oedman, C. *Liquid Crystals* 2003, **30**(6), 643.
- [21] Gupta, V. K.; Abbot, N. L. *Phys. Rev. E* 1996, **54**(5), R4540.
- [22] C. Vena, C. Versace, G. Strangi, S. D'Elia, R. Bartolino "Light Depolarization effects during Fréedericksz transition", *Optics Express* 2007, **15** (25), 17063-17071.
- [23] Bain, C. D.; Troughton, E. B.; Yu-Tai T.; Evall, J.; Whitesides, G. M.; Nuzzo, R. G. *J. Am. Chem. Soc.* 1989, **111**, 321.
- [24] Almanza-Workman, A. M.; Raghavan, S.; Petrovic, S.; Gogoi, B.; Deymier, P.; Monk, D. J.; Roop, R. *Thin Solid Films* 2003, **423**, 77.
- [25] de Gennes, P. G. *Reviews of Modern Physics* 1985, **57** (3); Part I.
- [26] Decker, E.L.; Garoff, S. *Langmuir* 1997, **13**, 6321.
- [27] Cassie, A. B. D. *Discuss. Faraday Soc.* 1952, **75**, 5041.
- [28] Israelachvili, J. N.; Gee, M. L. *Langmuir* 1989, **5**, 288.
- [29] Genell Med auf Floarglas - Balzers Thin Films Prod. ID. BD051149, BATCH 1400-655-(1999)
- [30] D'Elia, S.; Castriota, M.; Policicchio, A.; Versace, C.; Scaramuzza, N.; Agostino, R.; Cazzanelli, E.; Vena, C.; Strangi, G.; Bartolino, R. *J. Applied Physics*, accepted (2008).
- [31] D'Elia, S.; Ciuchi, F.; Versace, C.; Scaramuzza, N.; Vena, C.; Strangi, G.; Bartolino, R. *Surface Science*, submitted (2008).
- [32] Tompkins, H. G.; Irene, E. A. *Handbook of Ellipsometry*, William Andrew Publishing, Springer, 2005.
- [33] D. E. Aspnes, *Thin Solid Films* 1982, **89**, 249.
- [34] Azzam, R.M.A.; Bashara, N.M. *Ellipsometry and polarized light*, North-Holland P-L, 1992.
- [35] Hillebrant, H.; Tanoka, M. *J. Phys. Chem. B* 2001, **105**, 4270.
- [36] Kulinich, S.A.; Farzaneh, M. *App. Surface Science* 2004, **230**, 232.
- [37] Miyama, M.; Yang, Y.; Yasuda, T.; Okuno, T.; Yasuda, H. K. *Langmuir* 1997, **13**, 5494.
- [38] Seki, S.; Aoyama, T.; Sawada, Y.; Ogawa, M.; Sano, M.; Miyabayashi, N.; Yoshida, H.; Hoshi, Y.; Ide, M.; Shida, A. *J. of Thermal Analysis and Calorimetry* 2002, **69**, 1021-1029
- [39] Sawada, Y.; Seki, Sano, M.; Miyabayashi, N.; Ninomiya, K.; Iwasawa, A.; Tsugashi, T.; Ozao, R.; Nishimoto, Y. *J. of Thermal Analysis and Calorimetry* 2004, **77**, 751-757.
- [40] Ryzhikov, I.A.; Pukhov, A.A.; Il'in, A.S.; Glukhova, N.P.; Afanasiev, K.N.; Ryzhikov, A.S. *Microelectronic Engineering* 2003, **69**, 270-273.

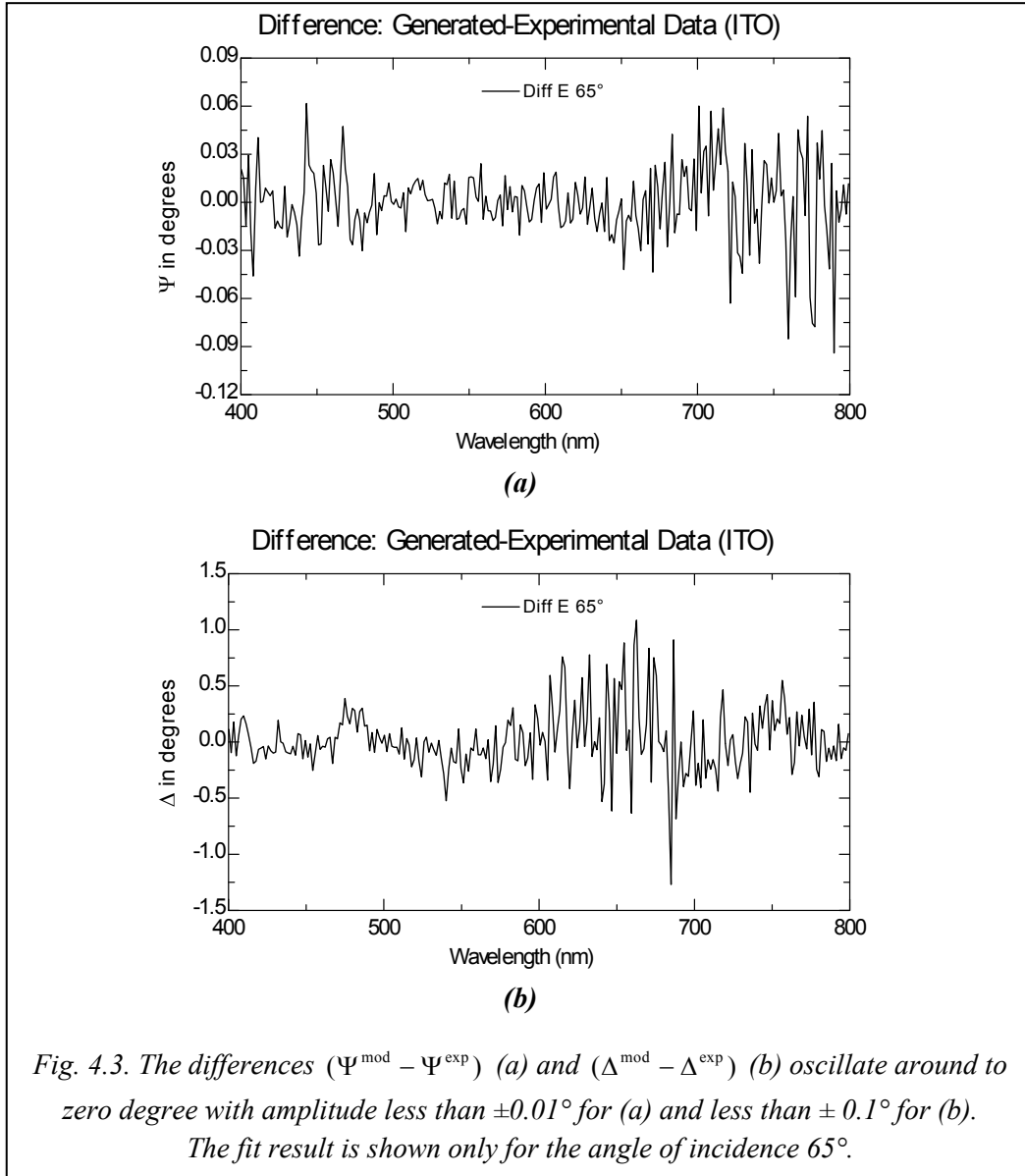
4.3.1. Appendix A – Check of the validity of the ellipsometric experimental data acquired on the glass/ITO substrates and DMOAP thin films.

This section shows some information concerning the experimental ellipsometry angles, measured on the DMOAP covered samples. Homogeneous thin film of the surfactant molecules (DMOAP) is characterized by a layer thickness less than 2-3nm. This system is a typical example of ultra thin film limit in the ellipsometry technique.

First of all, it is important recall that the ellipsometry technique doesn't provide direct information of the physical system by the measured ellipsometry angles. Only the interpretation of the experimental data by using an optical model provides access to the physical information.

The glass/ITO substrates ($25\Omega/\square$, purchased from Balzers FAB), used in this work, have been studied intensively. The optical model, studied and built for this substrate, allows us to obtain different structural and morphological information as widely showed in chapter 3 of this dissertation.

The figure 4.3 shows the difference between the generated and experimental ellipsometry angles for the glass/ITO substrates. The generated data ($\Psi^{\text{mod}}, \Delta^{\text{mod}}$) were simulated by the ITO/glass optical model, while the experimental data ($\Psi^{\text{exp}}, \Delta^{\text{exp}}$) were measured directly on the glass/ITO substrates. The difference between generated and experimental data are normally dispersed around to the zero degree with maximum amplitudes less than $\pm 0.01^\circ$ for Ψ angle and less than $\pm 0.1^\circ$ for Δ angle, in the spectral range between 400-800nm, and AOI equal to 65° .



When the DMOAP surfactant is deposited onto glass/ITO substrates, a ultra-thin film is created. In the ultra-thin film regime (sect. 4.2 of this chapter), the measured ellipsometry angles on the samples (thin film/substrates) $(\Psi_{\text{samples}}^{\text{exp}}, \Delta_{\text{samples}}^{\text{exp}})$ can be defined as a small variation of the measured ellipsometry angles on the uncovered substrate $(\Psi_{\text{ITO}}^{\text{exp}}, \Delta_{\text{ITO}}^{\text{exp}})$ i.e. $(\Psi_{\text{samples}}^{\text{exp}}, \Delta_{\text{samples}}^{\text{exp}}) = (\Psi_{\text{ITO}}^{\text{exp}} + \delta\Psi, \Delta_{\text{ITO}}^{\text{exp}} + \delta\Delta)$ [11].

By using these approximations, we can try to extract some information concerning the thickness of the DMOAP layer, directly from experimental data.

We have calculated the difference between the ITO experimental ellipsometry angles ($\Psi_{ITO}^{exp}, \Delta_{ITO}^{exp}$) and the experimental data acquired on the samples subject at different dipping treatments ($\Psi_{N-dip}^{exp}, \Delta_{N-dip}^{exp}$), by using these formulas:

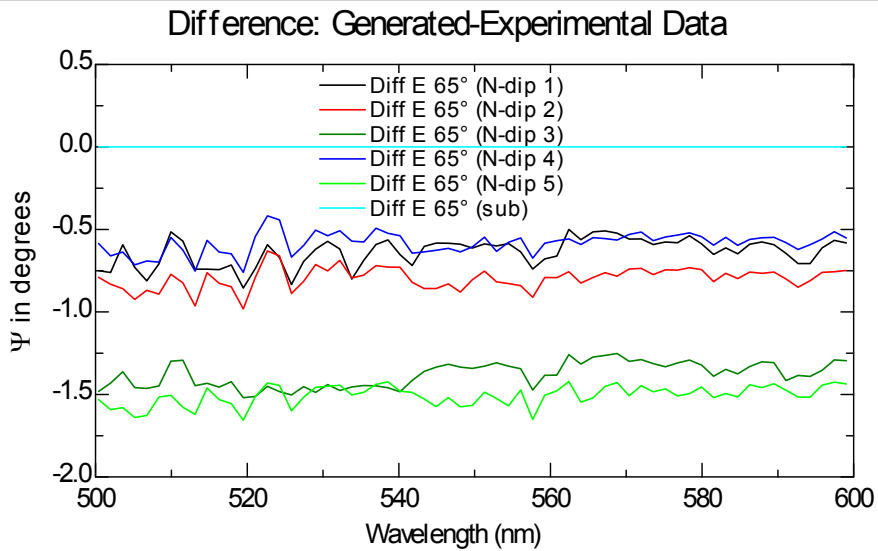
$$\Psi_{ITO}^{exp} - \Psi_{N-dip}^{exp} = \Psi \text{ in degree } \propto \delta\Psi \tag{4.2}$$

$$\Delta_{ITO}^{exp} - \Delta_{N-dip}^{exp} = \Delta \text{ in degree } \propto \delta\Delta$$

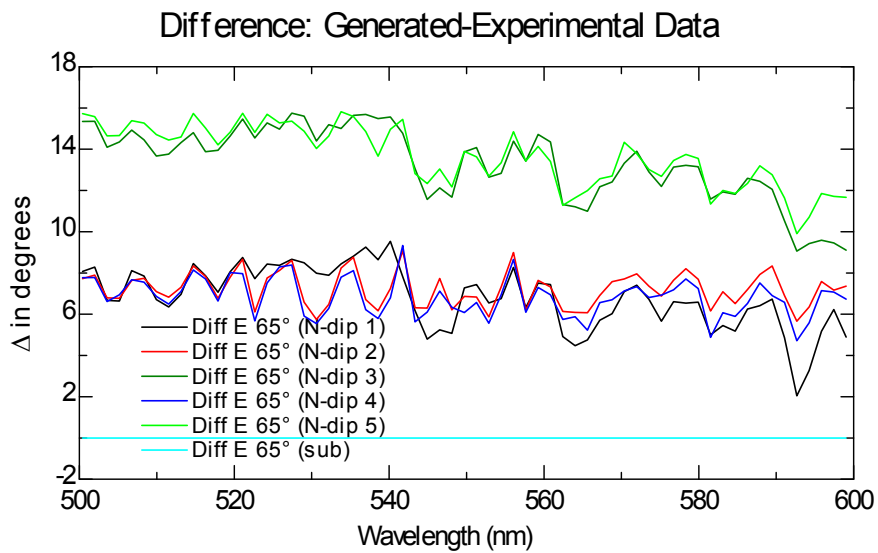
The figures 4.4 and 4.5 show the differences between the ellipsometry angles calculated by the Eq.(s) (4.2). The figure 4.4 shows the calculated results for the samples obtained with 0.005wt.% DMOAP in 2-propanol alcohol and drying temperature 85°C. The figure 4.5 are plotted the results calculated by the Eq. (4.2) for the sample obtained by using same DMOAP concentration but drying temperature were 120°C.

In these figures, we can recognize the ultra-thin film regime, in fact, the Ψ angle changes few (less than 2°) while the Δ angle changes in the range 10-15° when the dipping treatments increase.

It is important observe that any information, concerning the variation of the DMOAP layer thickness versus the dipping treatments, can be obtained from these figures without an optical model that described the multilayer structure of the samples.



(a)



(b)

Fig. 4.4. (a) $\Psi_{ITO}^{exp} - \Psi_{N-dip}^{exp} = \Psi$ in degree and (b) $\Delta_{ITO}^{exp} - \Delta_{N-dip}^{exp} = \Delta$ in degree.

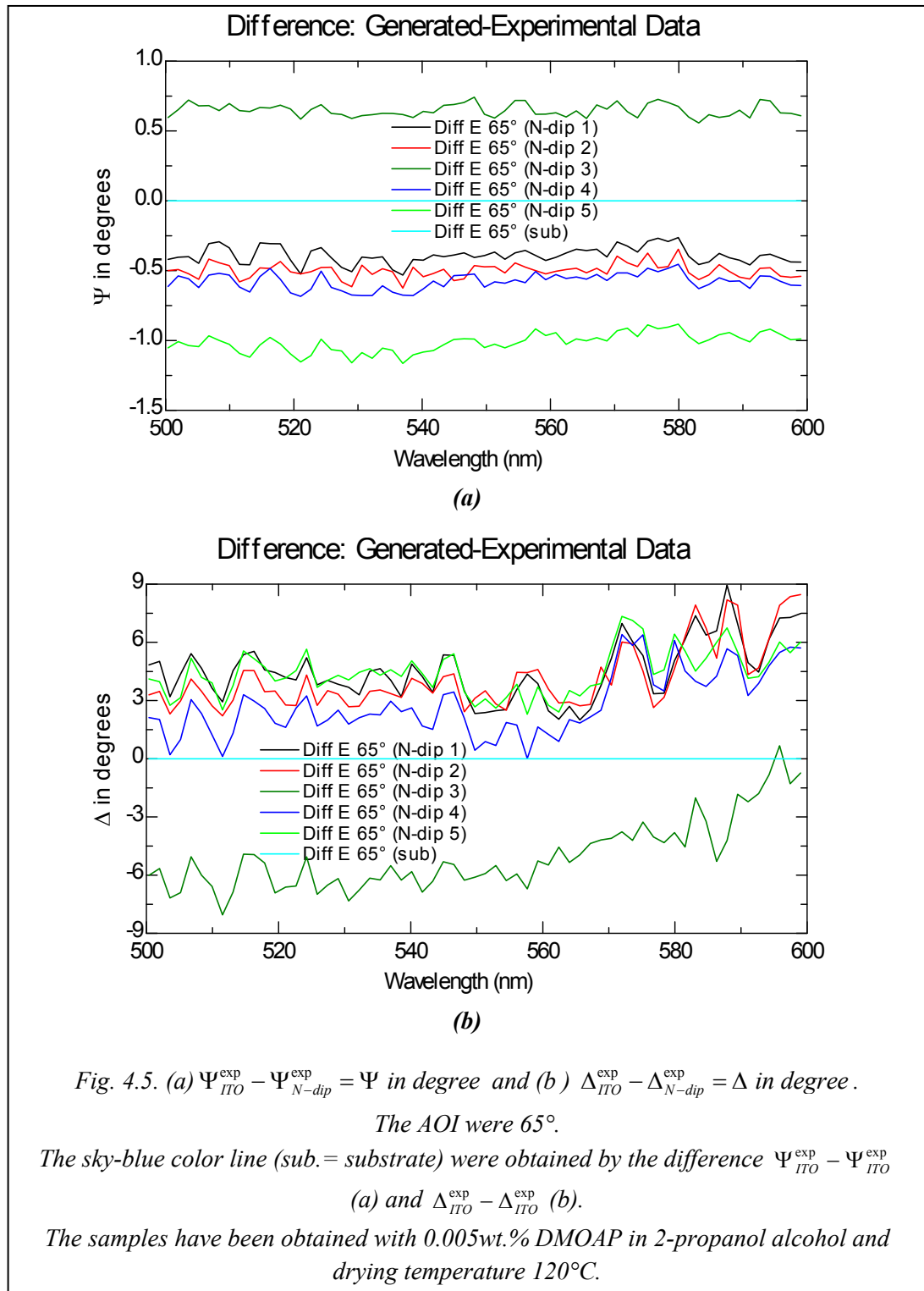
The AOI were 65° .

The sky-blue color line (sub.= substrate) were obtained by the difference: $\Psi_{ITO}^{exp} - \Psi_{ITO}^{exp}$

(a) and $\Delta_{ITO}^{exp} - \Delta_{ITO}^{exp}$ (b).

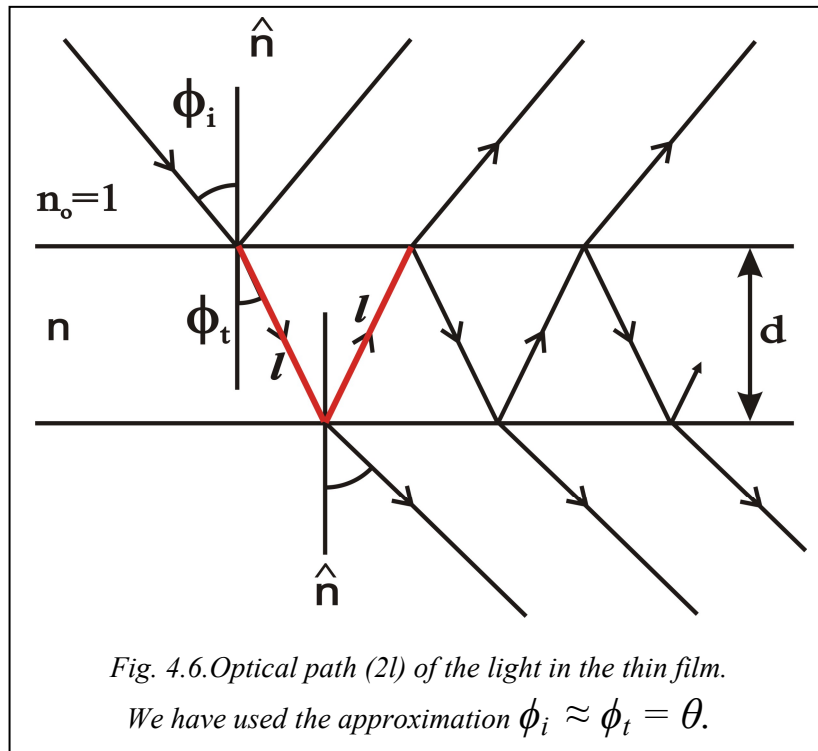
The samples have been obtained with 0.005wt.% DMOAP in 2-propanol alcohol and drying temperature 85°C .

We can estimate a maximum difference for the Δ angle (difference between the substrates and samples) more or less 14° .



In first approximation the Δ angle, calculated by using the eq. 4.2, measures the phase retarder between the p and s polarization components, when the polarized light

passes through the thin film (d is the thickness), following the optical path $2l$ as shown in the figure 4.6.



This phase retarder can be estimate by using the equation:

$$\Delta = \frac{2\pi}{\lambda} \cdot n \cdot 2l = \frac{2\pi}{\lambda} \cdot n \cdot 2 \cdot \frac{d}{\sin \theta} \quad (4.3)$$

where is the λ is light wavelength, n is the refractive index of the thin film, and $\theta = 90^\circ - 65^\circ = 25^\circ$ is related to the AOI, $\phi_i = 65^\circ$.

The layer thickness can be calculate by the Eq. (4.3)

$$d = \frac{\Delta \cdot \lambda \cdot \sin \theta}{4\pi \cdot n} \quad (4.4)$$

The maximum phase retarder estimated by the figure 4.4 is about 14° , while the refractive index of the DMOAP is 1.41 at $\lambda=589\text{nm}$, as reported by Sigma-Aldrich data sheet (sect. 4.3 of this chapter).

By using these data, we can estimate for the DMOAP layer a maximum thickness value of $d \approx 34\text{\AA}$. It is close to the thickness estimated by fit elaboration.

Chapter 4 - Reference

- [1] Abraham Ulman, "An Introduction to Ultrathin Organic Films from Langmuir-Blodgett to Self-Assembly", Academic Press, 1991
- [2] M.C. Petty, "Langmuir-Blodgett films. An introduction", University of Durham, UK, Cambridge Univ. Press, 1996.

- [3] R.K. Smith, P.A. Lewis, P.S. Weiss, "Review – Patterning self-assembled monolayers", *Progress in Surface Science* **75** (2004) 1-68
- [4] Mary E. Anderson, Charan Srinivasan, J. Nathan Hohman, Erin M. Carter, Mark W. Horn, and Paul S. Weiss, "Combining Conventional Lithography with Molecular Self-Assembly for Chemical Patterning", *Adv. Mater.* **18** (2006), 3258-3260.
- [5] George M. Whitesides and Mila Boncheva, "Beyond molecules: Self-assembly of mesoscopic and macroscopic components", *Proc Natl Acad Sci U S A.* 2002 April 16; **99**(8): 4769–4774; Lorena Nasalean, Stéphanie Baudrey, Neocles B. Leontis, and Luc Jaeger, "Controlling RNA self-assembly to form filaments", *Nucleic Acids Res.* 2006; **34**(5): 1381–1392.
- [6] J.B. Brzoska, N. Shahidzadeh, F. Rondelez, "Evidence of a transition temperature for the optimum deposition of grafted monolayer coatings", *Nature* **360**(1992), 719-721
- [7] **Stefano D'Elia**, Valentin Barna, Nicola Scaramuzza, Giuseppe Strangi, and Roberto Bartolino, "The influence of drying temperature on closed-packed structures of silanized mono-layers deposited on indium tin oxide (ITO) substrates", (in this: section 4.3). Submitted to *SURFACE SCIENCE*.
- [8] Wei Chen, Alexander Y Fadeev, Meng Che Hsieh, Didem Oner, Jeffrey Youngblood, and Thomas J. McCarthy, "Ultrahydrophobic and Ultralyophobic Surfaces: Some Comments and Examples", *Langmuir*, **15** (1999), 3395-3399.
- [9] Masashi Miwa, Akira Nakajima, Akira Fujishima, Kazuhito Hashimoto, and Toshiya Watanabe, "Effects of the Surface Roughness on Sliding Angles of Water Droplets on Superhydrophobic Surface", *Langmuir* **16**(2000), 5754-5760.
- [10] P. G. de Gennes "Wetting: static and dynamics" *Reviews of Modern Physics*, **57** (3), Part I, (1985).
- [11] R. M. A. Azzam, N. M. Bashara, "Ellipsometry and Polarized Light" (third printing), North-Holland, Elsevier Science Publishers B. V., Amsterdam, (1992).
- [12] K. Flock "The simultaneous determination of n , k , and t from polarimetric data", *Thin Solid Films*, **455-456** (2004) 349-355.
- [13] I.K. Kim and D.E. Aspnes "Toward nkd spectroscopy: Analytic solution of three-phase model of polarimetry in the thin-film limit", *App. Phys. Lett.* **88**, (2006)201107.
- [14] I.K. Kim and D.E. Aspnes "Analytic determination of n , k , and d of an absorbing film from polarimetric data in the thin-film limit", *J. App. Phys.* **101**, (2007) 033109.
- [15] J. Kattner and H. Hoffmann "Simultaneous determination of thickness and refractive indices of ultrathin films by multiple incidence medium ellipsometry", *J. Phys. Chem. B*, **106** (2002) 9723-9729.
- [16] H. G. Tompkins, E. A. Irene, "Handbook of Ellipsometry", William Andrew Publishing, Springer (2005).

- [17] M. Voué, J. De Coninck, S. Villette, M.P. Valignat, A.M. Cazabat “Investigation of layered microdroplets using ellipsometric techniques”, *Thin Solid Films* **313-314** (1998) 819-824.
- [18] O. Ou Ramdane, P. Aury, and P. Silberzan “Wetting of polymer brushes by a nematogenic compound”, *Phys. Rev. Lett.* **80** (1998) 23.
- [19] F. Heslot, A.M. Cazabat, P. Levinson, and N. Fraysse “Experiment on wetting on the scale of nanometers: influence of surface energy” *Phys. Rev. Lett.* **65** (1990) 5.
- [20] B. Lecourt, D. Blaudez, and J.-M. Turllet “Specific approach of generalized ellipsometry for the determination of weak in-plane anisotropy: application to Langmuir-Blodgett ultrathin films” *J. Opt. Am. A*, **15**(10), 1998.

Chapter 5

Summary and Outlook

The analyzed thin films materials ranged from fractions of a nanometer to several micrometers in thickness. Layered media play a very important role in many applications of modern technology and nanotechnology science, and thin films are as well significant competitors in many industrial applications. Thin films have been successfully used in many new technological applications, i.e. organic optoelectronic devices (Organic Light-Emitting Diodes (OLED), light emitting polymers (LEP) and organic electro-luminescence (OEL)), meta-material technology designs for optical application, linear and nonlinear optical applications (multilayered photonic crystals, nano-structured layers, optical surface coatings, etc); electronic semiconductor devices (solar cells, integrated nanochips, solid state memories). Other important application of thin films is the Self-assembly technique of organic materials, by which monomolecular thin films can be created, in order to develop the new nanophotolithography technique, [full bibliography concerning these topics can be found in this thesis]. In order to find new technological applications for thin film materials, actually used only in a limited number of cases, any experimental investigations around these films are important nowadays.

In this dissertation, ellipsometrical technique, together with other several experimental methods (Scan Electron Microscope (SEM), Atomic Force Microscope (AFM), X-Ray diffraction, Optical Contact Angle Meter, spectrophotometer etc) have been used for studying organic and inorganic thin films.

The properties of inorganic (organic) systems play an important role to the properties of organic (inorganic) ones. The reciprocal interactions between organic-inorganic structures were investigated considering two different physical systems. The first one is represented by the ferroelectric thin films, obtained via the sol-gel synthesis. These organic precursors transform themselves in inorganic ferroelectric materials following a thermal annealing process. The second physical system that was investigated was characterized by the order formation of self-assembly monolayers of surfactant molecules on a Transparent Conductive Oxide (TCO).

Float glass substrates covered by high quality ITO thin films (Balzers) have been intensively used in this work, therefore a full optical and structural characterization of this TCO substrate has been required [1]. These substrates were subjected for an hour to single thermal treatments at different temperatures between 100°C and 600°C. For studying the electric and optical properties of annealed and not annealed ITO-covered float glasses, ellipsometry, spectrophotometry, impedance analysis, and X-Ray investigations were performed.

The dispersion law of the float glass slides does not depend on the annealing temperature as emphasized by the transmittance measurements [1, 2] and the far-IR ellipsometrical characterization (section 3.4, chapter 4). The ellipsometrical optical models, used to characterize the ITO thin film and study the thermal modification of its structural properties, were defined by two layers: the first one describes the dielectric surface roughness properties, while the second one illustrates the ITO thin film properties. The second layer is defined as a sum between a Lorentz oscillator (to describe bound carriers - dielectric properties) and a Drude oscillator (to explain the free-carriers - conductive properties). This optical model allows estimating the dispersion laws and structural properties (plasma frequency, collision frequency, carrier density, resistivity and optical band-gap energy) of the annealed ITO samples.

Advanced spectrophotometrical investigations have been used to estimate the optical band-gap energy of the samples. The optical band-gap energy values estimated by transmittance measurements were proven to be smaller than the ones obtained via the ellipsometrical characterization. The difference between the two results was found in the range between 0.2 and 0.4eV. Transmittance and impedance characterizations have been compared to ellipsometry investigations to complete the scientific picture for the obtained experimental data.

The thermal annealing strongly changes the structural and optical properties of ITO thin films, as the ITO thin film absorbs oxygen from air during the thermal curing. Absorption decreases the oxygen vacancies and increases the crystalline order of the ITO thin films as confirmed both by ellipsometry and X-ray measurements. When the annealing temperature increases both the carrier density and optical band-gap energy decrease according with the Burstein-Moss theory, while the resistivity increases according to the performed electrical measurements. Optical band-gap energies were found to decrease from 4.5eV to 4.2eV with increasing annealing temperature [1].

An easy way for growing Lead Zirconium Titanate, $\text{PbZr}_{0.53}\text{Ti}_{0.47}\text{O}_3$, (PZT) films (with stoichiometric amount indicated in the formula) has been obtained by hybrid (carboxylate and alkoxides) sol gel method [3] and spin coating deposition of the main solution on different substrates (float glasses, ITO coated float glasses, and intrinsic silicon wafers) [2, 3]. Moreover, the effects of different thermal treatments on the structural and morphological properties of PZT films and substrates have been investigated. All of the annealing treatments had a one hour duration. The temperature ranged from 100 to 700 °C, with the chosen experimental values every 100°C. Preliminary investigations on the bare substrates indicate that the float glasses and silicon wafers properties did not change during annealing and, on the contrary, changes to structural and morphological properties were found for the ITO thin films because the annealing favors the thermal adsorption of atmospheric oxygen. Consequently, we measured an increase of the resistance and decrease of the optical band gap, in good agreement with the Burstein-Moss model. The substrates properties and their changes under annealing are not noticeably influenced by the

presence of deposited PZT layers, because these layers are not a significant barrier for the oxygen diffusion into the substrate materials [2].

We used the estimated optical model for the uncoated substrate at every temperature to describe the PZT behavior when annealed at the same temperatures. Our hypothesis allows to simulate, with good approximation, all the measured ellipsometrical angles acquired on different samples. We also obtained good results with the optical models for the system glass/ITO/PZT.

The optical models of the PZT layers deposited on float glasses, silicon wafers and ITO-coated float glasses, estimated for each annealing temperature, show that structural properties modifications of these thin films, obtained by sol-gel synthesis on different substrates, are similar. The heating process allows the elimination of water molecules and residual organic impurities from the PZT layers, even for lower annealing temperatures. The as-deposited PZT layer on different substrates is amorphous, but with increasing annealing temperatures a transformation toward a crystalline phase occurs and consequently an increase in the optical density is observed. There also is a good agreement between the changes in the optical band gap energy estimated for the samples deposited on the three substrates. We have observed that the optical band-gap energies of the perovskite and pyrochlore phases are simultaneously present below 600 °C, while for higher temperatures the pyrochlore phase was completely transformed in perovskite phase.

The optical band gap energy decreases towards the typical values of the band gap energy of the pyrochlore phase (3.7eV) and perovskite phases (4.2eV) when the annealing temperature is between 100 - 500 °C.

The highest amount of ferroelectric perovskite structures obtained by high annealing temperatures has been associated to the best efficiency, in the electro-optical response, obtained in asymmetric nematic liquid crystal (ANLC) cells having PZT electrodes annealed at 600°C [3,4]. This electro-optical response can be also attributed to the charge distribution present at the PZT-ITO interface, found by means of the ellipsometrical investigations. During the structural modifications, caused by the annealing process, the thickness of the PZT layers slowly decrease for temperatures between 100-500 °C, and collapses by 50% for temperatures around 600°C. This structural reorganization indicates the transition from amorphous to polycrystalline phase, as confirmed by SEM analysis.

The ellipsometrical characterization allows observing an interesting interaction between the PZT layers and respective substrates. The dispersion laws of PZT deposited on ITO covered float glasses show a small absorption resonance in the near IR region. This is not observed in the PZT samples deposited on float glass and intrinsic silicon wafer substrates. We suggest that the absorption resonance depends on the interfacial effects between ITO thin films and PZT material.

EDX measurements show an interdiffusion of lead and indium ions across the PZT-ITO interface, that probably generates a peculiar intermediate layer between the PZT and ITO layers. The newly detected band on the near-IR region can be attributed to the charge distribution in this region [2, 3].

In order to obtain novel physical information, the thermally induced modifications of the dielectric function for these organic-inorganic thin film systems have been investigated by means of far-IR (1.4 - 43 μ m) ellipsometry. This experimental work have been performed at the University of Nebraska-Lincoln (USA), Department of Electrical Engineering, and Nebraska Center for Materials and Nanoscience. Prof. Mathias Schubert and Dr. Tino Hofmann were the supervisors [5].

During this study, we have tried to find new information concerning the complex optical system characterized by the multilayer structure: float glass/ITO/PZT. For characterizing the modifications of the organic PZT precursors, (e.i. as they transform in ferroelectric materials by means of annealing processes) the typical resonances of the organic chemical groups that appear in the dielectric function were studied by using far-IR ellipsometry.

Preliminary investigations have showed that the water molecules and residual organic impurities seem to appear also after the pyrolysis process of the PZT samples. These impurities demonstrate to be present in the PZT thin films annealed at low temperatures, confirming the previous results (described in section 3.2 - chapter 3 of the PhD thesis [2]). In fact, there are several open questions concerning the experimental investigations performed in far-IR spectra. In order to get a clear picture of this systems new experimental investigations and theoretical analysis are underway for comparing the obtained results with RAMAN characterizations.

Self-Assembled monolayers have been obtained by using DMOAP surfactant molecules on ITO thin film substrates [6]. The protocol deposition of the DMOAP surfactant consists in a dipping treatment of the clean substrates in the DMOAP solution by means of an accurate experimental setup assembled in the clean room. We studied DMOAP thin film formation at two different drying temperatures (85°C and 120°C respectively). The layers thicknesses were determined by ellipsometrical investigations and we obtained helpful information about the molecular organization at the substrate by performing static contact angle measurements.

We propose a self-consistent model to explain the obtained experimental results. In addition, the drying temperature is demonstrated to be a relevant experimental control parameter in characterizing molecular reorganization. For $T_{\text{drying}} = 85^{\circ}\text{C}$, near the 2-propanol boiling range temperature (81-83°C), we measured the maximum water contact angle value of 80° and found the layer thickness value of 26~27Å, which is consistent with the molecular monolayer thickness reported in literature. Therefore, at 85°C, we consent that we obtained a single monolayer of DMOAP molecules, characterized by closed-packet structure of the hydrocarbon chains. At $T_{\text{drying}} = 120^{\circ}\text{C}$, the layer thickness increases to some extent, and the acquired data reveal smaller contact angle values, suggesting that DMOAP molecules bend on the substrates and they stack in disordered formations. In this case, we expect that some

solvent molecules were still present when the samples were extracted from the surfactant solution. Moderate drying temperatures favored the gradual removing of the solvent molecules from the DMOAP molecular layer. Such a slow process privileged the molecular reorganization of the hydrocarbon chains inside the film, greatly increasing the molecular order. On the contrary, both a rapid removal of the solvent (at a higher drying temperature) and chemical reaction between the head polar groups inhibited the ongoing molecular reorganization reducing considerably the level of molecular ordering.

These investigations could prove very important in further analysis and understanding of self-assembly monolayer physics by showing the high impact of some initial parameters, such as the drying temperature that ought to be taken into consideration.

Special thanks to Prof. Nicola Scaramuzza.

Author: Stefano D'Elia

Chapter 5 - Reference

[1] **Stefano D'Elia**, Federica Ciuchi, Carlo Versace, Nicola Scaramuzza, Carlo Vena, "Effects of annealing temperature on the structural and morphological properties of high quality indium tin oxide thin films", (in this PhD thesis: chapter 3, sect: 3.1). Submitted to *SURFACE SCIENCE* (2008).

[2] **Stefano D'Elia**, Marco Castriota, Alfonso Policicchio, Carlo Versace, Nicola Scaramuzza, Enzo Cazzanelli, Raffaele Agostino, Carlo Vena, Giuseppe Strangi and Roberto Bartolino, "Thermally induced modifications of the optic properties of Lead Zirconate Titanate thin films obtained on different substrates by sol-gel synthesis", (in this PhD thesis: chapter 3, sect: 3.2). Accepted, *JOURNAL OF APPLIED PHYSICS* (2008).

[3] Marco Castriota, **Stefano D'Elia**, Salvatore Marino, Enzo Cazzanelli, Nicola Scaramuzza, Carlo Versace and Roberto Bartolino, "Effects of thermal treatments on structural and optical properties of Lead Zirconium Titanate thin films obtained by sol gel technique", (in this PhD thesis: chapter 3, sect: 3.3). Submitted to *THIN SOLID FILMS* (2008).

[4] S. Marino, M. Castriota, G. Strangi, E. Cazzanelli, N. Scaramuzza, *J. Appl. Phys.* **102**, (2007) 013112-1.

[5] **Prof. Mathias Schubert** "Complex Materials Optics Network - University of Nebraska-Lincoln, Department of Electrical Engineering, and Nebraska Center for Materials and Nanoscience". Link Web: <http://ellipsometry.unl.edu/index.php>

[6] **Stefano D'Elia**, Valentin Barna, Nicola Scaramuzza, Giuseppe Strangi, and Roberto Bartolino, "The influence of drying temperature on closed-packed structures of silanized mono-layers deposited on indium tin oxide (ITO) substrates", (in this PhD thesis: chapter 4, sect: 4.3). Submitted to *SURFACE SCIENCE*.

Appendix - A

Introduction

*The appendix A collects different papers results of the **Joint Research project between CNR – Italy (Physics Department - University of Calabria (UNICAL)) and BAS – Bulgaria (Institute of Solid State Physic Bulgarian Academy of Sciences, Sofia 1784)**. This international project has been started in the 2004 and the time duration were of three years. The guide line of the project were: “**Confined and nanostructured liquid crystals studied by the method of flexoelectric spectroscopy**”. Coordinators of the project were prof. Nicola Scaramuzza (Department of Physic - University of Calabria - UNICAL) and prof. Alexander G. Petrov (Institute of Solid State Physic Bulgarian).*

The interface effects between the solid substrates and the liquid crystal phases has been studied during this project, performed in Italy and Bulgaria [1]. The experimental investigations were performed with the supervision of the prof. Alexander G. Petrov and dr. Y. Marinov of the Institute of Solid State Physics, Bulgarian Academy of Sciences, Sofia 1784, Bulgaria.

JOB MOBILITY

*[1] “**Institute of Solid State Physics, Bulgarian Academy of Science, Sofia – Bulgaria**”
Prof. A. G. Petrov. Joint Research project between CNR - Italy and BAS – Bulgaria.
TIME DURATION OF THE COLLABORATION: 2 MONTHS; (APRIL-JUNE 2006)
Concentrations: Dielectric and flexoelectric oscillations in PDLC cells.*

Orientation effects of PTFE nanolayers upon the nematic 5CB

Y. MARINOV[†], S. D'ELIA[‡], L. TODOROVA[†], A.G. PETROV[†], C. VERSACE[‡] and N. SCARAMUZZA^{*‡}

[†]Institute of Solid State Physics, Bulgarian Academy of Sciences, Sofia 1784, Bulgaria

[‡]LICRYL-INFM and Center of Excellence CEMIF.CAL, Department of Physics, University of Calabria, Via P. Bucci, Cubo 33B, I-87036 Rende (CS), Italy

(Received 12 December 2005; in final form 7 August 2006; accepted 15 August 2006)

Planar nematic layers of 5CB oriented by 'sliding on' nanolayers of PTFE were studied by electro-optic methods. Deposited layers were characterized by AFM and spectroscopic ellipsometry. It was found that at 100°C presumably single PTFE chains (4 nm thickness) are deposited. By ellipsometry measurements *c.* 0.1° pretilt angle of the nematic layer was determined. In planar nematic layers low frequency flexoelectric splay oscillations were excited. An overall *1/f* shape of the oscillation spectrum was found in the range 1 to 1000 Hz, giving no evidence of a surface viscosity effect in this range.

1. Introduction

Producing highly oriented liquid crystal films is important in many electro-optical applications such as displays, temperature sensors optical processing, etc. A wide variety of techniques has been developed to promote LC orientation. One common technique makes use of rubbed oriented layers of different kinds of organic materials. Treated surfaces affect the orientation phenomena of the LC–solid interface, in a process known as anchoring. The anchoring properties are not easy to predict since they involve a wide variety of physical properties ranging from intermolecular and surface energies to flexoelectricity and adsorption–desorption processes. Recently a new highly versatile method for orienting liquid crystals was demonstrated [1]. It consists in mechanical deposition of a thin crystal-like film of poly(tetrafluoroethylene) (PTFE) on a smooth glass substrate. In fact PTFE induces homogeneous alignment of the liquid crystals. This method is innovative with respect to the enabling of a new generation of fast switchable surface driven displays, nanodevice elements and nanoassembly for molecular electronics.

PTFE layers are also interesting candidates for testing the flexoelectricity of nematics. Flexoelectric effects provide linear coupling between an electric field and the nematic director orientation. Due to the flexoelectricity (representing a LC analogue of piezoelectricity) [2], an applied field not only orients the nematic director along the field direction but also causes

a slight fan-like distortion, called splay, of the director field. The most important aspect of this effect is that positive and negative voltages cause opposite splays, thus producing a first harmonic electro-optic response. Flexoelectric deformations depend strongly on the boundary conditions. Our recently developed flexoelectric spectroscopy [3] provides a fine tool for analysing the orientational surface viscosity, thus revealing important dynamical aspects of the interaction between a nematic liquid crystal and a solid surface.

The purpose of the present work is to present some new results on liquid crystal orientation alignment promoted by nanostructured PTFE films, as studied by AFM, polarizing videomicroscopy and ellipsometry. In addition, the flexoelectric spectra of a planar nematic 5CB liquid crystal film, oriented by an ultrathin PTFE layer, were recorded by the method of flexoelectric spectroscopy. In the frequency domain below 1000 Hz the flexoelectric measurements provide evidence that surface viscosity for planar anchoring is lower than for homeotropic anchoring.

2. Materials And Methods

PTFE (Teflon[®]) nanolayers were deposited on clean glass plates by the method of rubbing a preheated glass by a piece of Teflon [1]. A scheme of the deposition set-up is shown in figure 1. This frictional transfer method consists of using smooth microscope glass slides as hot substrates; PTFE film is then deposited by sliding a solid PTFE bar against the preheated substrate surface at 100°C and a constant pressure of 130 N cm⁻², and at a sliding rate of 0.2 cm s⁻¹. Using this technique, the

*Corresponding author. Email: scaramuzza@fis.unical.it

3b2 Version Number : 7.51c/W (Jun 11 2001)
File path : p:/Santype/Journals/Taylor&Francis/Gmcl/v465n1/gmcl220536/gmcl220536.3d
Date and Time : 28/1/07 and 17:19

Mol. Cryst. Liq. Cryst., Vol. 465, pp. 301–308, 2007
Copyright © Taylor & Francis Group, LLC
ISSN: 1542-1406 print/1563-5287 online
DOI: 10.1080/15421400701206154



Pretilted Nematic Layers of 5CB on PTFE Treated Glass Supports

S. D'Elia

C. Versace

N. Scaramuzza

Dipartimento di Fisica, UNICAL, Rende (CS), Italy

5

Y. Marinov

A. G. Petrov

Institute of Solid State Physics, Bulgarian Academy of Sciences,
Sofia, Bulgaria

10

Planar nematic layers of 5CB oriented by “sliding on” nanolayers of PTFE were studied by electrooptic methods. Deposited layers have been characterized by AFM and polarizing videomicroscopy. By using a drop method it was established that the preferred director alignment is tilted opposite to the sliding direction. In some of these samples an unusual modulated domain pattern after switching off a prolonged a.c. excitation was observed for the first time. A possible relation between the domain origin and loosely deposited PTFE layers was suggested.

Keywords: interfaces; liquid crystals; polytetrafluoro-ethylen coating; pretilt angle

Nanometer thick layers of PTFE (TeflonTM) have been deposited on clean glass plates by the method of rubbing a preheated glass by a piece of Teflon [1]. This frictional transfer method uses smooth microscope glass slides as hot substrates. PTFE film was deposited by sliding a solid PTFE bar against the preheated substrate's surface at a 100°C and constant pressure of 130 N/cm². Sliding rate was 0.2 cm/s. Deposited layers have been characterized by AFM (PERCEPTION, Assing) in the no contact mode.

This study was performed in the framework of a CNR-BAS joint project. The authors are indebted to Maria DeSanto for AFM characterization.

Address correspondence to C. Versace, Institute of Solid State Physics, Bulgarian Academy of Sciences, Sofia, 1784, Bulgaria. E-mail: ■

Q3
Q1

Dielectric and flexoelectric oscillations in PDLC studied by flexoelectric spectroscopy and laser light diffraction

A. G. PETROV^{a*}, Y. MARINOV^a, S. D'ELIA^b, S. MARINO^b, C. VERSACE^b, N. SCARAMUZZA^b

^aInstitute of Solid State Physics, Bulgarian Academy of Sciences, 72 Tzarigradsko Chaussee Blvd., 1784 Sofia, Bulgaria

^bLICRYL (CNR-INFN) and Center of Excellence CEMF. CAL, Dipartimento di Fisica, Università degli Studi della Calabria, Ponte P. Bucci, Cubo 31C, 87036 Rende (CS), Italy

Nematic droplets of variable size of E7 were dispersed in a photopolymer NOA65 matrix by the method of UV photopolymerization-induced phase separation. Dielectric and flexoelectric oscillation of the director orientation in the droplets were excited by an ac driving voltage in the range 1 Hz to 3 kHz. Both the linear and quadratic electro-optical response of the PDLC films were studied by the flexoelectric spectroscopy method and by laser light diffraction. The temperature and voltage dependence of the 1st and 2nd harmonic electro-optic spectra (amplitude and phase of the transmitted light vs frequency) were obtained, and strikingly deep minima in all spectra were found. These minima were interpreted as resulted from a spatial filtering (i.e. selective diffraction) of the time-modulated components of the transmitted light.

(Received November 1, 2006; accepted December 21, 2006)

Keywords: Polymer dispersed liquid crystals, Flexoelectric spectroscopy, Diffraction, Spatial filtering of time modulated light beams

1. Introduction

Polymer dispersed liquid crystal (PDLC) films, consisting of micron sized droplets of a nematic liquid crystal dispersed in a polymer binder, are of particular current interest for projection television, direct view flexible displays and switchable window applications [1]. Understanding the optical response of these smart optical materials at higher frequencies is important from both a fundamental and an applied point of view.

2. Materials and methods

Polymer: NOA65 (Norland Optical Adhesive 65, Norland Products Inc., New Brunswick, N.J.) is a clear, colorless, liquid photopolymer. It is cured by UV light, with a maximum absorption within the range 350-380 nm. The refractive index of the cured polymer is $n = 1.524$.

Liquid crystal: The eutectic cyanobiphenyl mixture E7 (BDH Limited Pool, England) was used, showing a nematic-to-isotropic (N-I) transition at 59-60°C, and a smectic-to-nematic transition below -20°C. The refractive indices of the LC material at a 633 nm for extraordinary and ordinary light are 1.737 and 1.5185, respectively [2]; the dielectric anisotropy is positive, $\epsilon_{\parallel} = 19$ and $\epsilon_{\perp} = 5.2$ at 1 kHz frequency and room temperature [3]. Therefore, the random-like LC orientation in the droplets in the absence of an applied field creates a refractive index contrast, giving rise to intense light scattering. However, this scattering is field-reducible, and when the a.c. field is of sufficiently low frequency, it is also time-modulated (see below).

Samples: The PDLC samples were prepared by a photopolymerization-induced phase separation (PIPS) technique. Predetermined mixtures of NOA65 and E7 in the ratio 50:50 wt % were heated to 60°C in an isotropic phase to achieve homogeneous mixing. The blended compounds were sandwiched between two In-Sn oxide (ITO) coated glass plates and set to a thickness of 25 μm or 5 μm using polymer spacers. The UV curing was performed by either homogeneous irradiation of the whole sample area, or by a lateral gradient of the UV intensity, thereby producing a gradient in droplet size.

Experimental set-up: The technique for exciting and recording the dielectro-optic and flexoelectro-optic response of the PDLC films has been described previously for continuous nematic layers [4, 5]. The frequency dependence of the 1st and 2nd harmonics of time-modulated He-Ne laser light of normal incidence transmitted through the film (forward scattered) was registered by a photodiode and fed to a lock-in amplifier (SR530, Stanford Research Systems). The lock-in in-built function generator was interfaced to a computer, thus providing a frequency sweep of variable range and rate. The amplified generator output was applied to the sample by means of ITO electrodes.

Diffraction patterns were obtained by a 628 nm He-Ne laser (Melles-Griot) on a black screen placed 50 cm away from the sample, and photo images at different voltages were taken by a HP 735 digital camera. The spatial distributions of the 1st and 2nd harmonics were obtained during a scan along the equatorial section of a diffraction pattern, by the photodiode being fixed to a translator.

Appendix - B

Introduction

The appendix B collects different papers concerning various scientific arguments. In order to prepare these work, interesting scientific discussions have been performed with dr. Carlo Vena.

*Interesting investigations have been developed concerning depolarization processes in nematic liquid crystal (NLC) cells during Fréedericksz transition. The results of these studies were submitted to the 4th **International Conference on Spectroscopic Ellipsometry (ICSE4)** - 11 - 16 June, 2007, Stockholm – Sweden as poster presentation and paper submission [1], as reported in my scientific curriculum (to the end of this thesis).*

In these experimental investigations has been used homeotropically aligned NLC cells [2]. The homeotropic alignment were obtained by deposition of monolayer of DMOAP molecules onto the conductive glass substrates.

In order to obtain high quality homeotropically aligned NLC cells, the investigations concerning the self-assembly of the DMOAP molecules, widely reported in the chapter 4 of this thesis, have been used usefully.

Reference

[1] C. Vena, C. Versace, G. Strangi, S. D'Elia, R. Bartolino "Fréedericksz Transition in Homeotropically Aligned Liquid Crystals: a Photopolarimetric Characterization", *phys. stat. sol. (c)*, Vol. 5, Issue 5, May 2008, pp. 1257-1260.

[2] C. Vena, C. Versace, G. Strangi, S. D'Elia, R. Bartolino "Light Depolarization effects during Fréedericksz transition", *Optics Express*, Vol. 15, No. 25 December 2007, pp. 17063-17071.

Light depolarization effects during the Fréedericksz transition in nematic liquid crystals

Carlo Vena, Carlo Versace*, Giuseppe Strangi, Stefano D'Elia and Roberto Bartolino

INFN-LiCryl Laboratory and Centro d'Ecceellenza Materiali Innovativi Funzionali (Cemifcal)

Dipartimento di Fisica Università della Calabria, 87036 Rende, Cosenza, Italy

*Corresponding author: versace@fis.unical.it

Abstract: This work is aimed to the photopolarimetric characterization of the disorder evolution occurring in homeotropically aligned nematic liquid crystal films during the electrically induced Fréedericksz transition. The molecular director dynamics and the transversal reorientation modes are investigated by the analysis of the depolarization of the light beam emerging from the sample. Our measurements reveal unexpected depolarization effects at the transition, which we interpret in terms of director field inhomogeneity and defects creation.

©2007 Optical Society of America

OCIS codes: (120.5410) Polarimetry; (160.3710) Liquid Crystals; (290.5855) Scattering and Polarization.

References and links

1. P. G. de Gennes and J. Prost, *The Physics of Liquid Crystals* (Oxford Science Publications, Clarendon Press, second edition, 1993).
2. V. Fréedericksz and V. Zolina, "Forces causing the orientation of an anisotropic liquid," *Trans. Faraday Soc.* **29**, 919 (1933).
3. M. Golubitsky and D. G. Schaeffer, *Singularities and Groups in Bifurcation Theory: Vol. I*, Applied Mathematical Sciences **51** (Springer-Verlag, New York, 1985).
4. G. I. Blake, T. Mullin and S. J. Tavener, "The Fréedericksz transition as a bifurcation problem," *Dynamics and Stability of Systems* **14**, 299 (1999).
5. M. Kléman, "Defects in liquid crystals," *Rep. Prog. Phys.* **52**, 555 (1989); R. Repnik, L. Mathelitsch, M. Svetec and S. Kralj, "Physics of defects in nematic liquid crystals," *Eur. J. Phys.* **24**, 481 (2003).
6. M.G. Clerc, T. Nagaya, A. Petrossian, S. Residori and C.S. Riera, "First-order Fréedericksz transition and front propagation in a liquid crystal light valve with feedback," *Eur. Phys. J. D* **28**, 435 (2004).
7. A. Buka and L. Kramer, "Linear and Nonlinear Transient Patterns in the Splay Fréedericksz Transition of Nematics," *J. Phys. II France* **2**, 315 (1992).
8. N. Scaramuzza, G. Strangi and C. Versace, "Electro-Optic Behavior of a Non Polar Nematic Liquid Crystal and Its Mixture," *Liq. Cryst.* **28**, 307 (2001).
9. C. Vena, C. Versace, G. Strangi, V. Bruno, N. Scaramuzza, R. Bartolino, "Light Depolarization Effect by Electrohydrodynamic Turbulence in Nematic Liquid Crystals," *Mol. Cryst. Liq. Cryst.* **441**, 1 (2005).
10. R. M. A. Azzam, "Beam splitters for the division-of-amplitude photopolarimeter," *Opt. Acta* **32**, 1407 (1985).
11. R.M.A. Azzam, E. Masetti, I.M. Elmiyawi, F.G. Grosz, "Construction, calibration, and testing of a four-detector photopolarimeter," *Rev. Sci. Instrum.* **59** (1), 84 (1988).
12. E. Masetti, M.P. de Silva, "Development of a novel ellipsometer based on a four-detector photopolarimeter," *Thin Solid Films* **264**, 47 (1994).
13. K. Brudzewski, "Static Stokes Ellipsometer: General Analysis and Optimization," *J. Mod. Opt.* **38**, 889 (1991).
14. D. Bicout, C. Brosseau, A. S. Martinez and J. M. Schmitt, "Depolarization of multiply scattered waves by spherical diffusers: Influence of the size parameter," *Phys. Rev. E* **49**, 1767 (1994).
15. C. Brosseau and D. Bicout, "Entropy production in multiple scattering of light by a spatially random medium," *Phys. Rev. E* **50**, 4997 (1994).
16. R. A. Chipman, "Polarizers, retarders and depolarizers," http://www.optics.arizona.edu/chipman/Publications/Polarizers_and_Polarized_Light_Preview.pdf
17. N. Eber, S. A. Rozanski, Sz. Nemeth, A. Buka, W. Pesch and L. Kramer, "Decay of spatially periodic patterns in a Nematic Liquid Crystal," *Phys. Rev. E* **70**, 061706 (2004).
18. S. T. Bramwell, K. Christensen, J.-Y. Fortin, P. C.W. Holdsworth, H. J. Jensen, S. Lise, J. M. López, M. Nicodemi, J.-F. Pinton, and M. Sellitto, "Universal Fluctuations in Correlated Systems," *Phys. Rev. Lett.* **84**, 3744 (2000).

#87200 - \$15.00 USD
(C) 2007 OSA

Received 4 Sep 2007; revised 23 Oct 2007; accepted 1 Nov 2007; published 5 Dec 2007
10 December 2007 / Vol. 15, No. 25 / OPTICS EXPRESS 17063

Fréedericksz transition in homeotropically aligned liquid crystals: a photopolarimetric characterization

C. Vena^{*}, C. Versace^{**}, G. Strangi, St. D'Elia, and R. Bartolino

Dipartimento di Fisica, Università della Calabria, 87036 Rende, Cosenza, Italy

Received 27 August 2007, revised 28 January 2008, accepted 29 January 2008
Published online 20 March 2008

PACS 78.20.Ci, 78.66.Qn

^{*} Corresponding author: e-mail cvena@fis.unical.it

^{**} e-mail versace@fis.unical.it

This work is aimed to the photopolarimetric characterization of the disorder evolution occurring in homeotropically aligned nematic liquid crystal films during the Fréedericksz transition. This order-disorder transition is studied by monitoring the depolarization effects of the transmitted light. De-

polarization mainly occurs because light undergoes random and local phase displacements. The measurements reveal unexpected depolarization effects at the transition, which we interpret in terms of director field inhomogeneity.

© 2008 WILEY-VCH Verlag GmbH & Co. KGaA, Weinheim

1 Introduction In this paper we report an ellipsometric study of the Fréedericksz transition (FT) in homeotropically aligned nematic liquid crystal samples. We use a new theoretical approach to explain our experimental results and gain further understandings. During the transition we observed an unexpected light depolarization of the transmitted light beam [1]. Recently, it was observed a substantial difference between the homeotropic and planar cases of initial configuration of the nematic film [1]. The depolarization effects during Fréedericksz transition occurs only in the homeotropic case. In the planar case the orientational director dynamics is established by the geometry of the system, which unambiguously fixes the initial and the final directions of the director. In homeotropic case only the initial director orientation is fixed (perpendicular to the cell plates), then, during the transition, the director is free to revolve in all the directions around the initial one. This is a further degree of freedom which is not present in the planar case. This symmetry breaking produces a local director orientation which is different in the various points of the cell. As a consequence the wave-front of the transmitted light undergoes a local phase displacement and light depolarization occurs [1].

In Ref. [2] it was essentially studied the depolarization effects due to different polarization states between differ-

ent regions of the same light wave-front. In this case Stokes parameters are averaged across the wave-front surface and accounted in the model as a simple plane wave-front. In this model the wave-front is divided in N regions. Every region has well defined polarization, but there is no correlation between the polarization states of different regions. By this model the wave front depolarization can be expressed as a easy function on N , i.e $N=(1/P)^2$. In this work we compare the theoretical results and the experimental data and we tend to understand the complex scenario that occurs during FT.

2 Experimental We applied an alternate electric voltage (1000 Hz) to a nematic liquid crystal film (M7 nematic mixture [3]) confined between two transparent electrodes (glass slides coated by an ITO layer), being 25 μ m the cell thickness, each ITO electrode was coated by a surfactant (DMOAP) to induce a homeotropic alignment. The M7 parameters values reported in the literature are the following: the rotational viscosity is $\gamma_1=41$ cP; the dielectric anisotropy is $\Delta\epsilon=-0.31$ and the bend elastic constant is $K_{33}=8.1\cdot 10^{-7}$ dyne. Because M7 has a negative dielectric anisotropy ($\epsilon_{\parallel} < \epsilon_{\perp}$), the nematic molecular director tends to align itself perpendicular to the electric field and, above a certain threshold voltage, the Fréedericksz transi-

Electrohydrodynamic Instabilities in Doped M5 Nematic Liquid Crystals

C. Vena
C. Versace
G. Strangi
S. D'Elia
R. Bartolino

Licryl INFM-CNR Regional Laboratory and Centro d'Eccellenza
CEMIF.CA. Dipartimento di Fisica, Università della Calabria, Rende, CS

We report the study of the electrodynamic behavior of the nematic mixture M5 doped at several percentages by its reaction precursors 4-(n-Octyloxy)phenol and 4-Heptylbenzoic acid [1]. The influence of the doping impurities on the M5 clearing temperature has been studied by micro differential scanning calorimetry and their conductivities have been determined by impedance analysis as well as their dielectric constants. Finally we studied by polarizing microscopy the influence of the dopants on the voltage threshold for the onset of the orientational instabilities and we determined the cut-off frequency of the low frequency conductive regime.

Keywords: anisotropic media; electrodynamics; instabilities; liquid crystals

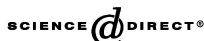
1. INTRODUCTION

Electrohydrodynamic convection (EHC) in nematic liquid crystals is a well known standard system for dissipative pattern formation (for a general review, see [2]). It provides a rich scenario of dissipative structures which can be readily controlled by experimental parameters as electric field strength and frequency. Moreover, the hydrodynamic and electric equations involved are well known and the observation of the textures is straightforward by means of optical microscopy. These characteristics have allowed to liquid crystals to become an important paradigm to study generic aspects of pattern forming

Address correspondence to C. Vena, Licryl INFM-CNR Regional Laboratory and Centro d'Eccellenza CEMIF.CA., Dipartimento di Fisica, Università della Calabria, 87036 Rende, CS. E-mail: cvena@fis.unical.it



Available online at www.sciencedirect.com



Thin Solid Films 455–456 (2004) 513–518



Photopolarimetric investigations of liquid crystals–electrochromic oxides interface

G. Strangi*, C. Versace, N. Scaramuzza, E. Cazzanelli, V. Bruno, C. Vena, S. D'Elia, R. Bartolino

LiCryl – INFM (Liquid Crystal Regional Laboratory), c/o Department of Physics, University of Calabria, Via P. Bucci Cubo 31/c, I-87036 Rende (CS), Italy

Abstract

Transmission ellipsometry studies of both nematic and smectic liquid crystals (LCs) confined by mixed conductor substrates are reported. By simultaneously measuring the Stokes parameters of transmitted light, we follow the modification of the polarization state of the monochromatic light propagating through the LC cells. The analysis of the polarization states of the probe beam during the application of a specific voltage waveform at the LC samples allows obtaining important physical information on the investigated systems. The weakening of the anchoring energy in nematic LC samples and the experimental evidence of the Goldstone mode during the switching process of smectic LCs are reported.

© 2003 Elsevier B.V. All rights reserved.

Keywords: Ellipsometry; Liquid crystals; Tungsten oxides

1. Introduction

The polarization optical technique represents one of the most important probe tools to investigate the physical and chemical properties of the 'soft matter'. Liquid crystals (LCs), polymers, molecular materials are the class of materials more representative and extensively studied of the 'soft matter' science. The electrical, mechanical and optical properties of the 'soft matter' make it extremely interesting for both basic scientific research and technological aspects. In particular, the optical properties have been largely exploited because of the intrinsically anisotropic physical characteristics. The aim of this work is the investigation of surface properties and optical switching mechanisms of LC cells by means of transmission ellipsometry (photopolarimetry) technique [1].

The physical behavior of LC is largely characterized by the surface properties and in particular the surface anchoring energy plays a fundamental role in the scenario of the LCs research. The bulk properties of the LC cells are greatly dependent on the surface regions that, being strongly anchored to the cell boundary substrates, does not undergo reorientation at usual operating voltage. Only for very intense field surface regions

can be reoriented, so that the surface anchoring energy represents the work needed to reorient the nematic LC surface region towards the bulk director orientation. Recently, the adsorption of ions (coming from the LC bulk) to the walls of the cell has been invoked to explain the anchoring energy dependence on the cell thickness [2–5]. We used an innovative cell as system-model in order to select properly the ion species as well as the amount of the injected charge at the NLC–substrate interface. The WO_3 is among the most exploited electrochromic materials as active electrodes, because of its mixed conduction property [6]. These materials present good ionic conductivity for small cations (H^+ , Li^+ , Na^+) coupled with a reasonable electronic conductivity, this allows a reversible intercalation–deintercalation processes of protons in bulk films. Here our intention is to exploit these properties in order to create surface charge-controlled systems, which allow a proper study of the influence of charge on the surface properties of the NLC.

The study has been carried out by applying opportune electric stimulus to the LC samples, and measuring the evolution of the polarization of the transmitted light by a four detectors polarimeter (FDP). The light transmitted through a LC cell is generally elliptically polarized, the modification of the incident state of polarization is related to the birefringence of the medium. The effective

*Corresponding author.

E-mail address: strangi@fis.unical.it (G. Strangi).

List of own publications

The following articles have been published or submitted for publication. References to these articles are partially in the Bibliography.

1. **Stefano D'Elia**, M. Castriota, C. Versace, N. Scaramuzza, E. Cazzanelli, C. Vena, G. Strangi, "Thermally induced modifications of the optic properties of Lead Zirconate Titanate thin films obtained on different substrates by sol-gel synthesis", *Journal of Applied Physics*, accepted (2008).
2. M. Castriota, **Stefano D'Elia**, S. Marino, E. Cazzanelli, N. Scaramuzza, C. Versace and R. Bartolino, "Effects of thermal treatments on structural and optical properties of Lead Zirconium Titanate thin films obtained by sol gel technique", *Thin Solid Films*, submitted (2008).
3. **Stefano D'Elia**, F. Ciuchi, C. Versace, N. Scaramuzza, G. Strangi, C. Vena and R. Bartolino "Ellipsometric investigation of the effects of annealing temperature on the optical properties of indium tin oxide thin films studied by Drude-Lorentz model", *Surface Science*, submitted (2008).
4. **Stefano D'Elia**, V. Barna, N. Scaramuzza, G. Strangi, and R. Bartolino "The influence of drying temperature on the closed-packed structure of silanized monolayers deposited on indium tin oxide (ITO) substrates", *Surface Science*, submitted (2008).
5. G. Petrov, Y. Marinov, **Stefano D'Elia**, S. Marino, C. Versace, N. Scaramuzza "Dielectric and flexoelectric oscillations in PDLC studied by flexoelectric spectroscopy and laser light diffraction", *Journal of Optoelectronics and Advanced Materials*, Vol. 9, No. 2, February 2007, pp. 420-423.
6. Y. Marinov, **Stefano D'Elia**, L. Todorova, A.G. Petrov, C. Versace, and N. Scaramuzza "Orientation effects of PTFE monolayers upon the nematic 5CB", *Liquid Crystals*, Vol. 33, No. 10, October 2006, pp. 1219-1225.
7. Y. Marinov, **Stefano D'Elia**, A.G. Petrov, C. Versace, and N. Scaramuzza "Pretilted nematic layers of 5CB on PTFE treated glass supports" *Molecular crystals and liquid crystals*, Vol 465, pp. 301-308, 2007.
8. C. Vena, C. Versace, G. Strangi, **Stefano D'Elia**, and R. Bartolino "Fréedericksz Transition in Homeotropically Aligned Liquid Crystals: a Photopolarimetric Characterization", *phys. stat. sol. (c)*, Vol. 5, Issue 5, May 2008, pp. 1257-1260.
9. C. Vena, C. Versace, G. Strangi, **Stefano D'Elia**, and R. Bartolino "Light Depolarization effects during Fréedericksz transition", *Optics Express*, Vol. 15, No. 25 December 2007, pp. 17063-17071.
10. C. Vena, C. Versace, G. Strangi, **Stefano D'Elia**, and R. Bartolino, "Electrohydrodynamic Instabilities in Doped M5 Nematic Liquid Crystals" *Molecular crystals and liquid crystals*, Vol 465, pp. 217-225, 2007.

11. G. Strangi, C. Versace, N. Scaramuzza, E. Cazzanelli, V. Bruno, C. Vena, **Stefano D'Elia**, and R. Bartolino "Photopolarimetric investigations of liquid crystals–electrochromic oxides interface". *Thin solid films*, 2004, Vol. 455-456, pp. 513-518.

WORKS PRESENTED AT CONFERENCES

1. **Stefano D'Elia**, M. Castriota, E. Bruno, A. Policicchio, C. Versace, C. Vena, R. Agostino, G. Strangi, E. Cazzanelli and N. Scaramuzza "Optical and morphological properties of PZT thin films deposited by sol-gel method on different substrates". **4th International Conference on Spectroscopic Ellipsometry (ICSE4)** - 11 - 16 June, 2007, Stockholm – Sweden. (Presentation type: *Poster*)
2. C. Vena, C. Versace, G. Strangi, **Stefano D'Elia** and R. Bartolino, "Light Depolarization Effects in Nematic Liquid Crystals" **4th International Conference on Spectroscopic Ellipsometry (ICSE4)** - 11 - 16 June, 2007, Stockholm – Sweden. (Presentation type: *Poster*)
3. **Sciences and Technologies of Mesophases and Molecular Materials (STM³) International Doctorate Workshop** – September 27 – October 01, 2006, Cetraro – Italy. (Presentation type: *oral*)
4. **Stefano D'Elia**, M. Castriota, C. Versace, C. Vena, E. Cazzanelli, N. Scaramuzza, M. De Santo, S. Marino and E. Bruno, "Structural and morphological characterization by VASE technique of lead zirconate-titanate (PZT) thin films deposited by sol-gel method". **1st International Symposium on Transparent Conducting Oxides (IS-TCO)** - 23 - 25 October, 2006 Hersonissos, Crete, Greece. (Presentation type: *Poster*)
5. C. Versace, G. Strangi, **Stefano D'Elia**, C. Vena, R. Bartolino, "Deposition of High-Oriented Molecular Films on Poly(tetrafluoroethylene) Substrates". **SICL'04 6TH National meeting**, Ishia, 02-04 Giugno 2004. (Presentation type: *Poster*)
6. P. Strangi, C. Versace, N. Scaramuzza, E. Cazzanelli, V. Bruno, C. Vena, **Stefano D'Elia** "Photopolarimetric Investigation of Liquid Crystals Electrochromatic Oxide Interface". **3rd International Conference on Spectroscopic Ellipsometry** - Vienna 6-11 July 2003. (Presentation type: *Poster*)

JOB MOBILITY

1. "Institute of Solid State Physics, Bulgarian Academy of Science, Sofia – Bulgaria" Prof. A. G. Petrov. **Joint Research project between CNR - Italy and BAS – Bulgaria.**

TIME DURATION OF THE COLLABORATION: 2 MONTHS;

Concentrations: Dielectric and flexoelectric oscillations in PDLC cells.

2. "University of Nebraska, Lincoln - USA" Prof. Mathias Schubert.

TIME DURATION OF THE COLLABORATION: 2 MONTHS;

Concentrations: Deep IR ellipsometry investigation of the PZT thin films obtained by sol-gel synthesis.

3. **J.A. Woollam “WVASE Trainings Course” - L.O.T.-Oriel GmbH & Co. KG**
**Im Tiefen See 58, Darmstadt, Germany. The Lecturer: James Hilfiker J:A:
Woollam Co.; The coordinator Dr. Thomas Wagner L.O.T. – Oriel**
TIME DURATION OF THE COLLABORATION: 5 DAYS;
Concentrations: Ellipsometry, Optical model theory isotropic and anisotropic
physical systems.

Scientific Curriculum Vitae

<i>Name</i>	<i>Stefano D'Elia</i>	
<i>Date of birth</i>	<i>January 11, 1974</i>	
<i>Place of birth</i>	<i>Cosenza, ITALY</i>	
<i>Nationality</i>	<i>Italian</i>	
<i>Education and scientific activities:</i>	<i>2003</i>	<p><i>M.S. Degree in Physics:</i> <i>Physics Department - University of Calabria, 87036 Rende (CS) – Italy</i> <i>Thesis:</i> “<i>Deposizione e caratterizzazione ellissometrica di film sottili molecolari</i>” <i>Concentrations:</i> <i>Ellipsometry technique, interactions between thin film and Liquid crystalline materials, Self-Assembly of molecular systems. Thin films of PTFE deposited by rubbing deposition. Dynamic light scattering, Polarimetry.</i> <i>Advisor:</i> <i>Prof. Carlo Versace - University of Calabria, 87036 Rende (CS) – Italy</i></p>
	<i>2004-2005</i>	<p><i>Post - M.S. Degree in the LiCryl-CNR laboratory supported by the Regione Calabria (ITALY).</i> <i>Concentrations:</i> <i>Ellipsometry characterization of molecular thin films deposited by Self-Assembly method.</i> <i>Advisor:</i> <i>Prof. Carlo Versace - University of Calabria, 87036 Rende (CS) – Italy.</i></p>

2004-2005

*Teaching Tutors of the "CALABRIA SCIENZA OGGI Foundation".
Facoltà di Scienze MM.FF.NN. -
Physics Department - University of
Calabria, 87036 Rende (CS) – Italy*

May 16 – June 25,
2005

*Teaching Tutors: An introduction to
Ellipsometry technique, "Alarico"
Summer school on nanoscience of soft
matter.
ALARICO CENTRE - Montalto
Uffugo (CS), Italy.*

2005-2008

*PhD Student at the University of
Calabria (UNICAL) Physics
Department - in the frame of the PhD
Program: "International Doctorate in
Science and Technology of Mesophases
and Molecular Materials" - XXI°
Cycle - Physics Department -
University of Calabria, 87036 Rende
(CS) – Italy.
Advisor: Prof. Carlo Versace.
Concentrations: Ellipsometry
characterization of thin films, theories
of optical model (isotropic and
anisotropic optical system), thin films
of oxide and organic materials, Self-
assembly, Liquid crystalline materials,
interactions between thin film and
Liquid crystalline materials, interface
effects between n-type semiconductor
(Indium tin oxide) and ferroelectric
materials (Lead Zirconate-Titanate
(PZT)).*

2008-now

*Secondary school professor at Istituto D'Istruzione Superiore "Giuseppe Veronese", Chioggia (VE) Italy.
Concentrations: Teaching Tutor of mathematic and physic at the Liceo Scientifico "G. Veronese", Chioggia (VE).*

The End!

Dr. Stefano D'Elia

